EXPERIMENTAL VALIDATION OF FINITE ELEMENT TECHNIQUES FOR BUCKLING AND POSTBUCKLING OF COMPOSITE SANDWICH SHELLS

by

Aaron Thomas Sears

A thesis submitted in partial fulfillment
of the requirements for the degree

of

Master of Science

in

Mechanical Engineering

MONTANA STATE UNIVERSITY-BOZEMAN
Bozeman, Montana

December, 1999

APPROVAL

of a thesis submitted by

Aaron Thomas Sears

This thesis has been read by each member of the thesis committee and has been found to be satisfactory regarding content, English usage, format, citations, bibliographic style, and consistency, and is ready for submission to the College of Graduate Studies.

Dr. Douglas Cairns _____
Chairman, Graduate Committee Date

Approved for the Department of Mechanical and Industrial Engineering

Dr. Vic Cundy _____
Department Head Date

Approved for the College of Graduate Studies

Dr. Bruce McLeod _____
Graduate Dean Date

STATEMENT OF PERMISSION TO USE

In presenting this thesis in partial fulfillment of the requirements for a master's degree at Montana State University-Bozeman, I agree that the Library shall make it available to borrowers under rules of the Library.

If I have indicated my intention to copyright this thesis by including a copyright notice page, copying is allowable only for scholarly purposes, consistent with "fair use" as prescribed in the U.S. Copyright Law. Requests for permission for extended quotation from or reproduction of this thesis in whole or in parts may be granted only by the copyright holder.

Signature _____

Date _____

ACKNOWLEDGEMENTS

The author would like to acknowledge the support of Dr. Doug Cairns and Dr. John Mandell for their guidance, advice and patience throughout this long project. Numerous other people have also helped this project towards fruition, in particular I would like to thank: Dan Samborsky for his advice and help with the testing and manufacturing of the panels; Dr. Ladean McKittrick with the nuts and bolts of the FEA code and techniques; Jon Skramstad for his help with the RTM equipment; Will Ritter for making the majority of the panels; and Cullen Davidson, Ross Rosseland, and Charlie Evertz for help with the grunt labor. This project was funded by grants from DOE EPSCoR, under account #292051.

Lastly, and most importantly, I would like to thank my parents, Dr. John and Carolyn Sears, for their love and support. I would have never finished without them.

TABLE OF CONTENTS

TABLE OF CONTENTS - Continued

Page

TABLE OF CONTENTS - Continued

Page

LIST OF TABLES

LIST OF FIGURES

ABSTRACT

This thesis reports on a series of experimental and finite element modeling studies of sandwich panels typical of wind turbine blade construction. Buckling is a common failure mode in composite structures such as fiberglass wind turbine blades and sandwich construction is often employed in sensitive areas to increase buckling resistance with minimum weight and cost. The panels were flat or curved with fiberglass facesheets and balsa cores. The primary objective of the study was to investigate the accuracy of linear and nonlinear finite element buckling predictions for panels of this type.

Modeling procedures used for composite structures like blades often utilize linear eigenbuckling and geometrically nonlinear incremental buckling analyses. Often, the nonlinear model used the linear mode shape to perturb the model and to produce a buckling shape on the perfect geometry. The present study uses the random nodal displacement perturbation method for the nonlinear analysis which is entirely independent of the linear mode shape. The random perturbation method can be used for complicated structures and does not impose a mode shape on the model which may or may not be correct. Both methods, linear and nonlinear, were validated with buckling experiments on idealized blade substructures: curved and flat fiberglass/balsa sandwich shells. Five different series of panels were tested incorporating changes to four parameters: support conditions (simple-free-simple-free and four sided simply supported), radius of curvature (flat, shallow and deep), facesheet lay-up, and core thickness.

Good correlation between tests and shell element FE modeling was found for both the linear and nonlinear cases for the critical buckling loads for most models. Good correlation was also found for the early postbuckling response, with late postbuckling strains becoming invalid and deflections being rough approximations after some response shift (mode shift or mesh rippling). Certain combinations of numerical and/or structural parameters were found to present problems to some of the analysis techniques. The combination of curvature and free side edges caused problems for predicting the correct critical buckling mode for both the linear and nonlinear analyses. Deep curvatures and high mesh densities also caused problems predicting the correct mode shape for four sided simply supported panels. Complex boundary conditions tended to compound these problems. Proper modeling of the boundary conditions was found to be critical for accurate results, especially for the curved panels. In this study, this required modeling the load supports of the test fixture. Finally, closed form solutions found in the literature had poor correlation for both critical buckling loads and mode shapes.

The random nodal displacement perturbation method was found to have several general characteristics. First, it tended to give conservative results as compared to the linear models. A statistical study demonstrated relatively consistent results with a standard deviation of 3.7% (down to 2.2% for smooth responses). The random method also tended to exacerbate any problems encountered with all nonlinear models, such as snap-through critical buckling responses, mode shifts to non-symmetric shapes and mesh rippling behavior. Additionally, a model would occasionlly pass the critical buckling mode and continue loading until finally buckling into a higher mode shape. These last two problems were a function of the average size of the perturbations (slight for the mode shifts, significant for snap-through and higher buckling modes). Finally, large perturbations would sometimes violate curvature requirements for sandwich modeling due to high local curvatures caused by the random displacements.

It is recommended that both linear and nonlinear random perturbation method analyses be run for sandwich structures with curvature or complex boundary conditions. The more conservative result of the two is generally the more accurate. If the nonlinear model buckles in a higher mode shape at a significantly higher critical buckling load, another nonlinear run is necessary to confirm the mode shape.

Numerical parametric studies were also performed to establish FE modeling guidelines for buckling analyses. In addition to the conclusions above several other observations were made. The effect of using sandwich modeling is very significant even for relatively thin cores. The analyses are not particularly sensitive to the core properties, only the approximate range is required for good predictions. The effects of angled loads up to 10% higher on one side are not significant. The mixed element model (solid brick element core and shell facesheets) did not provide accurate predictions (twice the experimental and shell predicted loads).

Chapter 1

INTRODUCTION

While wind power offers great potential in the United States, it currently provides only small amounts of localized energy within the United States [Sesto and Ancona (1995)]. To cultivate wind energy as a widespread renewable, alternative energy source, its cost per kilowatt must be reduced. One factor directly affecting cost is blade weight. Lower weight blades will produce more efficient systems with lighter weight support structures, thereby reducing cost. Current blades are constructed of laminated wood or fiber reinforced plastic materials (referred to as FRPs or composites hereafter). Blades are constructed with a hollow airfoil shell structure [McKittrick et al. (1999)]. Blade structure and design are important elements in the affordability of wind power. The blades are subjected to complex fatigue load spectra, extreme wind loads, and possible impacts during their lifetime of use. Most composite blades tend to be designed conservatively and heavier than necessary, due to the complicated analyses and load-material response predictions required to obtain more accurate results. Among FRPs, fiberglass systems have become popular as blade materials due to their lower cost.

Composite FRPs consist of fibers with high strength and stiffness bonded into a thermoset or thermoplastic polymer matrix. The fibers are usually arranged into layers in an XY plane, creating a shell structure. Within the XY plane, the fibers can be random (continuous or discontinuous strands) or directional (unidirectional or multidirectional). Most FRP structures use unidirectional fiber layers, oriented to resist various loads, arranged to create an orthotropic or even anisotropic shell structure [Jones (1975)]. Since FRPs have high in-plane strength and stiffness, these shells are often thin. Large, thin, unsupported shell structures tend to buckle under compression loads well below their compressive strength due to geometric instability.

To combat the buckling problem, the skin thickness is increased. The extra thickness raises the moment of inertia (I_i), and hence, also the bending stiffness (D_{ij}). Two major methods are used to add bending stiffness without adding significant weight: skin stiffeners and sandwich construction. Skin stiffeners add another shell structure in the *XZ* plane, creating a 'T' or 'I' shaped structure. Sandwich construction utilizes a lightweight material, called the core material, surrounded by the stiffer, thinner shell material, termed face sheets. A composite facesheet sandwich construction diagram is shown in Figure 1-1. Typical core materials include balsa, honeycomb and foam. Most fiberglass wind turbine blades use both methods to increase the bending stiffness of the blade.

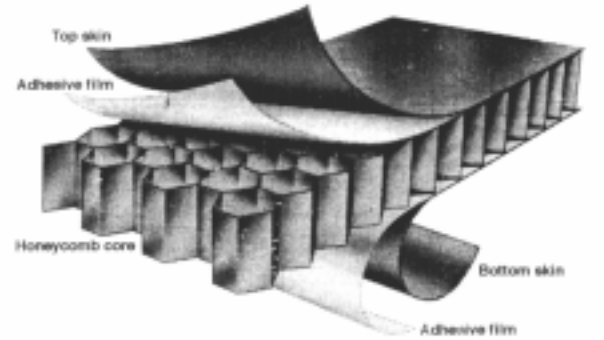

Figure 1-1. sandwich construction

The MSU Composites Group fiberglass AOC15/50 wind turbine blade design is shown in Figure 1-2. The span (skin stiffener) ties the windward and leeward shells together to increase the global bending stiffness of the blade. The sandwich construction on the trailing edge (which undergoes compression under wind loads), mitigates local shell buckling of the relatively flat airfoil surfaces under extreme wind loads.

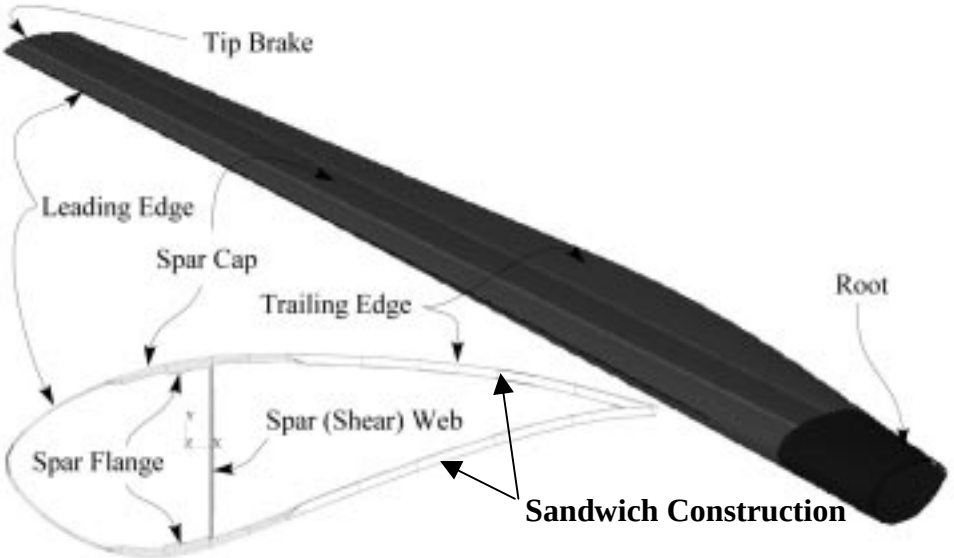

Figure 1-2. CAD drawing of the MSU fiberglass AOC15/50 wind turbine blade design with a cross section.

Both stiffening methods increase the complexity of an already difficult orthotropic shell analysis. Blade designs for the AOC15/50 are analyzed by finite element analysis (FEA) using the commercial code, Ansys [Ansys v5.5 (1999)]. FEA predicts the aforementioned local shell buckling to be a design driver for this style of blade design. To study the buckling phenomenon in the blade design, both linear eigenbuckling and non-linear analyses were performed by McKittrick (1999) on a model of the entire blade. To validate the Ansys prediction in this complex structure, simpler substructures such as I-beam/flange and sandwich panels were investigated as separate studies.

The present study focused on buckling of curved sandwich panels such as those found in the AOC15/50 blade design. Preliminary results with FEA for the overall blade deign showed buckling to occur at several locations along the trailing edge side consisting of sandwich construction. The critical eigenbuckling shape found in those preliminary results is shown Figure 1-3. The approach taken in this study was to test individual sections of sandwich panel, representative of the buckled region, with various face sheets layups, cores, curvature and edge supports. The experimental results were then used to validate the linear and nonlinear buckling predictions by Ansys.

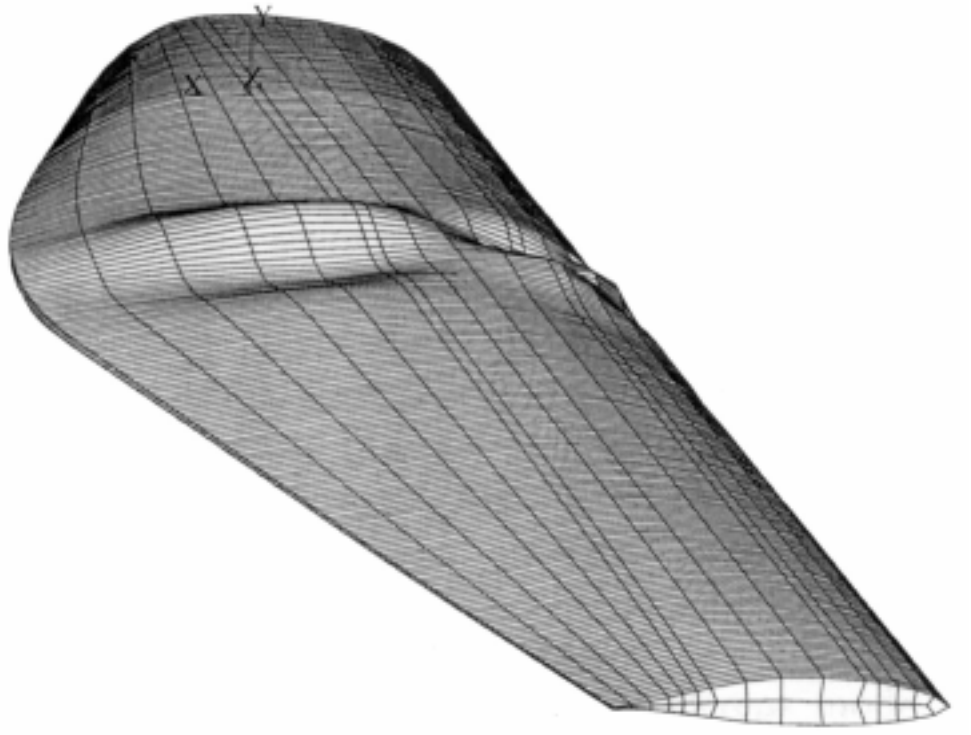

Figure 1-3. FEA eigenbuckling deformed shape of the MSU AOC15/50 blade design [McKittrick (1999)]

The goals of this study are twofold and listed below.

1. Validate the ability to predict critical buckling load and nonlinear response, including failure, of curved sandwich panels with finite element analysis. The numerical procedures used are directly applicable to complex, whole, structures and available in a commercially available package [Ansys].
2. Develop general design and analysis guidelines for sandwich construction. This is accomplished through panel and numerical parametric studies. The parameters studied include radius of curvature, core thickness, lay-up, support condition, mesh sensitivity, perturbation models, perturbation sensitivity and core material property sensitivity studies.

Chapter 2

BACKGROUND

MOTIVATION AND SCOPE

As noted earlier, the AOC15/50 fiberglass wind turbine blade was designed using finite element analysis. Vibration, bending stiffness and buckling analyses were all performed upon full blade models. Results from these analyses can be found in McKittrick et al. (1999). The structural design was iterated through these analyses to enhance the performance and mitigate potential problems before they occur in use. These models were the primary basis for the design, and as a consequence require a high level of confidence. To build that level of confidence, several smaller substructure studies were performed with these same numerical techniques and validated with experiments. Idealized substructures were chosen which could be tested experimentally, including I-beams and curved sandwich panels. I-beams represent the main spar section and are a complex, but controllable geometry. Curved sandwich panels represent the unsupported leeward structural section and are a simpler structural geometry with a more complicated material. This study focuses on the buckling analyses and techniques used by McKittrick et al. as applied to curved sandwich panels. Where possible, analytical solutions were also used to supplement the FEA solutions.

McKittrick et al. used the finite element package Ansys, versions 5.3 to 5.5, for all of their analyses. They used the layered quadratic shell element, shell91, for all of the elements. This element has sandwich modeling capabilities which were used for all areas with balsa cores. Both eigenbuckling and nonlinear incremental buckling analyses were performed. Many nonlinear buckling models impose eigenbuckling mode shapes as initial imperfections [Jeussette and Laschet (1990)]. Usually, the appropriate nodes are initially deflected a small amount conforming with the eigenbuckling shape. In such a large and complicated structure as a fiberglass wind turbine blade however, it is desirable to have methods which independently confirm, or

conflict, the eigenbuckling mode shape. Thus, McKittrick et al. used a random nodal out of plane deflection perturbation method for his nonlinear incremental buckling analyses.

The eigenbuckling analyses of McKittrick et al. predicted buckling within the sandwich construction, $(0/\pm45/0/b_{3/8})s$, on the leeward trailing edge of the blade (The nomenclature describing panel lay-ups in this paper is as follows: the facesheets are symmetric and represented by the numbers which describe the orientation of the fiber layers of one facesheet and end at the 'b'. The 'b' stands for a balsa core with the subscript denoting the full thickness). The mode shape is shown in Figure 2-1 along with a cut-away diagram depicting how a substructure was derived from that shape. If this shape is viewed as a wave, the nodal inflection points (those where no out of plane displacement occurs) can be used to truncate the shape. These nodal points can be viewed as boundary conditions of zero displacement, free rotation and zero moment, which correspond to the simply supported condition. If these supports are set into the three dimensional buckling shape, a roughly 64 x 64 cm square is formed. The enclosed section is a doubly curved shell, although the axial curve is very slight and considered negligible. The second curvature is significant with a radius of curvature of 178 cm (70 in.).

The section of the blade described above served as the base geometry for the present study. To obtain a wider field of confidence, several panel parameters were varied. Among the significant parameters are radius of curvature, core thickness, core material, face sheet lay-up, facesheet material, aspect ratio and support conditions. The following parameters were included in the study to determine first order effects for structural performance: radius of curvature, core thickness, lay-up, and support conditions. The facesheet and core materials were confined to fiberglass and balsa, respectively. Aspect ratio is a useful parameter to vary in order to study buckling modes and the transition between them and was initially included in the study. However, it was dropped primarily due to time constraints dealing specifically with machining new fixture parts. The aspect ratio was held constant at 1:1 throughout testing.

Support conditions were confined to four-sided, simply supported (SSSS) and simply supported loading with free edges (SFSF) for almost all tests. The two support conditions allowed for two distinct buckling characteristics to be studied for each panel and correlated with FEA prediction. Varying the layup also validates any design changes concerning facesheet changes. Changes in core thickness immediately change the bending stiffness, and therefore the buckling resistance of each layup. Changing the core thickness also affects how much transverse core shear influences the panels response, making this a good

parameter with which to study sandwich modeling techniques. Curvature also has a significant effect upon bending stiffness and buckling resistance. It also significantly complicates the mathematical solution and makes analytical solutions with cylindrical sandwich panels nearly impossible. This leaves finite element analyses as the only predictive tool. The methods and reasoning for the specific variations of each panel parameters are detailed in chapter 3, Experimental Methods.

The numerical parameters varied are either basic FEA modeling parameters specific to sandwich panels, or specific to tests performed. The purely numerical parameters studied are mesh density (sensitivity), perturbation method and perturbation sensitivity. Any good predictive FEA model must have values of the parameters listed above which are insensitive to changes. The numerical parameters specific to sandwich panels are core property sensitivity and sandwich modeling techniques. The last numerical parameter is only significant in this study, and is the effect of modeling the testing fixture used in the experiments. Methods, details and results of these studies can be found in chapter 4, Numerical Methods.

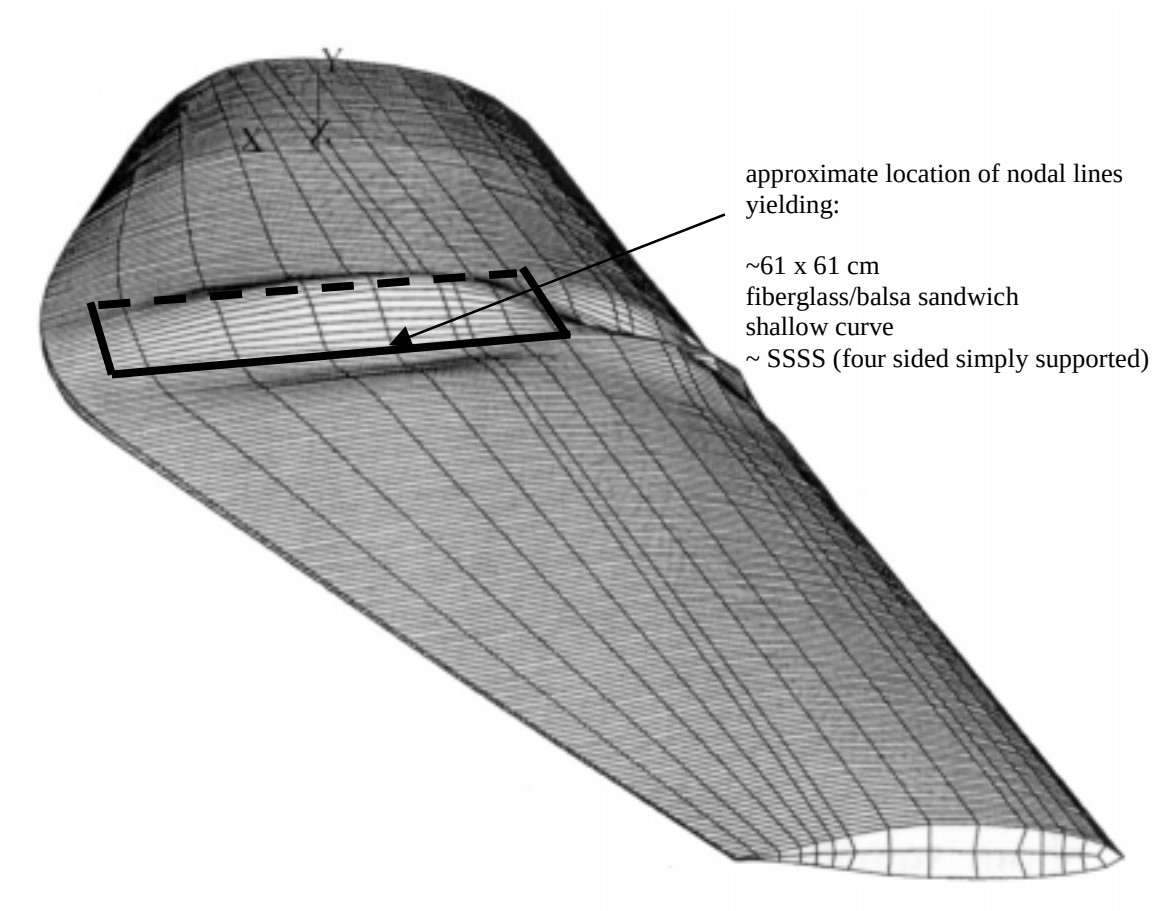

Figure 2-1. the idealized sandwich substructure derived from the blade FE mode shape

CONCEPTUAL OVERVIEW AND PREVIOUS WORK

Buckling

The buckling phenomenon has received extensive research and attention in engineering. Many different techniques have been used to study buckling in various structures, including experimental, linear stability, nonlinear, and finite element analysis. The structures susceptible to buckling can be categorized as one dimensional (columns), two dimensional (plates and cylindrical shells), or three dimensional (substructures and structures). Buckling can be caused by in-plane compression loads, shear loads or torsional loads. Most college introductory mechanics of materials courses cover the stability of columns. The textbook by Gere and Timoshenko (1984) gives a detailed examination of the basic, linear, mathematical modeling of buckling. Meanwhile, the textbook by Chia (1980) examines nonlinear plate and cylindrical shell buckling.

Stability. Pushing upon a straw is a simple demonstration of buckling. Even if the straw is pushed on perfectly straight, it will start to bend outwards at some load. The load where the straw begins to deform out of plane, or buckles, is termed the critical buckling load. Below this load, the straight shape is stable. If the straw is pushed sideways and then released, the straw will first bend outwards in a curved shape, but then return to the straight, original shape when unloaded. Above the critical buckling load, the bent or buckled shape is the stable one. If the axial load upon the straw is held constant and the straw pushed back into the straight shape, then released, it will return to the buckled shape. This demonstration shows how buckling can be viewed as a stability problem, with critical buckling load defining the point of instability. The buckling stability problem can be modeled with linear mathematics [Gere and Timoshenko (1984), Jones (1975), Plantema (1966)].

Buckling Responses. The straw example exemplifies one common definition of buckling as the phenomenon of small in-plane displacements/loads causing large out of plane displacements in a structure. This definition leads to some common engineering graphical representations of buckling called load history plots, in particular, the load versus maximum out of plane deflection plot (LOD). The three different phases of buckling can be graphically shown in these plots, as shown in Figure 2.2. The first phase, or region, is the linear region. Here, very little or no out of plane deflection occurs, so the structure performs as expected by linear elasticity. At some point, the structure will begin to deform out of plane significantly. This region is characterized by a quickly changing response including a ‘knee’. Different structures will have a more or less tightly defined

knee. The critical buckling load is found within this region of the plot and can be mathematically defined in several ways (described later p. 18, theoretical background). After the structure has buckled, it enters the postbuckling region where several different responses are possible. These general postbuckling responses are highly dependent upon the geometry and boundary conditions.

Figure 2.2 is a compilation of load deflection plots which show the four different postbuckling responses. The unsymmetric postbuckling response, 2.2b, is a highly unusual one which requires complex interacting geometries [Bushnell (1981)]. The path of this response is governed by the direction in which the structure buckles. The remaining three cases buckle with the same postbuckling behavior independently of the direction of buckling. The neutral postbuckling response, 2.2a, is common for simply supported plates with free edges. The stable postbuckling response is common for four sided simply supported plates, while the unstable postbuckling response is common for four sided simply supported thin cylindrical shells [Bushnell (1981)].

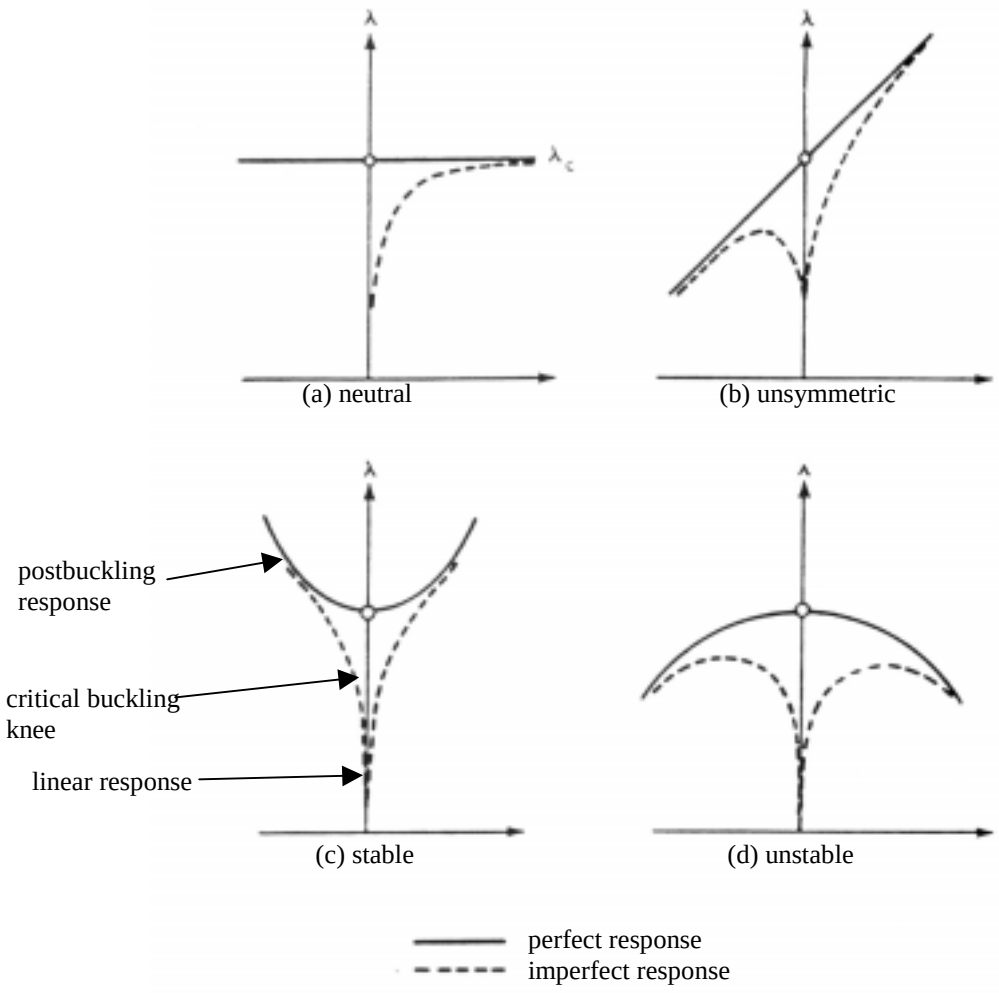

Figure 2-2. four postbuckling response types

Imperfect Responses. Another interesting buckling response characteristic is explored in Figure 2.2. Two different path types are possible for each structure or model, the perfect or imperfect response. A perfect structure would begin loading perfectly linearly, with no out of plane deflections. At the critical buckling load, the structure becomes mathematically unstable, immediately buckles and follows the postbuckling response. However, perfect structures are only encountered mathematically (although some are inherently asymmetric). Real structures contain slight, or even large imperfections which cause the structure to deform out of plane slightly, before the critical buckling load. The amount of deviation from the perfectly linear response is governed by the size and type of imperfection present. However, no matter the size of the imperfection, the response will eventually return asymptotically to the postbuckling response of the perfect structure. This occurs when the effects of global bending outfactor the effects of the local imperfections. These imperfections can be modeled mathematically, or their effects simulated, and therefore these 'real' responses can be modeled. These imperfections are simulated by perturbations upon the mathematical model. Since model geometries are usually perfect ones, they must be perturbed in some way to create the initial out of plane deflections in the linear range. Some common methods of perturbation are transverse force(s), edgewise moment(s), and geometric displacement(s) which can be either a defined shape (usually a buckling shape suggested by linear analysis) or randomly deformed. Jesuette and Laschette (1990) tie their stability and nonlinear models together: "First an initial bifurcation analysis is performed to introduce eventually a geometrical imperfection and to choose the first step load level from the estimated critical load."

Various Load History Plots. An example of one type of load history plot is given in Figure 2.2, the load versus out of plane deflection plot. With the definition of buckling given earlier, it is the most straightforward plot. Other load history plots can also be very useful to describe buckling responses. They are shown in Figure 2-3 b&c. Each part of Figure 2-3 is a different type of plot shown for the same FEA model. Fig. 2-3a is the load-out of plane deflection plot now familiar as a stable postbuckling response. Fig. 2-3b is a load-in-plane deflection (corresponding to the load) plot. Notice that as 2-3a begins to buckle out of plane, 2-3b has a knee which makes the structure more compliant. Figure 2-3c is a load-strain plot for the location of maximum out of plane displacement. This point is the point where the curvature due to bending is the greatest, and therefore the bending strains the highest. If the strains are recorded from the tension and compression sides at this XY location on the panel, they will be seen to diverge around the critical buckling load.

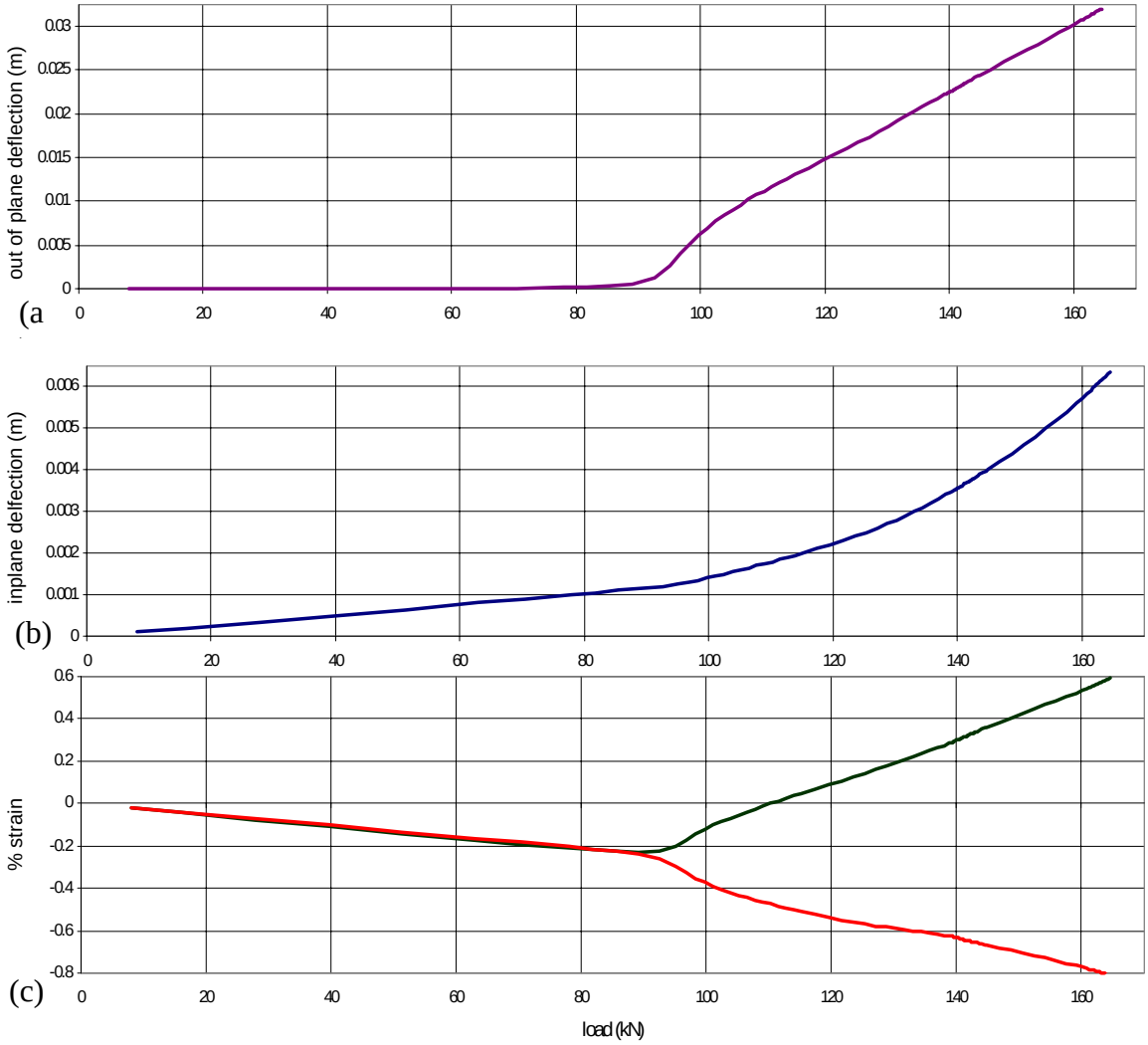

Figure 2-3. three load history plots for a stable response

Methods for Determination of Critical Buckling Load. Although far smoother, the data taken from the FE model, Figure 2-3, resembles the data available from a test of a real structure. While a critical buckling region can be roughly surmised from these plots, no critical buckling load can be precisely determined from just viewing the plot. A mathematical method is needed with which a critical buckling load can be determined from a full structural buckling response. Many methods are possible, and most focus on different points near the knee of the curve. Some popular methods are listed next:

- *maximum curvature*
  the point of maximum curvature of load versus in or out of plane deflection plots

- *inflection point*
  the inflection point of the LOD plot, or the first point where the postbuckling becomes a substantially straight line [Plantema (1966)]

- *strain reversal*
  the load where the convex side (tension) strain is a maximum (slope is zero). [Plantema (1966)]

- *normalized deflection*
  load where a specific out of plane deflection is reached, normalized to the structures thickness and overall dimensions

- *Southwell plots*
  bilinear postbuckling intersection point [Parida et al. (1997)]

Notice, in Figure 2-4, that for a neutral postbuckling response the point of inflection method predicts critical buckling at the asymptotic line, while the strain reversal method predicts it at a lower load. Plantema (1966) remarks upon the differences of these methods, "although in general the results obtained from different methods agree reasonably well, it will be clear that the definitions of the experimental buckling load are not free of some arbitrariness." The choice of method is therefore left to the user, with the ease of use, data availability and quality the main factors determining the best method.

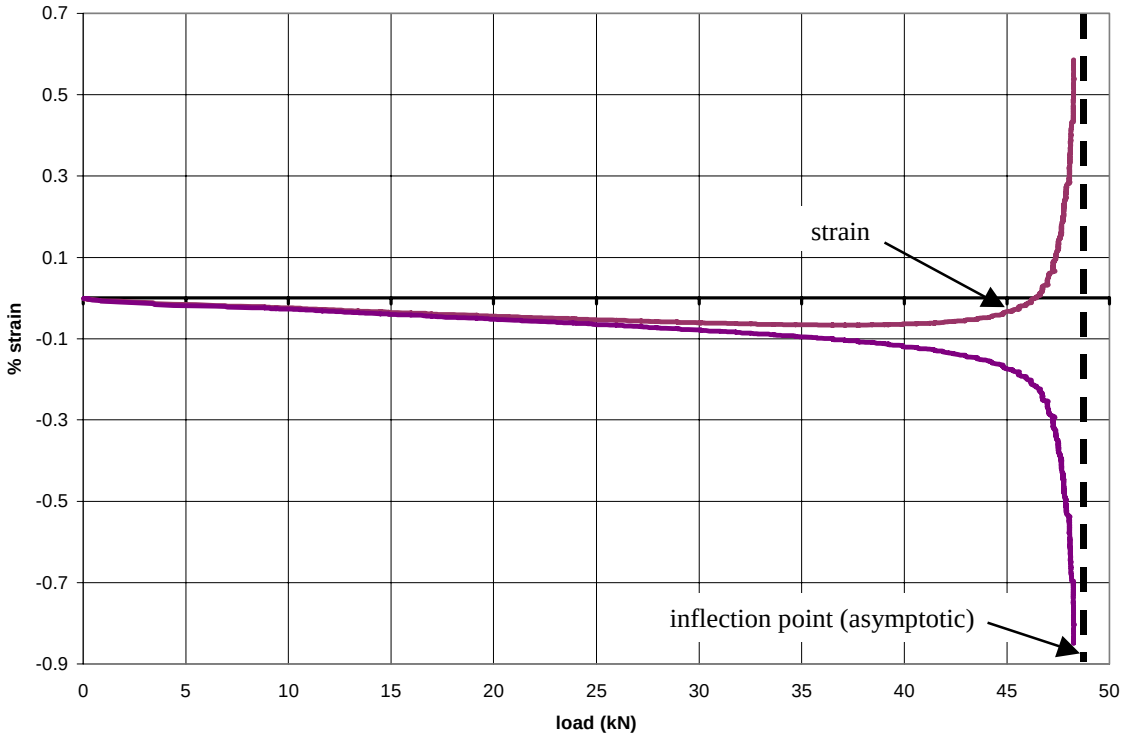

Figure 2-4. example of the difference between critical buckling determination methods

Testing. The best method of defining buckling may change from test to test depending on the special parameters and data acquisition involved in each individual test. Buckling tests are notoriously difficult to perform, especially those involving in-plane displacements upon plates or shells. Parida et al. states this (1997), "experimental simulation of boundary conditions while carrying out a panel buckling test has been known to be difficult." He obtained good results for the simply supported case for relatively thick (6mm) flat carbon fiber laminates with roughly the same buckling loads as experienced in the present study. This study provides a good insight into the level of research in buckling: the study of buckling of composite materials under hot and wet conditions, with extensive experimental work covering early postbuckling and FEM stability analysis. Plantema (1966) also remarks upon the problem of support conditions with special attention to sandwich construction, "the realization of either simply supported or clamped loaded edges is a difficult problem… In addition, buckling tests on sandwich panels often present problems peculiar to this type of construction."

Sandwich Construction

"The concept of sandwich construction has been traced back to the middle of the last century, although the principles of sandwich construction may have been applied much earlier" write Noor, Burton and Scott (1996). The principle of sandwich construction is to provide bending stiffness to shells, while keeping them light, by the addition of a thick but lightweight material. This material may be directly placed upon a surface of the shell creating an open face sandwich construction. More commonly, the lightweight material is inserted between two thin shells and is termed ordinary sandwich construction. The lightweight material is now called the core. It is this type of construction which gives the name, sandwich, to the principle. Typical core materials are either low density solids (foams, balsa wood, thermosetting resins containing lightweight fillers) or high density materials in cellular form (aluminum and composite, honeycomb or web). The thin shells on either face are high strength and stiffness materials termed the facesheets. Typical modern facesheets include engineering metals (steel alloys, aluminum,…) and fiber reinforced plastic composite materials (carbon/epoxy laminates, fiberglass/polyester laminates,…). The facesheets provide the load carrying capacity while the core transfers the load between the facesheets primarily through shear [Noor, Burton, Bert (1996)]. One other type of sandwich construction is multiple

sandwich construction which has multiple cores and a corresponding number of facesheets. The three types of sandwich construction, as well as various core materials, are shown in Figure 2-5.

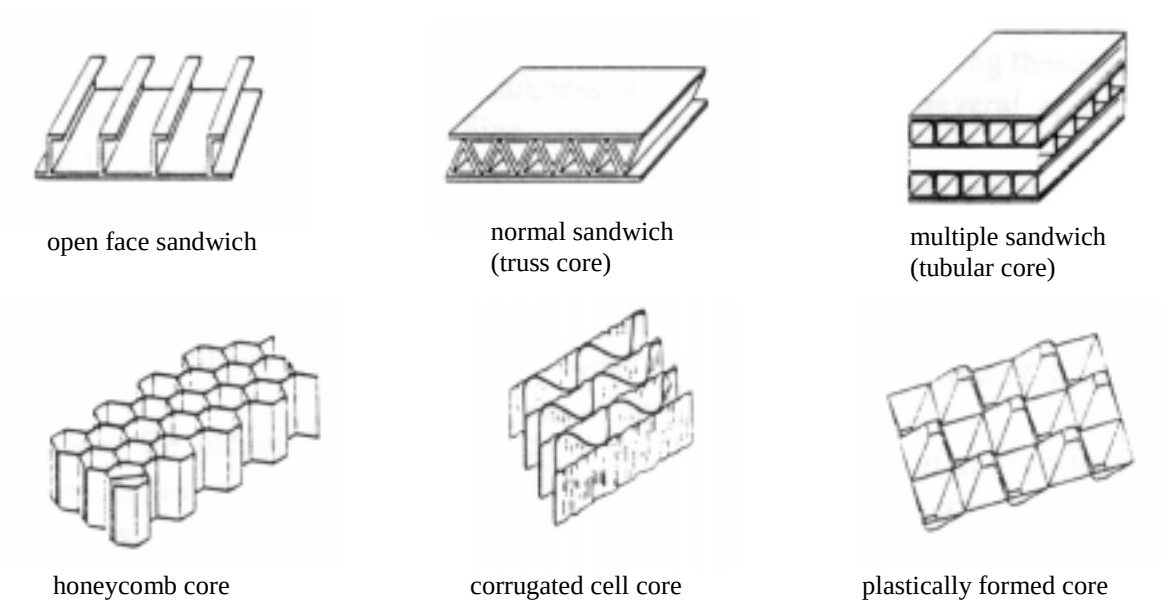

Figure 2-5. three types of sandwich construction and various core materials

Failure Modes Due to the multi-material nature of sandwich construction, several new mechanical failure and buckling modes are possible in addition to normal shell failure. The buckling modes possible are face sheet wrinkling, core shear buckling and global panel buckling, of which the former two are also catastrophic failures. Critical buckling is not necessarily a failure mode, but is often treated as one by designers because of its possible unstable behavior. Once buckled, the panel may fail by geometric collapse, transverse core shear or face sheet overstressing. Face sheet overstressing may also occur prior to buckling in the linear range. These modes are most easily understood with idealized diagrams, as shown in figure 2-6. Equations for the three buckling modes can be found in the theoretical background section and the following references for full derivations: Platema (1966), Vinson (1987), MIL-HDBK-23A (1968). Face sheet overstressing is simply an in-plane shell type failure and is predictable by thin shell failure theories such as maximum stress, maximum strain of Tsai-Wu failure criterion [Jones] for composite materials.

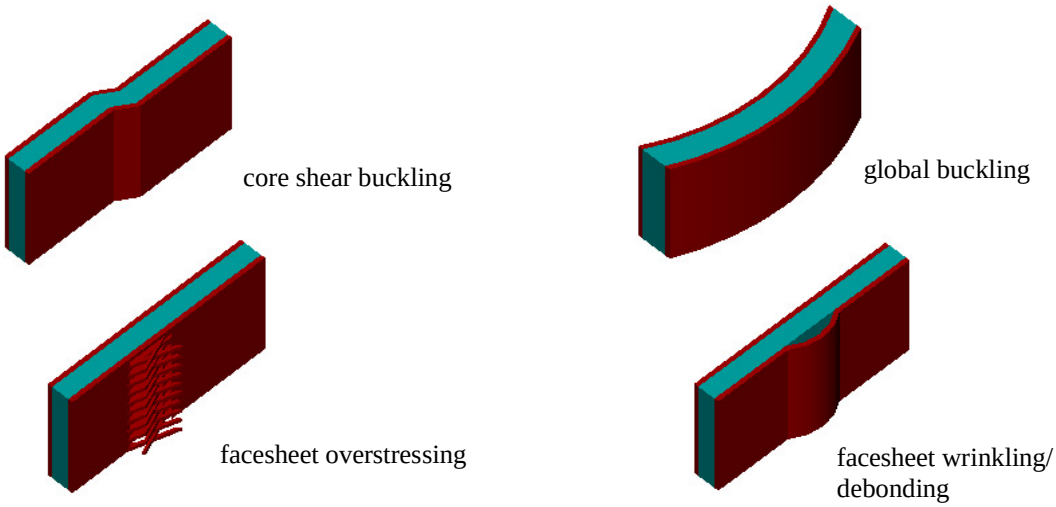

Figure 2-6. four failure modes of sandwich shells

Sandwich Modeling The multi-material nature of sandwich construction also requires separate modeling techniques be used rather than a classical thin shell theory, such as classical lamination theory. These theories disregard transverse shear effects which can become significant in thick shells; sandwich panels would generally fall in the thick shell category [Jones (1975)]. Two distinct approaches can be taken to model sandwich panels and their transverse shear effects: three dimensional models and two dimensional shell theory based models. The most common three dimension models are the continuum models which are generally analyzed with finite elements [Hanagud, Chen et al (1985), Chamis, Aiello et al (1988) and Juessette and Laschet (19990)] although Burton and Noor (1994) presented an analytical solution. Detailed finite element models where the honeycomb core geometry is represented have also been researched [Chamis, Aiello et al (1988), Elspass and Flemming (1990)].

More often, two dimensional shell theory based models are used to predict sandwich construction behavior. Noor, Burton, Bert (1996) divided the two dimensional models into three distinct categories: global approximation models, discrete layer models and predictor-corrector approaches. They describe and qualify the global approximations models as excerpted here;

> In the global approximation models the sandwich is replaced by an equivalent single-layer anisotropic plate of shell, and global through-the-thickness approximations for the displacements, strains and/or stresses are introduced…. Examples of these theories are the first-order shear deformation theories… and higher-order theories based on a nonlinear distribution of the displacements and/or strains in the thickness direction. …The range of validity of the first-order shear deformation theory is strongly dependent on the factors used in adjusting these stiffnesses (transverse shear).

The predictor-corrector approach is an iterative one, where information from a previous solution is used to correct certain parameters for the next solution. Noor and Burton (1994) are the only authors to have used this approach. They used first order shear deformation theory in the predictor phase and then corrected either transverse shear stiffnesses or the thickness distribution of displacements and/or transverse stresses [Noor, Burton and Bert (1996)].

The most often used models are the discrete layer models. These models divide each facesheet and core into one or more distinct layers with piecewise approximations made for through thickness response quantities. Most are linear models based on Grigolyuk three-layered sandwich shell theory, which has piecewise linear in-plane displacements and constant transverse through thickness displacements [Noor et al. (1996)]. Plantema (1996) is the author used most often in this study, although other models are Allen (1969) Monforton and Ibrahim (1975), Kanematsu, Hirano et al (1988) and Mukhopadhyay and Sierakowski (1990a, 1990b). Noor et al. (1996) also report discrete layer models with higher-order displacement approximations. The assumptions which lead to a linear three-layer model for a composite sandwich model are described next.

Three-Layer Theory. The nature of ordinary sandwich construction allows several key assumptions to be made. First, the core has a very low elastic modulus in the in-plane directions as compared to the face sheets (on the order of 1:100 for many typical constructions). Therefore its effects on the overall stiffness of the panel can be neglected, and the facesheets carry the all membrane loads. Since the core carries minimal loads, its stresses can be neglected. From this assumption, equilibrium demands that the shear stresses and hence shear strains be constant throughout the thickness of the core. The last assumption is specific to composite sandwich panels. Due to the relative thinness of the facesheets as compared to the thick core, the difference in distance from the panel center to different layers is negligible as compared to the average distance. This allows for the composite face sheet to be viewed as a single layer orthotropic sheet with smeared properties. In all other respects the facesheets are subject to the usual assumptions and resulting theories of thin shells (normal engineering theory of bending). These assumptions result in a modeling theory for sandwich construction called three-layer sandwich theory.

Genearal Sandwich Construction Research. Extensive research has been performed on sandwich construction. Textbooks such as Platema's *Sandwich Construction* are entirely dedicated to the subject. This text covers sandwich modeling, basic equations, bending and buckling of sandwich columns, plates

and some cylinders. Over 1300 references are cited in Noor, Burton and Bert's 1996 review of sandwich construction research, *Computational models for sandwich panels and shells.* Topics of research include thermo-mechanical effects, vibrations, viscoelasticity, global stability, local buckling, postbuckling, damage, geometric effects, impact and optimization to among others.

Postbuckling of Cylindrical Sandwich Shells. As of 1996, out of 1300 references, Noor et al. report only seven papers investigating nonlinear and static postbuckling. All seven used three-layer models, although Jeusette and Laschet (1990) also employed first order shear deformation and three dimensional models. The seven studies are: Akkas and Bauld (1971), Bauld (1974), Jeussette and Laschet (1990), Schmidt (1969); Sun (1992), Troshin (1986), and Wang and Kuo (1979). No experimental studies on the nonlinear and static postbuckling responses of sandwich cylindrical panels or cylinders are reported by Noor et al. By contrast, 27 studies were performed using three-layer theory to predict bifurcation buckling, and 8 experimental studies are reported. Plates and Beams get substantially more attention with 32 nonlinear and static postbuckling studies using three-layer theory and 5 experimental studies.

Noor et al. also state, "Most of the reported studies on nonlinear analyses of sandwich plates and shells used the finite element method." Very few or no analytical solutions to postbuckling of sandwich plates exist due to the complicated material and resulting equations. With the addition of a slightly more complicated geometry such as a cylindrical panel, the equations become too difficult to work. Even FEA can have difficulties with thin homogeneous cylindrical shells as commented by Bushnell (1981):

> "It is worth emphasizing that the problem of the axially compressed cylinder, which appears superficially to be an excellent, simple test case for a person learning to use a computer program that he has acquired elsewhere, is really quite demanding… the reader is urged to study that material before dismissing a computer program because it 'can't even predict the classical buckling load for an axially compressed monocoque cylindrical shell.'"

Jeussette and Laschet's paper (1990) is a fairly comprehensive study of nonlinear FEA analysis of cylindrical sandwich shells. They use three different models for sandwich construction with FEA: 1). third order shear deformation model 2). three-layer model 3). three dimensional model with shell element facesheets and a volume element core. The models were validated and evaluated by comparison with experimental and 2D analytical results. A three point bending test was chosen with a thick to insure a large portion of shear deformation in the final deflection plate (f/c = 0.075, L/h = 16; f = facesheet thickness, c = core thickness, L = length, h = total thickness). The first model gave poor results (best deflection correlation- 75%), the second good (best- 98%) and the third excellent results (100%).

They then used the multilayer shell element to model buckling and postbuckling of a highly curved cylindrical thin shell composite and compared it to an experiment. In the nonlinear analysis, the eigenbuckling shape is imposed upon the model geometry as the perturbation. Lastly, a typical aircraft curved sandwich panel is modeled. The three dimensional model was the only model used. No perturbation was necessary due to the eccentricity of the loaded flange edges (in effect a moment perturbation). No experimental results are cited for this panel. FEA predicted three different mode shapes with a prebuckled linear shape, followed by the first critical mode which eventually snaps through to the second mode. The first critical buckling mode contains five waveforms in the axial direction and one in the theta direction forming a ripple like pattern. This mode shape is an unusual one which is counterintuitive (a mode shape closer to the aspect ratio is usually expected). No experimental results are cited to confirm this unexpected buckling mode. The second mode is an end localized buckling shape which first coincides with a drop in load (127.8 kN to 115.29 kN) then begins a stable postbuckling path.

THEORETICAL BACKGROUND

Mathematics of Buckling: Linear Stability

Flat Four Sided Simply Supported Plates

A brief review of the derivation of the buckling solution for a thin composite plate will be presented as a base to compare the analytical procedure and the solution with the sandwich, cylindrical and nonlinear analyses.

According to linear mathematics [Jones (1975), Gere and Timoshenko (1984)], a structure above its critical buckling load can satisfy equilibrium in either its buckled or original shapes. However, the original shape is an unstable one. When viewed in terms of energy, the buckled shapes occupy lower energy levels than the 'straight' shape.. A useful analogy is the ball on a hill description. The ball will be at rest, equilibrium, on any flat surface. Three surfaces can be flat; the top of a hill, a flat plain, and the bottom of a hill. Above the critical buckling load, the straight shape is an unstable one and occupies a position at the top of the hill. Any slight push either direction (perturbation) will cause the ball to roll down the hill until it finds the bottom of the hill where it will settle. Any perturbation at the bottom position will only cause the ball roll back to its stable position. So, the critical buckling load can be found by finding the stable point in the equilibrium equations, which are the minimum energy levels.

For orthotropic flat plates, we start with the bending equilibrium equations (transverse loading is absent, so the q(x,y) term is zero; and, the transverse and shear loads are removed since they also equal zero [Jones (1975)]) are;

$$M_x, xx + 2M_{xy}, xy + M_y, yy + N_x \cdot w, xx + 2N_{xy} \cdot w, xy + N_y \cdot w, yy \tag{1}$$

The potential energy of such a loaded plate then becomes:

$$\Pi p = \tfrac{1}{2}\iint (\{\delta w''\}^T [D]\{\delta w''\} + \{\delta w'\}^T [N]\{\delta w'\}) dxdy \tag{2}$$

which for specially orthotropic laminates becomes:

$$\Pi p = \tfrac{1}{2}\iint (D_{11}\delta w, xxxx + 2(D_{12} + 2D_{66})\delta w, xxyy + N_x \delta w, xx) dxdy \tag{3}$$

Four sided simply supported plates are studied here, so an appropriate general displacement function must be chosen to satisfy the boundary conditions. The boundary conditions are, zero displacement and moment along the four edges. A double fourier series displacement function satisfies these conditions;

$$w(x,y) = \sum\sum A_{mn} \sin(\frac{m\pi x}{a}) \sin(\frac{n\pi y}{b}). \tag{4}$$

Variational calculus states that for a stable system, any small perturbation will not affect gross changes in the system. Hence, the displacement function is perturbed slightly, δA_{mn}. Instability occurs when the second variation (similar to a derivative) of the potential energy of the system with respect to the perturbed function (A_{mn}) is zero (the slope on either side is opposite, forcing the function back down to the stable point). Equation (3) is first differentiated twice with respect to A_{mn}, which disappears and makes the new function independent of the size of the perturbation (A_{mn}) i.e. the linear eigenvalue problem for buckling. This equation is then set to zero and integrated twice with respect to x and y. Since a fourier sine series is an orthogonal set of functions, for the entire equation to equal zero each term must separately be equal to zero (by the definition of orthogonal series). This allows the equation to become uncoupled and solved separately for each m and n. Each term equals zero when;

$$N_x = \frac{\pi^2}{m^2 a^2}[D_{11}m^4 + 2(D_{12} + 2D_{66})m^2 n^2 (\frac{a}{b})^2 + D_{22}n^4 (\frac{a}{b})^4] \tag{5}$$

Therefore an infinite matrix of stability loads, $N_x(m,n)$, is available with a value for each mode shape with 'm' half sine waves in the x-direction and 'n' in the y-direction. The lowest value is the critical buckling load, which changes for each panel with respect to its orthotropic properties and aspect ratio a/b.

Orthotropic Cylindrical Shell Buckling

Following similar procedures in the cylindrical coordinate system, a buckling solution can be found for a composite shell. The solution found by Whitney (1987) with the transverse pressure term eliminated, is presented here to compare with the plate solution;

$$N_0 = \frac{F_{mn}}{m^2 (H_{11mn} H_{22mn} - H_{12mn}^2)} \tag{6}$$

where;

$$F_{mn} = H_{11mn} H_{22mn} H_{33mn} + 2H_{12mn} H_{13mn} H_{23mn} - H_{22mn} H_{13mn}^2 - H_{33mn} H_{12mn}^2 - H_{11mn} H_{23mn}^2 \tag{a}$$

and

$$
\begin{aligned}
H_{11mn} &= A_{11}m^2 + A_{66}n^2R^2 \\
H_{12mn} &= (A_{12} + A_{66})mnR \\
H_{13mn} &= -\frac{m\pi}{a}[A_{12}\frac{a^2}{\pi^2 R} + B_{11}m^2 + (B_{12} + 2B_{66})n^2R^2] \\
H_{22mn} &= A_{66}m^2 + A_{22}n^2R^2 \\
H_{23mn} &= -\frac{nR\pi}{a}[A_{22}\frac{a^2}{\pi^2 R} + (B_{12} + 2B_{66})m^2 + B_{22}n^2R^2] \\
H_{33mn} &= \frac{\pi^2}{a^2}[D_{11}m^4 + 2(D_{12} + 2D_{66})m^2n^2R^2 + D_{22}n^4R^4]
\end{aligned}
\qquad \text{(b-g)}
$$

This solution is the general cylindrical solution, to compare it with the specially orthotropic solution found as equation (5) for the flat plates, the B_{ij} terms of equation (6, b-g) are all set to zero. This reduces the complexity of the equation significantly, however, this solution remains much more complex than the flat plate solution. Notice that the H_{33mn} term closely resembles the entire flat plate solution with the addition of the radius, R, in some terms and a factor of m^2 throughout. The H_{33mn} term is found within the F_{mn} term and always multiplied by another H_{ijmn} factor. This second factor contains the in-plane stiffness terms A_{ij} which were not found in the flat plate solution. In summary the cylindrical plate solution is significantly more complicated, a coupled function of the in-plane and bending stiffness terms, and a function of the radius of curvature, as well as the aspect ratio and sine wave mode shapes (m,n).

Mathematics of Sandwich Panels

Many engineers are not conversant with the intracacies of sandwich construction. The most common approach, three layer theory, will be explored and contrasted with basic shell theory. For more detailed investigations the reader is pointed towards Platema (1966), Whitney (1987), MIL-HDBK-23A (1968), and Vinson (1985). If a specific topic is sought, the reference paper by Noor, Burton and Bert (1996) is recommended.

Global Buckling

The mathematics of plate buckling for thin shell theory (including isotropic, orthotropic and classical lamination theory, CLT) was simplified by a major assumption: due to the thinness of the plate, transverse shear strains were considered negligible. Unfortunately, this assumption will not suffice for sandwich construction because by nature they possess soft and thick cores which combine to become

significant factors affecting the bending response. The major assumptions on which three layer theory is based are born from its bi-material nature and listed again;

- the core has a very low elastic modulus with respect to the face sheets
  - the core does not affect the overall in-plane stiffness
  - facesheets carry all of the membrane loads
  - the core carries no in-plane stresses
  - the equilibrium equations demand that the shear stresses and strains be constant throughout the thickness of the core because the in-plane stresses are constant (zero)
- the in-plane core displacements u_c and v_c are assumed to be linear finctions of the z coordinate.
- the core and face sheets have constant thickness
- the face sheets are very thin compared to the core
  - the distance from the center of the core to the outside ply is very close to the distance to the inside ply. Therefore, the average distance can be used for all plies and their stiffness properties smeared to create a single, orthotropic layer facesheet.
- the in-plane displacements u and v are uniform through the thickness of the facesheets
- the plate in-plane strains are small compared to unity (linear strain behavior)

For simplicity, isotropic face sheets and core are considered in the mathematical procedure portion to clarify the effects of the shear terms. The first difference between the thin and sandwich shell theories occurs in the plate deflections function which must now include the effects of shear deformation. This is accomplished by the use of partial deflections

$$w = w_b + w_s \tag{7}$$

where w_b and w_s are the transverse deflections resulting from bending and shear respectively. The shear deflection may be related to the bending deflection by the equation

$$w_s = \frac{-D}{S}\Delta w_b \tag{8}$$

where D is the bending stiffness and S the transverse shear stiffness per unit length (similar to the A,B & D terms of classical lamination theory).

The general equilibrium equation for buckling, and the boundary conditions remain the same as for the orthotropic thin shell. However, the addition of the shear term yields a solution of

$$Nx_{m,n} = \left(\frac{a^2}{m^2\pi^2}\right)\left(\frac{D(\frac{m^2\pi^2}{a^2}+\frac{n^2\pi^2}{b^2})}{1+\frac{D}{S}(\frac{m^2\pi^2}{a^2}+\frac{n^2\pi^2}{b^2})}\right) \tag{9}$$

where $Nx_{m,n}$ are the stability loads, a is the length of the panel, b the width and m and n the number of half sine waves in the length and width directions respectively.

In this case (fully isotropic) the ratio of the bending to shear stiffness determines the difference between three layer sandwich modeling and thin shell theory (the thickness of the core is included into the shear stiffness term S). For an infinitely shear stiff panel (either $S\rightarrow\infty$ or the panel becomes a thin shell as $h_c \rightarrow 0$) the solution reduces to that of a thin shell. When orthotropic (composite) sandwich panels are studied, the complexity increases greatly. The critical buckling equations which Vinson [1987] used were derived with the Rayleigh-Ritz energy method and are presented here;

$$C_1(n) := \frac{a^2}{n^2 \cdot b^2} \qquad C_4(n) := \frac{a^2}{n^2 \cdot b^2} \qquad C_2 := 1 \qquad C_3(n) := \frac{n^2 \cdot b^2}{a^2}$$

$$D_x := \frac{E_{fx} \cdot h_c^{\,2} \cdot t_f}{2 \cdot \left(1 - \nu_{xy} \cdot \nu_{yx}\right)} \qquad D_y := \frac{E_{fy} \cdot h_c^{\,2} \cdot t_f}{2 \cdot \left(1 - \nu_{xy} \cdot \nu_{yx}\right)} \qquad D_{xy} := \frac{G_{xy} \cdot h_c^{\,2} \cdot t_f}{2 \cdot \left(1 - \nu_{xy} \cdot \nu_{yx}\right)}$$

$$B_1 := \sqrt{\frac{D_y}{D_x}} \qquad B_2 := \frac{D_y \cdot \nu_{xy}}{\sqrt{D_x \cdot D_y}} \qquad B_3 := \frac{D_{xy}}{\sqrt{D_x \cdot D_y}}$$

$$A(n) := C_1(n) \cdot C_3(n) - B_2 \cdot C_2^{\,2} + B_3 \cdot C_2 \cdot \left(B_1 \cdot C_1(n) + 2 \cdot B_2 \cdot C_2 + \frac{C_3(n)}{B_1}\right) \tag{11}$$

$$V_x := \frac{\pi^2 \cdot \sqrt{D_x \cdot D_y}}{b^2 \cdot G_c \cdot h_c} \qquad V_y := \frac{\pi^2 \cdot \sqrt{D_x \cdot D_y}}{b^2 \cdot G_c \cdot h_c}$$

$$K(n) := \frac{B_1 \cdot C_1(n) + 2 \cdot B_2 \cdot C_2 + A(n) \cdot \left(\frac{V_y}{C_4(n)} + V_x\right)}{1 + \left(B_1 \cdot C_1(n) + B_3 \cdot C_2\right) \cdot \frac{V_y}{C_4(n)} + \left(\frac{C_3(n)}{B_1} + B_3 \cdot C_2\right) \cdot V_x + V_y \cdot V_x \cdot \frac{A(n)}{C_4(n)}}$$

$$\sigma_{cr}(n) := \frac{\pi^2}{4 \cdot \left(1 - \nu_{xy} \cdot \nu_{yx}\right)} \cdot \left(\sqrt{E_{fx} \cdot E_{fy}}\right) \cdot \frac{h_c^{\,2}}{b^2} \cdot K(n)$$

where E_{fx} and E_{fy} are the elastic moduli of the facesheets in the x and y directions, n the number of half sine waves in the x (loading) direction, ν_{xy} and ν_{yx} are the facesheet Poisson's ratios, and σ_{cr} the n^{th} stability loads

The $C_i(n)$ terms are support condition factors (the SSSS factors are shown here). They are highly dependent on the aspect ratio and the number of sine waves, n, axially. This equation is for m = 1 transverse waves since it is assumed to yield the lowest values. The D_i terms are the bending stiffness terms very similar to D (isotropic, thin shell) and D_{ij} of CLT. Notice that they are a function of the face sheet stiffness ($E_i t_f$) and the face sheet Poisson's ratios. However, the height of the core is an even more influential factor since it is a squared term. The B_i and A(n) terms are just place keeping equations, which also demonstrate the complex interactions occurring between the support conditions and orthotropic bending stiffnesses. The V_x and V_y terms calculate the effect that shear stiffness ($G_c h_c$) will have on the solution. Notice, that as with the isotropic case, it is the ratio between D (of the united face sheets) and the shear stiffness ($G_c h_c$, ~ to S) of the core which determines the effect of three layer theory as compared to thin plate theory.

The final effects of the terms, shown in the coefficient K(n) and the final solution equation (11), can only be described as complex. It follows that a closed form solution has not been found for a cylindrical sandwich shell. The added complexities of a curved panel, to the already complex three-layer model, makes a closed form solution cumbersome enough that FEA becomes a more viable option.

Core Shear Buckling and Facesheet Wrinkling Failures

Core shear buckling and facesheet wrinkling were found to be an improbable failure mode in the linear response for the present study. The two equations used to predict these failures, for solid cores in the linear range were taken from Vinson (1987) and are shown below for completeness.

core shear buckling

$$\sigma_{cs} = \frac{G_c h_c}{2t} \tag{12}$$

face sheet wrinkling

$$\sigma_{fw} = \sqrt{\frac{2t_f E_c \sqrt{E_{fx} E_{fy}}}{3h_c\left(1-\upsilon_{xy}\upsilon_{yx}\right)}} \tag{13}$$

Mathematics of Nonlinear Plate Theory

In linear plate buckling analysis, the only results available are the stability loads and corresponding mode shapes. This occured because the out of plane delfections, A_{mn}, were independent of the loads, N_i. To study the postbuckling response, the out of plane (and in-plane) deflections must be known in relation to the loads. To accomplish this, nonlinear analyses must be used. Nonlinear strain theory is substituted into the plate bending equilibrium equation (1) which introduces additional and coupled terms into the potential energy equation (2) (or similar solution method).

In linear strain theory, the higher order terms are considered small compared to the linear term because the deformations are small compared to the original shape. This allows those terms to be neglected without introducing appreciable error. However, when deflections become finite compared to the original shape, the higher order terms become important. The Lagrangian description for finite deformations of an elastic body yield a second order nonlinear strain-displacement relation of the form

$$\varepsilon_x = e_x + \tfrac{1}{2}\left[e_x^2 + \left(\tfrac{1}{2} e_{yx} + \omega_z\right)^2 + \left(\tfrac{1}{2} e_{zx} + \omega_y\right)^2 \right] \tag{14}$$

where

$$e_x = u_{,x} \qquad e_{yx} = u_{,y} + v_{,x} \qquad e_{zx} = u_{,z} + w_{,x}$$

$$\omega z = \tfrac{1}{2}\left(v_{,z} - y_{,y}\right) \qquad \omega_y = \tfrac{1}{2}\left(u_{,z} - w_{,x}\right)$$

In plate postbuckling and/or bending analyses (with small in-plane strains), linear strains and the squares of the angles of rotation are small compared to unity, which simplifies equation (14) to

$$\varepsilon_x = e_x + \tfrac{1}{2}\left(\omega_z^2 + \omega_y^2\right) \tag{15}$$

Lastly since a plate is massive body in its plane, the rotation about the axis normal to the plate (w_z) is very small, and can be neglected. This assumption leads to the set of nonlinear strains which are used in nonlinear plate theory

$$\varepsilon_x = e_x + \tfrac{1}{2}\omega_y^2 \qquad \varepsilon_y = e_y + \tfrac{1}{2}\omega_x^2 \qquad \varepsilon_z = e_z + \tfrac{1}{2}\left(\omega_x^2 + \omega_y^2\right)$$

$$\varepsilon_{yz} = e_{yz} \qquad \varepsilon_{zx} = e_{zx} \qquad \varepsilon_{xy} = e_{xy} + \omega_x \omega_y \tag{16}$$

When this equation set is used in the equilibrium equation (1), the resulting nonlinear governing equation becomes

$$D\nabla^4 w = \frac{Eh}{1-\nu^2}\left[\left(u^0_{,x} + \tfrac{1}{2}w^2_{,x}\right)\left(w_{,xx} + \nu w_{,yy}\right) + \left(v^0_{,y} + \tfrac{1}{2}w^2_{,y}\right)\left(w_{,yy} + \nu w_{,xx}\right) + (1-\nu)w_{,xy}\left(u^0_{,y} + v^0_{,x} + w_{,x}w_{,y}\right)\right] \quad (17)$$

for isotropic plates. Notice that the loads N_i, have been replaced with in-plane displacements loads, u^0 and v^0. The resultant loads are defined as functions, with N_x being

$$N_x = \frac{Eh}{1-\nu^2}\left[u^0_{,x} + \nu u^0_{,y} + \tfrac{1}{2}\left(w^2_{,x} + \nu w^2_{,y}\right)\right] \quad (18)$$

Notice that w terms are now present which are above the second order, and therefore, A_{mn} is as well. During minimization of A_{mn} to the second derivative, the A_{mn} terms will not vanish, and load to out of plane deflection relationships will exist which are nonlinear and have multiple potential solutions.

The minimization of potential energy solution method is not the only method with which these equations can be solved. Other methods include: double Fourier series, generalized double Fourier series (or the combination), and power series for exact solutions of certain geometries; approximate solutions available are; principle of minimum potential energy, Ritz method, Galerkin method, perturbation technique, finite difference and finite element analysis. This nonlinear plate theory contains systems of equations of the eighth order. The linear equations were of the fourth order. Hence, four more boundary conditions must be found in order to solve the equations.

The resulting solution set is a complex system of coupled equations which would require several pages to fully cover. Since these equations were not used in the present study, the reader is referenced to Chia (1980) for the details. What is important from this discussion is the set of nonlinear strains and how they allow for the study of postbuckling. It is this set on nonlinear strain equations that is requested when the NLGEOM command is turned on in Ansys.

Chapter3

EXPERIMENTAL METHODS

Test Parameters and Matrix

As mentioned in the introduction, the locally buckled portion of the AOC15/50 blade design served as the base for this study. The buckled section provided the parameters and dimensions for the experimentally tested sandwich panels. The eigenbuckling mode resembled a four sided simply supported mode 1 shape, and so the four sided simply supported support condition (SSSS) was chosen as the base support condition. The buckling mode was about 64 x 64 cm in dimension, however, due to testing and machining constraints, 45.7 x 45.7 cm panels were tested. The buckled section was also curved shallowly with a 1.78 m radius of curvature (~70 inches) in the transverse (y) direction while the loading direction was very slightly curved. To simplify testing and analysis, the axial curvature was considered neglible and only single curvature (cylindrical) panels were tested. The entire blade is manufactured of fiberglass and balsa, with the buckled section having a $(0/\pm45/0/b_{3/8})s$ layup. The resulting, initial base study panel therefore is a $(0/\pm45/0/b_{3/8})s$, SSSS, cylindrical panel (1.78m radius) panel. (Note: in the panel lay-up notation, 'b' represents a balsa core with the subscript denoting its thickness; the numbers represent the plies and their orientation; the 's' denotes symmetric facesheets)

To provide more generality and confidence in the FEA validation across a wide range, four parameters were varied: radius of curvature, facesheet layup, core thickness and edge support condition. The parameters were varied one at a time, where possible, to isolate parametric effects. To study the effect of curvature, two other radii were chosen along with the 1.78m. The deepest curvature occurring in a leeward sandwich section of the blade design, had a 0.548m radius of curvature, and was chosen as the deep curvature radius to study. The third curvature to study was infinite radius, a flat panel. Flat panels are advantageous because, with their simple geometry, they can also be modeled analytically with sandwich

theory. For simplicity and generality, the flat panel was chosen as the base panel with which to study parameters rather than the 1.78m curved panels. Therefore, the base panel was a flat, 45.7 x 45.7 cm, $(0/\pm45/0/b_{3/8})s$ panel and designated as the blade or B series. The 0.548 and 1.78m (23 and 70") radius curved panels used the same layup and are designated as the 23p and 70p series respectively.

The effect of facesheet layup was studied by comparing the base panel with a $[90/0/90/b_{3/8}]s$ panel, designated as the cross or C series. This second layup was chosen for its distinctly different elastic properties from the baseline case while still maintaining the same total thickness. Maintaining a constant thickness was more important than keeping a constant fiber volume fraction because of the heavy influence of thickness on bending stiffness. Core thickness was studied with 6.35 mm thick cores in $(0/\pm45/b_{1/4})s$ panels, designated as the quarter or Q series. The second zero layer of the base face sheet was dropped to comply with the sandwich modeling requirements in Ansys. Lastly, tests were also ran with free edge sides, the SFSF condition, to provide another condition for FEA validation. Table 3.1 outlines the test matrix.

Table 3.1. Test Matrix

Test Series	Parameter studied	Layup	Radius	# of SFSF tests	# of SSSS tests
blade, B	none- base	$(0/\pm45/0/b_{3/8})s$	flat	6	6
23p	curvature	$(0/\pm45/0/b_{3/8})s$	23 inch	3	3
70p	curvature	$(0/\pm45/0/b_{3/8})s$	70 inch	3	2
cross, C	layup	$(90/0/90/b_{3/8})s$	flat	3	3
quarter. Q	core thickness	$(0/\pm45/b_{1/4})s$	flat	3	2

Materials and Manufacturing

All sandwich panels were manufactured at MSU-Bozeman using resin transfer molding (RTM). In RTM, dry fabric and balsa core is placed into a mold cavity and resin injected into the mold until the fibers are fully impregnated with resin and the cavity filled. The wet system is left to cure in the mold for a minimum time defined by the type of resin system. All panels in this study cured in the mold for one day and were not postcured at elevated temperatures. For more detail on RTM molding see the theses by Hedley (1994) and Skramstad (1999).

An unsaturated polyester matrix/E-glass fiber system was used for the FRP face sheets and Baltek Contourkore CK-100 was the balsa core material. This style of sandwich construction is typical of low cost FRP materials used in wind turbine blades. The resin used in this study was CoRezyn unsaturated

orthophthalic polyester (63-AX-051), made by Interplastic Corporation, with 2% MEKP (by volume) added as catalyst. The dry glass fabrics used were Owens-Corning (Knytex) stitched D155 fabric (areal weight of 526 g/m2) for all 0° and 90° layers, and stitched DB120 (areal weight of 407 g/m2) for the ±45° layer.

To allow for curved structures, Baltek Contourkore is a series of approximately 2.5 x 5.1 cm (1 x 2") balsa rectangles bonded to a thin fabric material creating balsa 'mats'. The mat allows the balsa grid to follow curved surfaces in a piecewise linear fashion. The mat and rectangles are shown in Figure 3-1 The left balsa mat shows the piecewise linear contour fitting ability. The left corner of the mat was raised ~2 cm and allowed to curve down to the lower flat surface naturally. The gaps between rectangles fill with polyester during RTM. The resulting polyester grid was ingored in the analysis (in particular, no effect on the elastic properties of the core).

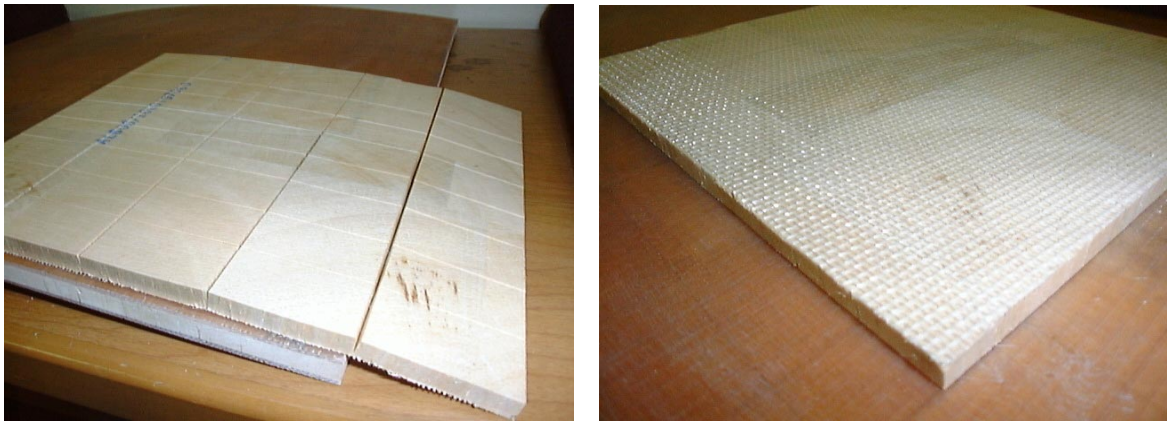

Figure 3-1. Baltek Contourkore; left, the rectangular gird for contour fitting of curved surfaces; right, (opposite face) the backing mat unifying the grid.

Sandwich Construction RTM Problems. The balsa should be placed in the mold, fabric facing upward, to allow for easier placement of the dry fabric onto the balsa. Care should also be taken during resin pumping to alleviate resin flow problems. High flow pressures can cause 'fiber wash', severe displacement of fabric layers within the mold which changes local and global properties. Relatively minor fiber wash occurs near the mold edges with fibers oriented parallel to the mold edge. Very high fiber contents can cause 'race-tracking' of the resin in the spaces between balsa rectangles. The resin may quickly fill the spatial gap around a square entirely, before complete impregnation, or 'wet-out', can occur.

This will stall or stop wet out and cause porosity problems for that face sheet area or at the very worst leave dry fabric. Panels with wet out or fiber wash problems were discarded.

RTM Molds. Three different molds were used to accommodate the three radii of curvature studied. The 1.78m and 0.584m radii molds were constructed with 9.5 mm (3/8") thick steel shells to increase bending stiffness and decrease deflection of the plate under resin injection pressures. The flat panel mold was constructed of 12.7mm (½") aluminum plates. The thickness of the sandwich panel was controlled by steel spacers with 9.5 x 12.7 mm cross sections. These two dimensions defined the total thickness of the sandwich panels for the 6.35 and 9.5mm (¼" & 3/8") thick balsa respectively. Silicone square rubber tubing of 9.5 or 12.7 mm cross section, with one strip per side, provided both the gasket seal and the outlet ports at the four corner gaps.

Test Fixture

Three criteria were required for the test fixture:

- edge supports should be a close approximation to ideal simple supports (free rotation with no transverse deflection)
- load distribution should be uniform across the width and thickness in the linear region
- post-buckling rotation/deflection should be unrestricted

Additional qualities desired were:

- low cost
- quick testing turn around from one panel to another
- accommodate the three curvatures

The final design incorporated rollers on flat plates for the loaded end simple supports and separate knife edge simple supports for the unloaded edges. A CAD drawing is shown in Figure 3-2 of the loaded and unloaded side simple support systems. Two load fixtures were used: one for flat panels and one for curved panels, which used the same loading principle and details. Commercial aluminum C-channel was attached to the panel edges, which in turned rested upon steel rollers. The rollers provided the load path and simple support by rotating freely on a flat steel plate during buckling. The C-channel transferred the load from the face sheets to the rollers. This system loaded the panels face sheets (rather than the soft core) while still supporting in the panel center. The rollers were machined from 4340 steel bar stock. One side was milled flat and 1.6mm (1/16") clearance holes drilled into the midline of the flat surface at 25.4mm (1") intervals.

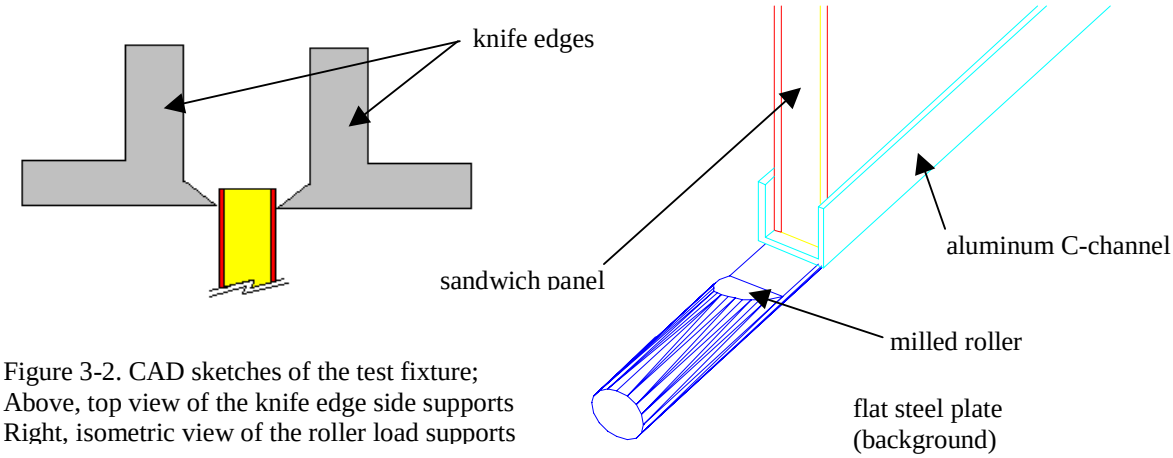

Figure 3-2. CAD sketches of the test fixture;
Above, top view of the knife edge side supports
Right, isometric view of the roller load supports

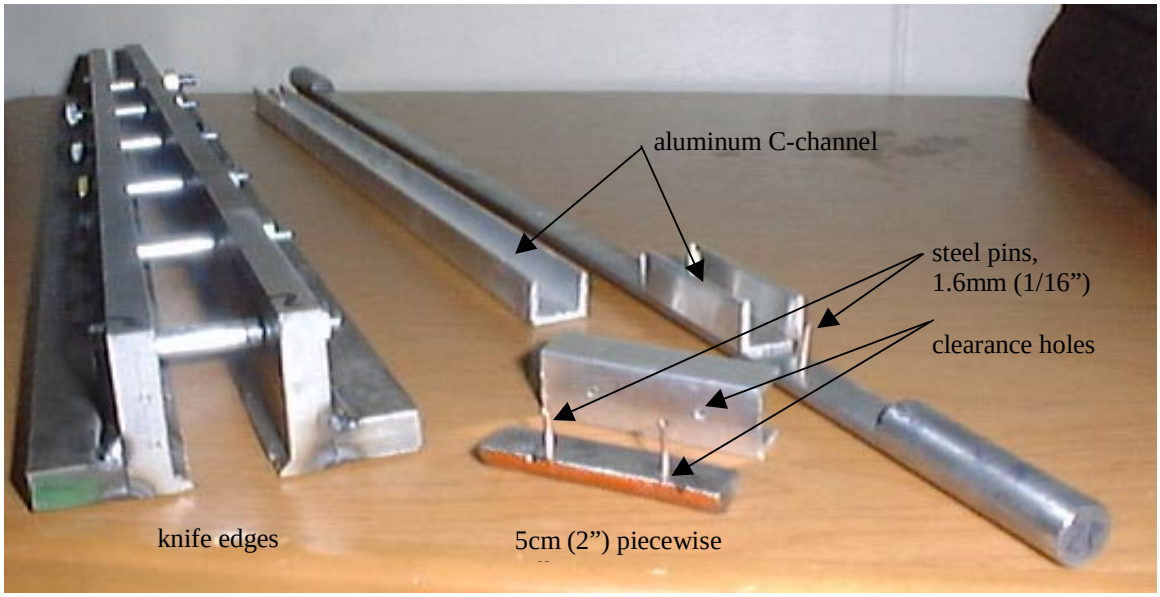

Figure 3-3. The various individual test fixture pieces

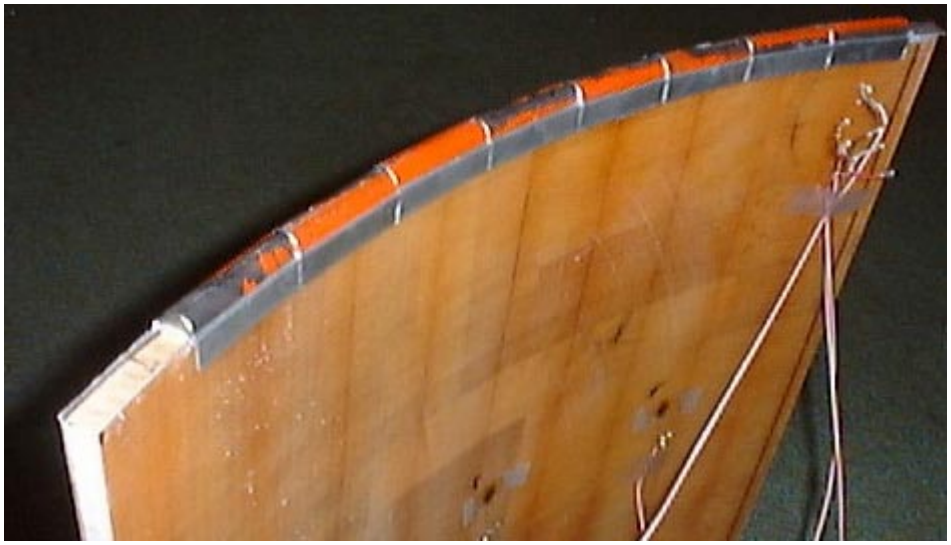

Figure 3-4. the curved test fixture attached to the panel, shown after testing

steel pins were placed in the clearance holes, passed through aligned holes in the aluminum channel and penetrated the balsa wood. The pin/C-channel system provided a stable and removable connection between panel and roller. Additionally, a layer of epoxy bonded the panel to the aluminum and also served to fill any gaps between them. The epoxy served to transmit the load more evenly to the panel, improving load uniformity, as shown in loading exercises with strain gaged panels. The various simple support parts are shown in Figure 3-3.

While the flat plate fixture used a single roller per loaded edge, the curved fixture approximated a curved support with piecewise linear supports as shown in Figure 3-4. Ten similar 5cm rollers were used for loaded edge. A single curved support would have seriously inhibited buckling due to its ability to resist twist and inability to rotate freely. A single flat roller was much easier to manipulate and was therefore used throughout most of the flat panel tests.

This load system worked well for critical buckling and fairly well deep into postbuckling. During SFSF testing, the single piece rollers rotated smoothly through critical buckling and very deep into postbuckling. The load-strain data did not show any oscillations, jumps or discontinuities except when the operator changed the load very rapidly. To prove roller rotation, rather than panel rotation upon the roller, a straight edge was attached to the end of the bottom roller. Photographs of the test set up and deep postbuckling deformation are shown in Figure 3-5. The angle of the straight edge matches the angle of the panel at the roller, demonstrating buckling rotation was entirely from of the rollers.

For the four sided simply supported condition, roller rotation dominated buckling is shown through additional circumstantial evidence. During testing, the rollers were observed to have rotated in the middle, while the edges did not. This phenomenon was expected due to the mode 1 buckling shape of the SSSS condition. However, the observer could have been fooled if the panel rotated within the C-channel, the C-channel lifted slightly off the roller, or a combination of the two. Again the test data showed a smooth transition into and through critical buckling. (A test data example can be found on page 34), in figure TDE, in the data acquisition section.) Panel slippage or channel lifting would most likely be a drastic event and be expected to show a departure from the smooth data shown. Lastly, either from one test or an accumulation of deep postbuckling SSSS runs, the rollers became permanently twisted symmetrically in the middle. The permanent twist, and location, proves roller rotation, however, it also signifies that the single roller also provided a resistance to rotation through shear stress. This effect will be further examined in the Chapter 5.

Figure 3-5. demonstration of the free rolling ability of the test fixture a). SFSF setup for roller rotation test b). roller rotation in the buckled configuration

Since forces on the side fixtures was much smaller, knife edges were possible. The knife edges are shown schematicly in figure 3-2, and pictorially in figure 3-3. The knife edges were designed as separate units to allow for usage with any radii. The SFSF condition is tested by not engaging them. The knife edges are connected by bolting six, 6.35mm (¼") bolts per side to allow for easy engagement and disengagement. The bolts also provided the force keeping the knife edges from separating during buckling. The 9.5mm (3/8") thick steel welded behind the knife point increased the bending stiffness and was added after knife edge bending was observed in the initial design.

Data Acquisition

Load, strain and displacement data could be measured from each test. Each quantity was acquired through the HP34970A data acquisition unit. Load was taken directly from the load cell as a voltage. During testing visual confirmation of the load was available as direct output in pounds and used to determine the loading rate. Strain was measured with HBM or BLM strain gages (120 or 350 ohm, with k-factor 2.0). The gage output voltage was conditioned within the Measurements Group 2120A strain gage conditioner and output to the HP data acquisition unit directly as % strain. Finally, displacement data was gathered using Celesco strain pots. Unfortunately, the displacement data was extremely noisy. Load-displacement and load-strain graphs of panel FFA for the same test run are shown in Figures 3-6 and 3-7. The noise level of the displacement data is on the same order as the actual displacement rendering the data useless. The strain data, however, shows very little noise and shows the bifurcation phenomenon clearly. Only load and strain data were taken from most subsequent tests.

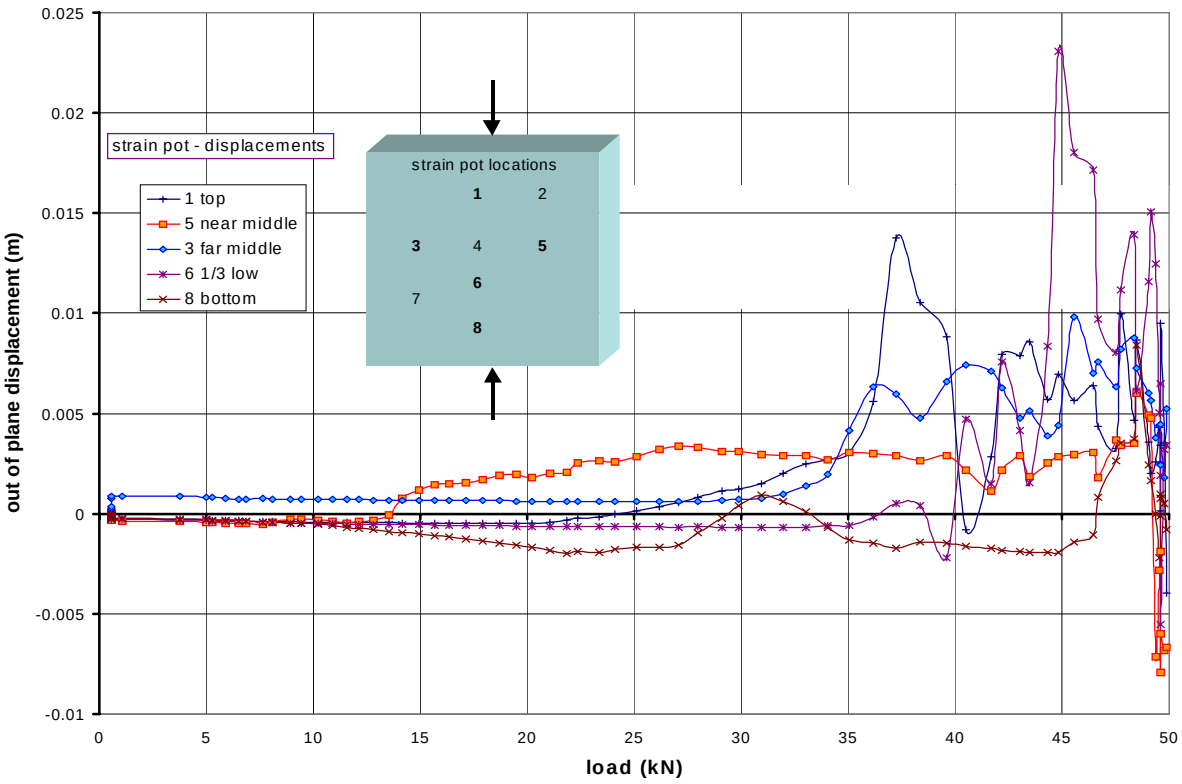

Figure 3-6. sample load-displacement data from panel FFA ($0_3/b_{3/8}$)s, test run #2

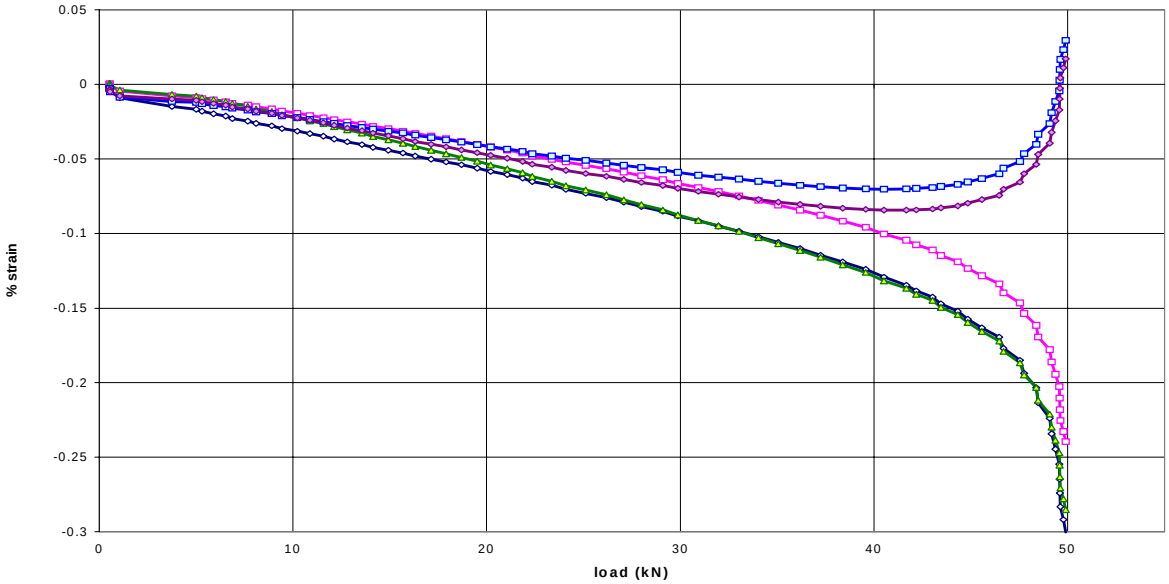

Figure 3-7. sample load-strain history data from the same panel and test run as Figure 3-6

Positioning

All of the tests utilized consistent strain gage placement and naming. Figure 3-8 is a diagram showing the dimensions and names for each gage position. To observe the load uniformity across the width and thickness, three strain gages were required on each face sheet. All were placed on the midlength of the panel where bifurcation is most apparent, due to the higher radius of curvature from buckling inches

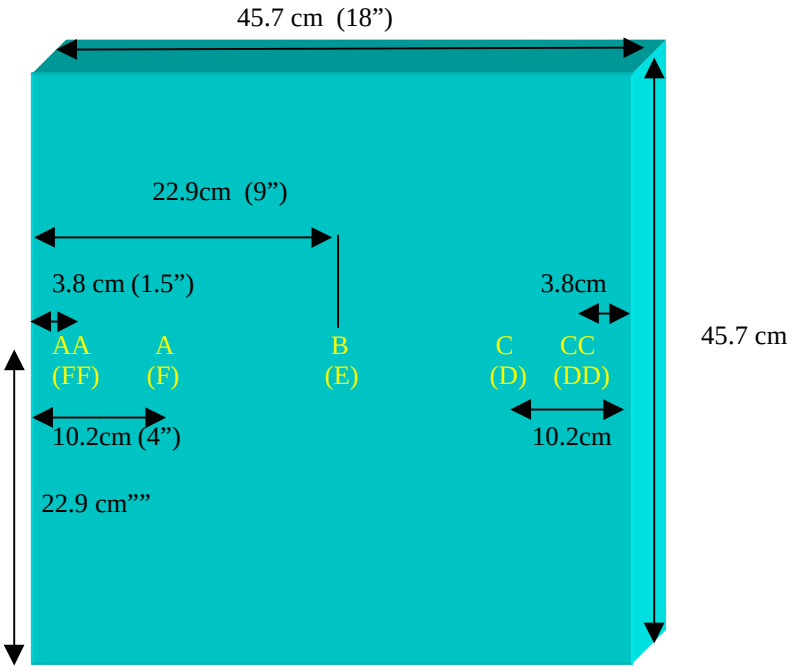

Figures 3-8. strain gage positions (gages AA-CC are located upon the convex side of curved panels)

deformation. Of the three, one was placed in the middle for similar reasons, and the other two, 5 or 7.5 to either side to best capture the strain distribution. The gages on the back face of the panel are located at the same positions and their names appear in parentheses. When out of plane displacements were taken, the numbering scheme was similar as shown in figure 3-6.

Test Procedure

Panel Preparation

To achieve a uniform load distribution during testing, the loaded edges of the panel had to be as flat through the width and thickness and parallel (top to bottom) as possible. The RTM manufactured plate was carefully cut with a diamond tip circular saw in a wet system, close to the desired dimensions. The flat loading edges and parallel dimensions were then tested with a flat granite block and scale. Most panels required further refinement which was accomplished by hand sanding on the granite block. This process provided length dimensions varying less than 0.4mm (1/64”) across the panel width and 0.8mm out of parallel. Panel width was allowed to vary up to a maximum of 1.6mm (1/16”).

For edge preparation, epoxy was mixed and applied generously as a gel to the ends of the panels which were to be loaded. The roller-pin-channel assembly was then attached and the system loaded in the Baldwin Testing Machine. The uncured system was loaded to approximately 9 kN. The pressure squeezed out excess epoxy, leaving only enough to fill the gaps between the panel and the aluminum c-channel. The load was left on the system overnight and the buckling test was run the next day. Best results occurred when the panel was tested without removing the system from the testing machine after the epoxy cured. This process mitigated the possible flat and parallel problems involving both the panel and the testing machine by aligning both in one step. Some panels needed shims placed on one side or the other for the best load uniformity.

Test turnover time could be greatly reduced if the epoxy was not necessary for load uniformity. Therefore, to determine the effect of the epoxy, a flat panel was tested with and without epoxy. The SFSF condition was chosen (which can be run repeatedly without panel damage) with the piecewise load fixture. The results are shown in Table B8E. The coefficient of variation (c.v.; percent standard deviation of strain at a particular load) drops significantly at both the 10kN load (by 43%), and the minimum c.v. (by 37%) with the addition of the epoxy filler layer. This affected the buckling phenomenon in two ways. If strain

variation is viewed as a type of perturbation, the greater strain perturbance in the no epoxy run caused the reversal point to occur drop. The 4% change in the reversal load is noticeable, but relatively minor. More curious was the drop in the asymptotic load. While smaller, this number is always more stable than the divergence load. During multiple tests of the same panel, with differing strain variations, the divergence load would vary up to 10%, while the flat load would rarely change by more than 1%. Intuition suggests that while the panel is still relatively straight, and in the linear response, the perturbance due to non-uniform load will have a significant effect upon initial out of plane deflection. However, the flat load occurs after large out of plane deflections have already occurred, and therefore is dominated by the bending properties of the panel rather than the fixture or strain variation. While slowing down the panel testing rate immensely, to minimize the strain variation the epoxy was deemed necessary to testing. Therefore, its effects upon divergence load, the primary buckling load for the SSSS tests, is also minimized. The effect of strain variation upon buckling is examined further in Chapter 5.

Table B8E. effect of the epoxy layer on strain uniformity and buckling in the piecewise fixture and SFSF condition

run #	epoxy layer	10 kN c.v.	minimum c.v.	@ load	reversal load (kN)	asymptotic load (kN)
4	no	40.1	21.3	32.4	39.6	47.1
9	yes	23.0	13.5	30.9	41.3	46.3

*c.v.: coefficient of variation (% standard deviation)

Undamaged panels could still be taken out of the Baldwin and off the rollers to be tested later. This process was limited by cracking of the epoxy during some high load tests and imperfect realignment of the panel relative to its curing position. Load uniformity was observed to degrade with each replacement. Panel B1 was taken out and replaced twice. The first time, it was removed from the testing machine and the rollers taken off. The second time it was only removed from the testing machine. Epoxy cracking was heard during initial loading during the last series of tests.

Procedure

Most panels were tested with free edges first to ascertain uniformity of load. Usually, several tests were run and which were stopped after critical buckling but before any damage took place. The knife edges were placed on the unloaded edges and one or more tests performed to find the critical buckling load. Often the first few SSSS tests were terminated with the response limited to very little post-buckling. The

final test(s) would reach further into the non-linear realm until damage occurred. A choice was then made whether to retire the panel after initial damage or continue loading until ultimate failure.

Data Reduction Methods.

Implementation of the strain reversal method. The load strain data was a fairly smooth set as seen earlier in Figure 3-6a. To find the strain reversal of the center convex strain gage, the data was differentiated with respect to load. The point, or area which the resulting curve crossed zero is then the strain reversal load. Due to the high sampling rate, the loads did not always change significantly from one datum to the next which results in a very noisy curve. A much smoother, and still accurate, set is found when the strain and load differences are taken from the tenth preceding datum. Examples of the noisy single and smoother tenth datum difference differentials are shown in Figure 3-9. The curve usually crosses zero back and forth several times inside a finite area due to still resident noise. The area is rarely larger than 1 kN and is often as small as 0.2 kN for the panels tested here. The area is termed the noise level and as a general rule all noise levels not directly stated should be assumed to be +- 0.5 kN.

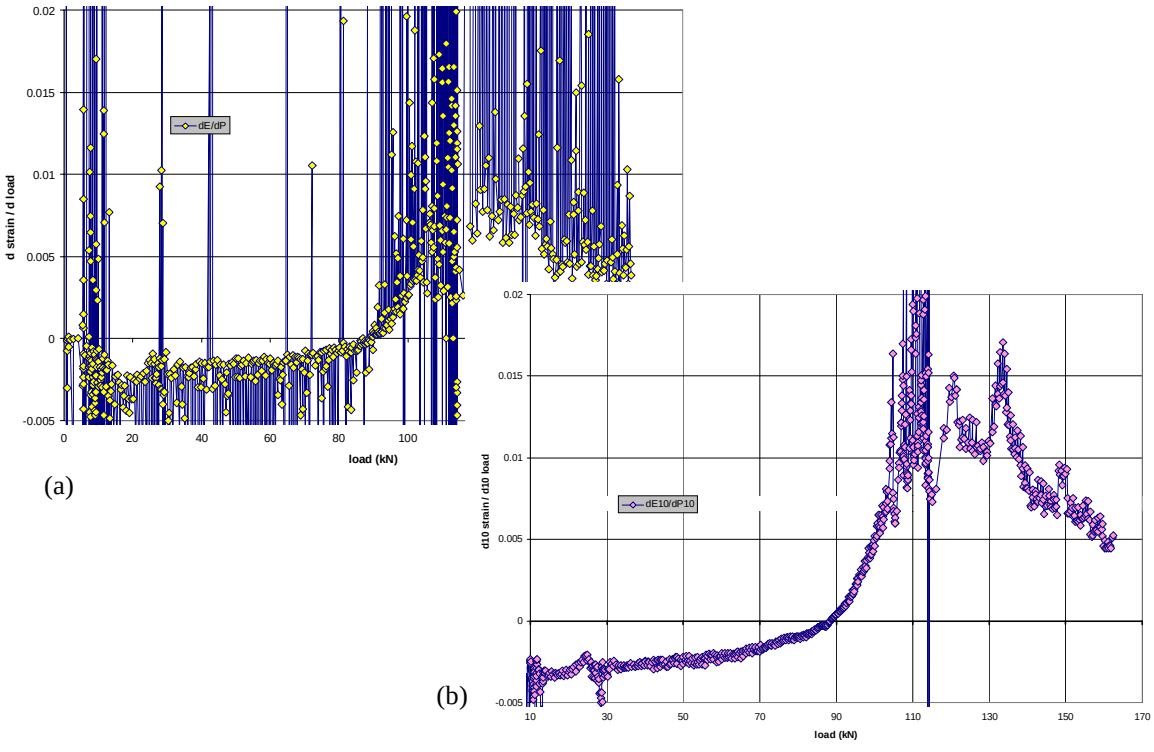

Figure 3-9. examples of the strain/load differential used for the strain reversal technique using the (a). single data difference and (b). tenth data difference.

Chapter 4

NUMERICAL METHODS

Finite Element Analysis was used to model all cases studied experimentally with additional cases further exploring the four experimental parameters (radius of curvature, core thickness, facesheet layup and support condition). This is the only type of predictive analysis available to investigate buckling of curved sandwich panels. The experiments were compared directly against FEA predictions to validate both the eigenbuckling and nonlinear analysis procedures used in designing the AOC15/50A related goal of this work was to establish guidelines for the modeling of sandwich panels.

The baseline case representing the simplified blade construction (flat, 45.7x45.7cm, SSSS, [0/45/0/b3/8]s; the experimental blade series) was used as the base panel to study FEA modeling parameter effects. The FEA parameter study, includes mesh convergence, perturbation convergence, perturbation model and fixture model studies. The studies where curvature might have a significant effect, such as the fixture model study, were also run as appropriate.

FEA Model Generation

Decks

All of the models used in this study were built and solved with parametric decks. Decks are the series of finite element code commands that create, solve and process models, compiled sequentially in a text form. When an FEA code reads a deck, it executes the commands without user input until completion, error or forced user intervention. Ansys allows decks to be read as text files, and therefore to be constructed within common word processing programs. Ansys also allows for parametric input for most commands and limited Fortran Programming commands (DO, FOR, etc…) and functions (SIN, ATAN, LOG, etc…). Any numeric input (panel width, maximum time step, displacement load, etc…) can be entered as a named variable. As an example, the parameter/variable, ‘gy’, was defined numerically early

in the deck as “gy = 18*0.0254.” Later, keypoint 2, a corner of the panel geometry, was given the location of (0,gy,0). The variable, ‘gy’, was used in many commands within the deck to define panel geometry, making changes from model to model, quick, simple and error free by changing a parameter only once (gy = 15*0.0254). Similarly, Fortran looping functions such as DO, can be incorporated into decks. One such DO loop was used to define a time-history post-processing variable in a ‘sub-deck’ by summing nodal reactions through the loop. ‘Sub-decks’ such as these are similar to program subroutines and are termed macros in Ansys. Macros are useful for performing tedious, often repeated tasks. In this study most post processing was handled by macros. While parametric decks and macros take longer to construct and ‘debug’ than interactively constructed models, they provide quick, consistent and repeatable models free from small discrepancies and mistakes. They offer the engineering analyst a highly efficient tool for parametric and convergence studies. Examples of decks used in this study can be found in the Appendices.

Panels

The sandwich panels were modeled using two different element systems, quadratic shell and mixed quadratic solid and shell elements. Shell models are more commonly used for sandwich construction, espicially in large structures or models because of user friendliness and to minimize model size. Since this study focuses on sandwich construction and its proper modeling,, the mixed element model was studied to gain further insight into its particular characteristics and usefulness. Both element models shared many common deck traits. They were modeled in the global cylindrical coordinate system, with R,Θ,Z correlating to X,Y,Z. The panels were loaded along the Z-axis and the layer orientations were defined according to angular offset from the Z-axis. When modeling with these elements, care must be taken to ensure whether the input given or output queried is defined in the global or local element coordinate system.

Both models utilized a base deck from which, with minor changes different panel parameters, FEA parameters and support conditions could easily be modeled. All four major panel parameters studied could be varied within a single deck. Flat sandwich panels were approximated by giving an extremely large radius or curvature (1e5 m). These ‘flat’ panels were compared to flat cartesian defined models for verification. Both decks were also capable of quickly changing mesh density and perturbations through

single numerical parametric changes. All three edge support conditions, simple, clamped and free were also easily accommodated with only minor changes. All loads were defined as displacements rather than pressure of force loads. Pressure loads are always defined normal to the element edge. As the panel buckles the element edge rotates creating a transverse load component which does not properly model the desired in-plane load and, therefore, was not chosen as the loading method. A uniform displacement was chosen over force for ease of modeling as well as a clearer, more accurate description of the true loading. The nodal reaction forces were summed along one loaded end to define the load, P. All decks also included failure criterion information and face sheet thickness to fiber volume fraction routines. Lastly both panel models had separate decks that included significant parts of the test fixture. The modeling of the fixture is described later.

Shell Models. Shell elements are useful in modeling thin shell structures which experience transverse displacement. These types of structures have very small thicknesses with respect to their in-plane dimensions. As a result, assumptions about the stiffness and strain in the transverse (thickness) direction may be made which eliminate the need for a three dimensional solid element and leave a two dimensional element with three dimensional degrees of freedom. To allow for bending (and shear) curvatures to develop within the element shell elements are quadratic elements (midside nodes). Additionally, to allow the element fully develop a curved deformed shape, the nodes have the ability to rotate about the in-plane axis (and sometimes the normal direction) giving five (or six) degrees of freedom per node. As a result of the assumptions made to gain a two dimensional element, shell elements are unable to calculate *z* stresses. The main advantage to shell elements is that they allow thin structures to be modeled without resorting to inordinately large meshes which would be required of solid elements for decent (or even relatively poor) aspect ratios.

The shell element models utilized the Ansys element shell91. Ansys provides two quadratic layered shell elements which both have six degrees of freedom, shell91 and shell99. Shell91 was chosen for its sandwich modeling option. Shell91 supports up to 16 distinct layers. Each layer can model a different orthotropic material in any desired XY orientation. Each layer contributes its material properties to the whole by the material property matrix $[D]_j$ (j^{th} layer) which is shown in the next lists. Notice that shear stiffness is calculated layer by layer as well. Interlaminar stresses can also be calculated because of

this layer by layer approach. The complete set of Ansys shell91 help files containing detailed data on element equations, options and output can be found in the Appendices. The thickness of each layer can be tapered linearly as well, by controlling the height of a layer at the four corners of an element. In general, a single ply was modeled as one layer. The ±45 plies were the exception and modeled as two separate layers.

Sandwich modeling in Shell91 is controlled by keyoption 9. When this option is turned on (the default is off) the middle layer, defined by number, becomes the core. While the number of layers either side of the core must be the same, their material, orientation and/or thickness may be different, thereby allowing for unsymmetric sandwich construction modeling. Several changes in the element equations are then triggered. These equation changes are based upon assumptions very similar to 3-Layer theory. The core carries all of the transverse shear, while the facesheets carry none. Secondly, the facesheets carry all, or almost all, of the bending load. This theory is a more general sandwich model, in that unbalanced or non-symmetric face sheets are permissible. The sandwich option also requires that certain conditions be met within the model geometry and material properties. The following two lists detail the element equation changes and model requirements.

Shell91 sandwich option element equation changes:

- The shear locking factor, f, in the layer material property matrix is set to one for the core, to obtain more accurate transverse shear response for the core. The shear locking fator *f* occurs in the layer property matrix $[D]_j$ terms;

$$[D]_j = \begin{bmatrix} BE_x j & Bv_{xy} jE_x j & 0 & 0 & 0 & 0 \\ Bv_{xy} jE_x j & BE_y j & 0 & 0 & 0 & 0 \\ 0 & 0 & 0 & 0 & 0 & 0 \\ 0 & 0 & 0 & G_{xy} j & 0 & 0 \\ 0 & 0 & 0 & 0 & \dfrac{G_{xy} j}{f} & 0 \\ 0 & 0 & 0 & 0 & 0 & \dfrac{G_{xz} j}{f} \end{bmatrix} \quad (19)$$

where: $B = \dfrac{E_y j}{E_y j - v_{xyj}^2 E_x j}$

$f = \left\{ \begin{matrix} 1.2 \\ 1 + 0.2 \dfrac{A}{25t^2} \end{matrix} \right\}$

A is the element area
t the average total thickness

- The transverse shear moduli, Gyz and Gxz, are set to zero for the top and bottom layers. Therefore, D_{55} and D_{66} also equal zero.
- The transverse shear strains and stresses in the facesheets are set to zero.
- The adjustments made to the transverse shear strains or stresses to ensure peak values at the shell center and zero at the free surfaces are not made.

Shell91 sandwich option model and material requirements:

- The ratio of the middle layer (core) thickness to the total thickness should be greater than 5/6, and must be greater than 5/7.
- The ratio of the peak elastic modulus of the face sheet over the elastic modulus of the core should be greater than 100 and must be greater than 4. Also, the ratio should be less than 10^4 and must be less than 10^6.
- For curved shells, the ratio of the radius of curvature to total thickness should be greater than 10 and must be greater than 8.

The shell element, in particular shell91, is perfectly suited to modeling the sandwich panels studied here. As a result, the model is a very simple looking one with a regular mesh. Figure 4-1 is an example of a shell SSSS shallow curved panel model. Figure 4-2 is a detailed view of one corner of the same panel with the /eshape command set to show the constituent layers and thickness of the elements.

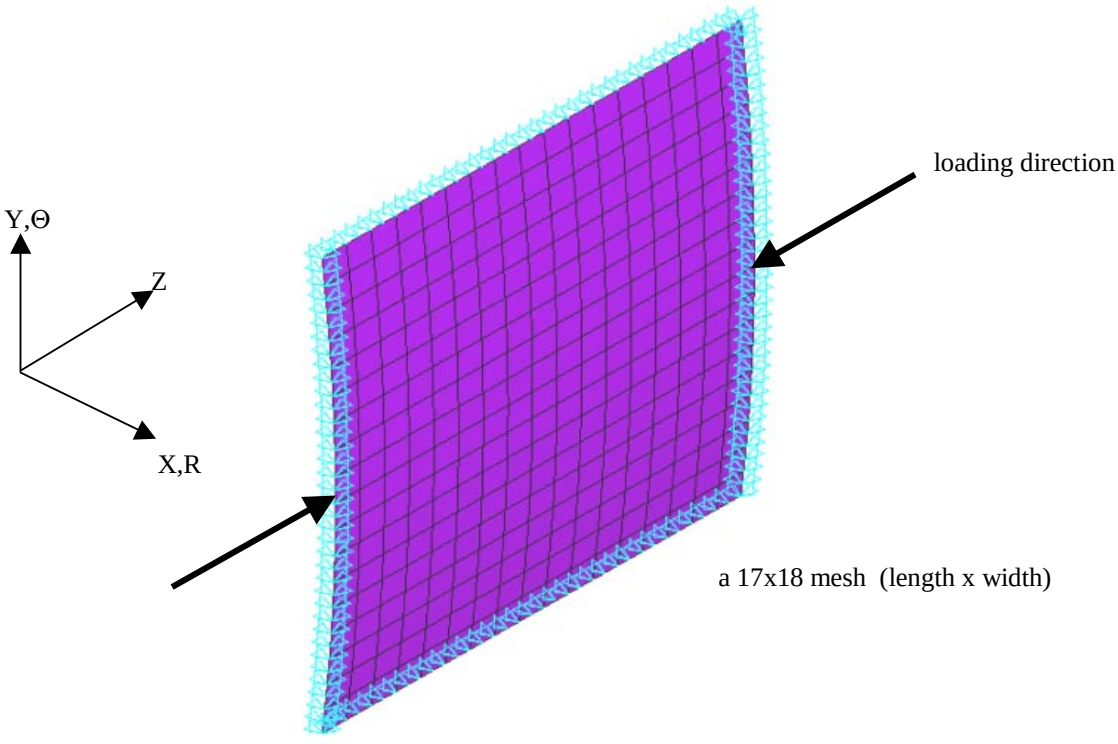

Figure 4-1. Shallow curved panel shell model with SSSS boundary conditions

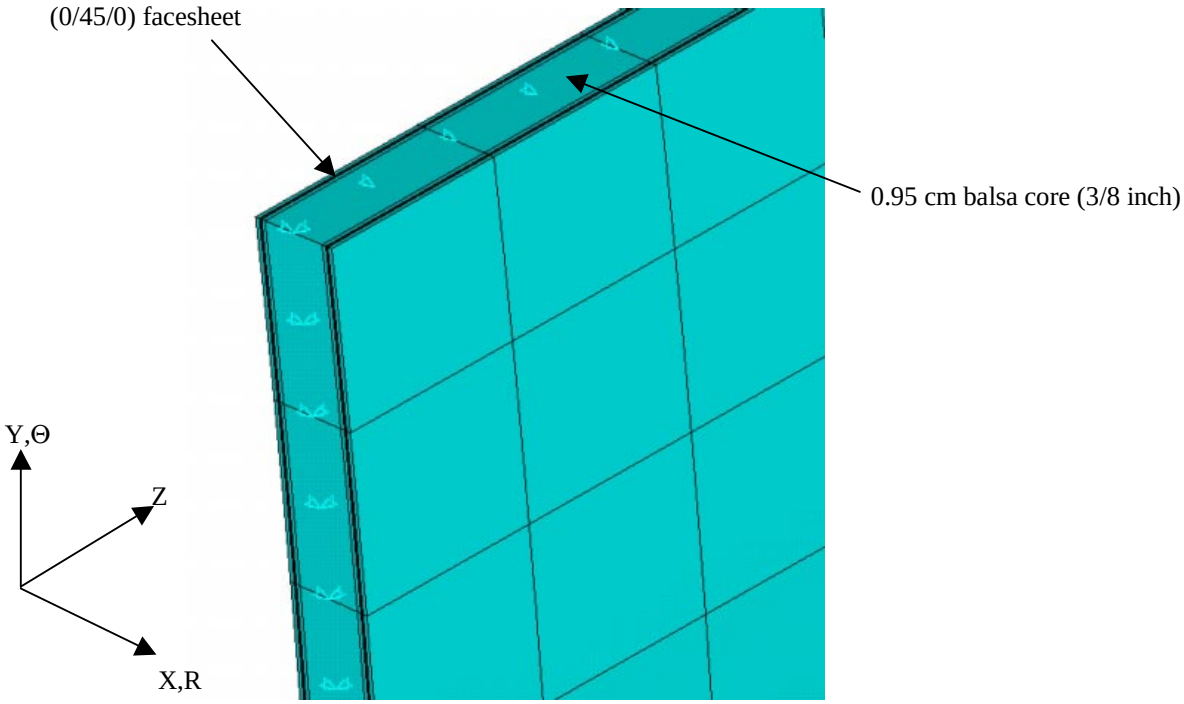

Figure 4-2. Magnified view of the above shell model with the layer thicknesses shown

Mixed Model. The second method used to model sandwich construction was a mixed element model with shell facesheets and a solid core. The core was built of solid96 elements. Solid96 is a 20 node quadratic brick element that can accommodate orthotropic materials. Two volumes were created to mesh the core. The volumes adjoined along the ΘZ plane at the desired radius, r, of the curved panel. Each extended hc/2 from that plane to yield the full core of thickness hc. This method ensures a line of nodes along the center of each core edge. The support conditions and loads can then be applied along these linear nodes at the panel center. The mesh density is controlled by the aspect ratio of the brick elements. Common FEA procedures suggest keeping element aspect ratios below 3:1:1, and optimally around 1:1:1 for accurate results. The disadvantages of this two volume approach lies in an aspect ratio versus model size dilemma. Low aspect ratios lead to very high numbers of nodes and degrees of freedom (DOF). This can cause extremely slow solving or solution errors due to RAM allocation or hard drive disk space problems in many computer systems. Even with a 5:1:1 element aspect ratio, a typical non-linear model takes approximately one week to solve on Sphinx, the computing system used in this study.

Once the volumes have been meshed, the face sheets were meshed upon the appropriate areas of the two volumes. The shell elements were meshed directly upon the nodes of the quadratic brick elements.

Through keyoption 11 of shell91, the shell nodes can be placed at the top, bottom or center of the element thickness. With this option, the face sheets can be properly modeled as extending out from the core, rather than overlapping in virtual FEA space. Figure 4-3 shows a detailed view of the model with the layer thickness and support conditions showing. Figure 4-4 shows a full view of a typical mixed model. This model has a mesh density of approximately 5:1:1 element aspect ratio for the brick elements.

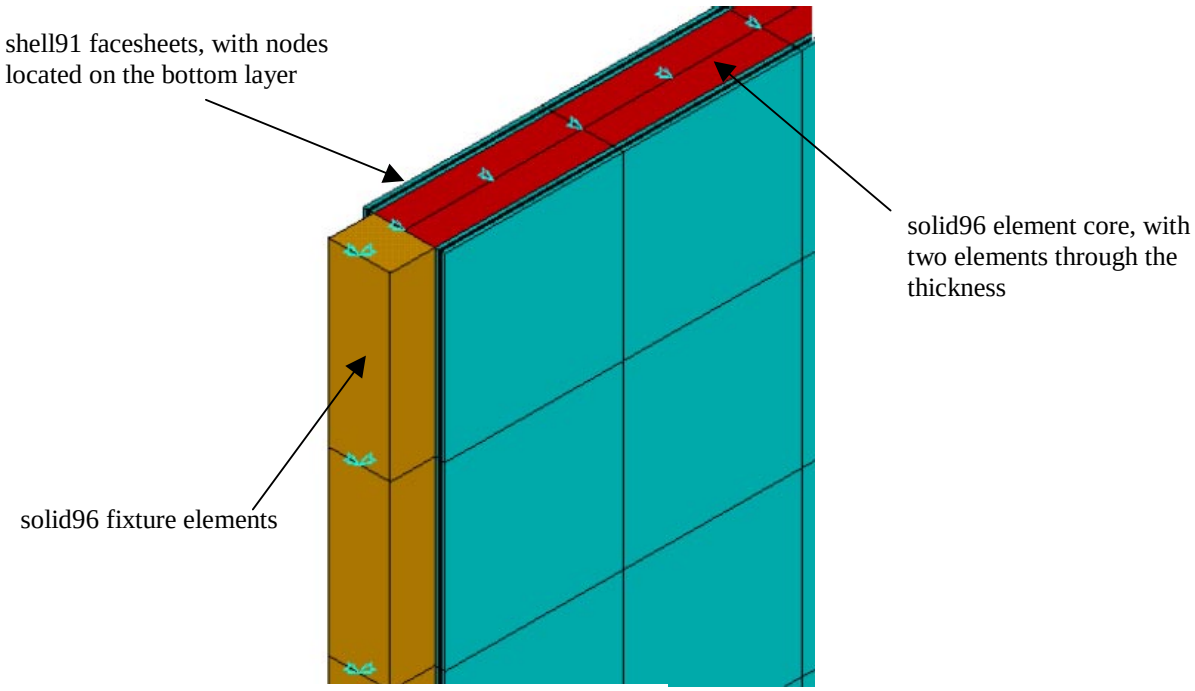

Figure 4-3. Detailed view of the mixed element model

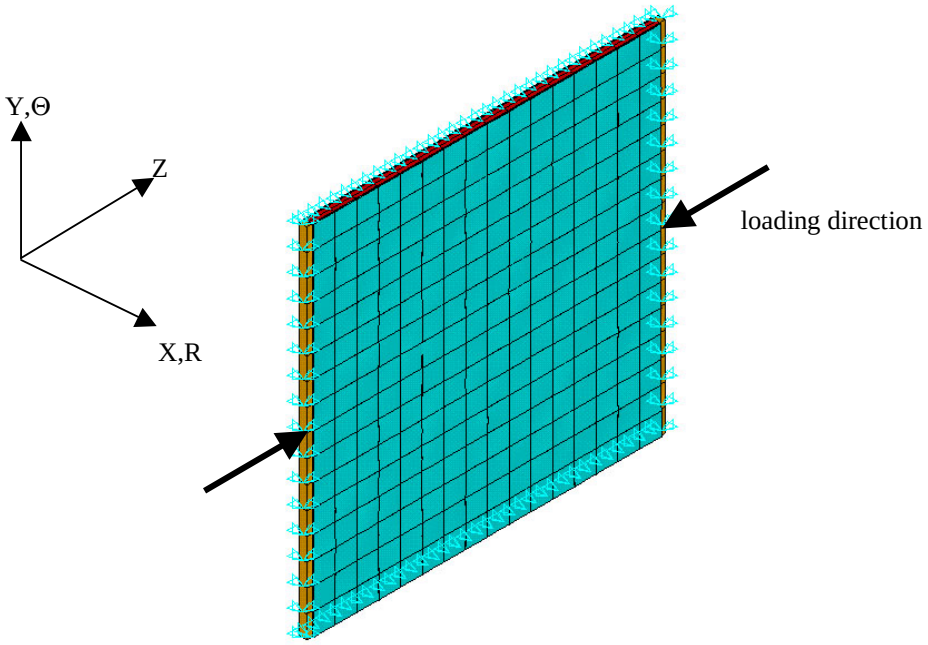

Figure 4-4. Full view of a mixed element model with a 5:1:1 brick element aspect ratio

Fixture Modeling

Intuition suggests that the fixture will affect a significant change upon the response of a tested panel from an ideally SSSS supported panel. The panel may rotate, lift or slide in the C-channel/pin system. That system may also rotate, lift or slide on the steel roller. Friction between the load plate and steel roller may change the equilibrium position of the buckled panel. While the analyst remains unable to model many of the response-changing phenomena in implicit FEA codes, the elastic response change from the addition of the steel supports to the end of a panel may be modeled.

The fixture was modeled differently for the shell and mixed models. Three separate models were built to study the effect of the fixture on the buckling response of the panel. The first model used only degree of freedom boundary conditions to model the fixture. This model represents the ideal simply supported FEA panel, where the four edges are restrained from moving out of plane. This model is referred to hereafter as the pure model. Free or clamped edges are possible by deleting a line of code, or adding a rotational restraint respectively. This model was used as the base model, without any fixture effects. The side support knife edges were only modeled as ideal simply supported boundary conditions. Any possible effects induced upon the panel response by the knife edges were treated as negligible and therefore not modeled.

Only the load supports were viewed as potentially affecting a change in the panel from the ideal (pure) case and therefore only these supports were modeled. Consistent with the experimental fixtures, both single and piecewise supports were modeled. The support model used shell91 elements, in the same global orientation as the panel, with a single steel layer. Only a single element was meshed through the height, while the number of elements across the width was predefined by the number of elements through the width of the panel. The element heighth per roller was the combined height of the roller and C-channel. The thickness was tapered linearly from the panel width to the bottom width, calculated to yield an equal stiffness by area of the experimental system. The piecewise model used nine separate element areas per edge. The three fixture models are pictured in Figure 4-5, in a closeup view of a corner to show the details clearly. The panel response differences due to these models are tabulated in Chapter 6, Numerical Results.

The mixed element fixture model is similar to the single piece shell model except that it was not tapered and was constructed of solid96 elements. It is shown in Figure 4-6 along with the boundary conditions. Unlike the shell model, with this model structure, a pure sandwich panel model is not feasible.

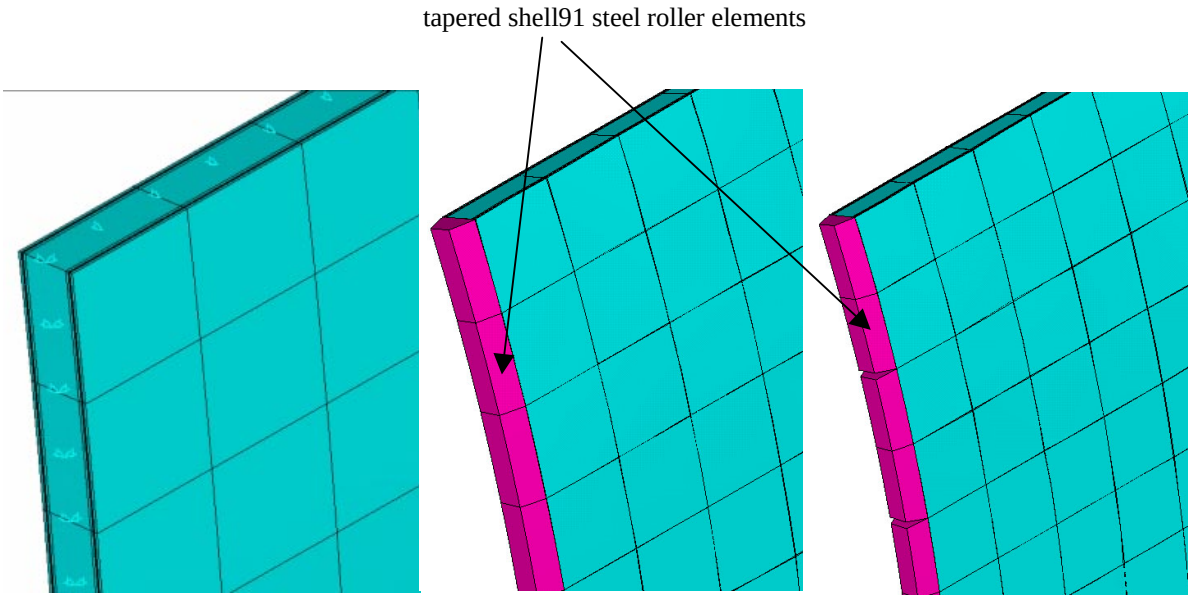

Figure 4-5. Three shell fixture models, pure, single and piecewise, left to right

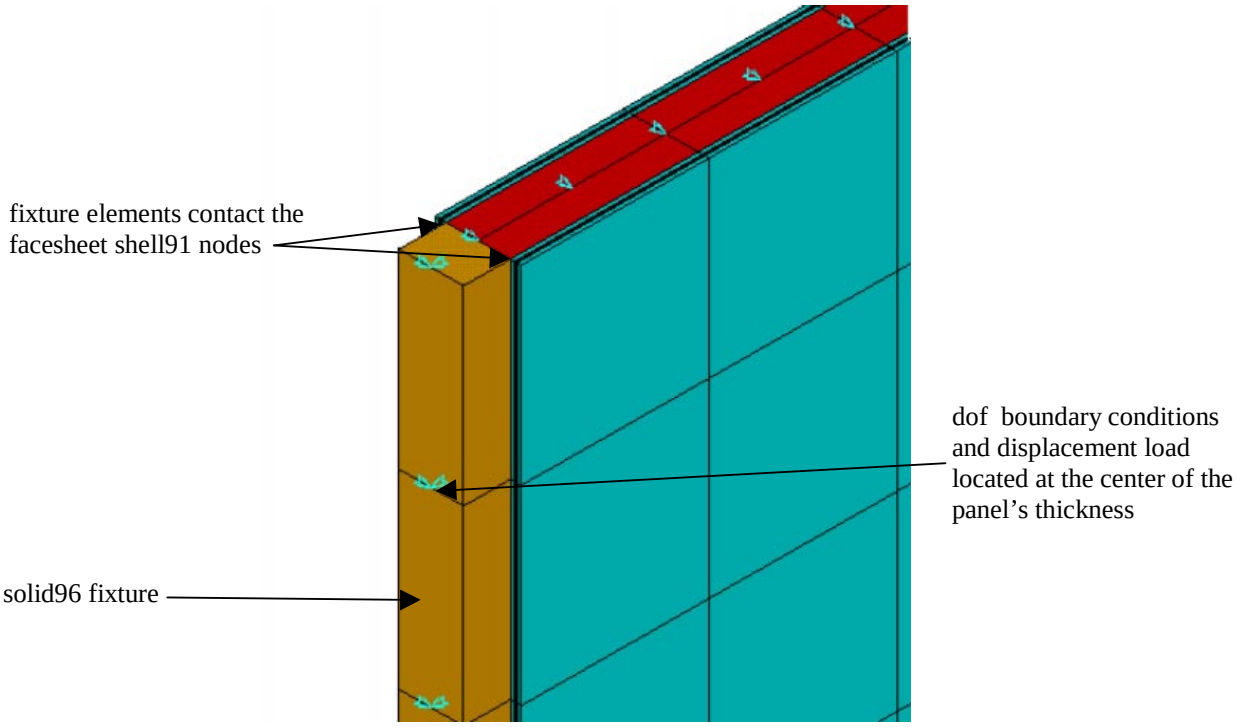

Figure 4-6. Mixed element fixture model

To achieve a simply supported structure, the panel must be loaded in the center of the panel, which is the soft core solid elements. If these balsa elements are loaded directly, they will deform in a V-shaped pattern. The soft core will not shear lag load the facesheets, therefore improperly modeling sandwich construction. Therefore, in order to load in the center of the panel, a stiff system must be employed which will load the facesheets.

Material Properties

All fiberglass material properties were derived from the DOE/MSU materials database [Mandell & Samborsky (1997)]. Elastic properties were calculated from fiber fraction formulas while failure data was taken directly from the nearest fiber fraction. The face sheet thickness of the sandwich panels was set constant for all numerical panels as t_{fs} = 1.588mm (1/16”) for 9.525 mm (3/8”) cores, and 1.07 mm (0.042”) for 6.35 mm (1/4”) cores. This results in different percent fiber volumes for different layups. Constant thickness was chosen over constant fiber volume between layups due to the heavy dependence of bending stiffness upon thickness. Percent fiber volume (%fv) of the face sheets was predicted by a subroutine in the decks.

Given the face sheet thickness, a function relating thickness fiber fraction for different layups was required. Data from the DOE/MSU material database was plotted and quadratic relationships derived using average ply thicknesses. DB120 fabric (all ±45 layers) have a different ply thickness than D155 fabrics. This data was also plotted and another quadratic relationship derived. From these two relationships, %fv and ply thickness were calculated. Elastic moduli were then calculated from equations supplied by the database. The subroutine can be found in the Appendices, along with the graphs and quadratic equations mentioned earlier. All FEA models used this subroutine. All fiberglass properties were predictive in nature (sandwich panel test data was not used to derive any properties). Table 4.1 is the results of this subroutine, for the material properties of each lay-up in the test matrix.

All failure data was also taken from the MSU-CG database (except all balsa properties), although no calculations were performed upon them. Balsa properties were all gathered from data given by the Baltek Co., the suppliers of all the balsa used in this study. Two widely different sets of data were delivered by Baltek. One set was the manufacturers product data sheet which was an incomplete set giving

Table 4.1. Fiberglass material properties used in FEA analyses for each lay-up

fiberglass material	#	elastic moduli (GPa) Ex	Ey	Ez	Poisson's ratios Prxy	Pryz	PRxz	shear moduli (GPa) Gxy	Gyz	Gxz
panels: blade, 70p, 23p; (0/45/0/b3/8)s, f = 1.59 mm, Vf = 35.5%										
db120	2	21.46	6.29	6.29	0.407	0.334	0.334	3.327	3.327	3.327
d155	4	29.26	7.52	7.52	0.323	0.323	0.323	3.311	3.311	3.311
panel: cross; (90/0/90/b3/8)s, f = 1.59 mm, Vf = 39.1%										
db120	2	23.34	6.72	6.72	0.400	0.328	0.328	3.601	2.709	2.709
d155	4	32.58	8.03	8.03	0.318	0.318	0.318	3.583	3.583	3.583
panel: quarter; (0/45/b1/4)s, f = 1.07 mm, Vf = 35.2%										
db120	2	21.29	6.26	6.26	0.407	0.334	0.334	3.304	2.486	2.486
d155	4	29.73	7.48	7.48	0.324	0.324	0.324	3.288	3.288	3.288

only the compression modulus and transverse shear. The second was an orthotropic data set as a function of wood density. These data sheets can be found in Appendix (). The orthotropic data was derived from a single piece of wood, which is influenced by the grain, and radial directions severely. However, the balsa mats are orientated randomly with respect to the radial and theta directions, yielding a smeared transversely isotropic material. The orthotropic data set was a more complete set, and therefore smeared into a transversely isotropic material to be used as the core properties. Since the data sets were both contradictory and manipulated, a core property parametric study was implemented to determine the necessity of accurate core properties. The balsa properties and any other material used to model the fixture are listed below in Table 4.2.

Table 4.2. core and fixture material properties used in the FEA analyses

material	#	elastic moduli (Gpa) Ex	Ey	Ez	Poisson's ratios Prxy	Pryz	PRxz	shear moduli (Gpa) Gxy	Gyz	Gxz
balsa; isotropic	3	0.148			0.300				0.0569	
balsa; orthotropic	3	0.187	0.061	4.07	0.67	0.01	0.02	0.0203	0.150	0.220
balsa: transv. iso.	3	0.148	0.148	4.07	0.67	0.02	0.02	0.0203	0.200	0.200
steel	5	200			0.300					

Non-linear Incremental Buckling Models

Apart from three changes made to the nonlinear models, the linear and nonlinear were essentially the same. These changes were; 1). the nonlinear shell strain equations were induced (see Theoretical Background, nonlinear mathematics section), 2). Some sort of perturbation was applied to the model to cause initial out of plane deformations 3). The displacement load was incremented linearly up through four different displacements. The eigenbuckling models were loaded 0.1 mm to find the stiffening matrix. Instability loads for the desired number of modes were given as a multiple of this pre-load. Out of plane deflection plots of the mode shapes are valid only as ratios, yielding a general shape, but not true deflections.

Perturbation Methods

Three types of perturbation were considered in this study to induce out of plane deflections on the geometrically perfect FEA model. These methods were force, moment and random nodal displacement perturbations. The three perturbation methods used upon shell models with all nodal loads and supports are shown in Figure 4-7.

The force perturbation method applies an initial normal force load onto a node or nodes. The disadvantage of this method is that the placement of the normal force(s) can artificially impose a mode shape upon the panel. This mode shape may or may not be the 'natural' first mode of the panel. This mode shape inducing quality can be used to impose certain mode shapes. A center panel normal load attempts to force a mode 1, while those with opposing quarter (Z direction) point loads imposes mode 2.

The moment perturbation method is less likely to impose a mode shape upon the model. With this method, moment loads were applied to the nodes on a loaded edge of the model. This method might inhibit nx2 or other multiple transverse wave form mode shapes. These first two methods were handled as independent load steps. The first load step isolated the perturbation load while the following time steps incremented the in-plane displacement loads.

The last method, the nodal random displacement method, is least likely to induce a mode shape. This method was the one used upon the blade design nonlinear buckling analysis. It is particularly useful with complex structures where the mode shape and location is unknown. The random displacement method moves each selected node a random, small distance in any axis direction. The maximum

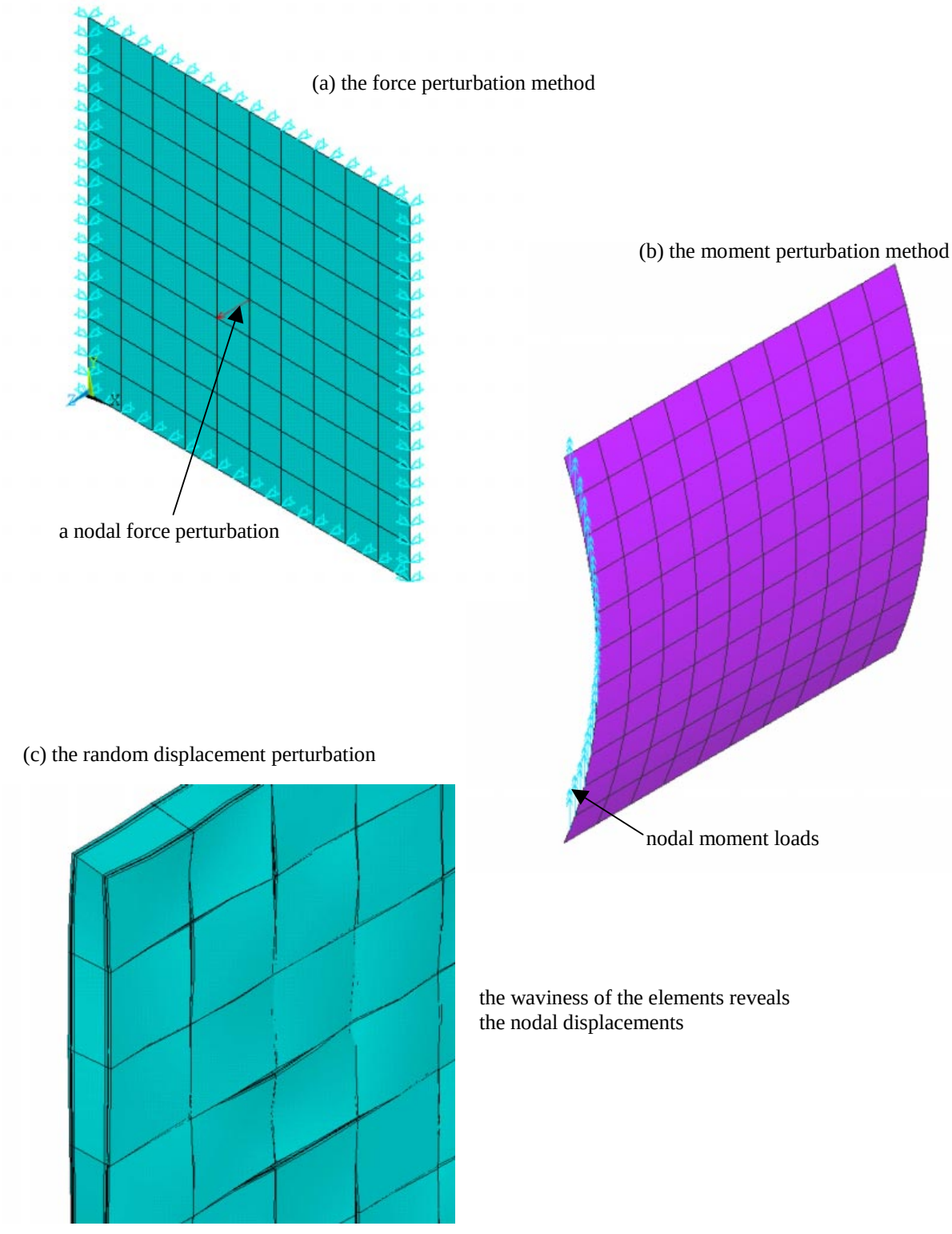

Figure 4-7. three perturbation models

displacement size is bounded by a user defined parameter. In this study, only out of plane displacement perturbations were performed upon the model. For the shell model all panel nodes were selected to be perturbed. Only the facesheet nodes were perturbed in the mixed element model. The magnitude of the displacement was governed by a Gaussian distribution formula. The formula is given below as equation (20),

$$f(x) = \frac{1}{\sqrt{2\pi\sigma^2}} e^{-(x-\mu)^2/2\sigma^2} \tag{20}$$

where;

μ = mean (zero here)
σ = standard deviation

A macro called by the decks performed this function upon the model. It was named u_def.mac and can be found in Appendix (A). The nominal maximum random perturbation size is input into this macro as the parameter, rp, which corresponds to 3σ in equation (20). The main disadvantage of the random displacement method is due to perturbation size limitations. Certain ratios of mesh size to displacement caused deep local curvatures. Some of these curves exceeded the maximum curvature allowable dictated by the sandwich option. This problem is detailed further in the numerical results chapter in the mesh and perturbation convergence study sections.

Timesteps and Output

The displacement load was ramped up over four fixed loads. Each load step was further divided into an indeterminate number of substeps. The first, maximum and minimum substep sizes were defined for each load step (normal to one). Ansys uses a line search method to determine the size of the next substep within the given parameters. The maximum number of equilibrium iterations was also defined. When exceeded, Ansys chooses a smaller substep, resolves and iterates until the minimum size is reached. If convergence is not reached at this minimum substep the solution ends. Results for each layer and substep were saved and therefore all previous results were valid and available for postprocessing. This accounts for the various degrees of postbuckling reached by different models.

The first loadstep was set just below critical buckling and its substeps were defined coarsely due to the linear response. The second load step incorporated the critical buckling region and its parameters

were set finely to capture the quickly changing response well. The last two loadsteps were set with high loads and relatively fine substeps to capture the panels response deep into the postbuckling region.

FEA Response Validation

A myriad of styles are available to describe the critical and postbuckling response of shells. Load-strain plots were chosen for this study because that is what was used for the experimental results. FEA nodal strain locations were chosen which directly corresponded to the strain gage locations. Strains for each layer in shell91 elements are available, therefore the outermost layers were chosen to best correspond with the gage locations on the outsides of the facesheets. FEA strains are denoted with the prefix 'n' before the strain location (i.e., nA corresponds to strain gage location ,A). FEA validation was ultimately determined by quantitative and qualitative correlation with experimental data. On the quantitative level, the same critical buckling determination methods were used on the nonlinear FEA as the experimental models to acquire hard numbers. Qualitatively, comparisons were made by simply overlaying the FEA load-strain plots onto the experimental plots.

Chapter 5

NUMERICAL MODELING STUDIES

Several numerical studies were performed to insure convergent models, study differences in different modeling techniques, determine the necessity of modeling certain structures or parameters, and obtain results for buckling techniques which may not be feasible for more complicated models. Several interesting and unexpected results for simple, common modeling parameters are identified.

Statistical Analysis of the Random Perturbation Method

The random perturbation method yields a unique solution for each case because each model has a slightly different and unique original shape. The question then arises, how much confidence can be placed on a single solution? Twenty cases were solved using the same deck, hence all parameters were held constant: (0/45/0/b3/8)s, ideal SSSS, 45.7 x 45.7 cm, 18x18 element grid, rp = hc/50. This model was considered mesh and perturbation size convergent (see next two sections). Figure 5-1 is a load versus out of plane deflection plot (LOD) compiling all 20 runs. It can be quickly observed that all but two of the runs behaved similarly. The similar eighteen all buckled in the mode one shape with an average critical buckling load (strain reversal) of 82.1 kN and a standard deviation of 3.03 kN (3.69%). Mode 1 was also the critical eigen-buckling mode, with a stability load of 88.1 kN. Therefore, nonlinear models using the random perturbation method tend to yield strain reversal loads more conservative than linear eigenbuckling models (shown to be true throughout the study of various panel parameters). To statistically study the postbuckling response, two other buckling related loads were also taken from the runs; the load where tension first occurs on the convex face and where the center node deflects out of plane one sandwich thickness (12.7 mm). The standard deviation drops as the model buckles through these two points from 1.75 kN (1.82%) to 0.93 kN (0.91%). This implies that critical buckling is more sensitive to the random perturbation than the early postbuckling response.

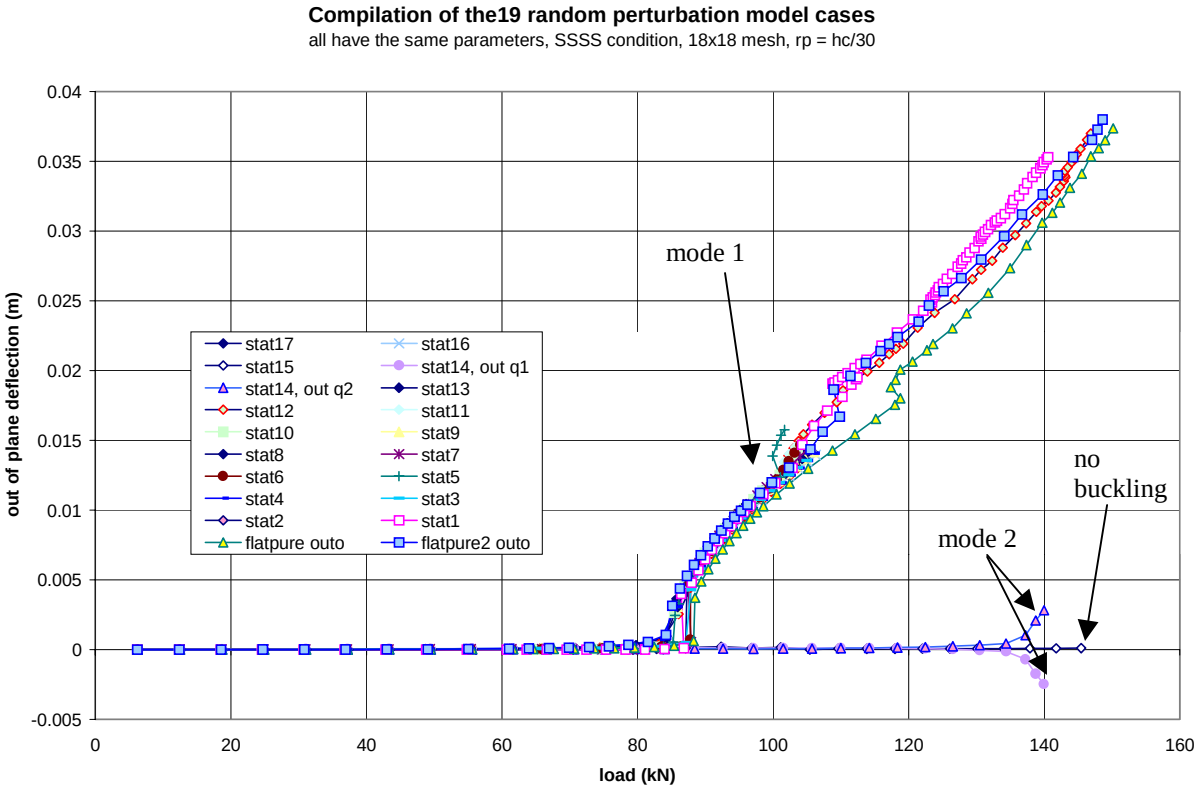

Figure 5-1. statistical case study of the random perturbation method (the only difference between the cases are their original unique perturbed shapes)

Closer inspection of the knee of the LOD plot shows two general types of responses, the 'smooth' and the 'load drop' types. These two types are shown in Figure 5-2, which is a magnified view of Figure 5-1, around the knee area, and with only eight runs for clarity. Four of the 18 mode one responses experienced drops in load, coinciding with the final development of the buckled shape. These four immediately snap back to the convergent early postbuckling response. This type of response is indicative of a non-convergent (too small) perturbation size. In fact, the perturbation study section shows that this perturbation size, although the largest possible for 18x18 element panels, is balanced between full and non-convergence. Since this phenomenon is confined to this type of numerical analysis, it has been termed numerical 'pop-in' buckling to differentiate it from true snap-through buckling behavior. If the responses are grouped into the smooth (convergent) and numerical pop-in (non-convergent), they have critical buckling loads and standard deviations of 80.8 kN (1.76 kN, 2.17%) and 87.2 kN (0.69 kN, 0.8%) repsectively. Any model which experiences a load drop around the critical buckling region tends to predict a critical buckling load slightly higher than a converged model (early estimate of about10% higher).

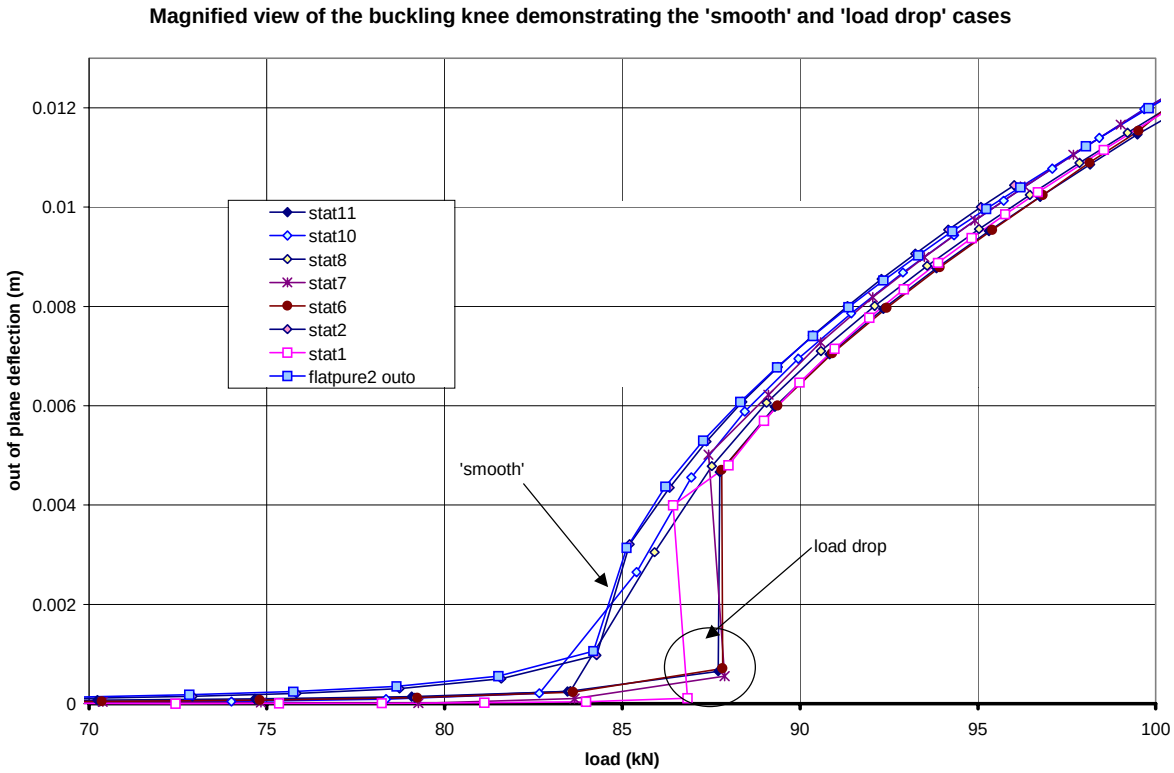

Figure 5-2. magnified view of the buckling knees for several statistical study cases to exhibiting the 'smooth' knee and 'load drop' responses.

The four cases run deep into postbuckling start to diverge somewhere after one thickness out of plane deflection. Often the divergence starts with a subtle mode shape shift and a slight load drop. In these four cases the symmetric mode one shape shifted slightly towards one corner, creating a asymmetric mode shape. An example of such a mode shift is shown in Figure 5-3. These mode shifts occurred only for models with sandwich modeling, and therefore the transverse shear in the core is a factor in their causation. The mode shifts did not occur for models with isotropic facesheets (although rippling did, see p.73). Therefore the orthotropic properties and layer orientation of the composite facesheets tended to influence the core transverse shear, and the combination caused the shift.

While more divergent than the consistent early postbuckling response, the late postbuckling response of these panels all follow similar paths and can be considered convergent. If the analyst wishes to study deep postbuckling responses, though, this study suggests running several cases because the random perturbation technique does have some divergence with flat SSSS panels, and may experience wider divergence with a more complicated structure.

The two responses not mentioned so far are the aberrant mode2 and non-buckled responses of runs 14 and 15. As mentioned earlier, the perturbation size used here is not always convergent, as shown in the load drop cases. Occasionally, the random deformations of these models are either too small or actually combat the development of a mode one shape around the first stability load (eigenbuckling). In these cases, if the load becomes sufficiently higher than the critical load, the original (straight) shape remains stable until another stability load is reached. Run 14 reached the second stability load and developed the corresponding mode shape, mode two. Once again, this nonlinear technique predicts buckling lower than the linear one, 130.8 kN versus 138.6 kN respectively. Run 15, however, passed the second stability point too and will reach the third at 178 kN. If a nonlinear structural model using the random perturbation technique develops a mode shape that seems unlikely or is well above the linear critical buckling load, another case run is required to confirm the response. Thus, it is important to first obtain the linear eigenbucking load for the first mode.

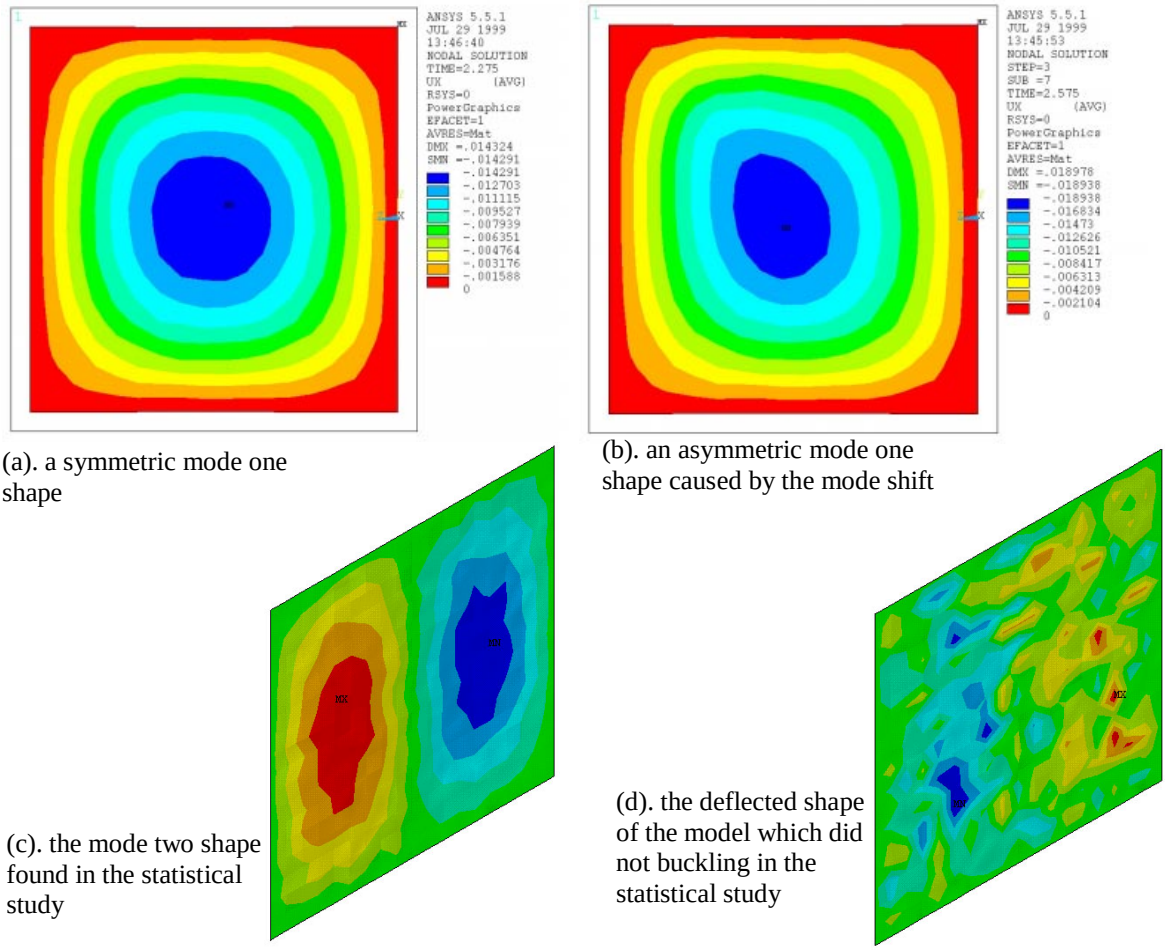

(a). a symmetric mode one shape

(b). an asymmetric mode one shape caused by the mode shift

(c). the mode two shape found in the statistical study

(d). the deflected shape of the model which did not buckling in the statistical study

Figure 5-3. examples of the buckling mode shapes for the random perturbation models (contours are of the out of plane deflection)

Mesh Convergence Study

Often, large structural models use relatively coarse meshes the buckling analysis. The mesh convergence study was performed to both confirm that the results stated in the present study are valid, and to give the analyst modeling large structures the number of elements per buckling wave required to yield good results. The mesh convergence and perturbation convergence studies were performed in parallel before the statistical study. Mesh convergence studies were performed separately for the eigenbuckling, moment perturbation method and the random nodal displacement method. The nonlinear methods used convergent perturbation sizes (next section). Five different element grids were used for each analytical method. The results from these studies are tabulated in Tables 5.1 & 5.2, and plotted in Figures 5-4 & 5-5.

Table 5.1. Mesh dependence of critical buckling for three analytical methods

element grid	linear stability loads (kN) mode 1	mode 2	nonlinear critical buckling loads (kN) moment	random
2x2	88.83	157.3		
6x6	88.42	138.8	75.5	83.4
9x9			75.8*	88.9*
12x12	88.41	138.6	75.4	84.4
18x18			75.4	79.8
24x24	88.41	138.6	75.4	82.0

* not evaluated at center of panel due to an odd numbered grid, therefor results tend to be slightly high

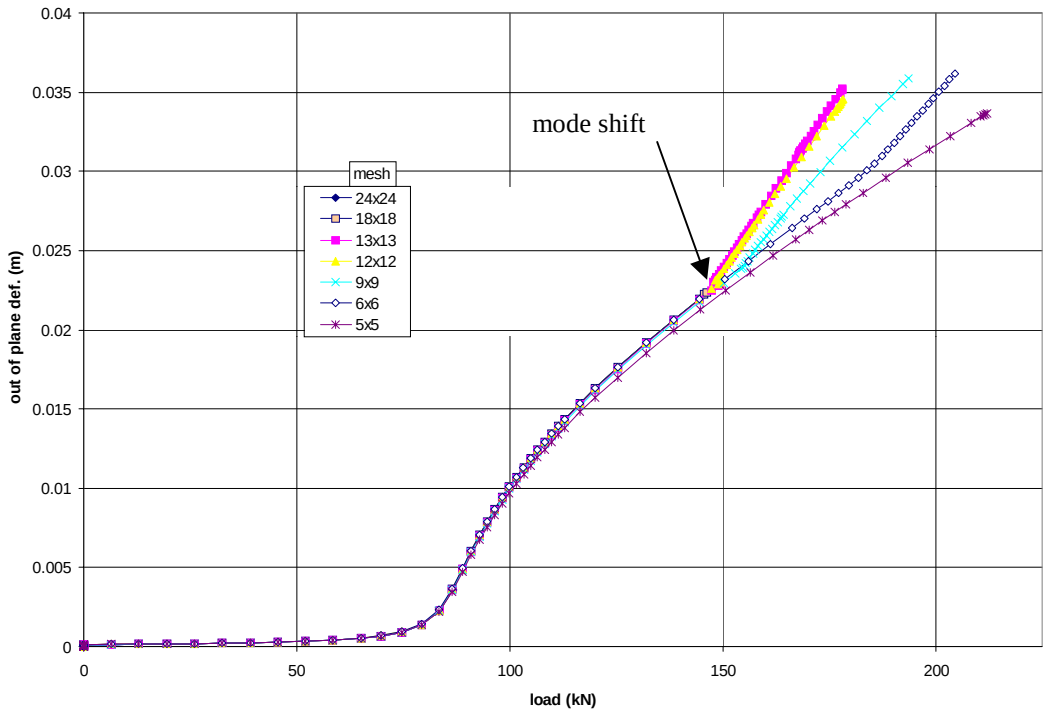

Figure 5-4. the mesh convergence study for a moment perturbation, ideal SSSS model

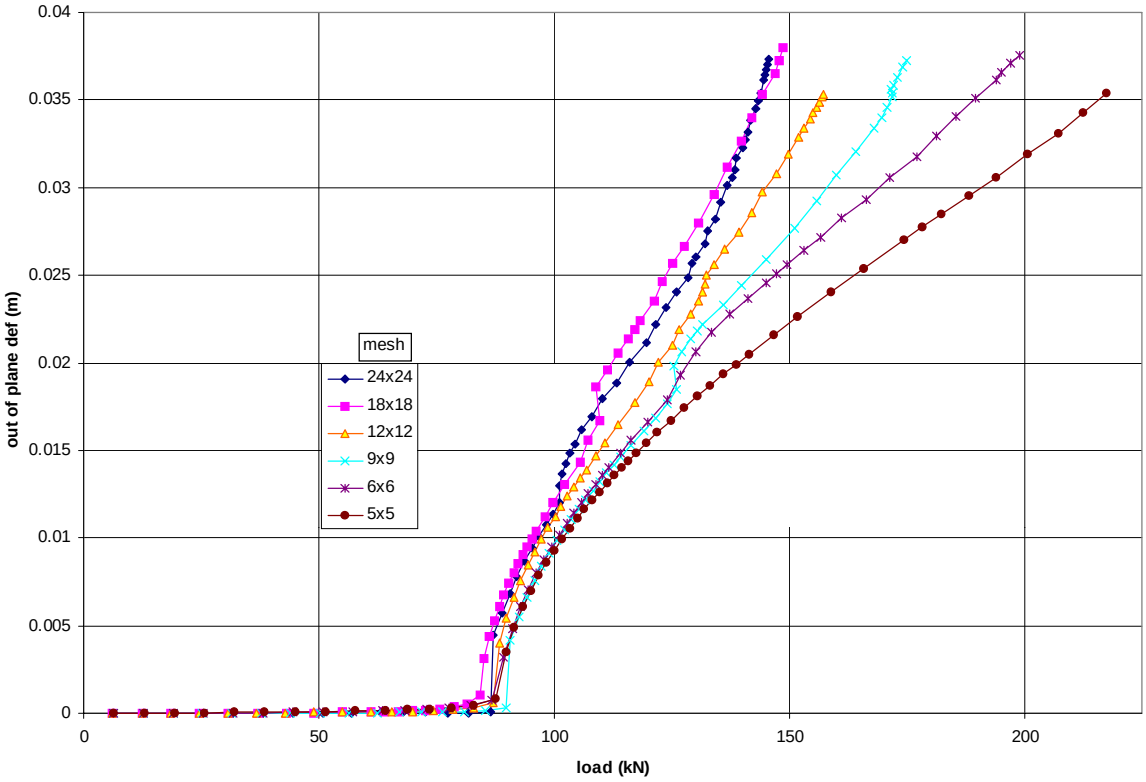

Figure 5-5. mesh convergence study for the random perturbation method (with ideal SSSS, B-series panels)

Eigenbuckling is very insensitive to mesh size. A 2x2 grid yields results within 0.5% of the very fine mesh of 24x24. For such a simple case as buckling of a flat sandwich panel, any grid size with at least two elements per half (sine) wave will give good results. At least three per wave will give convergent results (from mode 2, 6x6 grid). Convergent nonlinear methods, using the strain reversal critical buckling technique, give conservative results as compared to linear stability results. For this simple case, the random perturbation technique gives critical buckling loads 10% lower than eigenbuckling. Even relatively coarse nonconvergent mesh sizes give results on the order of 1% conservative.

Table 5.2. Mesh dependence of nonlinear buckling and postbuckling loads

element grid	moment method buckling loads pmy (Nm)	reversal (kN)	tension (kN)	1 thickness	random method buckling loads rp (m)	reversal (kN)	tension (kN)	1 thickness
5x5						85.8	108.1	109.9
6x6	20	75.5	101.6	107.4	hc/30	83.4	99.0	107.7
9x9	20	75.8*	101.3*	107.9*	hc/30	88.9*	104.2*	108.2
12x12	20	75.4	99.1	107.4	hc/30	84.4	96.0	103.7
18x18	20	75.4	98.9	107.4	hc/45	79.8	94.0	101.5
24x24	20	75.4	98.9	107.4	hc/100	82.0	93.7	101.1

* not evaluated at center of panel due to an odd numbered grid, therefor results tend to be slightly high

The moment perturbation method is very consistent and relatively independent of mesh size, with a 6x6 grid yielding acceptable results for critical buckling. The full LOD responses are shown in Figure 5-4. The early and middle postbuckling response is also very consistent. Differences only arise between the meshes deep into postbuckling where a mode shift occurs, with the finer meshes shifting earlier and into more compliant responses. Overall, the moment perturbation method is very independent of mesh sizes with 6x6 more than adequate to predict responses well into postbuckling.

The random perturbation method is relatively mesh independent. The results in Table 5.2 are not as straightforward as in Table 5.1 for the moment method. First, the odd 9x9 grid yields relatively high results due offcenter nodal evaluations. The 24x24 grid cannot use a fully convergent perturbation size, and so experiences a load drop and correspondingly slightly higher critical buckling load. The convergent mesh size is an 18x18 grid with a critical buckling load of 79.8 kN. However, results which are conservative of the eigenbuckling load of 88.4 kN are possible with grids as small as 5x5.

The random perturbation method becomes more mesh dependent as the panel buckles further into the postbuckling range. The full LOD responses are shown in Figure 5-5. Examination of this figure, and the postbuckling loads in Table 5.2 show a definite direct relationship between mesh density and more compliant responses. The 18 and 24 element grids seem to have reached a convergent response, as they closely mirror each other. The 12x12 remains close to this convergent response, while the deep postbuckling response of 6x6 meshes and below are significantly stiffer. All grids but the very coarse (5 and below) undergo a modal shift, and more compliant response, just above the one thickness out of plane deflection region. Relatively coarse meshes (5 to 12 grids) can effectively model critical buckling and early postbuckling while deep postbuckling or highly accurate critical buckling predictions require fine meshes (18 or more element grids).

With a moment of 20 Nm along one edge, the moment method gives lower critical buckling loads (for convergent models, see next section) and much smoother ‘knees’. The moment method also yields much stiffer postbuckling responses that the random method due to its still smooth geometry. The very coarse mesh (5x5) random method postbuckling response follows the same path as the moment method responses until their modal shifts. The early postbuckling responses of both methods, all element grids, are very similar in the half thickness out of plane deflection range.

Two other small mesh convergence studies were performed to see gross effects of mesh on panels with more complicated structural aspects. First, a panel with an aspect ratio of 3:1 (137.1 x 45.7 cm) was modeled. The in plane deflection results were divided by 3 to make direct comparisons with aspect ratio 1:1 panels. These psuedo-normal results are plotted in Figure 5-6. The panel buckled in the expected mode three shape, and seems to follow the same trends found with the aspect ratio one panels.

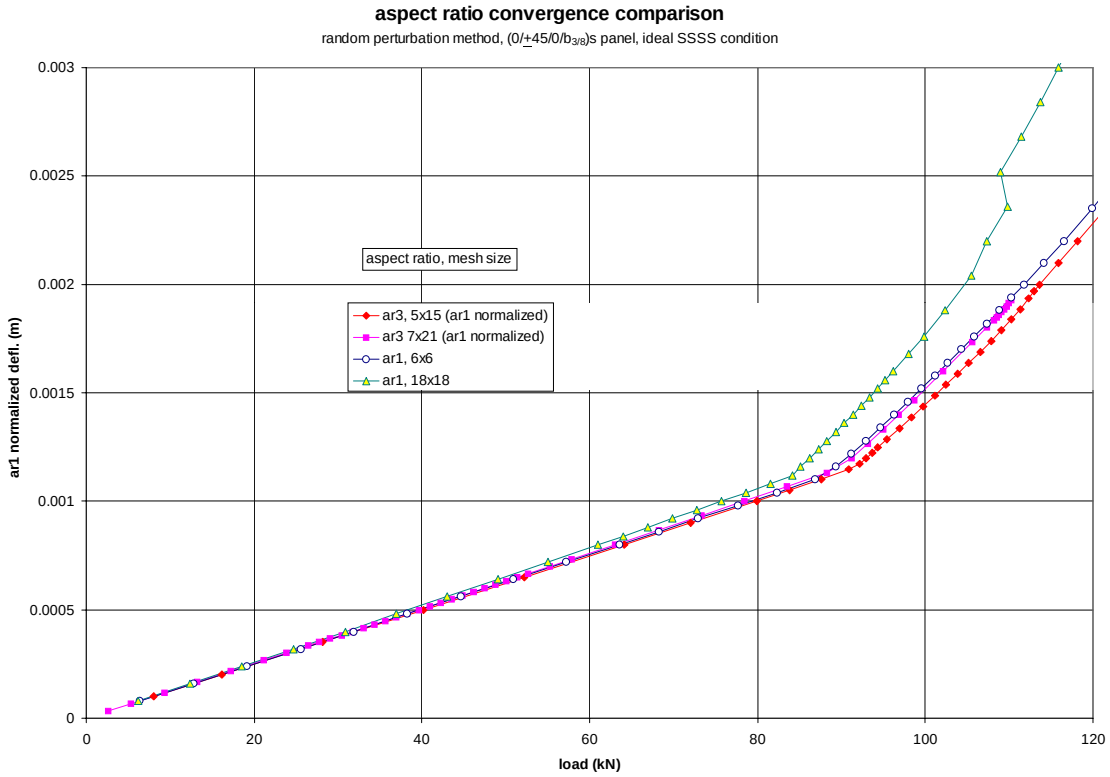

Figure 5-6. effect of aspect ratio on the mesh dependence of ideal SSSS panels

Curved panel mesh dependence was also studied with the 23p series panels. Two element grids were studied, 7x8 and 17x18, for the nonlinear analyses, while five meshes were studied with linear stability analyses. The linear mesh study produced some interesting results. The critical buckling loads are tabulated below for all three methods in Table 5.3. Due to the deep cylindrical curvature, more elements were required to obtain a converged solution. The 2x2 and 3x3 coarse meshes yielded good results which were only 3% and 1% away from convergence respectively. Between 4x4 and 15x16 the model is converged for the mode 1 stability load, which is also the critical buckling load. At the 16x17 grid the mode stability eigenvector disappears, or the eigenload suddenly becomes much greater. No mode 1 stability load is found within the first eight stability loads. Mode 2 now becomes the critical buckling load

predicted by FEA. Mode 2 was in convergence at the coarser meshes as well, and remains in convergence at 204.5 kN. This result defies common sense and engineering intuition. These results suggest that for curved sandwich shells, there is an upper limit to the number of elements per wave for linear eigenbuckling analyses. The sandwich option was turned off and the model run again for 16x17 and 24x25 grids. Both gave convergent mode 1 and 2 results, with 229 and 337 kN stability loads respectively, as the critical and second modes. The reason for the loss of mode 1 stability must therefore be tied into the sandwich option and its interaction with curved structures. The most likely culprit is the effect of transverse shear in the core, which is not present for the no sandwich option cases, which obey thin shell theory. The 17x18 grid nonlinear cases also gave mode 1 buckling shapes, so the problem is restricted to eigenbuckling analyses.

Table 5.3. A mesh convergence study for curved, ideal SSSS sandwich shells

	linear stability loads (kN)		nonlinear critical buckling loads (kN)		1 th. out of plane load (kN)	
element grid	mode 1	mode 2	moment	random	moment	random
2x2	160.5	223.5				
3x3	158.7	206.5				
4x4	157.1	205.0				
7x8			138.6	144.3	NA	173.1
12x13	156.6	204.5				
15x16	156.6	204.5				
16x17	NP	204.5				
17x18	NP	204.5	139.3	140.5	183.6	175.5

NP: not present

The LOD responses of these two models are shown in Figure 5-7. The critical buckling region of the curved panels seems less dependent on mesh size than for the flat panels, while the postbuckling response does seem to have mesh dependence. The 7x8 grid model undergoes a severe mode shift and load drop fairly early into the postbuckling response. The mode shifts from central symmetric mode one to a load end. The 17x18 grid does not shift modes and continues to develop mode one deformation throughout postbuckling. A load drop does occur very deep into postbuckling and corresponds to a mesh rippling effect. Both mode one shapes and mode shifts for each of the element grids are shown in Figure RIP found and explained in the core sensitivity section on page 68.

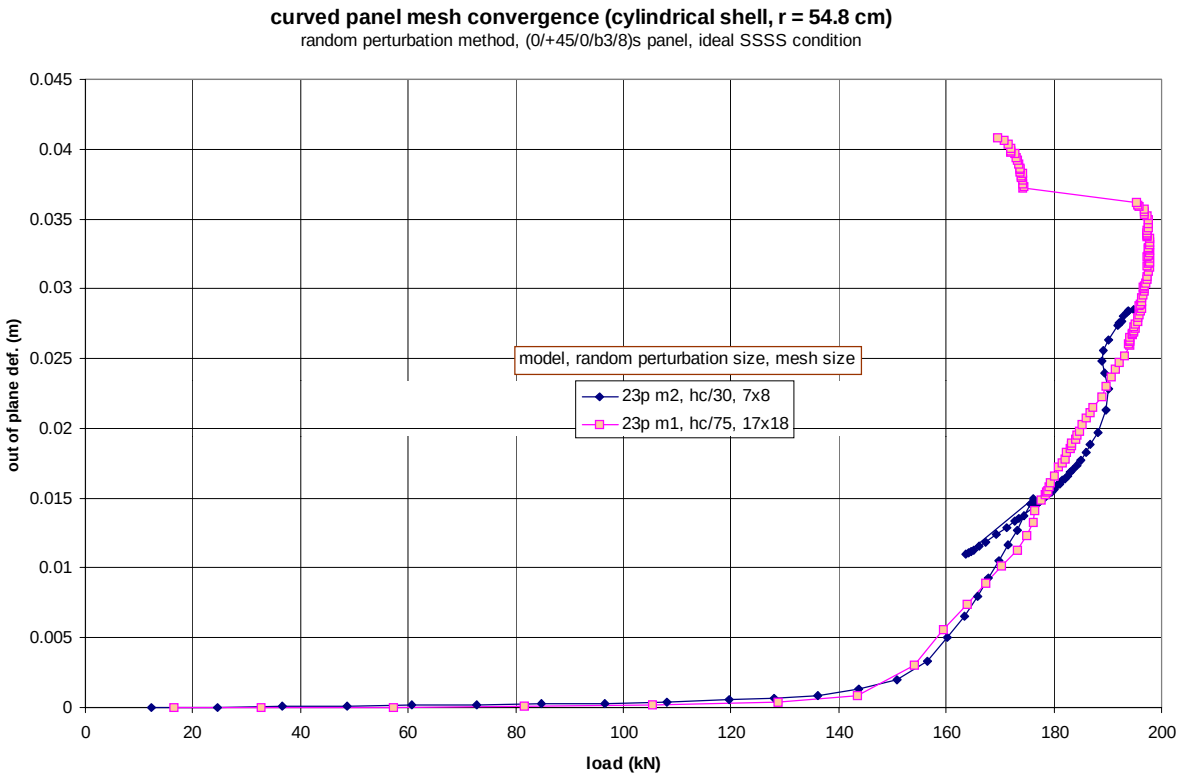

Figure 5-7. effect of panel curvature on the mesh dependence of random perturbation method, ideal SSSS panels

Perturbation Convergence Study

A perturbation convergence study was performed in parallel with the mesh convergence study. The 12x12 element grid was chosen for this study because it was nearly convergent for the random perturbation method and was convergent for the mesh independent moment method. The fully convergent models, 17x17 grids or greater, took up to a day to solve with the random perturbation method, and also proved to have local curvature errors with barely convergent perturbation sizes, which will be detailed in this section.

The results for each perturbation method are shown in Table 5.4. The three buckling loads used in the earlier studies are also used here. Columns in the random method which have ‘NS’ labels for buckling loads represent models which could not be solved due to their perturbation size. In this size range, it was

inevitable that at least one set of three neighbor nodes would have perturbations that caused a deep curvature locally, which exceeded the limit proscribed by the sandwich option. These perturbation-caused local curvature errors might also be present in smaller perturbation sizes as well.

Table 5.4. perturbation size convergence study for the random and moment perturbation methods.

moment perturbation models					random perturbation models				
pert. size		buckling data loads (kN)			pert. size		buckling data loads (kN)		
pmy (N-m)	mode	reversal	tension	1 thickness	**rp**	mode	reversal	tension	1 th.
0.005	1	87.2	100.5	108.4	hc/20		NS		
0.2	1	81.1	100.5	108.4	hc/30	1	84.4	96.0	103.7
1	1	80.9	100.5	108.4	hc/30	1	77.8	NA	
20	1	75.4	99.1	107.4	hc/50	1	88.5	NA	
50	1	70.0	96.9	105.9	hc/100	1	84.0	97.9	104.5
100	1	NA			hc/200	1	84.7	101.5	107.3
					hc/1000	1	114.2	114.2	108.0
					hc/1000	2	144.6	172.5	NA

The LOD plots for each of the cases listed above are shown in Figures 5-8 and 5-9 according to their perturbation type. From Table 5.4 and Figure 5-8 it is clear that the moment size influences the critical buckling load greatly. The greater the moment, the lower the critical buckling load and the more gradual the critical buckling knee. Moments which are very large, in this case 100 Nm and above, cause convergence problems by creating large out of plane displacements within the linear response, well before critical buckling. If the model reaches critical buckling, the moment method response paths will converge somewhere in the postbuckling region. The lower the perturbation, the earlier the path will converge. A great majority, from 20 to 0.005 N,m converge in the early postbuckling response, usually within one thickness out of plane deflection. No load-drop or snap-through buckling responses were found for the moment method models, although such a response might exist below a 0.005 Nm edge moment which had a very sharp, almost vertical knee.

The random nodal displacement perturbation method has a more complicated size sensitivity than the moment method. Two very distinct response paths that the model may follow are revealed in Figure 5-9. The model may buckle smoothly around the critical buckling region or may pass it and remain in the ‘straight’ shape until numerical pop-in back to a mode one response, or smoothly into a higher mode shape. The likelihood of remaining straight, past the critical buckling region is directly proportional to the

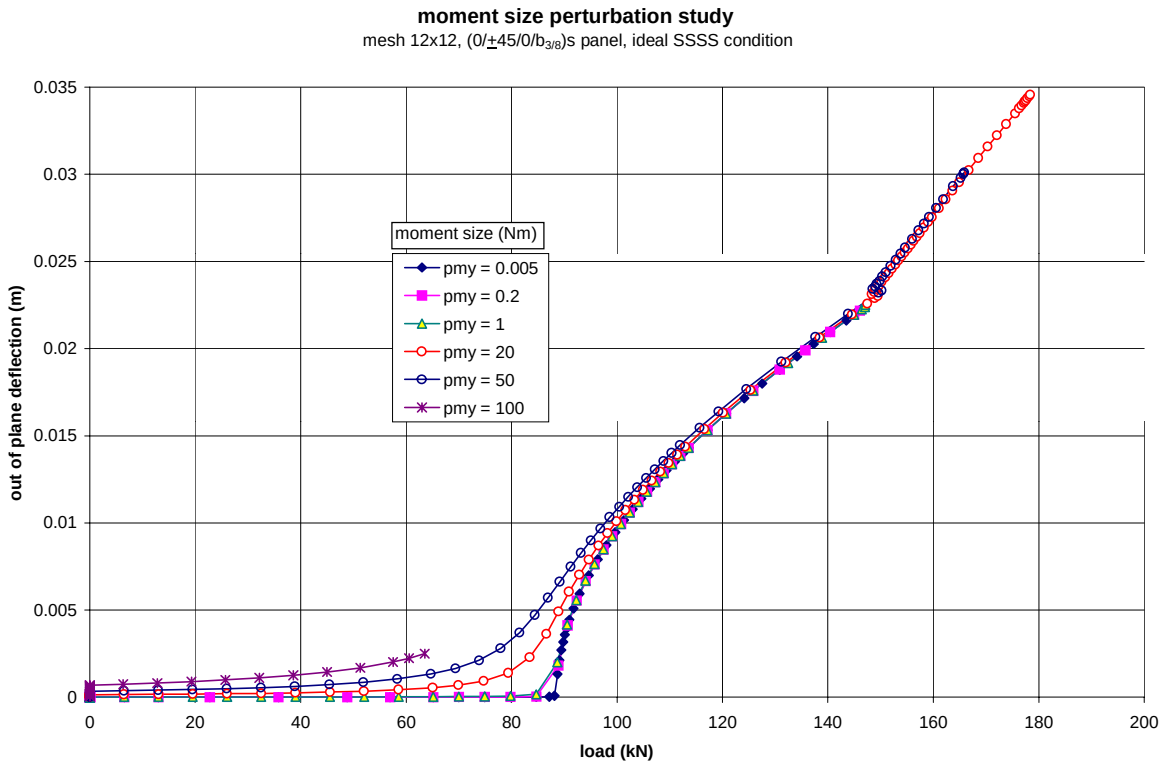

Figure 5-8. moment size perturbation study

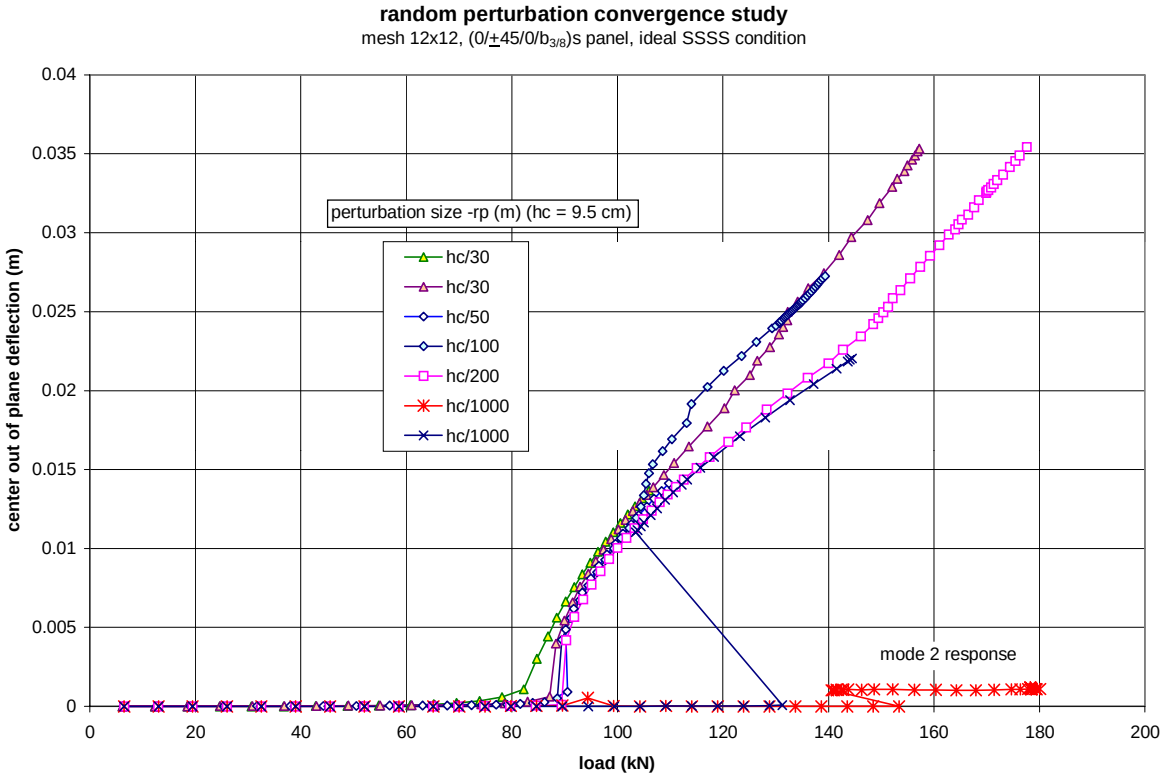

Figure 5-9. random perturbation size convergence study

perturbation size. In these cases, all sizes buckled smoothly into mode one except the very small, hc/1000 displacement size. One model snapped back into a mode one shape at about 130 kN. It immediately followed a convergent postbuckling path from just under one thickness out of plane deflection. The other hc/1000 model appropriately assumed a mode 2 shape at the second stability load. Due to the uniqueness of each perturbed shape, any size perturbation may cause the load drop phenomenon. However, the probability of this phenomenon occurring relates to the perturbation size. The statistical survey was run with a perturbation size of hc/50 and of the 20 runs, six experienced load drop or a higher mode shape. Meanwhile, over the course of this study 10 to 20 hc/30 size cases were solved and none experienced a load drop.

Among the convergent (smooth) critical buckling cases a slight perturbation size trend was found. The smaller perturbations usually had slightly higher critical buckling loads than the largest sizes. However, the scatter found due to the uniqueness of each solution was of the same order. Therefore, the analyst should use the largest possible perturbation size to assure the most conservative critical buckling loads (this was done in the present study). However, any perturbation method model which experiences a smooth critical buckling knee gives good results.

Perturbation size also has an effect upon the postbuckling response path. The larger the perturbation size the more compliant the postbuckling response. At one out of plane thickness the hc/30 load is 4% lower than the hc/1000 case load. The hc/1000 load is within 1% of the moment method load and the path of the hc/1000 case is very smooth. This is very similar to the smooth moment method responses. In contrast, the hc/30 and hc/100 cases experience a mode shift around one thickness out of plane deflection, resulting in a more compliant and ‘bumpy’ path. Like the critical buckling knee, the probability and location of a mode shift is influenced by the size of the perturbation, but a scatter band also occurs due to the uniqueness of each original shape (see the statistical survey section).

Perturbation size also affects models through effective stiffness changes. Table 5.4 tabulates the effective panel stiffness for each of the cases in the perturbation study. Each stiffness was calculated at 0.8 mm in-plane deflection of the loaded edge which lies within the linear response. As the perturbation size increases, the effective stiffness will drop. This is due to the greater amount of out of plane deflection, in

each element, in the linear range, which must be reacted out, thereby dropping the stiffness. The cases converge at the smaller perturbations at 81.4 GN/m, which is the expected panel stiffness calculated by classical lamination theory. The random perturbation method affects the effective stiffness more, with a 7% drop in stiffness. For the random method, the effective stiffness drop is also a function of the mesh size and uniqueness of each model. The mesh effect is shown by the 18x18 mesh, hc/45 case (used in the mesh study) which has an effective stiffness of 76.3 GN/m.

Table 5.4. the effective stiffness of each panel in the perturbation study, calculated at 0.8 mm load deflection.

pmy	stiffness (GN/m)	**rp**	stiffness (GN/m)
100	79.4	hc/30	76.0
50	80.8	hc/30	76.2
20	81.3	hc/50	78.8
1	81.4	hc/100	80.8
0.02	81.4	hc/200	81.3
0.005	81.4	hc/1000	81.4
		hc/1000	81.4

Damage Modeling

An easily implemented method for monitoring and modeling damage for the nonlinear models was sought. The method developed could monitor for, and then apply damage and failure zones in the facesheets and core for common CLT layer by layer failures. The shell91 and shell99 elements in Ansys can check for material failures in each element, layer by layer, and for each solution step. It uses the common CLT failure theories of maximum strain, maximum stress and Tsai-Wu. Three user defined failure criteria can also be coded and then used with similar procedures. Each material can have its maximum stress or strain defined in its material property data set. The failure criteria are output as ratios with a value greater than one signifying a failure. The resulting data set can be output in several ways, but to fully check the model, the highest ratio is output for each element, with its corresponding layer, for each solution step. The large data set must then be perused manually in a text format and the failed elements marked. The elements must then be checked for the exact failure type and direction.

Once damage has been found, a second model is generated which has the exact same parameters but loaded at a different rate and the damage modeled. The failed element layers are given a specific temperature at the correct load step. The material properties may be input as a function of temperature,

thereby allowing a second (or more) reduced/damaged property set to be defined. Temperature serves as a dummy variable which triggers the damaged property set to be used in the subsequent solution. This process is iterated until a catastrophic failure occurs.

This damage modeling method was implemented on a test model. A flat, 46 x 46 cm, $(0/\pm45/0/b_{3/8})s$, SSSS panel was modeled using the moment perturbation method. The model was not used as a predictive model of the experimental tests because it did not model the fixture (see fixture modeling section, this chapter). Two damage iterations were solved before a final catastrophic failure was found, fiber failure in the 0 degree layers along the length of the sides. The three resulting LOD plots are compiled together in Figure 5-10. The first damage zone is shown as the contour plot, and results in the first load drop and middle postbuckling response path. The second damage zone expanded the first slightly and dropped the response to the most compliant response path. The models took several days to solve and the three damage monitoring sessions each took around two hours of analysis. At this present stage of evolution, this damage modeling method is rather clumsy and unsophisticated.

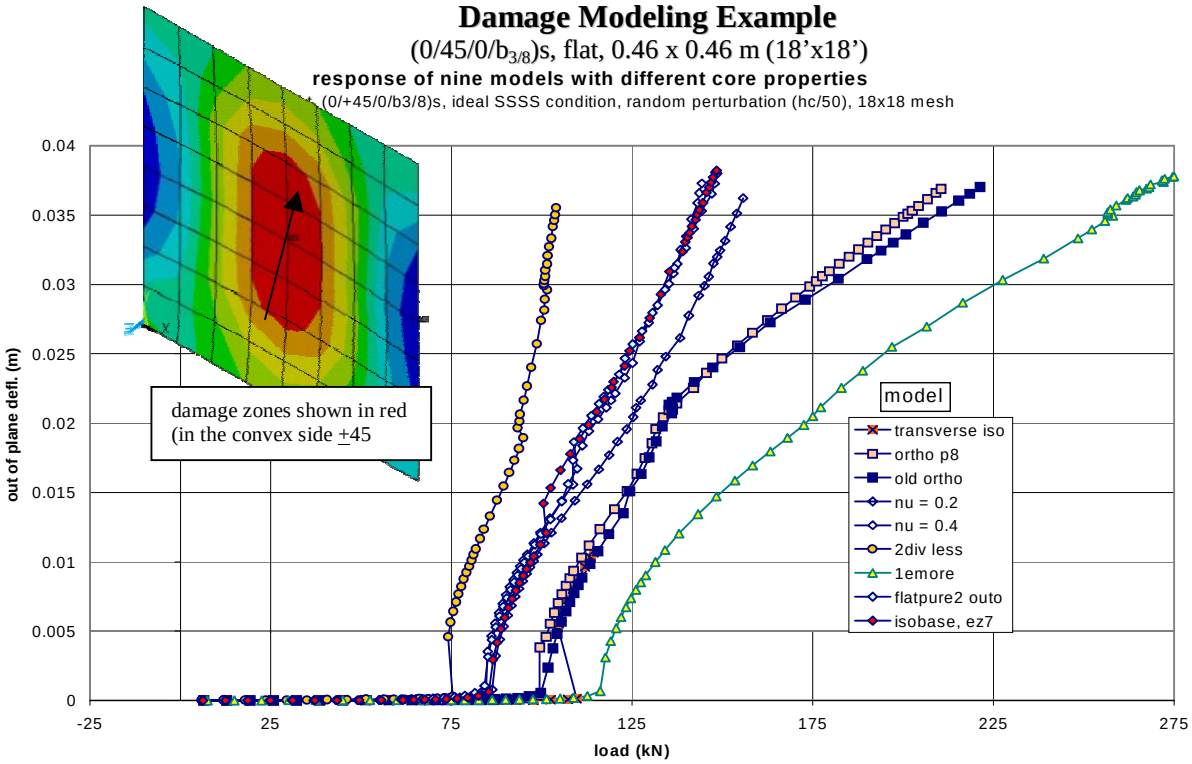

Figure 5-10. example of a damaged FE panel and the response changes (notice that the x-y axis have been flipped from the ordinates used normally in the present study)

Another serious problem is its portability to structural buckling models which require the use of the random perturbation method. The difficulty using this damage modeling method with the random perturbation method is demonstrated in Figure 5-11. The contour plot on the left shows the local, x strain distribution for layer one. The nodal strains deviate greatly within an element and are often discontinuous across elements. The strain discontinuities are directly caused by the random out of plane nodal displacements. The maximum and minimum strains at this solution step even occur within the same element. These discontinuities are present even when the deformed shape appears to be a smooth, regular mode shape. The right contour plot is an out of plane deflection plot for this model at the same solution step as the strain plot. Since it is these strains that determine the failure of an element layer, it is clear that the random perturbations would cause serious problems with the prediction of damage zones. For these two reasons, the damage modeling method was left to be developed by others as future work.

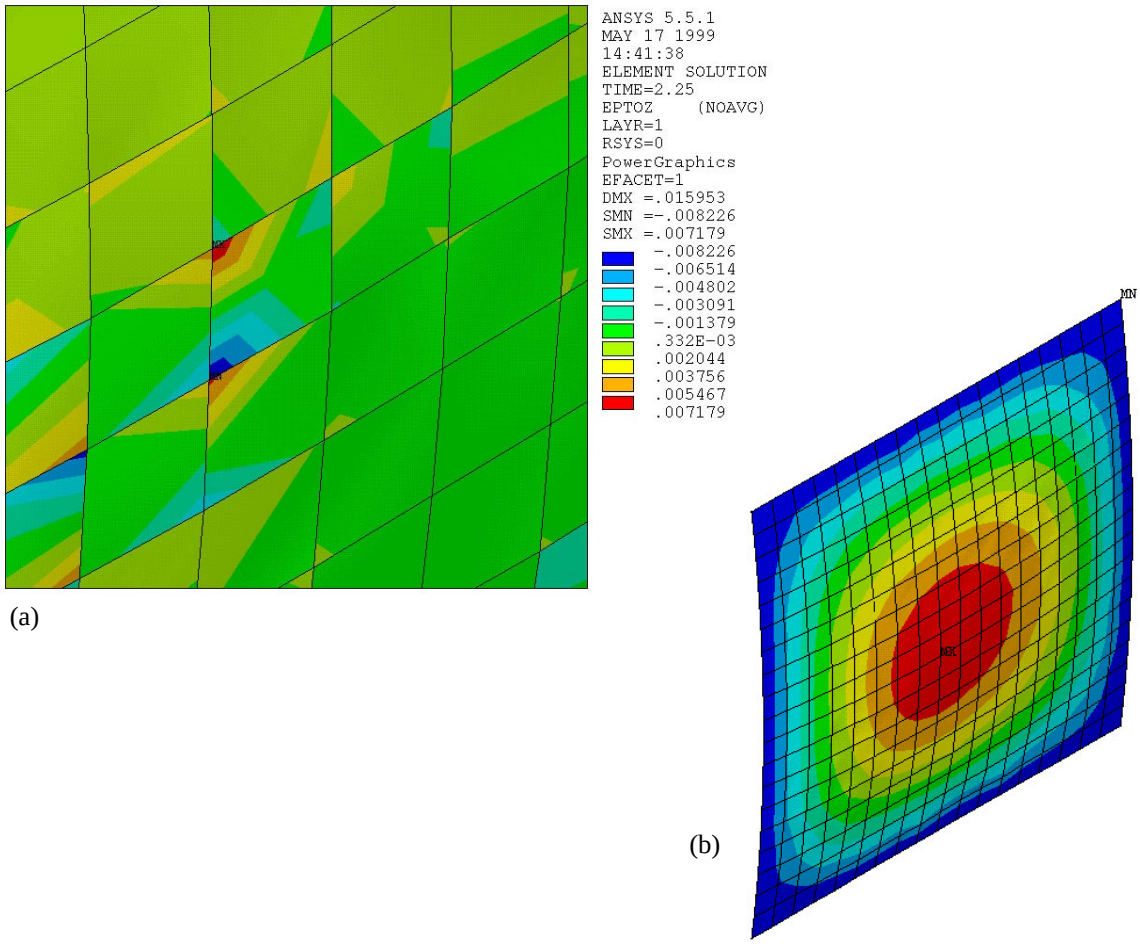

Figure 5-11. Example of the difficulty using the random perturbation method and element failure damage modeling. (a) close-up view of the nodal strains (b) out of plane deflection plot of the same model (and same time)

Effect of Sandwich Modeling

The effect of the sandwich modeling option was studied for both flat and curved panels. The results were predictable: the critical buckling loads increased from 25 to 40% with the postbuckling response diverging even more from these values. The critical buckling load increases for eight nonlinear (0/±45/0/b3/8)s panels are compiled in Table 5.6. Six of those models are plotted together in Figure 5-12 (response with shaded markers represent the models using the sandwich option). The modeling of the sandwich option (and the resulting effect of transverse shear upon the response) is most noticeable in the postbuckling responses of the deeply curved panels (23p). Those with the sandwich modeling have either barely stable (almost neutral) or unstable response types, while those without have stiff, stable responses. It is interesting to note that the models without the sandwich modeling also undergo a late postbuckling mode shift (suggested by a small load drop and path change, confirmed by inspection of the deformed shapes). Unlike many of the curved models, the mode shift did not correspond with a mesh rippling behavior, but instead a corner shift more like that found in the flat models.

Table 5.6. the effect of sandwich modeling upon the critical buckling load

	critical buckling load increase (%)		
	flat	shallow curved (70p)	deeply curved (23p)
ideal models	-	28	39
fixture models	32	-	26

The effect of sandwich modeling upon the mode shapes can be seen in Figure 5-13 parts (a) –(c). These figures are axial normal out of plane deflection plots, essentially central cross sections which have been normalized to a maximum value of one to compare shapes across models and solution steps. All shapes are from $(0/45/0/b_{3/8})s$ random perturbation nonlinear models: (a) are from flat panel models with and without sandwich modeling, (b)- shallow curved ‘no sandwich’ models, (c)- shallow curved models with sandwich modeling. The ‘no sandwich’ model in part (a) can be seen to almost exactly mirror the sample sine wave. The various sandwich modeled deformed shapes can be seen to be either shifted (t = 1.5,2) or sharper (t = 4). The shallow curved panels show that the ‘no sandwich’ models keep the nearly perfect sine wave shape once fully buckled (the random perturbations overcome). While in (c), the sandwich modeling seems to shift and broaden the buckling shape at its wave crest.

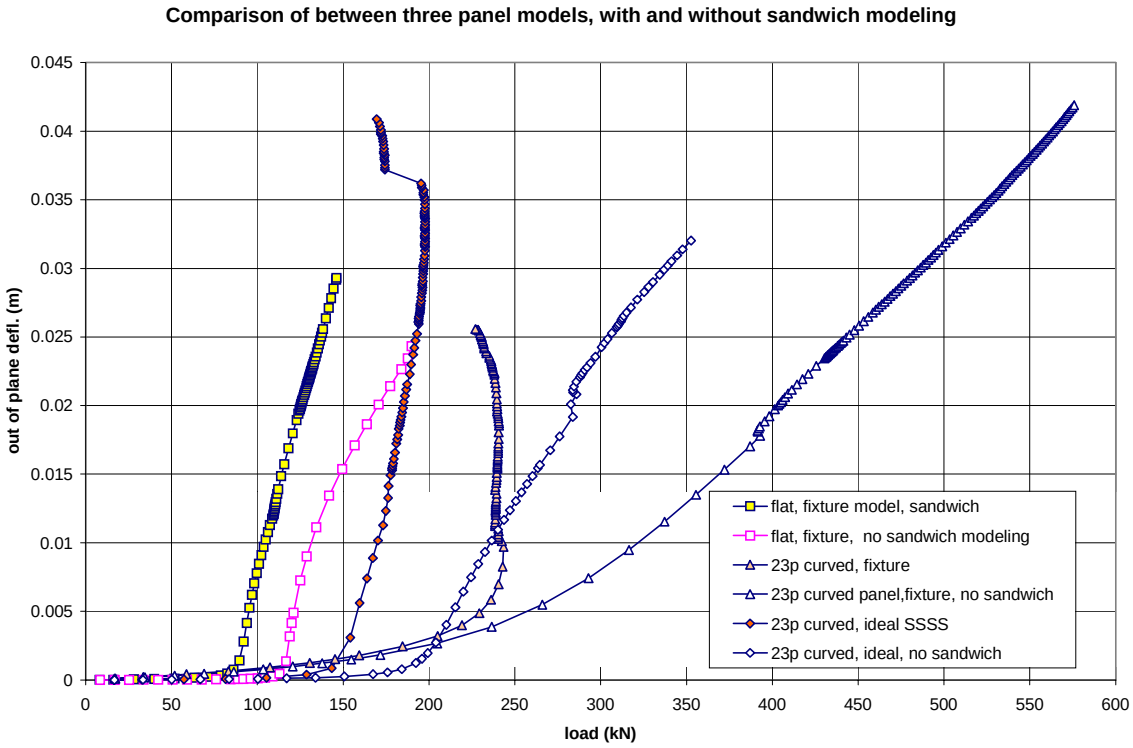

Figure 5-12. the effect of sandwich modeling demonstrated by three panel models

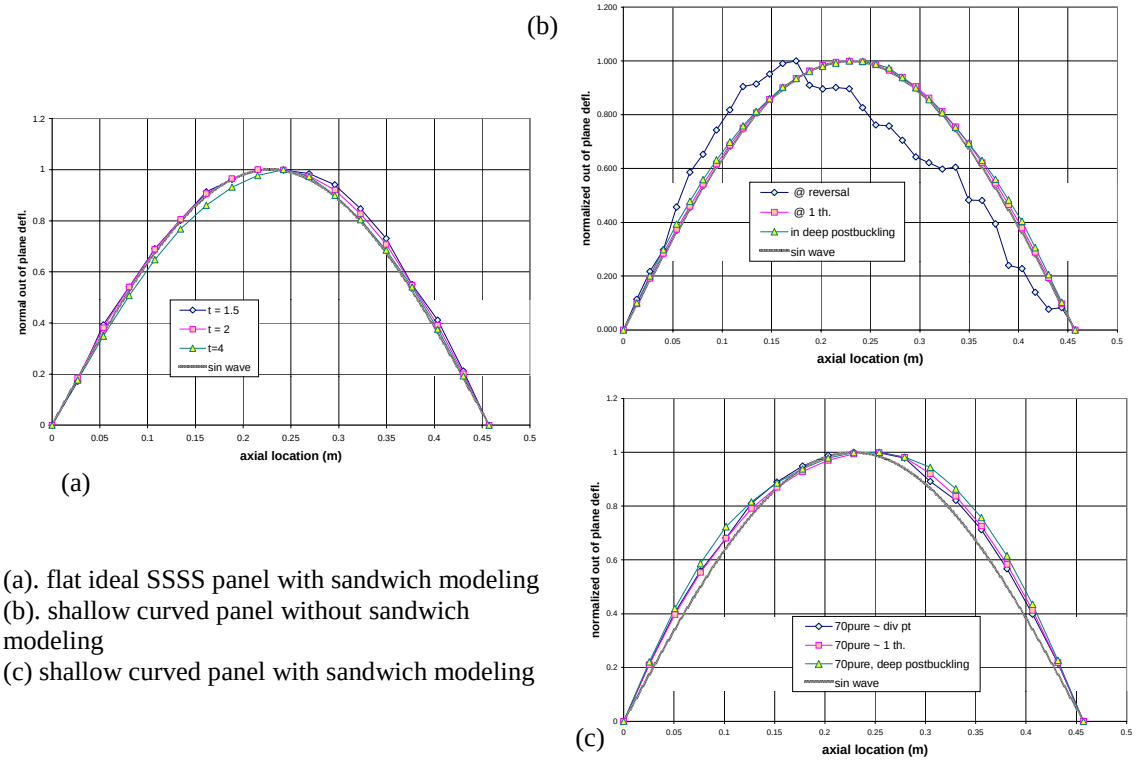

(a). flat ideal SSSS panel with sandwich modeling
(b). shallow curved panel without sandwich modeling
(c) shallow curved panel with sandwich modeling

Figure 5-13. effect of sandwich modeling on buckling axial buckling shapes

Core Property Sensitivity Study

As mentioned in chapter 4, the balsa data sets were contradictory and therefore a sensitivity study was initiated. The three base property sets used are shown below in Table 5.7. Nonlinear solutions were performed upon these three sets. Nonlinear models were chosen so that the postbuckling response could also be studied along with critical buckling. The models were all random perturbation, flat, (0/45/0/b3/8)s, ideal SSSS models, with 17x17 meshes and random perturbation sizes of hc/50. Other models were also solved which had core properties based upon one of the three sets. The numerical results from all of the models are shown in Table 5.8. The qualitative analysis of the models is derived from the combined LOD plot of these models which is found here as Figure 5-14.

Table 5.7. the base core material properties used in the FEA analyses

	elastic moduli (GPa)			Poissons ratios			shear moduli (GPa)		
balsa	Ex	Ey	Ez	Prxy	Pryz	PRxz	Gxy	Gyz	Gxz
isotropic	0.148			0.300				0.0569	
orthotropic	0.187	0.061	4.07	0.67	0.01	0.02	0.0203	0.150	0.220
transversely iso.	0.148	0.148	4.07	0.67	0.02	0.02	0.0203	0.200	0.200

Table 5.8. FEA results for three core property base sets and parametric changes

model name	core base	property change	stiffness (N/m)	critical buckling (reversal) , (kN)
iso base	isotropic	none	76.3 e6	80.8 $\pm$ 1.8
nu 0.4	"	G = 52.8 MPa	76.6 e6	81.3
nu 0.2	"	G = 61.7 MPa	77.7 e6	83.5
div2less	"	E = 74 MPa G = 28.5 MPa	74.4 e6	74.6
1eless	"	E = 14.8 MPa G = 5.69 MPa	58.3 e6	none, localized buckling
1emore	"	E = 1480 MPa G = 569 MPa	93.7 e6	111
EZ7	"	E = 14.8 MPa G no change	77.0 e6	82.8
ortho	orthotropic	none	80.5 e6	97.3
ortho p8	"	all properties at 80%	80.2 e6	97.2
transverse iso	trans. iso.	none	80.0 e6	load drop

The transverse shear modulus was expected to be the most influential material property and was tracked through the various changed models. From four of the isotropic models (the base, nu 0.2, nu 0.4,

and ez7), the two orthotropic models,, and the transversely isotropic model two results are drawn which are most clearly seen when looking at Figure 5-14. Predictably, higher transverse shear moduli will increase the buckling load, but the results are only sensitive on levels of whole factor differences. The four isotropic balsa models all follow very similar postbuckling response even though their shear moduli vary by up to 16%. The orthotropic balsa set has transverse moduli which are 3-4 times greater than the isotropic values, and produce critical buckling loads 20% higher. The div2less model has a property set which is exactly half of the base set, and has a critical buckling load only 7% lower. These results suggest that for accurate critical buckling conditions, only approximate material properties (within 30%) are required. For core properties an order of magnitude high, the critical buckling load is 40% high, which, although not acceptable, is lower than one might expect. The postbuckling responses follow similar trends as the critical buckling loads. Each gives a stable response which grows slowly stiffer as the shear modulus increases, and as the response moves further into postbuckling.

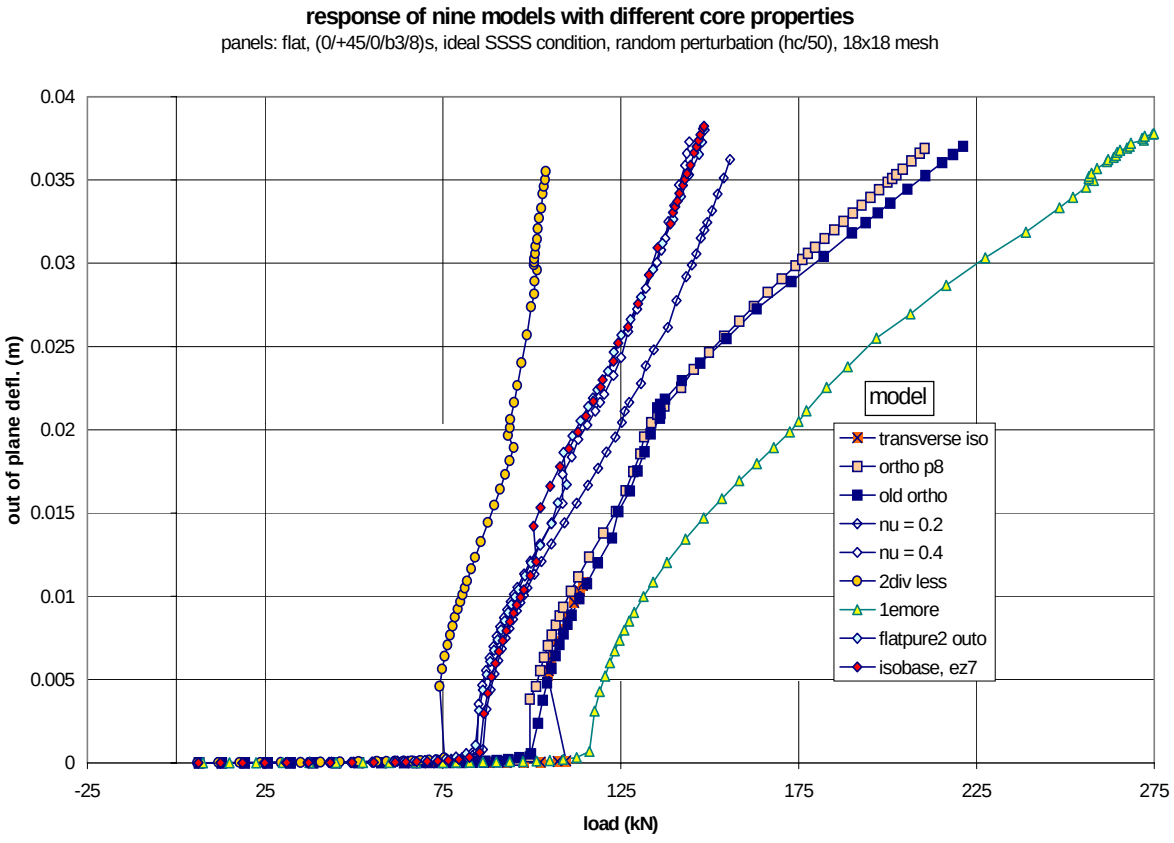

Figure 5-14. effect of core property on the buckling response of FE models

The response of the model, 1eless, is not shown in Figure 5-14 because this model did not undergo global buckling. Due to its low elastic properties a mode one response did not develop; instead, the panel underwent multiple local buckling. The resulting deformed shape is shown in Figure 5-15, (a). This case represents the result of a model with an extremely low transverse elastic and/or shear modulus. Other, similar problems can occur in models with higher core moduli in the postbuckling response. These models will tend to superpose local buckling along the edges onto the global buckling shape. This phenomenon was termed 'rippling'. The wavelength of the ripples tended to be dependent on the mesh size, with one half wave being two elements in length as can be seen below in Figure 5-15. The ripples are either caused by the high transverse shear strains in the core or are facesheet buckling on an elastic foundation. The resulting shapes from the rippling process are shown in Figure 5-15 parts (c) and (d). Part (d) can be seen to have ripples along its sides which are on the order of element size. This can also be seen on the bottom half of (b); however, the top half contains only a single 'ripple' (although it, too, is a single element in size). The rippling problem occurs most frequently in the curved panels which see much higher stresses and loads than their flat counterparts. This rippling was often the cause of a change in the postbuckling response path of the model to a more compliant slope in the same manner in which the mode shift would occur for the flat panels.

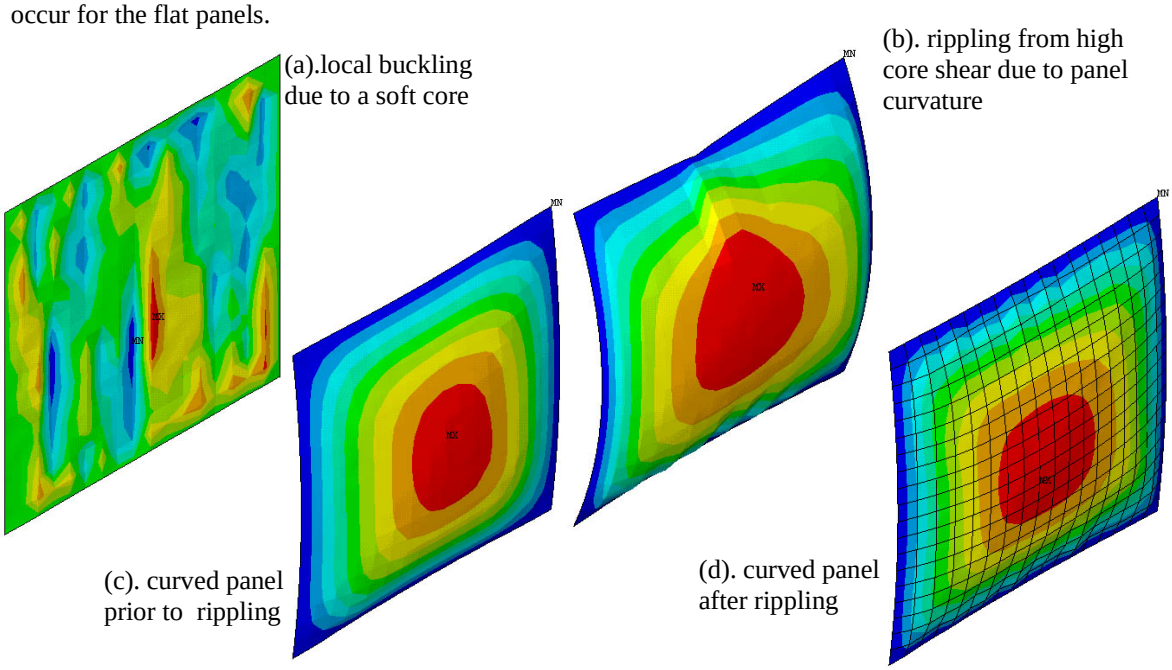

Figure 5-15. examples of soft cores (or high transverse core shear stresses) causing mesh dependent ripples in the buckling shapes

Fixture Modeling Study

The effect of modeling the loading support rollers was studied for both flat and deeply curved panels. The flat panels were studied using the ctvrf series of input files. The fixture was modeled as linearly tapered shell91 elements with a single layer of steel 14.3 mm in length (see Chapter 4 for a detailed description). Except where noted the models were all convergent random perturbation models. The difference between the flat, ideal SSSS pure sandwich model, and the single fixture model for various meshes is isolated in Figure 5-16. The single most striking observation is the response of the fixture model with a mesh density of 6x7 in the panel. The critical buckling load is approximately 70% higher for 6x7 mesh than the 17x18 mesh. The next denser mesh, 7x8, results in a response which much more closely resemble the ideal, pure case. This response discrepancy is not a statistical aberration, nor a mode two responses as seen in the statistical survey. It was consistently found throughout numerous tests of 6x7, 5x6 and 4x5 mesh grids.

The 'jump', or response shift, was caused by the extremely poor aspect ratio and either the perturbations upon the fixture nodes, or the steel (or steel to sandwich elastic discontinuity). The response shift was also found with the SFSF support conditions at the same gird sizes. However, it was not found to exist with eigenbuckling analyses. To isolate the cause of the shift in the nonlinear models, several different fixture parameters were changed. They are listed below according to their case filename series:

- *pure*: the ideal SSSS pure sandwich model
- *ctvrf:* the base fixture model described above
- *sandfix:* the steel fixture elements are replaced with the sandwich construction (no taper)
- *straight:* the fixture nodes were not perturbed
- *ctv mf:* the fixture model was perturbed by the moment method

The models were all run at mesh densities both above and below the panel grid response shift size. The panel responses are plotted together as LOD graphs in Figure 5-17. The only models which experienced the response shift were the base ctvrf and the straight model. All of the others showed small changes as expected, but remained relatively close to the pure models. This implies that the cause of the shift was a combination of the extremely poor aspect ratio, the random perturbation method and the steel. The analyst modeling nonlinear buckling with the random displacement method should be careful when modeling complicated support conditions or model discontinuities combined with poor aspect ratios (or low mesh densities per buckling wave). If the critical buckling load seems to be significantly higher than the

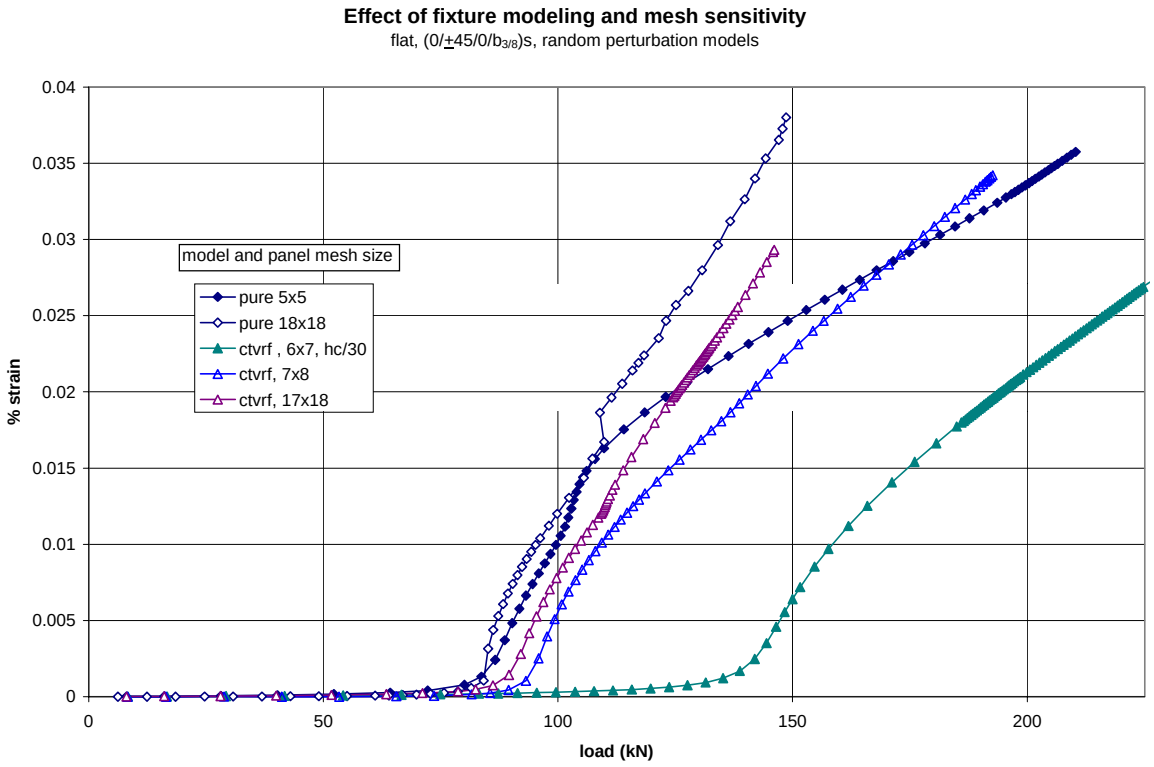

Figure 5-16. effect of modeling the fixture by response comparison versus the ideal SSSS support condtion

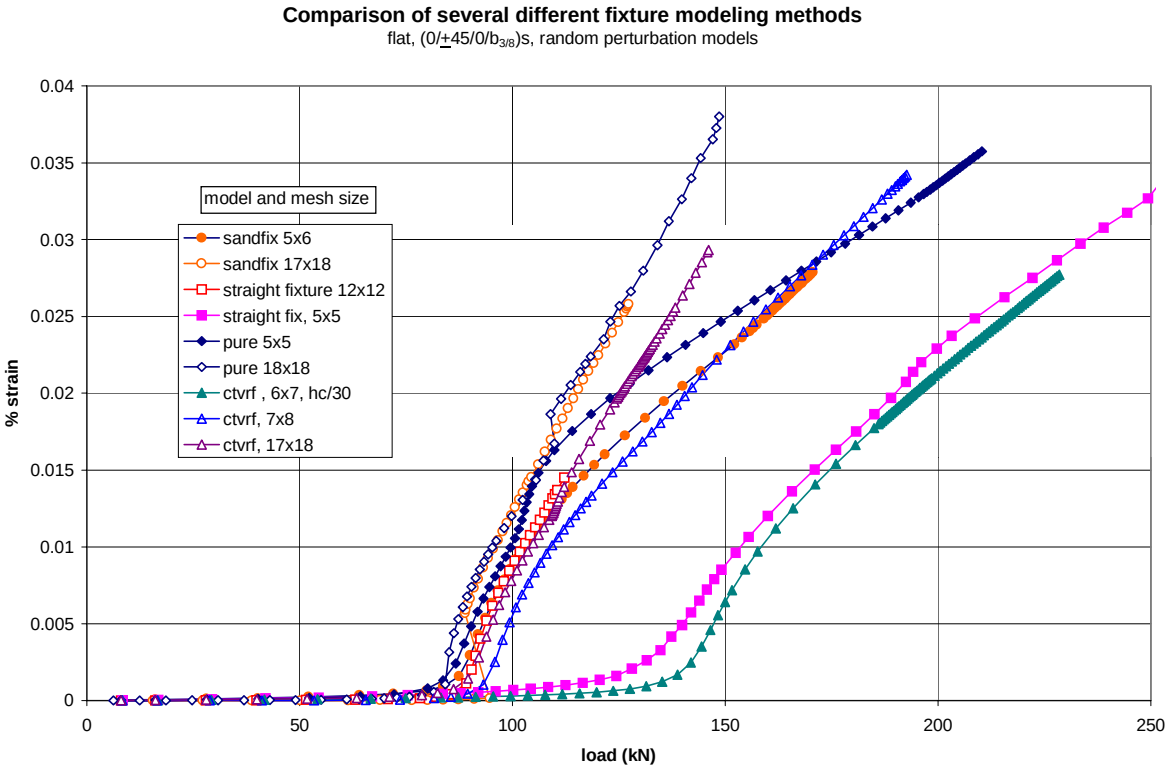

Figure 5-17. Comparison of several different methods to model the fixture

eigenbuckling critical load, even if the same mode shape, a response shift may have occurred. The mesh density of the section in question should be increased.

For fully convergent models, the critical buckling load is increased from 80.8 +-1.76 kN (ideal, pure case) to 83.3 kN with the addition of the fixture (ctvrf, run #3, 17x18 mesh, rp = hc/50). This increase is small, barely greater than the standard deviation, but is consistent. Other than the jump between mesh sizes above 7x8 and those below 6x7, the same mesh and perturbation size trends found for the ideal, pure, models are also found in the flat panel fixture models.

The effect of the fixture was small for flat sandwich plates, however; it was believed that its effects may become substantial with curved panels. Therefore, several models were also run with the 23p series panels (cylindrical ~58 cm radius). The models run and phenomenon studied are listed below according to their filename.

- *23 pure m17:* the baseline case
- *23 ctvrf m17:* the baseline fixture case
- *23 ctvrf m6:* tests whether the response shift is also found for curved fixture models
- *23 ctmf m17:* compares the moment method for curved fixture models
- *23 ctvrf piecewise:* attempts to model the piecewise roller experimental fixture
- *23 ctvrf uy=0:* studies the effect of not allowing the fixture to undergo Poissons effects (modeled because of questions which arose during testing)

Figure 5-18 is a compilation of LOD plots for the various models. The critical buckling loads are listed next to the filename in parenthesis. While the fixture had a minor effect on converged flat models, it had a large effect upon deeply curved models. The baseline fixture model has a 60% increase in the critical buckling load as compared to the pure model. The deeply curved model does not have the response shift seen for the flat fixture model for the 6x7 element grid. The longer linear response is due to the model having difficulty developing the mode one shape. The deformed shape which is found just prior to the significant load drop has two waves along the center axis on the convex side, and one asymetric, near the side, into the concave. The load drop represents snap-through behavior into a mode one shape buckling out into the concave side. The model immediately snapped back into convergence with the other curved fixture models. After following a similar path to the denser fixture models, the coarse model develops a stable postbuckling response. The stiffer response is typical of coarser meshes. It is uncertain whether the stiffer response in the deeply curved panels is caused because the coarser mesh has difficulties describing a highly

curved mode shape or because it does not develop the mesh rippling effect common to the curved models with fine meshes using the random perturbation method.

While modeling the fixture does greatly affect the response of the curved sandwich shells, the various fixture models remain fairly consistent for both the critical buckling load and the postbuckling response. While the pure model has a very compliant, but still, stable postbuckling response, the fixture models have neutral or even slightly unstable responses. As the models deform deeply into postbuckling, the responses of the pure and fixture model begin to converge. This occurs when the bending aspect of the response becomes more dominant than the local effects of the load supports. It is difficult to discern whether the models will fully converge beyond 2.4 thickness out of plane deflection. The effect of the fixture does significantly remain well into postbuckling, with load differences around 20% at 2.4 thickness out of plane deflection.

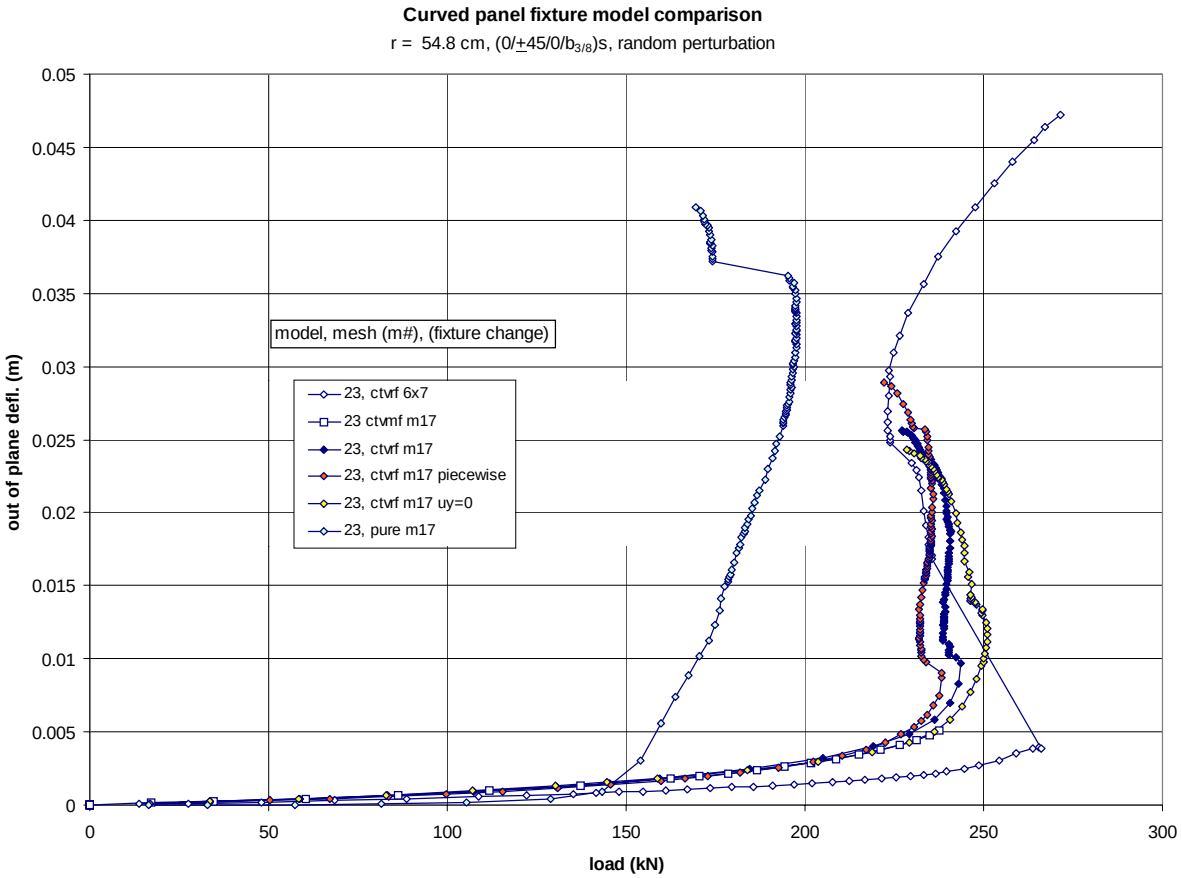

Figure 5-18. comparison of various fixture models for highly curved panels

Mixed Element Model Study

As described in chapter 4, the mixed element model was built and solved because it could provide information and possibilities that the shell models could not. A full set of core responses could be found, a continuum model used (no sandwich assumptions, but full transverse shear effects included) as well as the possibility of modeling the facesheet/core interface and the two remaining failure conditions (core shear buckling and face sheet wrinkling). Unfortunately, numerous problems arose hampering successful modeling. These problems included; proper modeling of the boundary conditions (which involved the necessity of modeling the load fixture and coupling of the side edge nodes which turned out to be very problematic), high aspect ratios or models which exceeded DOF limits set in the program for better aspect ratios, inability to reproduce the linear results, and numerous core property problems (orthotropic core properties, especially the given set, yielded poor linear results or were unsolvable).

Eventually a reasonable buckling response was found for a flat (0/45/0/b3/8)s model. Isotropic cores were required for good results. This model was a random perturbation nonlinear model in which only the facesheet nodes were perturbed. It had brick core aspect ratios of 5:1:1 and took fully 5 days to solve. The mode one deformed shape is shown in Figure 5-19. It is a very good looking, symmetric mode one shape. Unfortunately, the response of the model was highly unconservative in comparison with the shell models (and experiments, see chapter 6). The models are most easily compared in a load versus inplane deflection history plot, as in Figure 5-20. The shell models shown are ctvrf2 and 3 which are convergent fixture models.

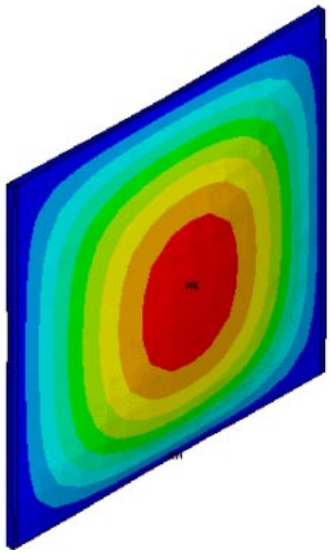

Figure 5-19. buckled shape of a mixed element sandwich panel model

The mixed model slightly stiffer in the linear response. Both models used the material property subroutine and had the same properties; therefore, the stiffer response must be due to the model itself. The load fixture model could have some effect. However, it is more likely that the difference occured because of the addition of the inplane stiffness of the balsa. The critical buckling load rises to about 140kN from the shell prediction of about 80kN, which constitutes a 75% increase. The postbuckling response is also much stiffer than the shell model. Because of the poor results, the many problems encountered and expected, and the estimated time to create a good model (if possible with this modeling procedure) the mixed element model was abandoned. As a reference for other researchers, the deck is included in the Appendices. Several possible changes which might improve the model are: eliminating the two volume approach for a single volume which would improve brick element aspect ratios and reduce the DOF (of course a new, more complicated side simple support would be necessary); the load fixture could be modeled as a cylinder rather than a rectangular bar; other techniques could be employed to solve the side edge problems (rather than nodal coupling of the facesheet nodes).

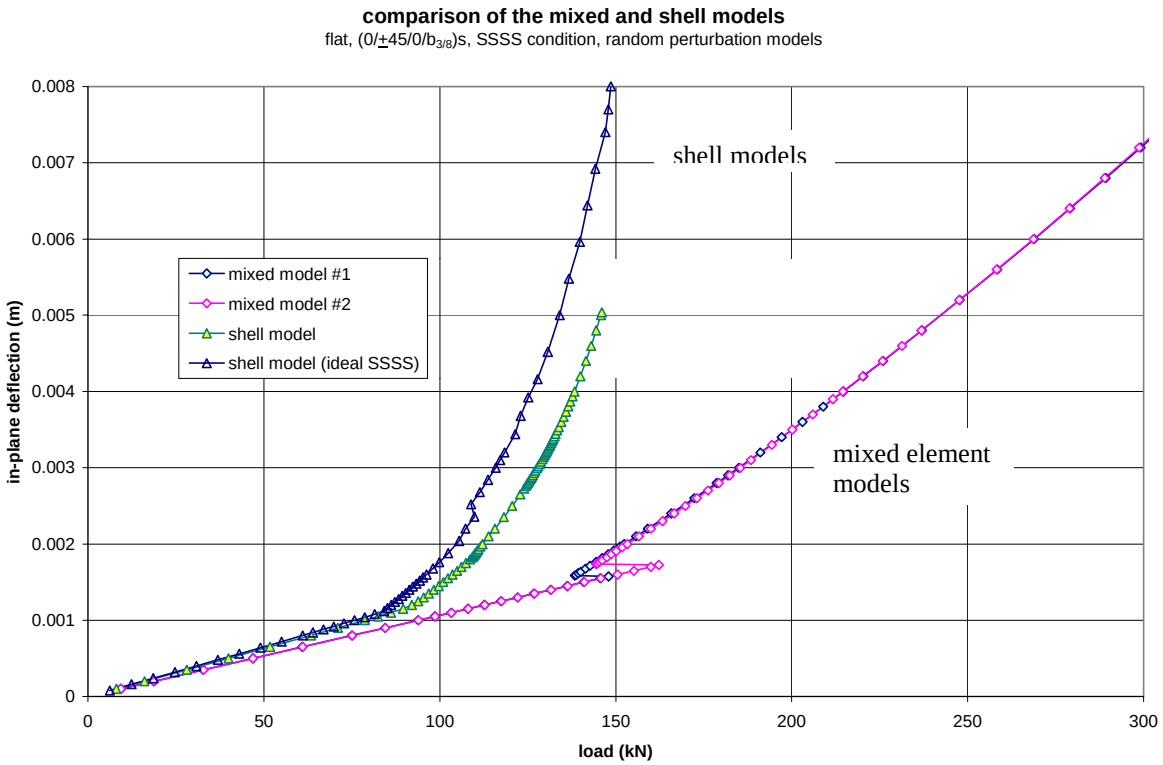

Figure 5-20. load versus in-plane deflection plot comparing the responses of the shell and mixed models

Angled Loading Study

During testing it was observed that the panel was not always loaded equally across the width of the panel. Often, shims were needed to mitigate light loading on one side. Naturally, the question arose; 'how much does the angle of loading effect the buckling response?' This study solved four different models to better understand this effect, and whether the issue would be a major one with the FEA validation of the tests. The responses for the models are compiled in Figure 5-21. The models were all (0/45/0/b3/8)s, flat, random perturbation fixture models. The baseline model was model ctvrf #4 (12x13, hc/30) and appears as 'no angle' in Figure ANG. The other three models had one end loaded a constant percentage more throughout the solution. The critical buckling load appears to be a mild function of the angle, however the general response is the same. The postbuckling responses are slightly more compliant with an increasingly angled load. The chance and severity of a mode shift also increases along with the angle, however, none of these problems are very severe and therefore the validation models will not incorporate an angled load. Separately, since it remains difficult to determine exactly how much angle (if any) each test had, the average buckling load of the tests should be assumed to be slightly lower than it would be for constant and uniform loading.

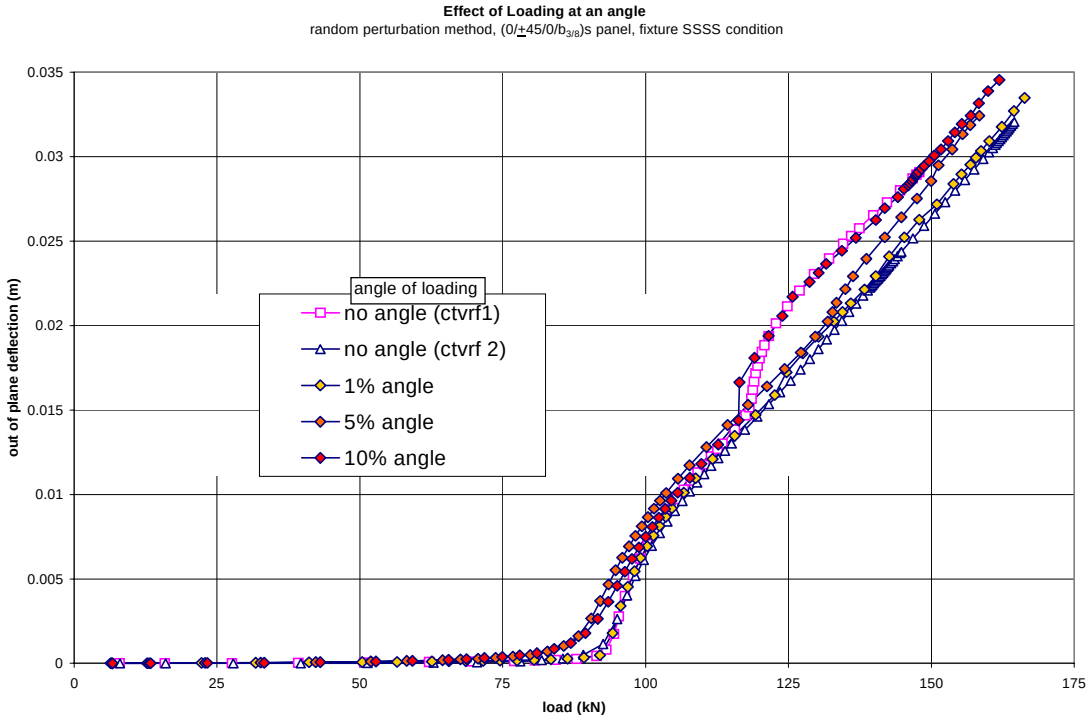

Figure 5-21. effect of loading the FE model with angular offsets

Chapter 6

EXPERIMENTAL RESULTS AND FEA VALIDATION

This chapter summarizes the results of all five test series, in both simple-free-simple-free (SFSF) and four sided simply supported (SSSS) support conditions. The five series are examined separately starting with the baseline test series. The experimental results are investigated first with special attention placed on consistency of results and any test irregularities. After adequate test results are confirmed, the finite element model predictions are compared to the tests results for FEA buckling technique validation. Finally, the FE model and test panels are compared to the baseline series and conclusions drawn about the effect of the parameter on the response and the ability of the FEA techniques to predict that behavior.

A quick review of some terms used often in this chapter is presented along with a reference to the section of this document where a more detailed examination can be found.

- *critical buckling load*- two methods were used to determine the load where buckling begins depending on the response type (see Chapter 2, Conceptual Overview and Chapter 3, implementation of the strain reversal method).
  - *(strain) reversal load*: the load where the slope of the convex side strains change from a negative slope to a positive one due to significant bending (at the point of maximum bending). Used mostly for stable or unstable buckling responses.
  - *asymptotic load:* the load which remains constant while the inplane displacement and out of plane deformation (and strains) continue to increase. Used only for neutral buckling responses and derived from the inflection point critical buckling method.
- *gage sets* (see Chapter 3, gage positioning)
  - *normal set* (ABC): gages positioned along midlength at center (B /E) and 10 cm from the sides (A,C / F,D)
  - *wide set:* midlength, at center (B / E) and 4 cm from sides (AA,CC / FF,DD)
- the five panel series (Chapter 3, Test Matrix)
  1. B-series (baseline): flat panel, $(0/\pm 45/0/b_{3/8})s$
  2. C-series (facesheet lay-up change): flat, $(90/0/90b_{3/8})s$
  3. Q-series (core thickness change): flat. $(0/\pm 45/b_{1/4})s$
  4. 70p-series (shallow radius of curvature): cylindrical shell- r = 1.78m, $(0/\pm 45/0/b_{3/8})s$
  5. 23p-series (deep radius): cylindrical shell- r = 0.58 m, $(0/\pm 45/0/b_{3/8})s$
- LOD: load versus out of plane deflection plot

Baseline Tests, B-Series

panel data: flat, $(0/\pm45/0/b_{3/8})$, ~46 x 46 cm

B-series Test Results

SFSF Tests

Six B-series panels were tested into the postbuckling range with the SFSF support condition. Four were tested with the single piece roller fixture (panels B1,3,4&5) while the last two used the piecewise fixture (B7&8). One typical run from each panel is plotted in Figure 6-1. For clarity, only the center back and front strain gages are shown for each panel. All six panels responded similarly in each buckling phase. The differences in the linear range are due to non-uniform loading. Figure 6-2 is a complete data set for eight gages on panel B8. The scatter band for the linear region can be seen to encompass the scatter of Figure 6-1. The average moduli of the panels, the linear regression of the average strain versus load, is found to be consistent from multiple tests on one panel, and from panel to panel (see Table 6.5 in the SSSS section). The results in show the critical buckling ranges to overlap. Each panel responded with a neutral postbuckling response, whose asymptote was between 45 and 50 kN. All of the panels were tested far enough into the postbuckling range to accurately deduce the asymptotic load, except B7 which is still well past strain reversal. The accurate deduction of the asymptotic load required at least some tension to occur on the convex side. Of the six panels tested, only B4 was tested to failure in the SFSF condition. Its load only increased 0.8 kN from the 0.1% strain tension load, until final failure at 0.6% strain (tension). This suggests that the asymptotic load may be identified within 1 kN, as soon as it is discerned from the load history plot.

An example of a complete data set for a SFSF test is plotted in Figure 6-2. This panel was instrumented with ten strain gages which incorporated both the normal and wide sets. However, only eight strain gages could be recorded for a single run. This test was run to a full asymptotic response at 47.1 kN. Several characteristic SFSF responses are shown in this plot, which can be confirmed by viewing other SFSF plots found in the Appendix. The loading response is always stiffer than the unloading response. Energy is lost to friction, heat, and occasionally damage to the epoxy filler, which accounts for the different elastic response paths (or slightly inelastic with damage). With very few exceptions, the gages returned to within 1 microstrain of zero (or the zero load strain output) when damage was not audible, and within 5 microstrain even when severe epoxy damage was audible.

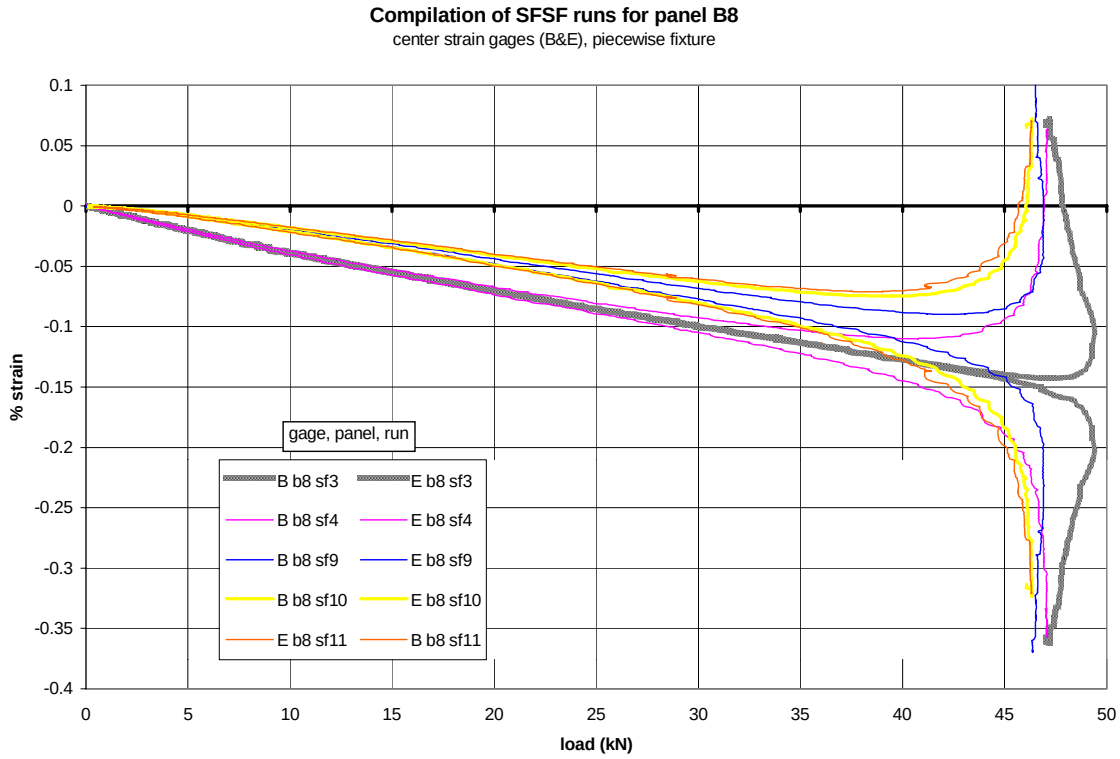

Figure 6-1. compilation of typical B-series SFSF tests for the six tested panels

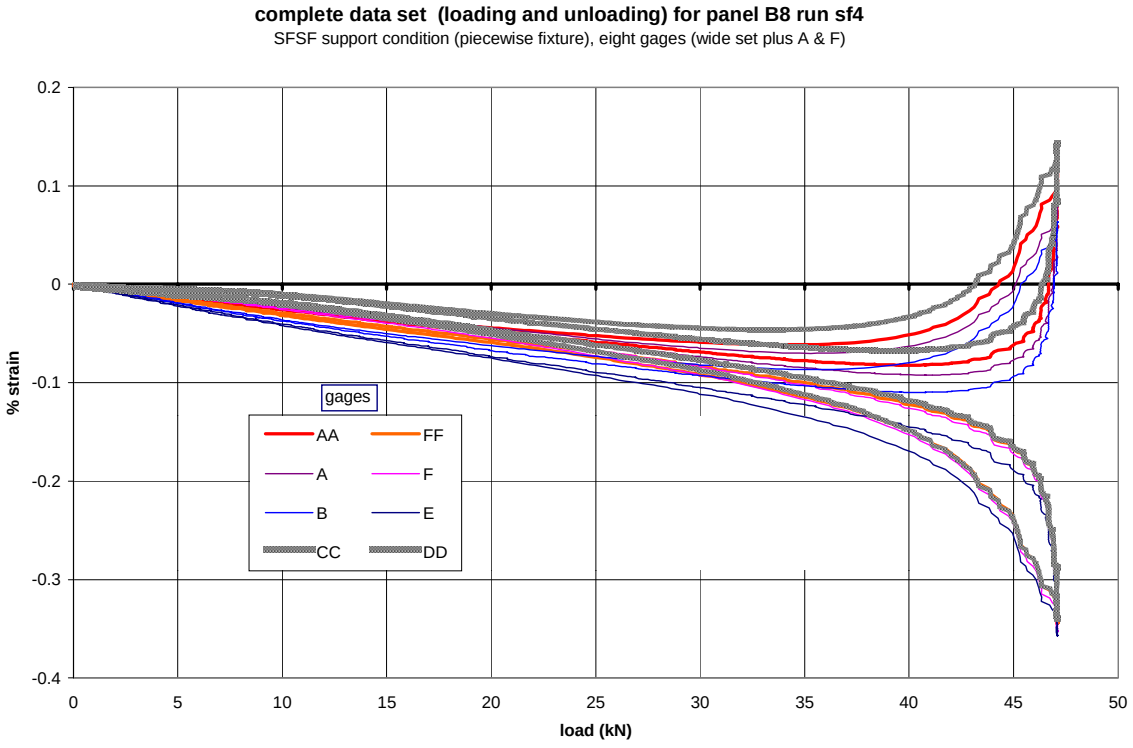

Figure6-2. a typical full data set for a B-series panel tested in the SFSF condition

The panel deflections and strains consistently responded across the width as a function of the free edges. The gages near the free edges experienced greater bending than the center. This suggests that the edges actually deflect more than the center, and the width direction buckling shape is also a wave, perhaps even sinusoidal. Table 6.1 gives the maximum strain values on the convex side for each panel, and the bending strains (front to back gage strain difference). For simplicity, the gages have been named by the front side only (ABC). B8 run 9, and B1 run3 actually buckled to the back side (DEF), although B8 run 4 (without epoxy) buckled frontwards. With only this exception, the panel always buckled in the same direction for each SFSF run, even when an SSSS test(s) was run between SFSF tests. The change in buckling direction in B8 from front to back, with the addition of the epoxy and subsequent realignment of the piecewise fixture, implies that the perturbations for B8 were dominated by the fixture placement and not the panel imperfections.

Table 6.1. the maximum convex (tension side) strains for typical loading runs on each panel

		maximum strains at each gage					bending strains		
panel	run	AA	A	B	C	CC	A (AA)	B	C (CC)
B1	3		0.0201	0.0157			0.346	0.338	
B3	4		0.0422	0.0364	0.0403		0.375	0.358	0.385
B4	10		0.574	0.586	0.592		1.49	1.436	1.474
B5	2		0.0693	0.0552	0.0602		0.409	0.41	0.423
B7	2		-0.0032	-0.011	-0.0073		0.287	0.256	0.257
B8	4		0.147	0.113	0.16		0.562	0.482	0.542
B8	9	0.117	0.79	0.0633		0.143	(0.482)	(0.420)	(0.461)

The general trend for the maximum strain and bending strain distribution is for the middle gage to be lower than the edge gages. B8 run 9 suggests that this is especially apparent for the wide gage set, where the strain gages are 7-8 cm closer to the edge than the normal gage set. The exceptions are the B4 tension strains and B5 bending strains, both of which have skewed distributions which are evenly distributed. The combination of the two data sets implies that the panel bends more at the edges, and the postbuckling strain distribution is not just a loading effect of the fixtures.

All five SFSF loading runs (to buckling) performed on B8 are shown in Figure 6-3. These five runs also yield important SFSF buckling information. First, runs 3 and 4 did not use an epoxy filler, while 9,10 and 11 had the epoxy filler. Runs 10 and 11 respond very similarly in the linear, critical and postbuckling regions and have asymptotic loads of 46.4 and 46.3 kN respectively. Run 9 loaded slightly past its asymptotic load of 46.3 kN, termed a softening response in the present study. Runs 3 and 4 react markedly differently than the other three. Both reach asymptotic loads of 47 kN, however run 4 follows the

classic neutral postbuckling path while run 3 experiences severe softening with a maximum load of 49.5 kN. Clearly the addition of the epoxy changed the asymptotic load. For SFSF panels, it is expected that panels with higher aspect ratios will buckle at lower loads, therefore the difference in this load could be accounted for by the increase in panel height from the epoxy. However, the excess epoxy was squeezed out by a lad of about 9 kN during test preparation, and the average increase in height throughout all panels tested was around 1mm, hardly enough to make a geometric difference. Runs 9,10 and 11 were shimmed with a single piece of aluminum on the CD gage side. The influences of the epoxy and shims (more uniform load) are responsible for the drop in the asymptotic load.

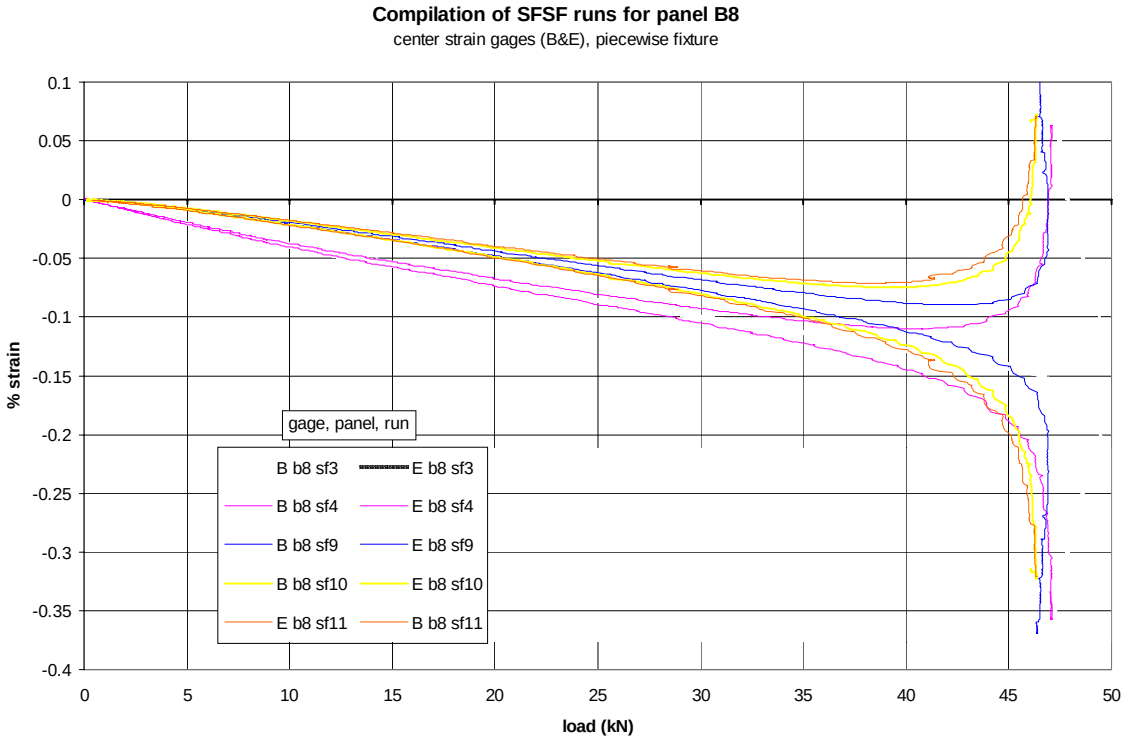

Figure 6-3. compilation of SFSF test runs for panel B8

The standard deviation statistics of strain and buckling data for the five SFSF buckling Blade8 runs are tabulated in Figure 6.2. The standard deviation statistics are presented as the coefficient of variation (CV), which is the percent standard deviation of the six strain gages (wide set). The addition of the epoxy dramatically reduced the coefficient of variation for strain data. The critical buckling loads (strain reversals) tend to vary much more than the asymptotic loads for panels with and without epoxy; in fact, the former overlap. The critical buckling loads seem to be more sensitive to initial imperfections, which may increase the coefficient of variation, than to the addition of epoxy with lower CV relating to

higher critical buckling loads. The CV of runs 9,10, and 11 becomes worse (higher) with each test, suggesting damage to the epoxy, while the critical buckling loads continue to drop. Other tests contradict the trend of higher CV causing lower critical buckling loads (see next section, SSSS tests on B1). The coefficient of variation may not reflect an increase in the number and size of imperfections. Whatever perturbation is the cause, critical buckling (strain reversal) is more sensitive to perturbations than the asymptotic buckling load. The stable asymptotic load of flat SFSF sandwich panels, compared with the more varying strain reversal loads, suggest than the asymptotic load is the value which should be used to make panel comparisons for statistical or parametric information in the present study. In contrast the design engineer should use the more conservative strain reversal buckling load, as well its greater sensitivity to initial imperfections.

Table 6.2. statistical and buckling data for the SFSF B8 runs (wide gage set)

run	min CV (%)	@ load (kN)	10 kN CV (%)	AA reversal (kN)	B reversal (kN)	CC reversal (kN)	asymptotic load (kN)
3	15	45	39	45.9	46.4	46.4	47.0
4	21	32	40	38.6	39.7	40.4	47.1
9	13	31	23	40.8	41.5	41.5	46.3
10	20	29	38	38.3	38.7	36.8	46.4
11	22	28	31	37.3	37.5	36.3	46.3

With most panels bending more at the edges, the strain reversal loads are expected to be lower for the end gages (CC and AA). Except for run 4, the center gage has the highest strain reversal (or tied for the highest). As with the bending strain (strain difference), this width-wise buckling shape effect is relatively small.

The tabulated results for the SFSF tested panels are shown in Table 6.3. The center gage (B) was chosen rather than the edge gages for the strain reversal critical buckling load to minimize eccentric or edge effects, and for consistency (it was the only gage position used for panels). The panels were of approximately equal dimension (length $\pm$1.6 %, width 1.5%) and modulus ($\pm$ 4.5 %) (the data is found in the next section in Table 6.5). Except where noted, the panels were tested with the single piece fixture and used the normal gage set. Every test which was run past the strain reversal critical buckling load is shown. All run numbers started from one and ran sequentially up. Any skips in number represent a test which was run only to verify the uniformity of the load. Most such tests ranged in maximum loads of 15 to 25 kN, with very minimal, if any, epoxy damage. The '#A' or '#P' in the shim column refers to the number of aluminum or paper shims used on the (CD) or (AF) gage side respectively. The coefficient of varition

statistics are presented from only the six gages comprising the normal or wide set even when eight strains were recorded. The min. CV column contains the lowest valid CV found for the entire data set, with its associated load in the '@ load' column. The CV at the 10 kN was deemed also be important and its values recorded in the last statistical column. The noise column after the 'reversal' column (strain reversal buckling load) is the qualitative assessment of the noise, and confidence, in the strain reversal data. The 'slope adjust' column after the asymptote buckling load is an estimate of the maximum possible change in to the asymptotic load based upon the slope and overall history of the test run. Those which are negative are still experiencing the softening effect.

An average strain reversal load was not calculated due to the highly variant results within one panel. Instead a critical buckling range is established with lower and upper bounds of 37 to 43 kN. Any runs which experienced softening were disregarded. The average asymptotic buckling load resultant (kN/m) is calculated due to its more stable nature. Only the B8 runs with epoxy are used for the sake of consistency. The average for all six panels is 101.3 kN/m with a standard deviation of 3.5 kN/m.

Table 6.3. statistical and buckling results for the B-series SFSF runs

			deviation statistics (CV,)			buckling data (kN)			*slope*	
panel	run	shim	min. CV (%)	*@ load (kN)*	10kN CV (%)	reversal	*noise*	asymptote	*adjust*	comments
B1	1	none	31.7	*24.4*	41	44.5	*0.1*	NA		rollers were very bent, sent back to machine shop
	3	none	6.5	*30.3*	17	40	*0.5*	47.4	*0.1*	much more linear data
B2	2	none	10.8	*31.6*	23	42.4	*0.5*	NA		very quickly loaded, barely buckled, max 49 kN
B3	4	2 P (?)	15.4	*15.9*	17	37.6	*0.5*	47.7	*0.3*	
B4	10	1 A (CD)	12.3	*11.3*	12	37	*0.5*	48.2 (47.4 @ 0.1%)	*0*	broken, fixture end delam, no cracking heard max 48.2 kN, 0.593/-0.850 % strain perm strains, A +3, B +4, C 0, D +6,, E +23, F +9 micro
B5	1	none				45.5	*0.5*	48.4	*-0.4*	softened
	2	none				41.8	*0.2*	48.7	*0.1*	
B7 *	2	2 P (CD)	9.9	*14.1*	11	37.8	*0.1*	45.7	*1*	
B8	3	none	14.8	*45.2*	39.3	46.4	*0.2*	47	*0.1*	
*	4	none	21.3	*32.4*	40.1	39.7	*0.2*	47.1	*-0.2*	significant softening, & still dropping
**										3,4 no epoxy, 9,10,11 w/epoxy
	9	1 A (CD)	13.5	*30.9*	23.0	41.5	*0.2*	46.3	*-0.1*	slight softening
	10	1 A (CD)	19.8	*28.7*	28.0	38.7	*0.2*	46.4	*0.1*	
	11	1 A (CD)	22.4	*28.4*	30.6	37.5	*0.2*	46.3	*0.1*	2 load rests

* piecewise fixture; ** wide gage set

It is expected that there would be a slight difference in the asymptotic buckling loads between panels tested in the single piece fixture, and those in the piecewise fixture. With a width-wise buckling shape that bends more at the edges, the panel would also need to rotate more at the edges of the load support. The single piece fixture would resist such a rotation with torsional stresses. However, the

piecewise fixture would allow for discrete rotation changes every five centimeters. This would allow the panel to buckle more freely into its desired shape (more deflection at free edges) dropping the buckling loads some finite amount. If the panels are separated by fixture, the single piece tested panels averaged asymptotic loads of 103.4 kN/m (standard deviation of 1.7). The two panels tested in the piecewise fixture had asymptotic loads of 97.3 and 97.0 kN/m (it was not fully asymptotic and with a possible final load of 99.1 kN). The two sets of panels did not differ significantly in dimensions, aspect ratios or axial modulus. The difference between the two is small and may not be statistically significant, but this small sample size warrants consideration.

SSSS Tests

Six panels were tested to failure in the SSSS support condition, B1,3,5,7 and 8. Again B7 and B8 were tested with the piecewise fixture and the remaining four with the single piece fixture. The center front and back strain responses for all six tests, which resulted in panel failure, are plotted in Figure 6-4. All of the B series panels buckled in the same direction in the SSSS tests as previously in the SFSF test (see section on crossply tests for the exception to this trend). The critical buckling region has a much larger range in the SSSS tests than the SFSF tests, from 80 to 120 kN. The postbuckling responses are also widely different. The differences are more easily understood if the six panels are categorized according to the fixture used.

All four single piece fixture panel tests responded with stable postbuckling paths, although the range of response paths is wide. The two extreme responses, B2 and B5, can be explained by poor fixture performance. For B2, the knife edges performed poorly with a significant gap, about 1 cm at failure, observed between the panel and the knife edges, as the panel pushed the supports away from each other. This allowed the panel edges to deform out of plane significantly and made the panel respond along a more bending compliant path than the tests where the knife edges performed well and the edges remained straight. More care was taken tightening the bolts on subsequent tests. The last panel to use the single piece fixture was B5. By this test, one of the fixtures had a significant, symmetric, permanent twist. This twist was the result of deep postbuckling tests, in which the middle had to rotate significantly while the ends remained straight. The roller offered a mild resistance to free rolling on the flat granite block. The middle twist was also a significant initial imperfection which perturbed the panel to buckle towards the twist. If other initial imperfections in the panel existed, which tended to force buckling in the other

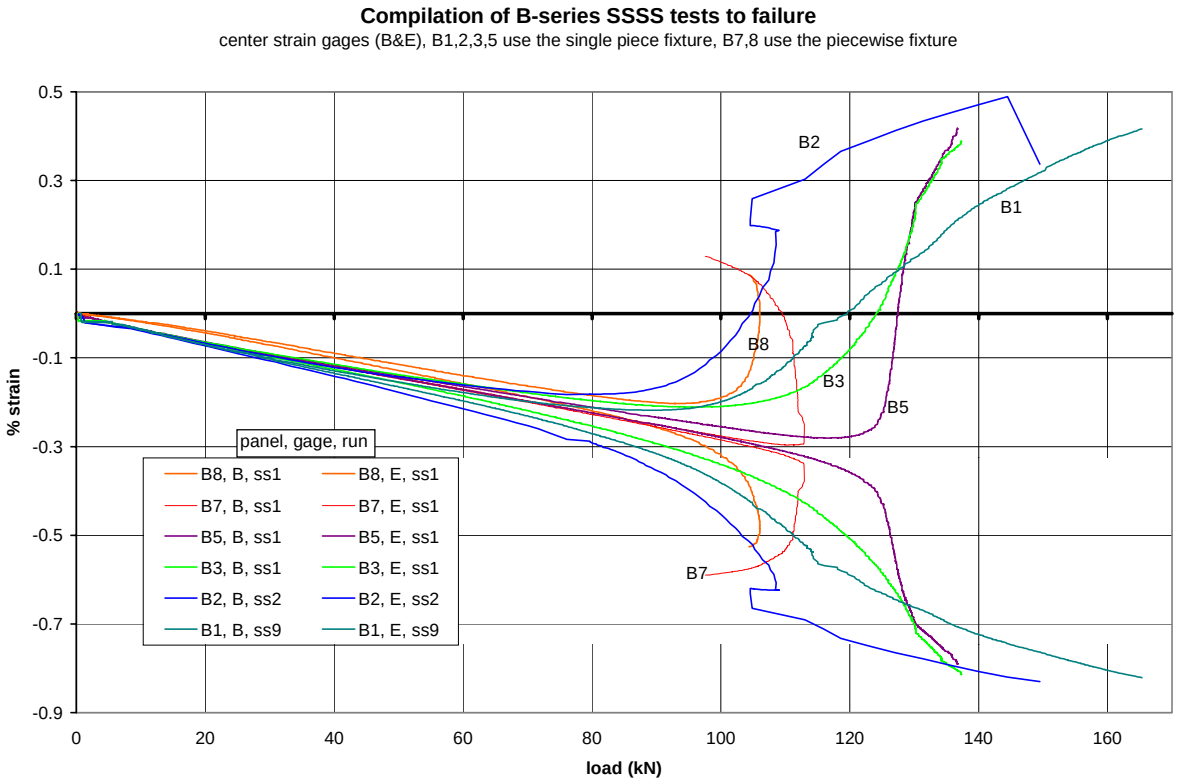

Figure 6-4. Compilation of the B-series SSSS tests to failure

direction, these two contradictory perturbations might factor out each other and delay critical buckling. No other contradictory perturbations were found within the strain data, however B5 does reach the critical buckling range at a much higher load than the other five tests. Once buckled, the panel deformed rapidly until it reached the equilibrium positions of B1 and B3. B5 then followed a stiffer postbuckling path which is very close to B3. Both failed at very similar loads and strains (with 1% load and 0.02 % strain differences). The load fixture and knife edges performed well for B1 and B3, which are bounded by B2 and B5 for the single fixture responses.

The piecewise fixture tests had critical buckling load ranges which lay within the single fixture range. The difference between the responses lay in the postbuckling response. While the single piece fixture provided stable responses the piecewise fixture provided unstable responses. B8 had an unstable response which failed early into the load drop. It failed at significantly lower buckling strains compared to the stable responses. B7 buckled at a high load, close to B5, then followed a strange unstable response that included two relatively flat sections and a failure load way below the critical buckling load. Its failure load and strains were similar to those of B8.

The stable postbuckling response was the expected response for a flat sandwich panel. As mentioned earlier in the SFSF section, the piecewise fixture allows for discrete changes of rotation in the load fixture to accommodate the different angles required by an ideal SSSS buckling mode shape. This allows the middle pieces to rotate freely of the end pieces, which do not rotate due to the effects of the knife edges. The pieces may also translate transversely if the panel deforms transversely at the load end, although friction must be overcome. The panel was observed closely during postbuckling, and was not seen to have translated. The panel was expected to provide the elastic continuity to the loaded ends for the stable response that is seen in the single fixture response and the FEA nonlinear analysis.

Whatever the reason, the unstable response of the piecewise fixture for flat plates places an uncertainty onto the postbuckling response of the curved panels, especially if an unstable response is found. The critical buckling and linear response of the piecewise fixture remains valid. Panels B1 and B3 give the most trusted postbuckling paths for comparisons. Four critical buckling ranges and strain reversals are trusted: B1,3,7 and 8. The buckling and statistical data for the B series SSSS tests are tabulated in Table 6.4.

Table 6.4. buckling and statistical data for the B series SSSS tests

			st. deviation statistics (%)			buckling data (kN)			failure data			
#	run	shim	min	@load	@10 kN	reversal	noise	damage	mode	load	@strain (%)	comments
1	7	none	6.7	58.5	19	**85.4**	0.5	115				
	8	none	8.3	50	20	**88**	1	none				
	9	none	5.8	55	15	**88.7**	0.5	115	fs delam / core shear	165.3	.416/-.846	stable postbuckling, smooth data
2	1	none	8.0	47.2	20	79	1	none				
	2	none	10.8	34	20	80	1	NA	fs delam / core shear	137.4	.389/-.880	knives separated! fast linear loading, not a good test
3	1	2 paper	7.4	46	16	**95.5**	0.5	120	fs delam / core shear	151.3	.389/-.814	similar to B1
5	1	3 P (CD) 1 P (AF)	2.6	61.8	17	114	2	125	fs delam / core shear	136.7	.418/-.837	was initially offset to opposite side to buckling
												fixture forced delayed buckling, very linear data
7	1	2 P (CD)	5.7	99.85	13	**110.4**	0.5		fs delam / core shear minor	max 112.8 failure 97.6	 -.250/-.380 .129/-.591	unstable postbuckling
8	1	1 A (CD)	11.9	80	23	**92.5**	0.3			104	.088/-.522	flattened, then dropped quickly at failure to 101 kN

Test Reproducibility. A full data set of all strain gages for panel B1, which did not fail or incur panel damage, is shown in Figure 6-5. Only five strain gages were working properly during this test (gage D was not). As with the SFSF tests, the unloading response was more bending compliant than the loading path, but was still elastic. As expected, the center convex gage (E) is seen to experience much more

bending strain than the left side (F). However, the center concave gage (B) did not experience a similarly larger bending strain than its neighbors (A and C). This response is typical of the SSSS tested panels, as confirmed in other load history plots found in this chapter and the Appendices. This phenomenon could result from either panel damage or strain redistribution along the concave facesheet. Strain redistribution would require a less bent facesheet, therefore necessitating the face sheet to pull away from the balsa core. The bending strain discrepancy occurs early in the postbuckling response when no panel damage was observed. A less bent facesheet buckling shape seems unlikely and this phenomenon remains unexplained. As a result of this discrepancy, the average modulus should become slightly more compliant. All of the SSSS runs (9,10 and 11) of B1 have this bending strain discrepancy as shown in Figure 6-6. Runs 9,10 and 11 show the SSSS response of B1 to be very consistent and repeatable for SSSS tests without support changes or panel damage.

Damage. The average strain of B3 ss1 is plotted with its six constituent strains in Figure 6-7. The average strain remains highly linear out to 120 kN, where it becomes significantly more compliant. Similar knees are also seen in B1 ss9 at ~115 kN, and B5 ss1 at 125 kN. Damage was also heard at 115, 120 and 125 kN on tests B1,3 and 5 respectively. These loads correspond with the change in average strain for each run. The average strains for B1,2,3 and 5 are plotted in Figure 6-8. A damage initiation load was not recorded for B5, but can be guessed as 125 kN from the evidence observed from the other three. After the change, the tangential moduli actually become greater than or equal to zero. Once begun, the damage was heard continuously as medium volume, quick, successive pops until failure. By comparison final failure was a single, intensely loud and sudden crack. Most panels could still hold a moderate load, ~40 kN with a neutrally stable response (steady load with increasing in plane deflection) for the short time before the panel could be unloaded.

Panel Modulus. Linear regression of the average strain of B3 ss1 in Figure 6-7 at the 30, 60 and 117 kN loads yields face sheet moduli of 22.6, 23.5 and 24.1 GPa respectively, with regression coefficients of 0.99 for each. It was common for the stiffness of a panel to change as the load increased. Most panels tended to become stiffer with increasing load. Two reasons have been postulated to explain this occurrence. First, the gaps and load points at the roller-plate interface, and roller-C-channel system are filled and widened as the contact surfaces become larger due to deformation. Second, the load paths set up

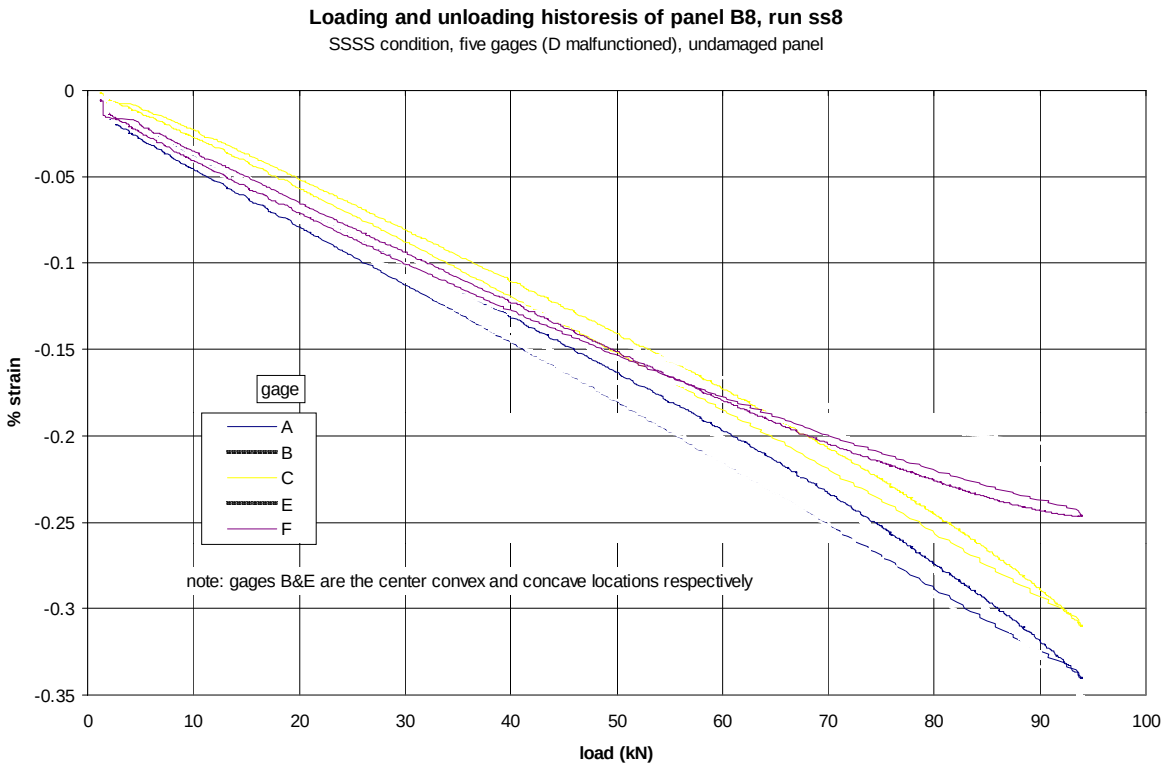

Figure 6-5. typical loading and unloading historesis for a B-series SSSS tested panel without audible matrix cracking.

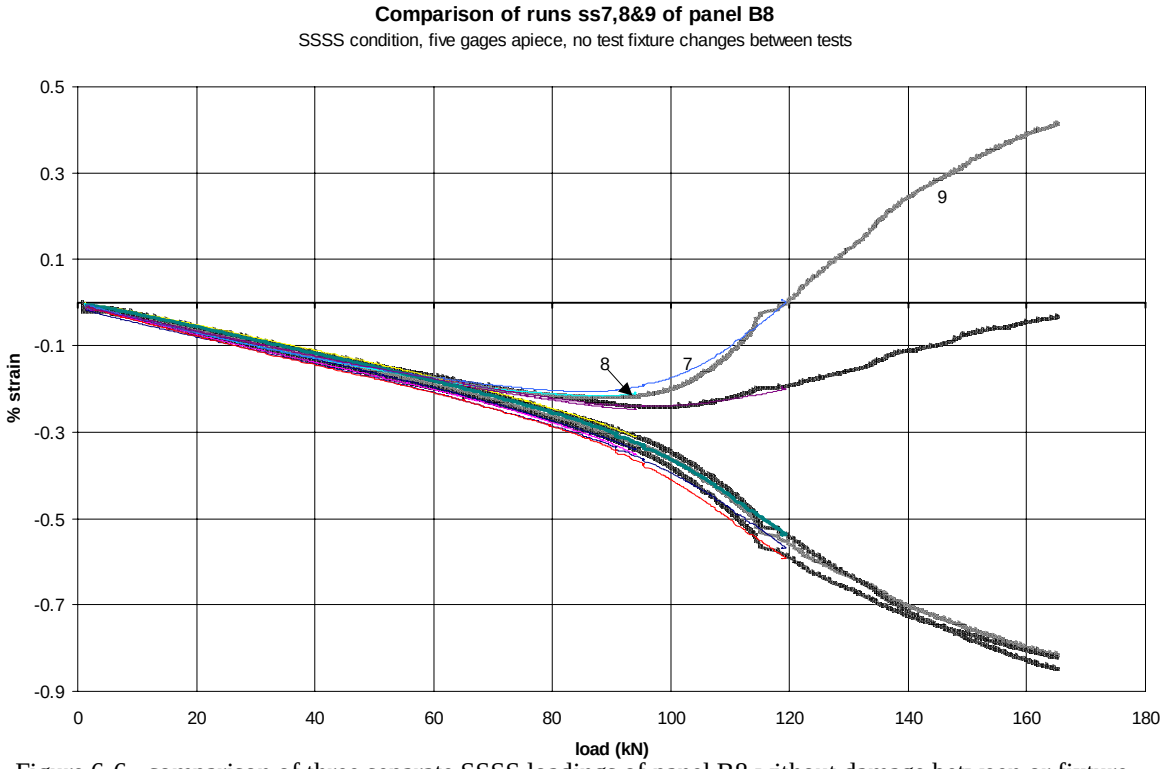

Figure 6-6. comparison of three separate SSSS loadings of panel B8 without damage between or fixture changes

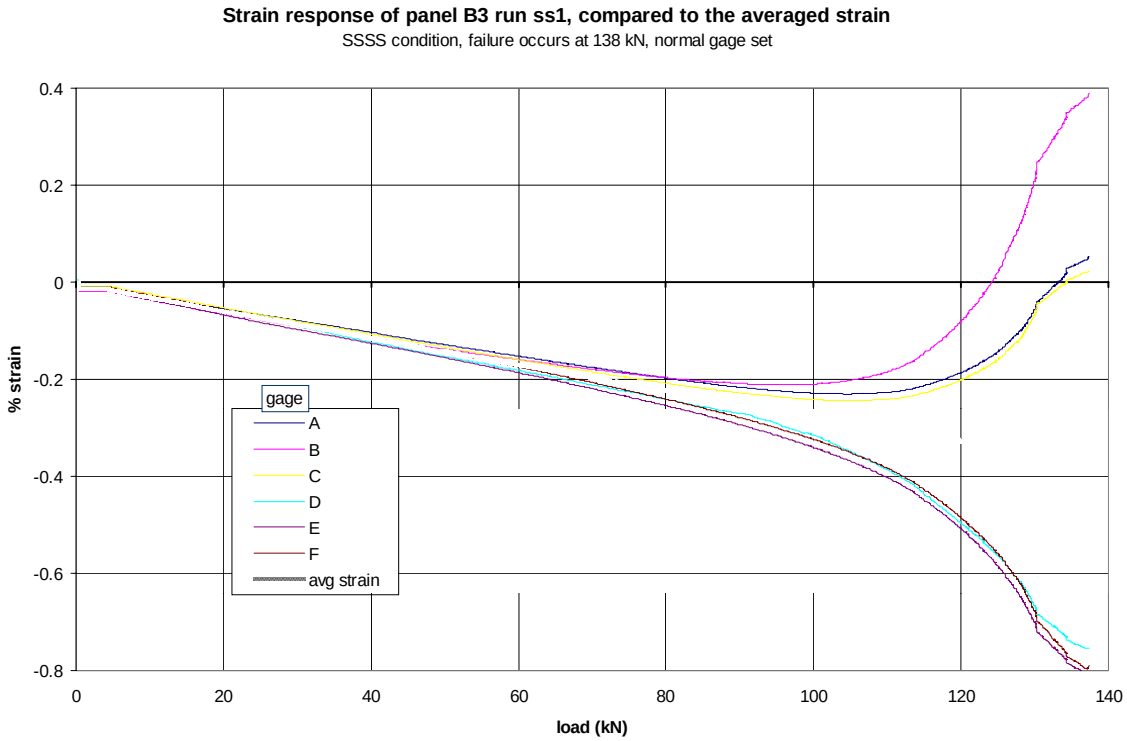

Figure 6-7. typical B-series SSSS strain response plotted along with the average strain response

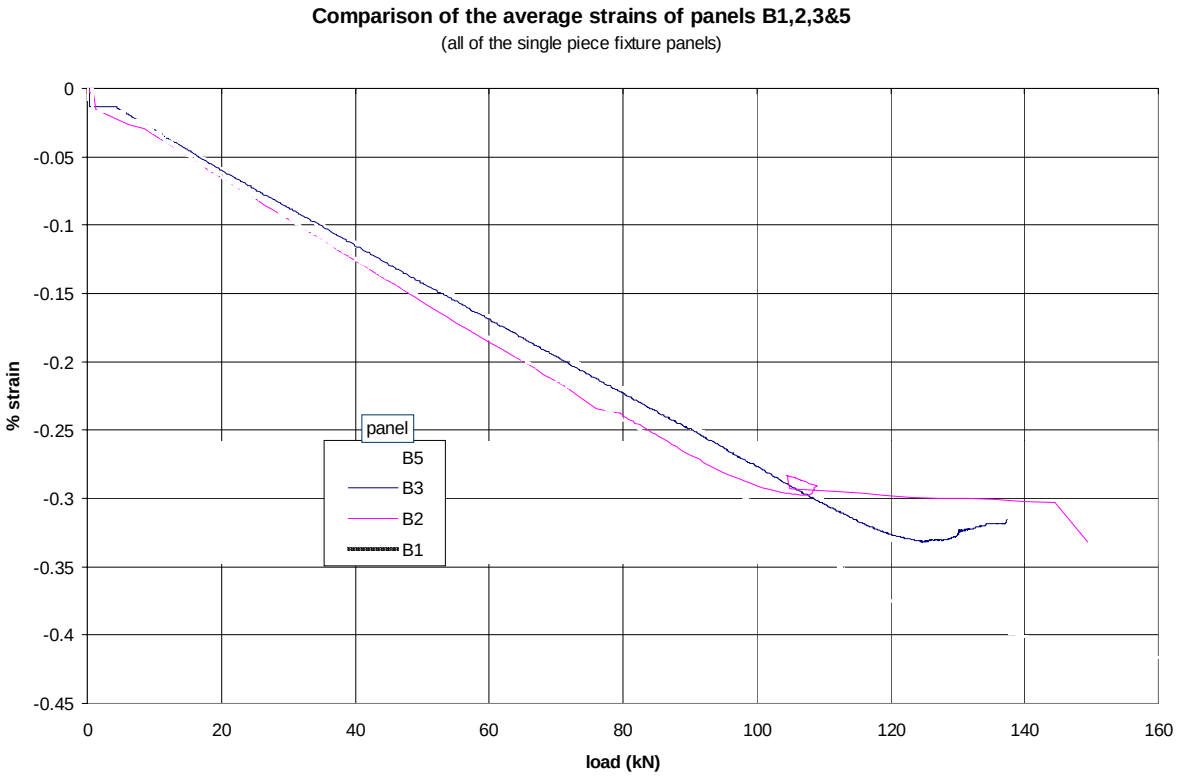

Figure 6-8. compilation of the average strain of the single piece fixture panels

Table 6.5. B series panel dimensions and calculated axial moduli from testing

dimensions (cm), +-0.08						face sheet modulus (Pa)			
#	fixture	length	width	supp.	#	@30 kN	@60 kN	@max linear	@ load (kN)
1	one	45.2	46.0		ave	**2.09E+10**			
				sf	1	2.14E+10			
					2	2.11E+10			
					3	2.07E+10		2.08E+10	44
					ave	**2.10E+10**			
				ss	1	2.11E+10	2.18E+10		
					2	2.09E+10	2.15E+10		
					3	2.06E+10	2.15E+10		
					4	2.18E+10	2.18E+10		
					5	2.12E+10	2.19E+10	2.22E+10	100
					6	2.08E+10	2.19E+10	2.23E+10	100
					7	1.95E+10	2.15E+10		
					8	2.06E+10	2.17E+10	2.23E+10	94
					9	2.16E+10	2.21E+10	2.23E+10	110
					ave	**2.09E+10**	**2.17E+10**	**2.23E+10**	
2	one	45.2	46.5		ave	**2.13E+10**	**2.19E+10**		
				sf	1	2.16E+10			
				ss	1		2.21E+10		
					2	2.10E+10	2.17E+10		
3	one	45.7	47.0		ave	**2.17E+07**			
				sf	4	2.09E+07		2.15E+10	47
				ss	1	2.26E+07	**2.35E+07**	**2.41E+07**	117
4	one	44.9	45.6		ave				
				sf	10	**2.40E+10**		**2.44E+10**	45
5	one	45.4	47.0		ave	**2.20E+10**			
				sf	1	2.17E+10		2.23E+10	49.5
					2	2.18E+10		2.25E+10	48.7
				ss	1	2.26E+10	**2.36E+10**	**2.44E+10**	125
7	piece	46.0	47.1		ave	**2.20E+10**			
				sf	2	2.19E+10		2.22E+10	45.5
				ss	1	2.20E+10	**2.29E+10**	**2.32E+10**	112
8	piece	43.8	47.6		ave	**2.32E+10**		**2.35E+10**	
				sf	3	2.44E+10		2.45E+10	49.3
					4	2.45E+10		2.50E+10	47.1
					9	2.34E+10		2.37E+10	46.9
					10	2.30E+10		2.33E+10	46
					11	2.32E+10		2.34E+10	46.2
				ss	1	2.57E+10	**2.49E+10**	**2.43E+10**	104

by these load distributions merge and overlap. The panel dimensions and different load moduli for each test is tabulated in Table 6.5. Occasionally, as with B8 ss1, a panel has a high modulus at 30 kN and drops rather than rises with loading. As is seen with this case, the final modulus approaches the range at which the SFSF tests are approaching with the more typical trend. The reason for the few atypical modulus trends could be either: 1).highly non-uniform loading distributions that simply have paths focused upon the gages or; 2). (with SSSS runs) excessive friction between the knife edges and panel which loads the steel, and which is eventually overcome as the axial load to friction load ratio rises. Throughout all panel series test runs, those with the decreasing moduli are all SSSS runs. In general, SSSS tests had higher moduli at the 30 kN load than SFSF tests on the same panel. This difference is ascribed to loading of the knife edges due

to friction. One panel that conspicuously lacks this behavior is B2, which had knife edge separation due to inadequate bolt tightening (and subsequently lower normal force on the panel supplying friction between steel and facesheet).

Panel Failure. The single piece fixture, B series SSSS failures, all failed at the bottom roller. The concave side facesheet would debond from the balsa core, and the balsa would fail in shear someplace between the debond and the C-channel. The damage zone was largest at the midwidth (furthest towards the middle of the panel) and would curve down to the C-channel at the edges. Those failures which occured concurrent with knife edges slipping off, had damage zones concentrated along that edge. For all B series panels, it was unclear whether core shear or face sheet debonding was the first failure mode. However, it is clear that the fixture influenced the B series failures and that the failure data may not be predictable by the analyses used in this study. An example B series failure, panel B5, is pictured in Figure 6-9. Pictures of other failed panels are compiled in Figure 6-10, with a closeup of B3 shown in Figure 6-10 b. The panel tested to failure in SFSF, B4, also failed at the bottom roller and is shown if Figure 6-11. The panel bent, and subsequently slipped through the C-channel interface. In the process it broke whatever bond it had with the epoxy and shredded the balsa in shear failure.

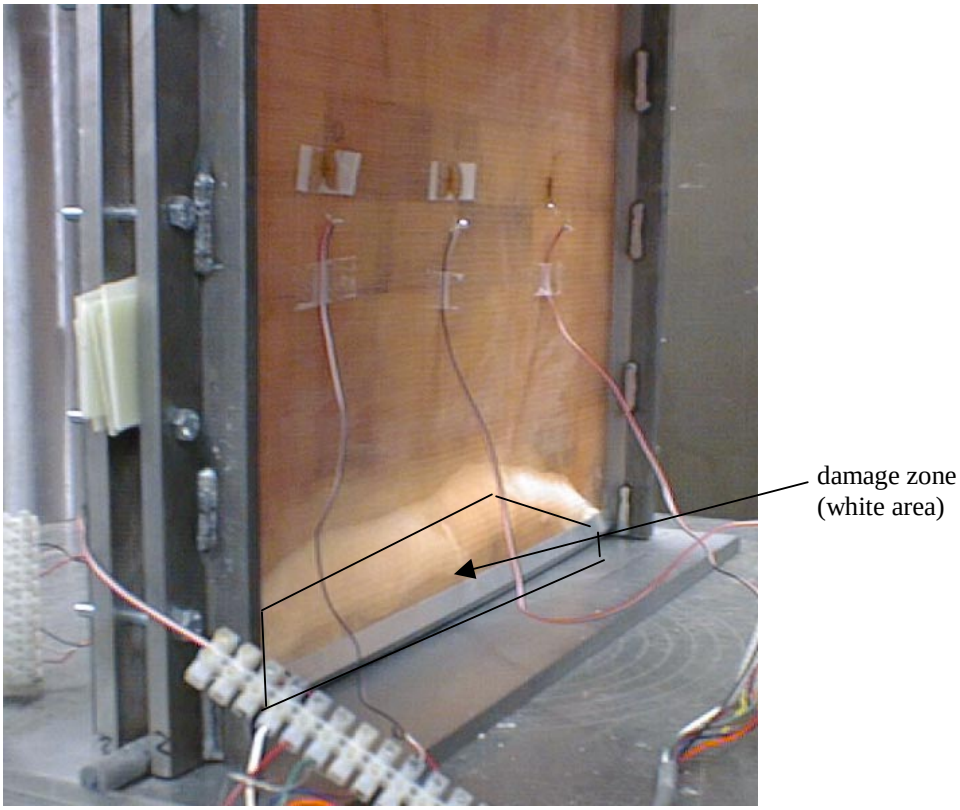

Figure 6-9. panel B5 shown after failure in the test fixture (SSSS condition)

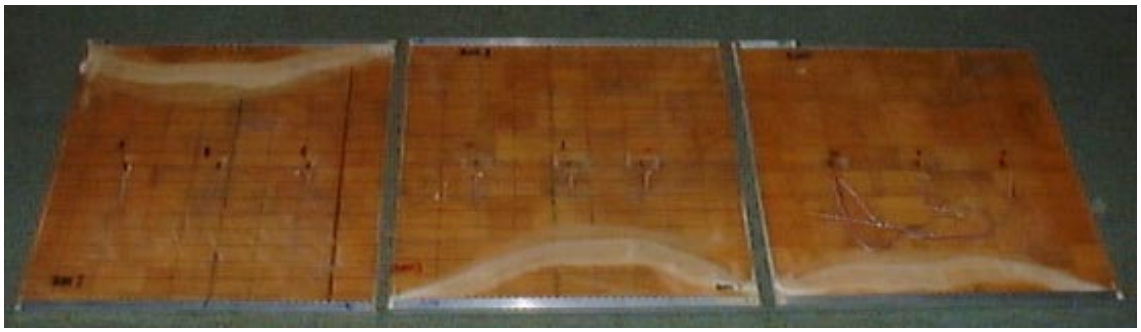

(a). comparison of the failure modes of panel B1,3&5 (all tested with the single piece fixture)

(b). close-up of the failure mode of panel B3 (damage zone is the white area)

Figure 6-10. failures of the B-series panels tested in the SSSS condition

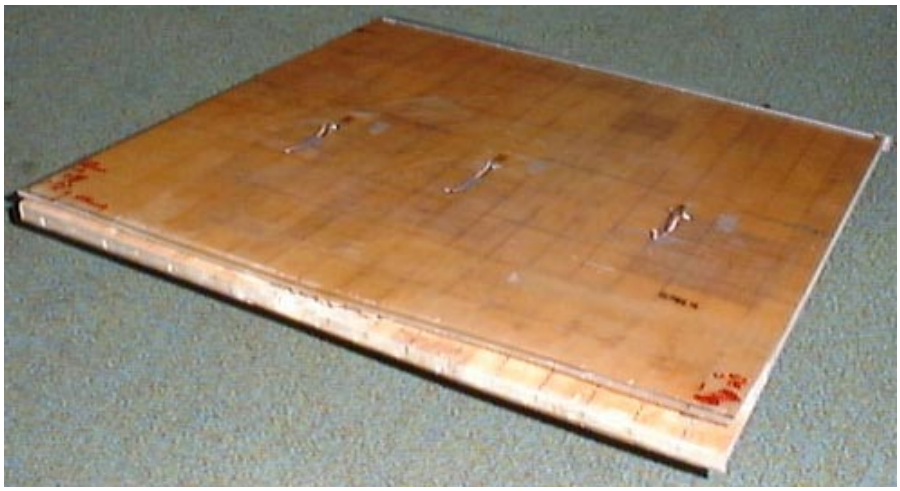

Figure 6-12. failure of panel B4 which which failed in the single piece fixture, in the SFSF condition

FEA Validation of the B-Series

SFSF Validation

In the previous section, consistent results were found for the SFSF support condition, especially with regard to the asymptotic (neutral) buckling load. All six panels buckled with the neutral postbuckling response. Therefore, the asymptotic buckling load was used as the main factor in determining the validity of the FEA nonlinear response prediction. Of the six panels, B4 was tested fully to failure, and consequently the furthest into postbuckling. For this reason, B4 was chosen as the representative experimental panel to compare with FEA response paths. The SFSF, FEA models were built with nearly the same deck as the SSSS decks, the only difference being that the side boundary conditions were removed. Mesh and perturbation convergence studies were also performed upon the B series, SFSF fixture models.

The random perturbation convergence load versus out of plane deflection (LOD) plot yields some characteristic FEA responses for SFSF models. It is shown in Figure 6-12 along with a single moment method response for comparison. The only critical buckling convergent responses are the hc/30 perturbation and the moment method cases. Smaller random displacements cause load drops (buckling shape snap through) while greater displacements cause local curvature errors and unsolvable models. Once into the postbuckling response, the random models follow neutral postbuckling responses over some range. For each model, sometime after the out of plane deflection exceeds one thickness (seldomly before) the model begins an unstable path (or the solution becomes non-convergent). The response seems to inflect again after the initial drop in load, and perhaps follow another neutral response at a lower asymptotic load. However, the solution usually becomes non-convergent before any such deduction may be made conclusively. Two responses are shown for different models with hc/30 perturbation sizes (cases #3 & 4). They demonstrate that the asymptotic load and load drop are fairly consistent for a particular random perturbation. The strain at which the load drop occurs and its slope are also dictated by the size of the perturbations. With exceptions due to unique displacement patterns, the smaller the displacement size the higher the strain at which it the drop occurs and the more gradual the slope followed. The two models without random displacements, the no perturbation and moment method cases, do not experience load drops. Both cases follow nearly the same postbuckling patterns, which again demonstrates the effects of the random displacements.

The random perturbation mesh convergence study LOD plot can be found in Appendix () along with the complete LOD plots for all the models solved. While the SFSF fixture models also experienced the mesh size response shift (see Chapter 4), once above the 6x7 panel grid density, no discernable mesh size dependence was detected. If one exists, it is overshadowed by the effect of the random perturbations upon the asymptotic load.

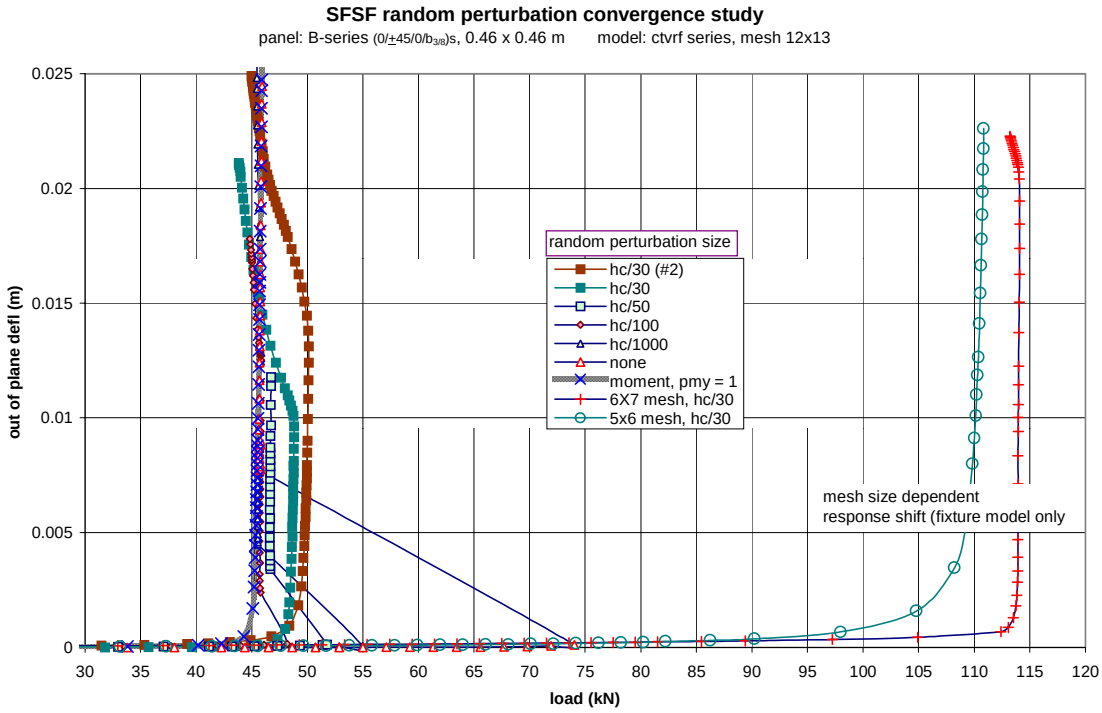

Figure 6-12. Perturbation convergence and other response characteristics of SFSF condition flat FE models

As a consequence, four different FEA models are plotted versus experimental B4 in Figure 6-13. The FEA critical buckling loads are seen to bound B4. While B4 eases into the asymptotic load through a broad knee (as do the rest of the experimental panels), the FEA models all experience very sharp knees. The early neutral postbuckling responses quickly flatten in load to the asymptotic load. The early random method FEA postbuckling responses seem to be fairly accurate, however all experience a load drop not seen in the experiments. While some experimental runs softened a bit before dropping back to their asymptotic loads, they never reached a seemingly neutral response before dropping. The random method postbuckling load drop is therefore considered a purely FEA random perturbation phenomenon and not an

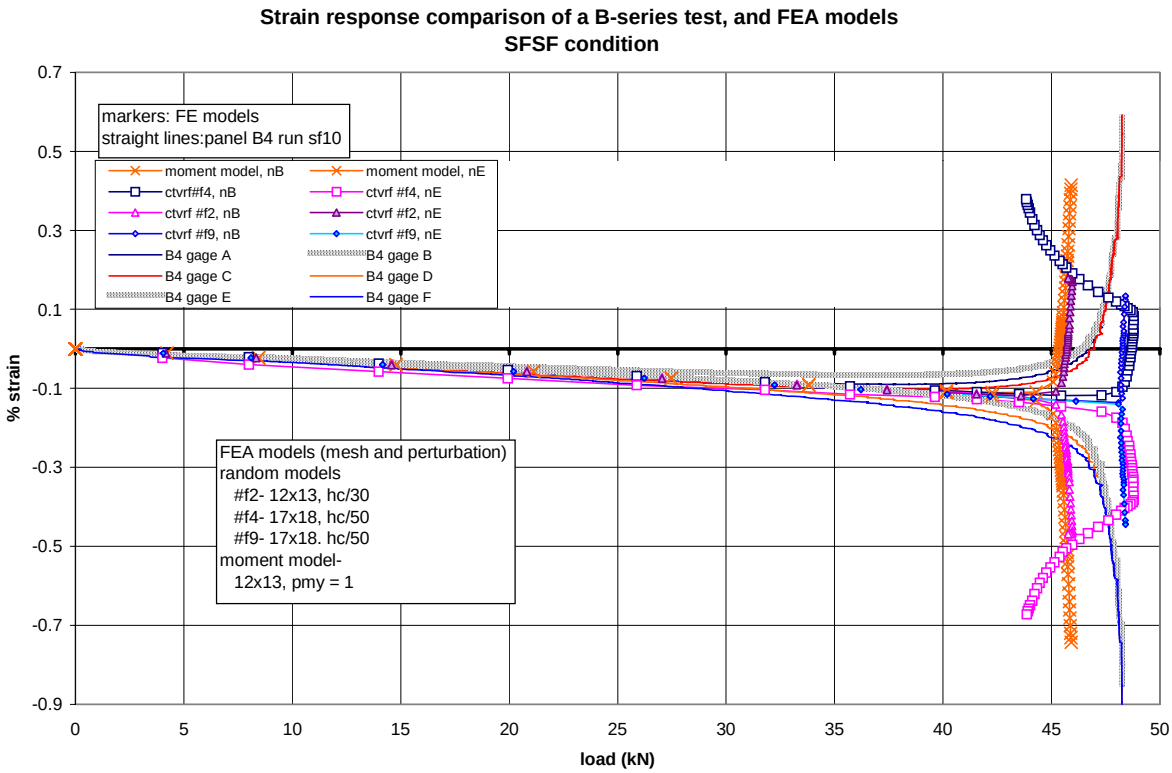

Figure 6-13. B-series SFSF, FEA to test comparison of load-strain histories

accurate prediction of the true postbuckling response of a flat SFSF sandwich plate. In contrast, the moment method seems to give accurate critical, early and late postbuckling responses.

The FEA models all had exactly the same dimensions with panel length of 44.45 cm (45.8 with the fixture) and widths of 45.7 cm. The experimental panels had slightly varying dimensions ($\pm$ 1.5%). To make better numerical comparisons, the width was divided out to yield resultant loads per unit width. Any difference due to length was considered negligible since all had very close aspect ratios. Table 6.6 contains the results for the six experimental asymptotic resultant loads and the early FEA asymptotic resultant ranges.

Both perturbation methods give accurate early buckling results. The random perturbation early asymptotic loads closely mirror the single piece fixture asymptotic load range, both ranging from 101 to 106 kN/m. The piecewise fixture asymptotic loads are just below this at a maximum of 4%, with the possibility of rising into the same range for B7. The moment method gives a ‘stable’ neutral postbuckling response, with a late postbuckling asymptotic load of 100.6 kN/M, which is the lower bound for the random perturbation asymptotic loads (those with the smallest perturbations).

Table 6.6. comparison of the asymptotic loads for the experimental panels and FEA models

EXP panel	resultant asymptotic load	slope adjust
B1	103.0	0.22
B3	101.5	0.64
B4	105.7	0.00
B5	103.3	0.43
B7	99.2	2.12
B8	97.3	0.21
FEA model		
random method minimum (early asym)	101	
random method maximum (early asym)	106	
moment method or no perturbation	100.6	0.44

* linear FEA critical buckling predicted at 97.3 kN/m

As noted earlier, the strain results from the experimental panels suggest that the free edges deform out of plane more than the center for these panels. The finite element models definitely deform this way. An example of a typical out of plane deflection shape is depicted in Figure 6-14. The edges can be seen to deflect more than the center by the contour lines around the midlength of the panel.

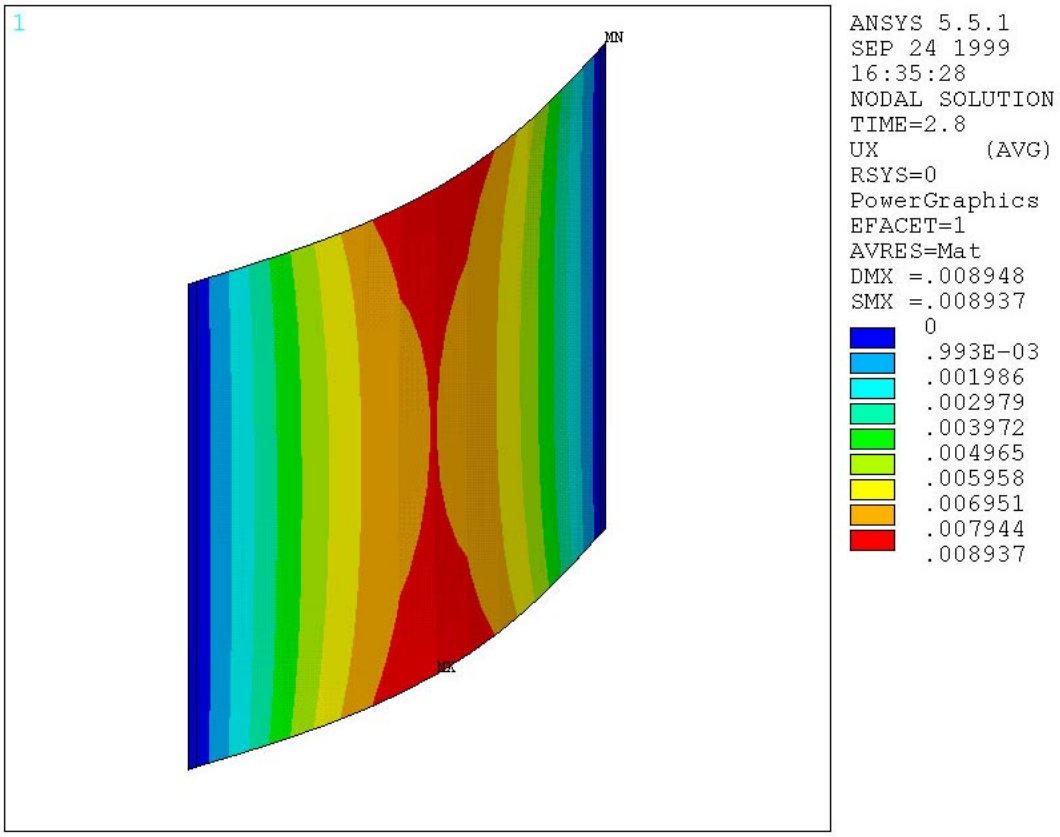

Figure 6-14. example of a SFSF, FE model buckling shape

SSSS FEA Validation

Because of its consistent, neutral postbuckling response, the SFSF support condition was an easy response with which to test the validity of the FEA buckling analysis techniques. The stable postbuckling response of the SSSS B series (single piece fixture) flat panels are more difficult to compare. The critical buckling (strain reversal) load of these panels has been shown to be sensitive to perturbations (see Chapter 4 for FEA and the previous section for tested panels). The experimental panels in particular have critical buckling loads ranging from 88 to 110 kN. Therefore, some criterion must be established with which the FEA validation is to be judged. Three major points must be satisfied and are listed below:

- The FEA critical buckling must be within the accepted testing values (88-110 kN) or slightly lower (conservative by up to 15%).
- FEA must predict the correct mode shape (mode 1 here).
- FEA must predict the correct postbuckling response (stable), and have fairly similar slopes and values found in the experimental strains versus load plots (qualitative judgement).

The first two points are examined together below in Table 6.7. In addition to the various FEA analyses, two 3-layer analytical techniques, and the classical lamination theory stability (CLT) analyses, were solved for the B series panels and are shown also. The 3-layer solutions and CLT are all for ideal SSSS sandwich panels. The fixture was not accounted for in the material properties or any other support condition constants. For this reason, the 'pure' FEA analyses (ideal SSSS) are also included as reference values to qualitatively examine the effect of the fixture to predictive analyses. All predictive analyses used panel dimensions of 45.7 x 45.7 cm, hc = 0.935 cm, t_t = 1.27 cm.

To find the face sheet properties to be used in the equations used by Vinson, the individual ply elastic properties were taken from the FEA material property deck subroutine, and entered into the laminate program Composite Pro ™. Composite Pro uses standard classical lamination theory to find laminate properties for the face sheets. Composite Pro then uses these properties to solve for 4 sandwich failure/buckling theories, (overall panel critical buckling, facesheet overstressing, facesheet wrinkling and core shear buckling) and outputs the critical mode [MIL-HDBK-23A (1968)]. These facesheet properties were then entered into a MathCad ™ worksheet and the equations used by Vinson (1987) were used to solve for each of the four failure modes again. This worksheet can be found in the Appendix. Overall panel buckling was found to be the critical mode for both sets of linear equations. The Vinson equations

give facesheet wrinkling and coreshear failures at least an order of magnitude higher than overall buckling. The loads at which they would occur are 14.74 and 2.34 GN, respectively. The CLT stability loads were found by transporting the Dij bending stiffness terms of CLT calculated by Composite Pro (assuming the core to be just another ply layer) into the common stability solution proposed by Jones (1975).

Table 6.7. the critical buckling loads and mode shapes for the B-series, SSSS condition, tested panels and predictive analyses

	fixture models		ideal sandwich models		ideal sandwich models	
analyses	critical buckling (kN)	mode	critical buckling (kN)	mode	2nd stability (kN)	2nd mode
experimental	**88-110**	**1**				
moment method FEA	90.7*	1	80.9*	1		
random method FEA	83.3*	1	80.8 +- 1.8	1		
eigenbuckling FEA	96.5	1	88.4	1	138.6	2
Vinson eqns			24.4	1	25.4	2
Com. Pro eqns.			72.5	2		
classical lamination theory (Jones)			158	1	312	2

* values from single FEA runs (convergent)

The FEA models, both the fixture, ideal, linear and nonlinear models, predict the correct mode shape of one. The moment method and eigenbuckling finite element analyses predict critical buckling to occur within the experimental range for the models including the loading fixture. The random perturbation is slightly more conservative, having a critical buckling load about 5% lower than the experimental range. As shown in chapter 4, the ideal FEA models all predict lower critical buckling loads than the fixture models. The nonlinear methods were about 5% conservative of the experimental range, while the linear model was just at the lower end of the range. These models all used the isotropic balsa data set, which again is the average of the orthotropic data. If the orthotropic, or transversely isotropic data set were used, the core property sensitivity study predicts the critical buckling load to increase 15-20%. For the B-series panels this would raise the critical buckling load to ~100 kN which is still within the experimental range. The remaining series also use the isotropic balsa data set and as long as the predictions are conservative the orthotropic data would also be valid. The various FEA analyses all pass the first two validation requirements, with the fixture models yielding more accurate, but still conservative results.

The two sets of FEA model results, fixture and ideal, were included to show the elastic effects of the fixture on FEA results and be a reference for the results from the 3-layer analytical results. Both analytical models have trouble predicting an accurate response. The CompositePro program predicts

critical buckling to occur near the correct load, however, it predicts a mode two shape. This result is counterintuitive and contrary to most plate buckling problems involving aspect ratios of one. A mode two response for a panel with an aspect ratio one might be intuited to occur when the elastic modulus in the load direction was much more compliant than the offload direction. With this particular lay-up, the opposite is true and mode one is still expected. As a result, a significant effort was made changing dimension parameters and material properties trying to find possible input mistakes or properties which would yield critical buckling modes of one half sine wave. An aspect ratio of 3:4 (45.7x61 cm) finally yielded a mode one buckling shape with the Composite Pro program. No material property changes attempted (centered on E_{fx}, ply orientation, face sheet Poisson's ratio and the core shear modulus) produced mode one critical buckling.

The equations used by Vinson predict the correct mode shape of one, however the load is approximately three times too low. A critical buckling prediction this low is not an accurate one, and not one in which an engineer could place enough confidence in to design with. Note that the sandwich panels studied here are relatively thin and compliant ones which may produce problems for these two three-layer buckling solutions by placing them outside of their valid ranges. The possibility of a user mistake exists as well.

The two surprising and counterintuitive three-layer theory results are contrasted by the CLT results which produced the expected mode shapes and loads. The correct, and intuitive mode one shape was predicted as the critical buckling mode. Without the effects of transverse shear included, the critical buckling load was 75% too high. The CLT solution used the exact same material properties as the two three-layer results and was initiated as a check for simple errors. The expected and reasonable results from CLT reduces the probability of user mistakes and increases the suspicion that the three-layer theories simply perform poorly and inadequately over this parametric range and material property set.

However, these two 3-layer critical buckling solutions are well established and trusted in the literature, as exemplified by their use in a commercial laminated theory program and as a base for optimization studies. As used in the present study, they performed poorly and could not predict the correct mode shape and critical buckling load of a flat, aspect ratio one, solid core, sandwich panel. Considerable time was spent to find user errors or any possible explanation, however none were found. In light of this problem, the critical buckling solutions from these sources are deemed as invalid as used here, and all

subsequent results viewed with skepticism within the study. It is stressed that the results from the closed form three-layer solutions are preliminary, with further study and confirmation required before a serious case can be made against their validity as applied to these sandwich panels as the possibility of user error still exists.

The next part of the FEA validation procedure involves only the nonlinear FEA models. (in regards to the orthotropic data set: the early and middle postbuckling response followed very similarly sloped paths, only in the deep postbuckling repsonse did the responses differ noticeably as the orthotropic balsa models took on a stiffer path) One of the main focuses of the study was to validate nonlinear buckling techniques which could be used on whole complex structures, with tests upon smaller, simpler substructures. The technique which is best suited to study structures is the random perturbation technique. As seen in the preceding SFSF section, the random perturbation technique often had problems predicting the deep postbuckling response. Usually the problems centered upon slight mode shape shifts caused by the random nodal displacement perturbations. Similar problems can be found within the SSSS flat panels as well, although in SSSS panels, the effects of the mode shift are more subtle and less harmful to predictive ability than in the SFSF. For this reason several different FEA models are compared to experimental values. Earlier, panels B1 and B3 were deemed the best test cases and therefore are the two with which the models are compared. B1 and B3 show different response paths, especially in the critical buckling and early postbuckling regions. Therefore, depending upon which model is shown with which test, the results can be manipulated to look better or worse. In this case, the best cases and worst cases are shown in order to fully understand the problem.

The best cases involve comparing B1 to either of two FEA models, ctvrf #2 (fixture model, random pert., rp = hc/30, 12x13 panel mesh) or ctvmf 3 (fixture model, moment pert., pmy = 20 Nm, 17x18 mesh). The two comparisons are plotted in Figures 6-16 and 6-17 respectively. Case ctvrf #2 shows two values for the center strains (i.e. nE and nE(2)) because the model did not have a node at the true center, and the two nodes on either side were the best fit. As seen in the SFSF comparisons, the FEA models have a much sharper critical buckling knee than the tests. The FEA and experimental critical buckling regions overlap, with the FEA knee occurring slightly earlier. For both FEA models, the early postbuckling response is more bending compliant than B1 (slope is higher). From there, the center convex response

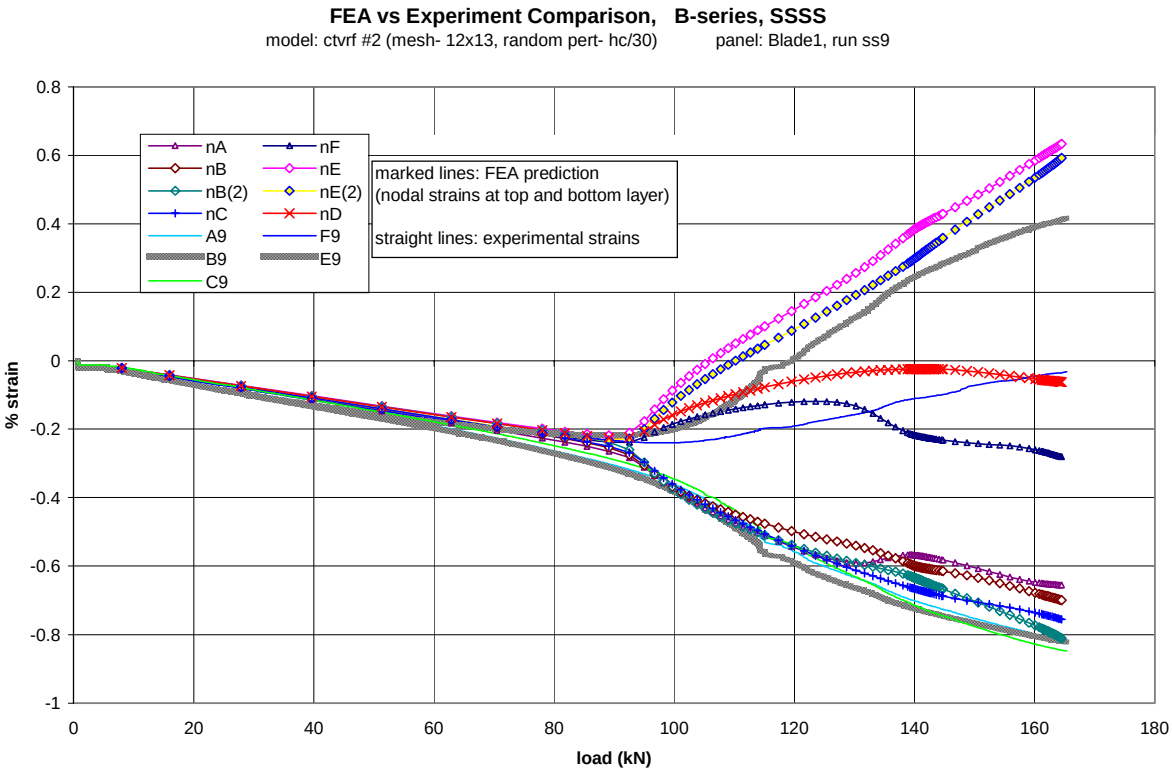

Figure 6-16. B-series, SSSS, FEA to test comparison of load-strain histories showing good postbuckling correlation

paths of ctvrf #2 begin to converge with B1, then parallel the experimental path with slightly higher strains. The side strain locations (A and C) show similar responses, although once into late postbuckling, rather than paralleling the experimental path, the strains converge at loads past 120 kN. The concave side strains, both FEA and B1, all follow very similar paths. As noted earlier in the experimental section, the center concave strain gage (B) does not show the difference in strain from the sides (A,C) that the convex side does (E from F). This FEA model does not show any significant difference either. Run ctvrf #2 shows very good agreement on the concave side with experimental panel B1. Throughout the strain locations, this FEA model predicts the linear, critical buckling and posbuckling responses very well. The only notable difference involves the noticeable shift in the paths of nodal locations nA and nF (which are from the same node). These path shifts occur because of a mode shape shift slightly away from that side, which does not show up in locations nC and nD.

Case ctvmf #10 (Figutr 6-17) shows similarly good agreement, especially on the concave side. Again the strain difference in the convex side between center and sides is not seen on the concave strains. On the convex side, after initially higher slopes, the nodal strains converge back to the experimental strains.

Until the mode shape shift late into postbuckling, the moment method has a stiffer, stable, late postbuckling response than either B1 or ctvrf #2. The mode shape shift can be detected in the slight difference between the strains of nA and nC (also nD and nF). The strains had been almost exactly the same due to the perfect geometry and symmetric mode shape. The shift can be inferred as towards side AF due to nA having a slightly higher strain than nC. The shift forces a more compliant path, which agrees better with panel B1 run ss9. Both of the best cases predict the buckling and postbuckling response of a flat, SSSS, sandwich panel very well.

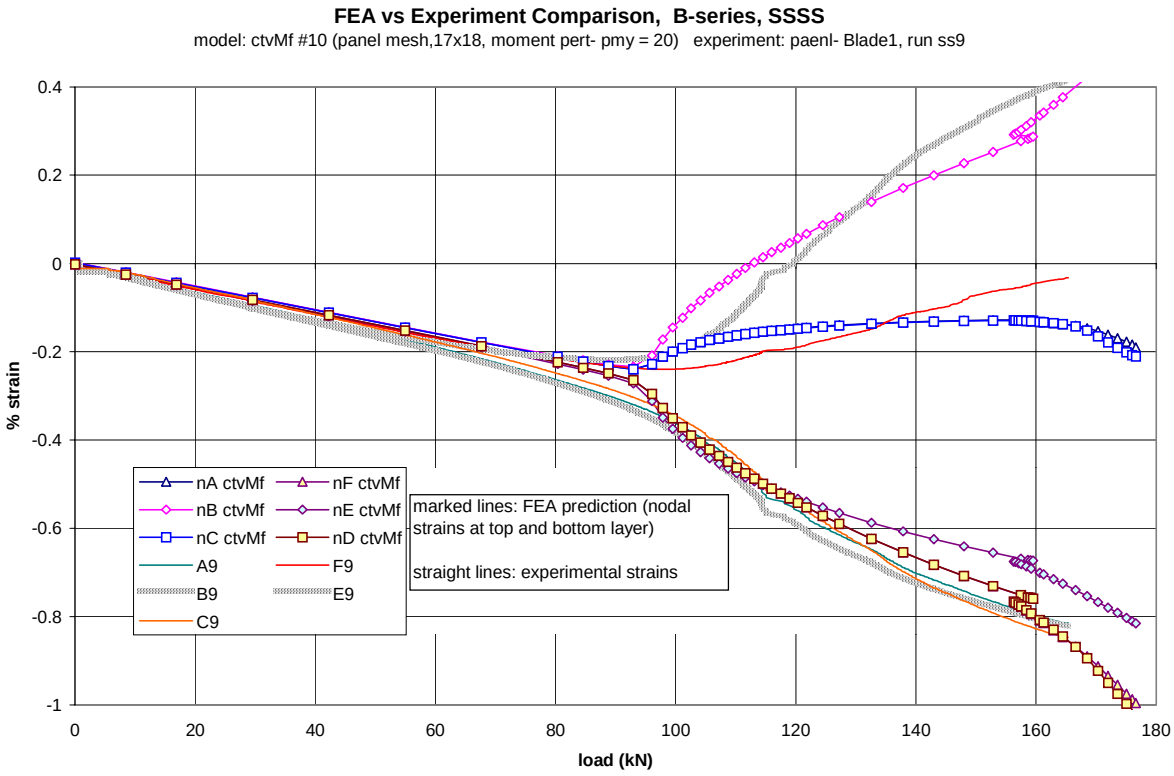

Figure 6-17. another B-series, SSSS, FEA to test comparison of load-strain histories showing good postbuckling correlation

The worst case is shown in Figure 6-18. Panel B3, run ss1 is plotted next to FEA model ctvrf #3 (fixture model, random pert., rp = hc/50, 17x18 mesh). B3 has a later and more gradual knee than B1, while ctvrf #3 has the typical FEA sharp knee. In the linear response, model ctvrf #3 has a wider spread than the two previous models. This is due to the random perturbations and a finer mesh than the 12x13 model. This combination allows for a more complex perturbed shape and the possibility of higher local curvatures which cause the strain field to diverge more. The high spread of the strains in the linear

response means that similar imperfections in the experimental panels can cause the strain differences, not just misaligned, crooked loading. Whether or not this relationship is true, the result is the same within the linear realm. As with the two earlier comparisons, the center convex FEA strain begins with a higher slope in the early postbuckling response than the experiment. Rather than slowly converging, though, this FEA model experiences an early and severe mode shift. This mode shift actually causes the center convex strain to follow a negative slope for a short time (from ~110 to 125 kN). The shift is so severe that the center convex strain (nE) converges with a side convex strain (nC) at 145 kN. The shift can also be dramatically seen on the concave side strains. Nodal strain nD follows a much more compliant path than any other strain, FEA or experimental. Meanwhile, nB follows a very high positive slope and nears the convex, opposite side strain of nD. The mode shift in ctvrf #3 makes FEA unable to properly model the late postbuckling response with respect to nodal strains. It is worth emphasizing that in this worst case comparison, the FEA critical buckling load is conservative by about 15% which is a serviceable result.

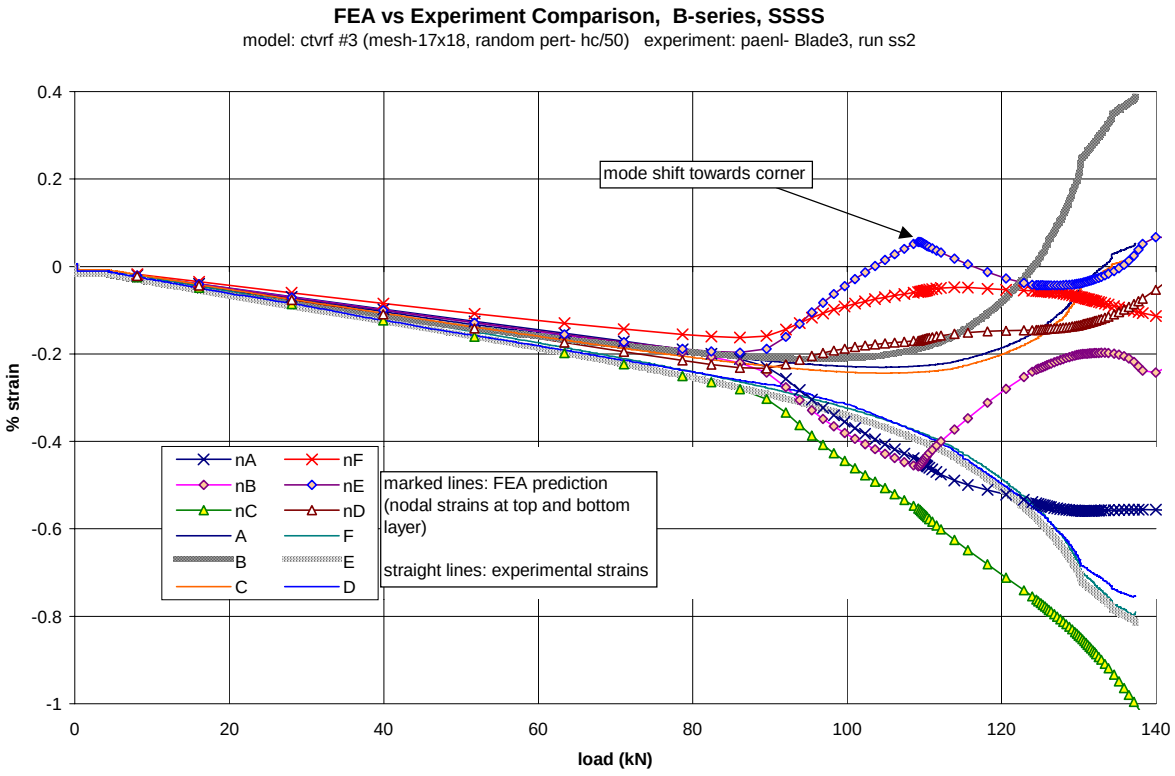

Figure 6-18. third B-series, SSSS, FEA to test comparison of load-strain histories showing relatively poor postbuckling correlation

A different look at ctvrf #3 reveals a more definitive judgement of late postbuckling response prediction using the random perturbation method. Figure 6-19 is an LOD plot for the three FEA models used above as comparisons. The mode shift which caused such a severe change in the nodal strains appears as only a slight drop in the slope of the LOD stable postbuckling response. Run ctvrf #2 does not show any slope changes in the LOD path and only a small change in the strain response. This demonstrates the extreme effect mode shifts can have on nodal strains without affecting the more general out of plane deflection plots. Consequently, after a mode shift, although the nodal strains may no longer be valid data, the general buckling response (indicated by in and out of plane deflection load histories) remains valid.

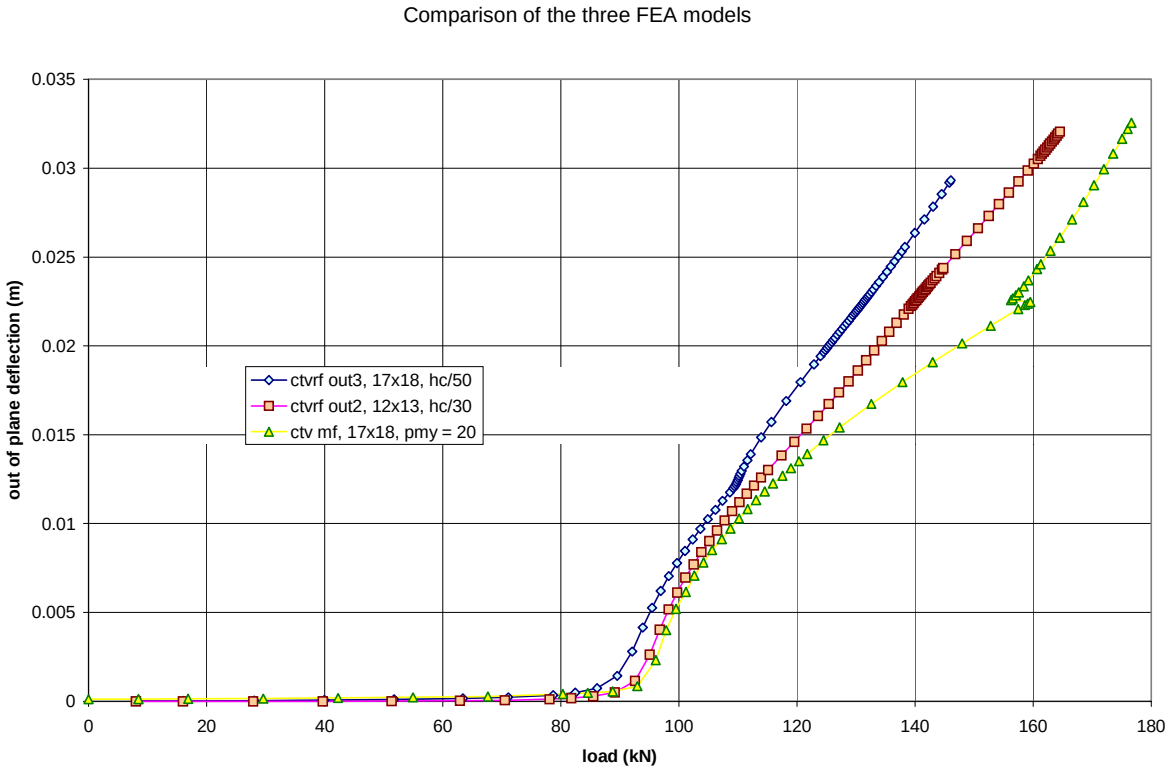

Figure 6-19. LOD plot of the three FE models used for qualitative validation of the B-series, SSSS tests

Facesheet Lay-up, C-series

panel data: flat, (90/0/90/$b_{3/8}$), ~46 x 46 cm

The same requirements met by the B-series must again be met for the C-series to show that the FEA techniques used are valid for a wide range of facesheet lay-ups. The C-series has facesheets which behave very differently than the B-series (all subsequent values quoted are FEA subroutine ply properties transformed into facesheet properties by classical lamination theory with the CompositePro program). The C-series has a (90/0/90) lay-up which is much stiffer in the width direction than in the load direction (axial moduli of 24 and 16 GPa respectively). This contrasts with the B-series which had facesheet moduli of 25 and 8 GPa respectively for Ex and Ey. Additionally, without 45 degree plies the in-plane shear modulus, Gxy, of the C-series is significantly lower than the B-series (3.5 versus 8.0 Gpa). Finally the Poisson's ratios for the two are also quite different due to the lack of 45's in the C-series. The B and C-series xy and yx ratios are; B-series, 0.37 and 0.12; C-series, 0.10 and 0.15. It was expected that these greatly different facesheet properties would create different buckling responses in the SFSF and SSSS support conditions with which the FEA techniques must be able to cope and predict accurately.

The C-series tests are first discussed and evaluated. Then the FEA predictions for the C-series are compared and validated versus the valid test data for each support condition separately. Then the C and B-series FEA and experimental buckling responses are compared to deduce the effect of the lay-up change and any problems thereby created in the FEA prediction.

C-series Test Results

SFSF Tests

Three C-series experimental panels were tested in the SFSF support condition, panels C1,2,&5. All three panels were tested with the single piece load support fixture. A sample load-strain history for each panel is plotted in Figure 6-20. Panels C1 and C5 were tested fully to asymptotic buckling, while C2 was only tested past its strain reversal. The final slope of C2 sf5 suggests that it will have an asymptotic load around the same load as C1 and C5. Further testing of C-series panels was not required because these three provided good confidence in the results with asymptotic buckling in the 31-35 kN range.

The C-series SFSF tests showed the same trends as the baseline, B-series panels. Figure 6-21 is a plot for each of the SFSF full buckling runs (sf3,4&5) of panel C5. The figure shows that a panel would

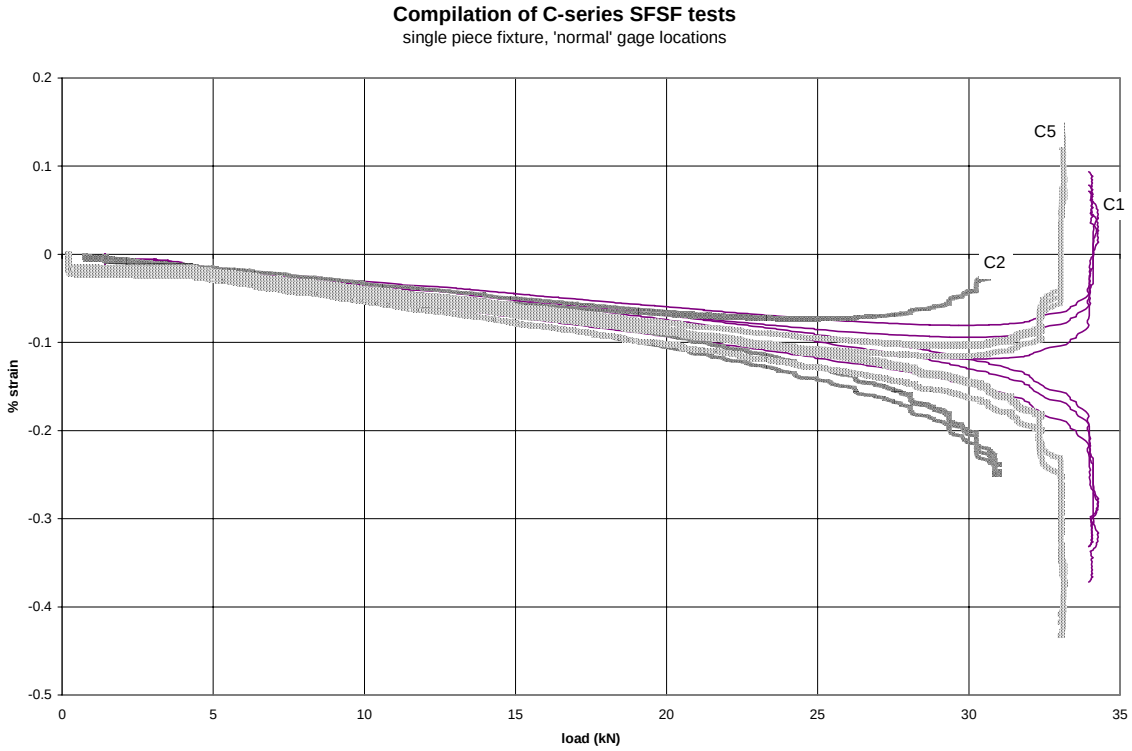

Figure 6-20. compilation of C-series SFSF tests containing one example test per panel

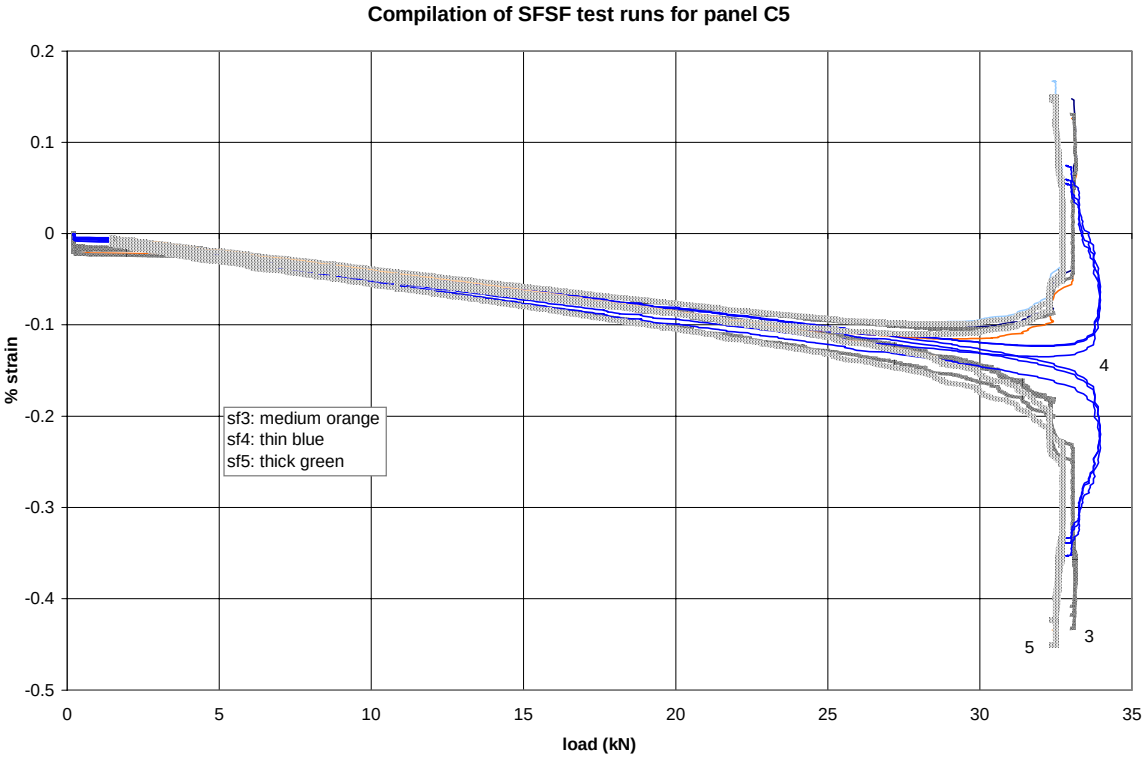

Figure 6-21. compilation of the three SFSF tests of panel C5 tested into the postbuckling range

consistently buckle at, or be converging to the same asymptotic load. Table 6.8 tabulates the statistical and buckling data from the C-series SFSF buckling tests. C5 shows that consistent asymptotic buckling loads are found for flat SFSF sandwich panels, while their strain reversals may vary due to loading imperfections (resulting in different coefficients of variation of strain). A similar investigation into the widthwise strain and bending strain distributions as performed on the B-series panels confirms that flat SFSF panels tend to deform more at the free edges than in the middle. The same characteristic responses of the C-series and B-series was expected because they share the same geometry and support condition.

Table 6.8. the statistical and buckling data for the C-series SFSF buckling tests

			deviation statistics (CV%)			buckling data (kN)				
panel	run	shim	min.	*@ load*	10 kN	reversal	*noise*	asymptote	*adjust*	comments
C1	3		13.9	26.9	23.5	26.0	1			
	4		13.5	30.2	23.7	32.5	0.5			
	5		16.6	23.7	23.6	29.5	0.5	34.1	-0.1	
C2	4	flipped	57.4	9.1	58.9	20.4	0.2	NA		max load, 27.9 kN
	5		16.1	11.3	16.3	24.4	0.3	NA		max, 31 (nearing asym)
C5	3		7.1	27.9	12.4	31.6	0.2	32.6	-0.5	at 18.4 kN; 8.9% CV
	4		10.4	18.7	13.2	29.0	0.5	32.8	-0.5	
	5		11.9	18.6	14.8	28.4	0.2	32.1	-0.3	

SSSS Tests

The same three panels that were tested in SFSF were tested in SSSS as well, C1,2 and 5. Similarly, all three were tested with the single piece load support fixture. The final test responses for each panel, the ones to failure, are compiled together in Figure 6-22. The data from all six strain gages are shown for each panel. Panel C1 appears to have a stable postbuckling path, although it fails before membrane stiffening can occur. C2 also appears to be on the beginning of a stable postbuckling path as well, but it fails even sooner in the early postbuckling response. C5 definitely followed an unstable postbuckling path, however, this response was due to poor fixture performance. A large gap, approximately 2 cm, was present between the top of the knife edges and the end of the panel. Once buckled, the rollers were seen to rotate at the side edge of the panel. Meanwhile, the knife edges were seen to rotate as a solid unit from bottom rollers. This created a complicated buckled shape and a complicated response. The response before this complicated buckling shape, before finite roller rotation, is assumed to

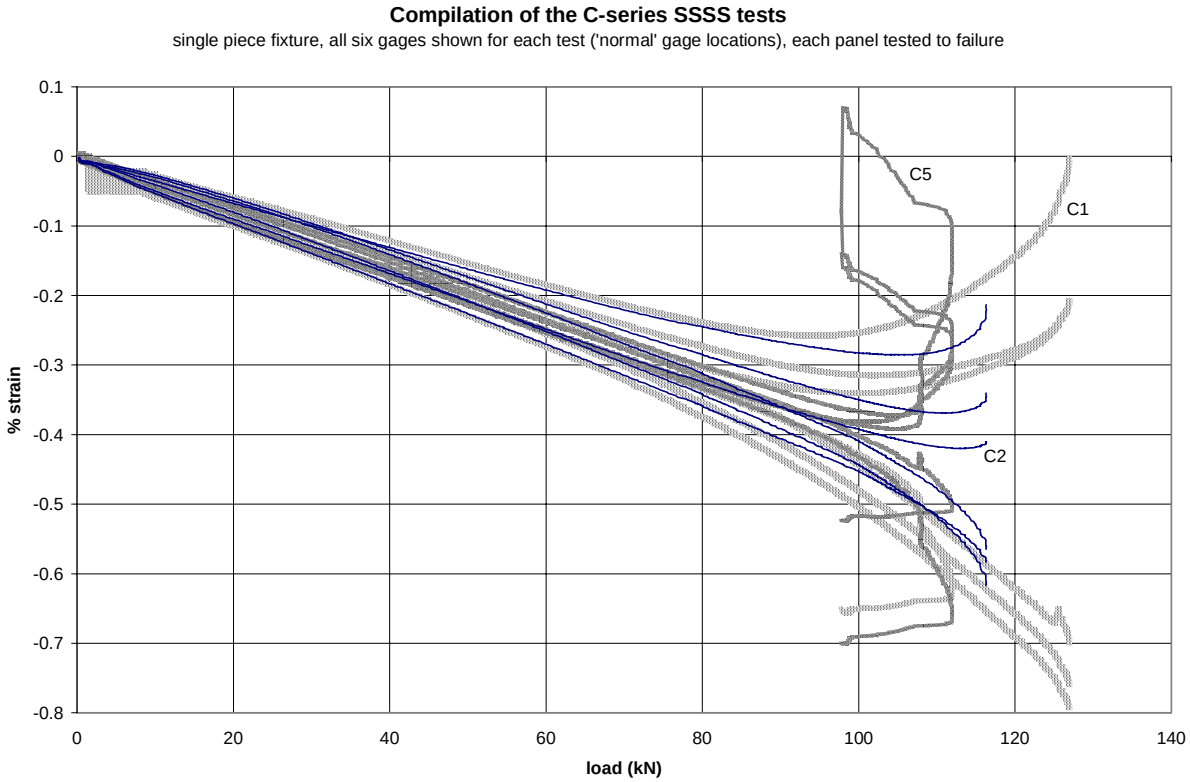

Figure 6-22. compilation of the C-series SSSS tests, one example shown for each panel (the test to failure)

be accurate and correlates well with the other two panel responses. Therefore, the critical buckling load of C5 is trusted as valid, while the postbuckling path is not.

The average modulus data for each test at the 30 kN, 60 kN and maximum linear response are compiled in Table 6.9. The same loading trends which occured in the B-series tests also happened to the C-series; the SSSS runs tended to have slightly higher moduli; and the values generally tend to asymptote towards a median value. The median axial modulus here is between 17 and 18 GPa. The calculated face sheet modulus from the FEA subroutines is 16.8 GPa (24.6 in the width direction).

Table 6.9. C-series panel dimensions and calculated axial moduli from tests

dimensions (cm)			(+-0.08 cm)		face sheet modulus (sandwich theory) Pa		
#	length	width	supp.	#	@30 kN	@60 kN	@max linear
1	44.6	45.72	SFSF	av	1.86E+10		
			SFSF	1	1.86E+10		
				2	1.91E+10		
				3	1.84E+10		
				4	1.84E+10		
				5	1.85E+10		
			SSSS	1	2.04E+10	2.01E+10	1.93E+10
				2	1.85E+10	1.86E+10	
				3	1.83E+10	1.84E+10	1.82E+10
				av	1.90E+10	1.90E+10	1.87E+10
2	45.4	45.72	SFSF	5	1.69E+10		
			SSSS	1	1.92E+10	1.80E+10	1.75E+10
				3	1.84E+10	1.78E+10	1.73E+10
				3	1.86E+10	1.82E+10	1.78E+10
				4	1.79E+10	1.78E+10	1.77E+10
5	46.2	47.13	SFSF	3	1.55E+10		
				4	1.54E+10		
				5	1.54E+10		
			SSSS	1	1.58E+10	1.65E+10	1.66E+10

The statistical and buckling data for the C-series SSSS tests are presented in Table 6.10. The critical buckling loads for the C-series SSSS tests were very close to the B-series, ranging from 94 to 114 kN. The range was entirely encompassed by one panel, C1. The large difference between the critical buckling loads of C1 ss1 and ss3 is unknown. No panel damage was heard and the strains for C1 ss1 were seen to travel back to zero confirming an elastic response (no damage). These two runs are plotted together in Figure 6-23. The center convex gage records almost exactly the same data for the two tests up to 80 kN. At 80 kN, the ss3 response begins to deviate from ss1 dramatically. Both runs end at the same load, ~125 kN, however, ss1 was unloaded at ~-0.13 % strain for gage E while ss3 failed at zero strain. It was stated in the baseline tests that very good consistency was found in tests on the same panel when no changes were made (see Figure B1SC). The only accountable reason for the severe change in response here between the two runs is major changes in the initial imperfections of the system, most likely due to epoxy damage during testing. These major changes may be accounted for in the 10 kN strain coefficient of deviation, with

an 8% increase. C2 has more agreeable data between tests ss3 and ss4, with buckling loads of 98.5 and 104 kN respectively and a respectively smaller 4% drop in the 10 kN deviation to delay buckling a little longer.

Table 6.10. statistical and buckling data for the C-series SSSS tests

		deviation statistics (%)			buckling data (kN)			failure data			
panel	#	min	@load	@10 kN	reversal	*noise*	dam.	mode	load	@strain (%)	comments
C1	1	11.0	81.4	22	114	0.5	none				not great uniformity
											at 58.5 kN- 11.7% std dev
	3	14.0	58.5	30	94	2	none	fiber failure, fix	127	-1.73e-3/ -0.793	failure induced by knife slip, ugly uniformity
C2	3	14.6	38.4	30	98.5	2	none				
	4	12.3	61.4	26	104	2	none	fiber failure, fix	116	.101/-.620	slight separation at end
C5	1	3.8	84.1	18	100	2		end delam	max: 112		knife to roller gap too large, roller rolled
									failure: 98		also some separation. disregard all but early postbuckling

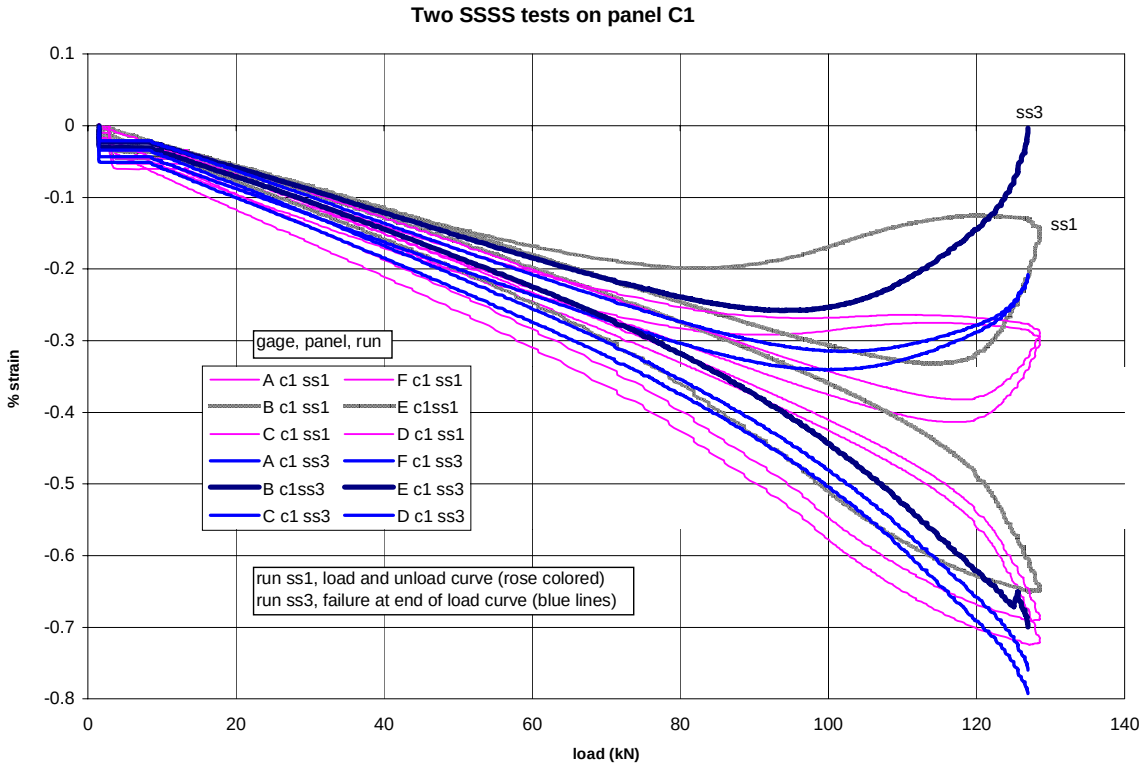

Figure 6-23. two SSSS tests on panel C1, first showing the loading and unloading historesis, second showing failure

Damage and Failure. Damage was not observed to occur before final failure in any of the three C-series panels. This is expected because these panels failed so early in the postbuckling response before the deformed shape could cause in any large bending strains. The C-series panels also failed in different failure modes than the SSSS B-series panels. C1 and C2 failed by face sheet failure across the midplane of the panel. In Figure 6-24, the convex side can be seen to have a linear crack with a narrow surrounding damage zone that travels across the entire midplane. The failure travels to the concave side via shear failure in the core. Unlike the B-series core failures, the balsa was not shredded, instead a single crack propagated cleanly through it. The convex side itself showed more damage, with face sheet delamination growing from the core shear failure. These failures occurred simultaneously with the knife edges slipping off the panels. The convex crack occured at the location of the slip. It is unclear whether the slip caused the failure, or the failure the slip. C5 failed at the top of the panel in the area between the roller and knife edges. The resulting damage zone was large and resembled the B-series failures.

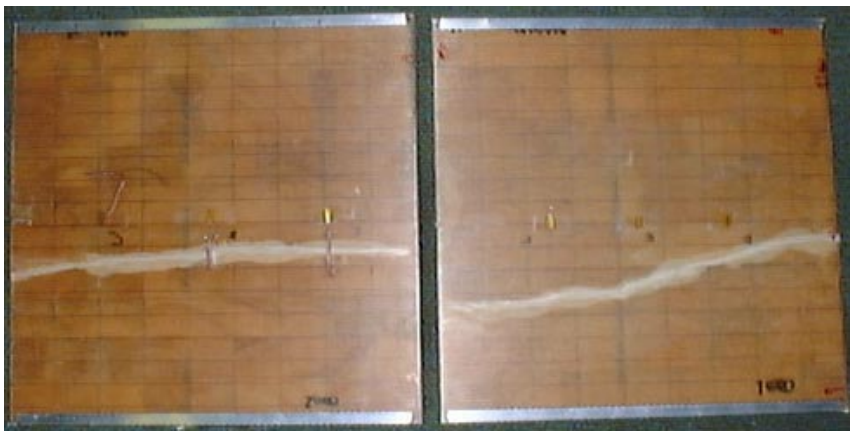

Figure 6-24. two C-series failures from testing in SSSS (the third was due to fixture problems)

The average strains of the three failed tests are shown in Figure 6-25. Only the valid portion, up to the critical buckling knee (~107 kN) of C5 is shown. The three panels are seen to have consistent average panel stiffnesses. Only C1 deviates from a linear path. Since no damage was observed before failure, the stiffness change must be due entirely to the expected center gage bending strain discrepancy seen in the B-series data. The six strains and their resulting average strain are plotted for test C1 ss3 in Figure 6-26. The expected bending strain discrepancy is present in this data. The three concave side strains can be seen to follow similar paths with no one gage changing at a greater rate than the others. Meanwhile, the center

convex gage (B) can be seen to have a much higher strain and a higher slope than the convex side gages. Since gage E is not experiencing the reverse trend due to the higher curvature and bending, the average strain begins to become more compliant. Therefore, the change in slope of the average strain is not a good indicator of damage to the panel and the simultaneous occurrence of damage and average strain nonlinearity in the B-series tests was just coincidence.

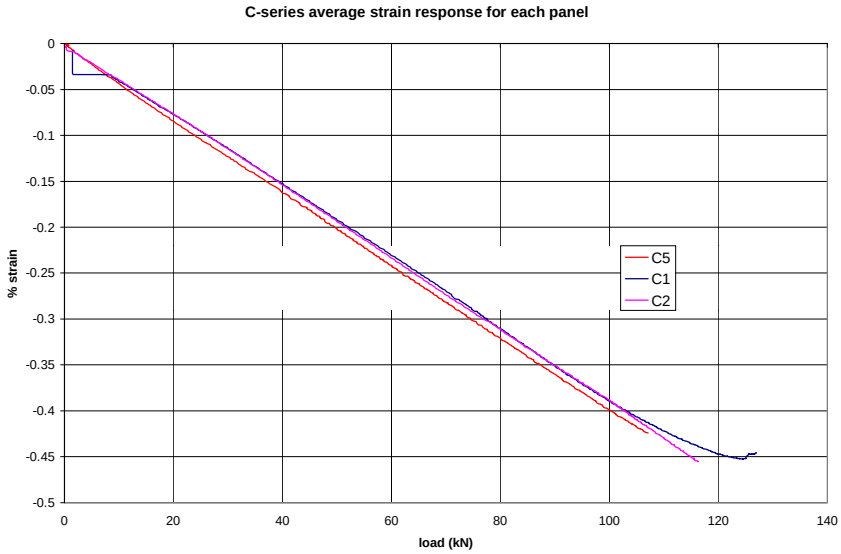

Figure 6-25. average strain responses for the C-series panels from the SSSS tests to failure

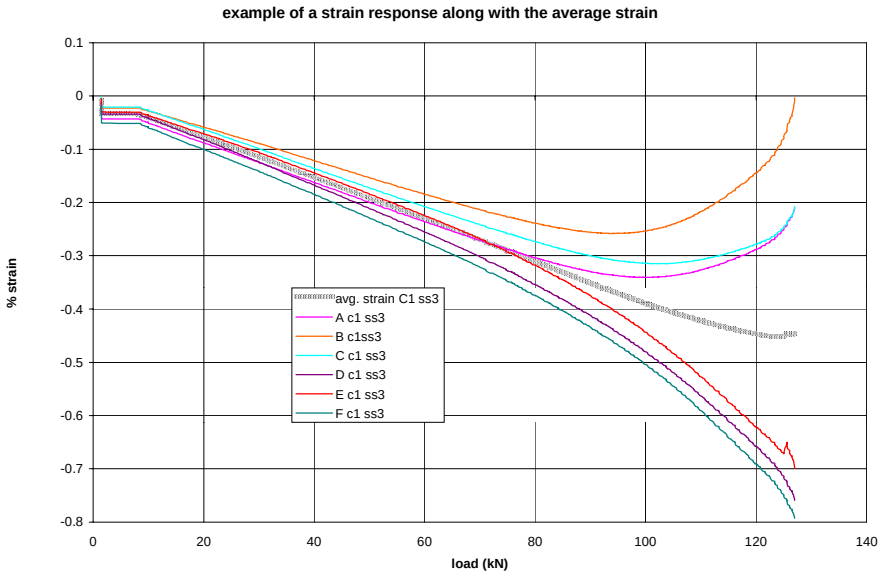

Figure 6-26. example of the load-strain C-series response in the SSSS condition, along with the resuliting average strain

C-series FEA Validation

SFSF Validation

The C-series and B-series SFSF tests responded with similar neutral responses. Therefore the asymptotic buckling load was used as the main determining factor of validity for the C-series FEA models. The same FEA trends found in the B-series SFSF models are also found for the C-series. The three C-series SFSF nonlinear FEA models are compared as LOD plots in Figure **6-27**. Each model has a different early asymptotic load due to its unique original shape. Each random perturbation model also becomes non-convergent or experiences a load drop due to a mode shift. Again, the early postbuckling neutral response is taken as the asymptotic load and any response past the load drop is considered invalid as a SFSF sandwich panel postbuckling response. The same mesh and perturbation size trends found in the B-series are assumed to be valid for this lay-up. The confidence in this assumption is very high due to the very similar nature of the model responses and exactly same boundary conditions and geometry.

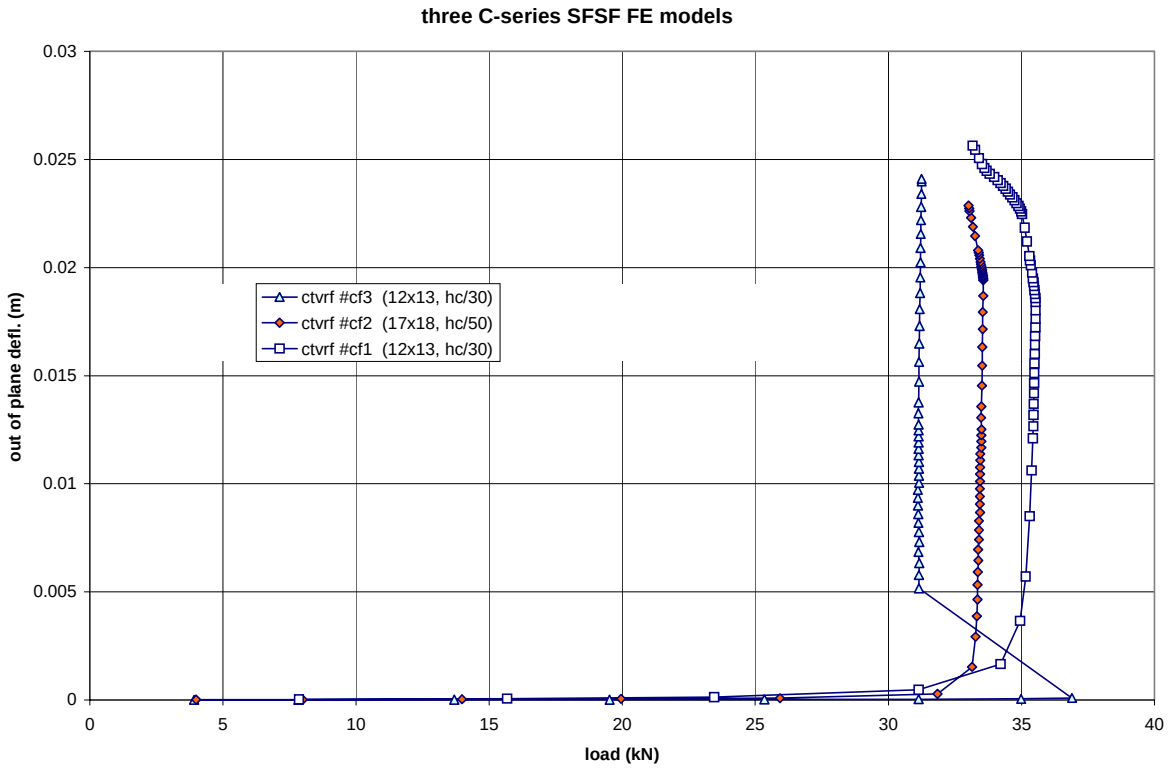

Figure 6-27. LOD plot comparison of three C-series SFSF, finite element models

Model cf2 (fixture model, 17x18 panel mesh, rp = hc/50) was chosen to plot versus the experimental tests in Figure 6-28. Again, the FEA model shows a sharp critical buckling knee and an almost immediate, flat neutral early postbuckling response. None of the experiments were tested deeply into their postbuckling response, but this FEA remains in a stable, neutral postbuckling response past the experiments (up to 0.4% strain). Table 6.11 tabulates the buckling data for the three experimental panels and the three FEA models.

Table 6.11. comparison of the C-series asymptotic loads for the experiments and FEA

experimental panels	asymptotic load (kN)	mode
C1	34.1 -0.1	1
C5 (ave.)	32.5 -0.5	1
FEA models		
nonlinear models		
cf1 (12x13, hc/30)	35.5	1
cf2 (17x18, hc/50)	33.5	1
cf3 (12x13, hc/30)	31.1	1
linear models	critical buckling (kN)	
ideal	32.3	1
fixture	30.8	1

The FEA buckling loads again compare favorably with the experimental for the SFSF support condition. The linear buckling model (fixture) was again the most conservative, as it was for the B-series. The random perturbation method, nonlinear models had early asymptotic loads surrounded the two full test cases and can be considered valid predictions. Interestingly, the pure linear model had a higher critical buckling load than the fixture model, opposite of intuition and the B-series results. The correct mode shape was predicted for each model. The second stability load was found at 65 kN and had a mode shape with 1 half sine wave in the load direction and 1 half sine wave in the width direction which was shifted a quarter wave to place a nodal point at the center of the panel. The third mode was the expected mode two, at a load of 90 kN.

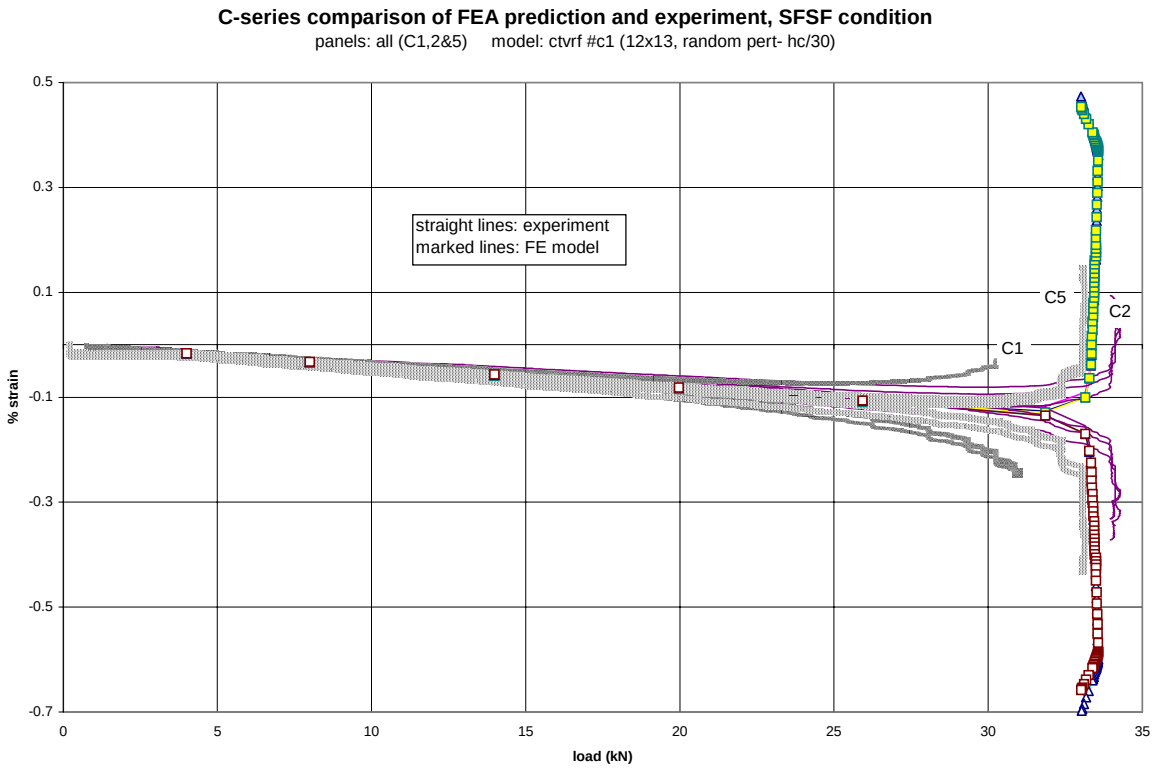

Figure 6-28. FE model prediction as compared to tests for the C-series in the SFSF condition

SSSS Validation

The same three requirements met by the B-series SSSS panels must again be met by the C-series. Three nonlinear random perturbation models (with the fixture modeled) were run, as well as linear FEA stability models with and without the fixture and finally the two, linear, 3-layer analytical solutions. The critical buckling and mode shape data are compiled for these models and the experiments in Table 6.12.

Table 6.12. the critical buckling loads and mode shapes for the C-series tested panels and all predictive analyses

	fixture models		ideal sandwich models		ideal sandwich models	
analyses	critical buckling (kN)	mode	critical buckling (kN)	mode	2nd stability (kN)	2nd mode
experimental (per test per panel)	**(94,114) , (98.5,104) , (100)**	**1**				
random method FEA	96.5	1				
eigenbuckling FEA	105.3	1	95.5	1	115.2	2
Vinson eqns			23.9	2	31.9	3
Com. Pro eqns.			29.9	2		
classical lamination theory (Jones)			100.1	1	166.7	2

All of the FEA analyses again predicted the correct mode shape, mode one. The nonlinear model critical buckling load was again lower than the linear model. All of the FEA models predicted critical buckling loads which fell within the experimental range. Again, the ideal sandwich panels had a lower critical buckling load than the fixture models by around 10%. Also, the analytical solutions had difficulty predicting the correct mode shape, or near the correct load. Due to the low ratio of Ex:Ey for this layup (<1), mode two is a reasonable predicted critical mode shape. However, the very low critical loads predicted, below even the SFSF critical buckling loads, are not reasonable. The classical lamination theory performs much better than the three layer theories. It predicts the correct mode shape, and curiously, a critical buckling load only 5% higher than the linear, ideal FEA load. This oddly accurate prediction must stem from the more compliant panel and relatively high width-wise stiffness.

The second stability load for the ideal FEA panel was fairly close to the critical load with only a 20% increase. The fixture model also had a close second stability load, 122 kN. None of the random perturbation nonlinear models passed on to mode two, however, only three case runs were solved. A proposed study to look at the relationship between the proximity of the second mode and the probability of the random perturbation models developing it, was not attempted, but suggested as future work.

The three nonlinear models are plotted together in a LOD plot in figure 6-29. Of the three models, only cf1 gave a smooth buckling knee and a convergent late postbuckling response. Run cf1 is the model

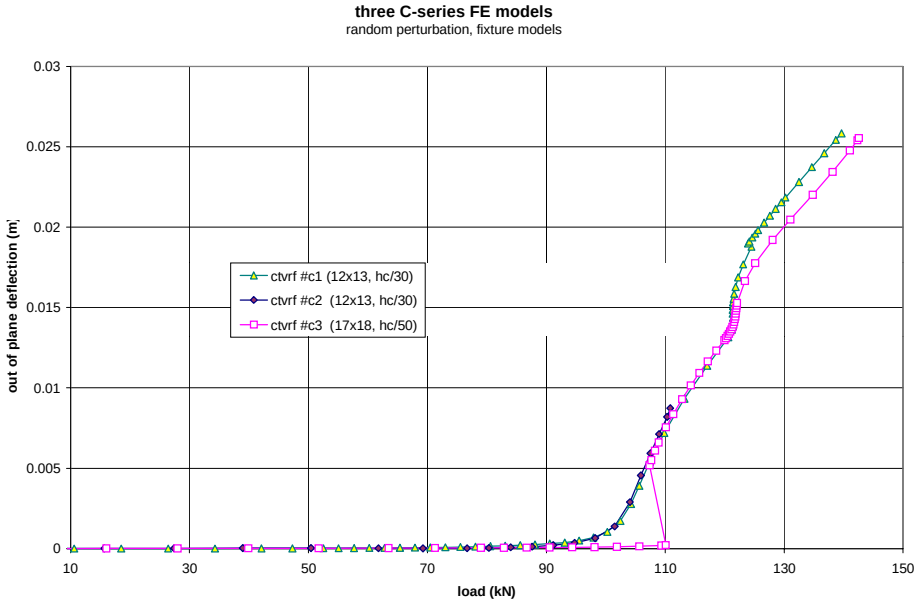

Figure 6-29. LOD plot of three C-series, SSSS, FE models

which supplied the critical buckling load for Table 6.12. Both models which were convergent into late postbuckling experienced a load drop and corresponding mode shift common to the random perturbation B-series models. All three models had very similar and convergent early postbuckling responses. Therefore, cf2 was the only choice to compare load-strain histories with the experiments.

FEA model cf1 is compared to tests C1 ss3 and C2 ss4 in Figures 6-30 and 6-31 respectively. Due to the early postbuckling failures of the experimental panels it is more difficult to compare the FEA response prediction and the test data. The linear responses correlate very well, with the test data showing a slightly higher scatter band. As usual, the FEA critical buckling knee is more pronounced than the experimental knee, which in these tests is very gradual. In the early postbuckling response, the strains and slope of the FEA response were both higher. This was typical of the B-series as well. The B-series FEA and test data would then typically slowly converge together with the FEA remaining slightly conservative. However, the C-series tests would fail before any such convergence could take place. FEA run cf2 also experiences an early and severe mode shift as well, making the comparison even more difficult.

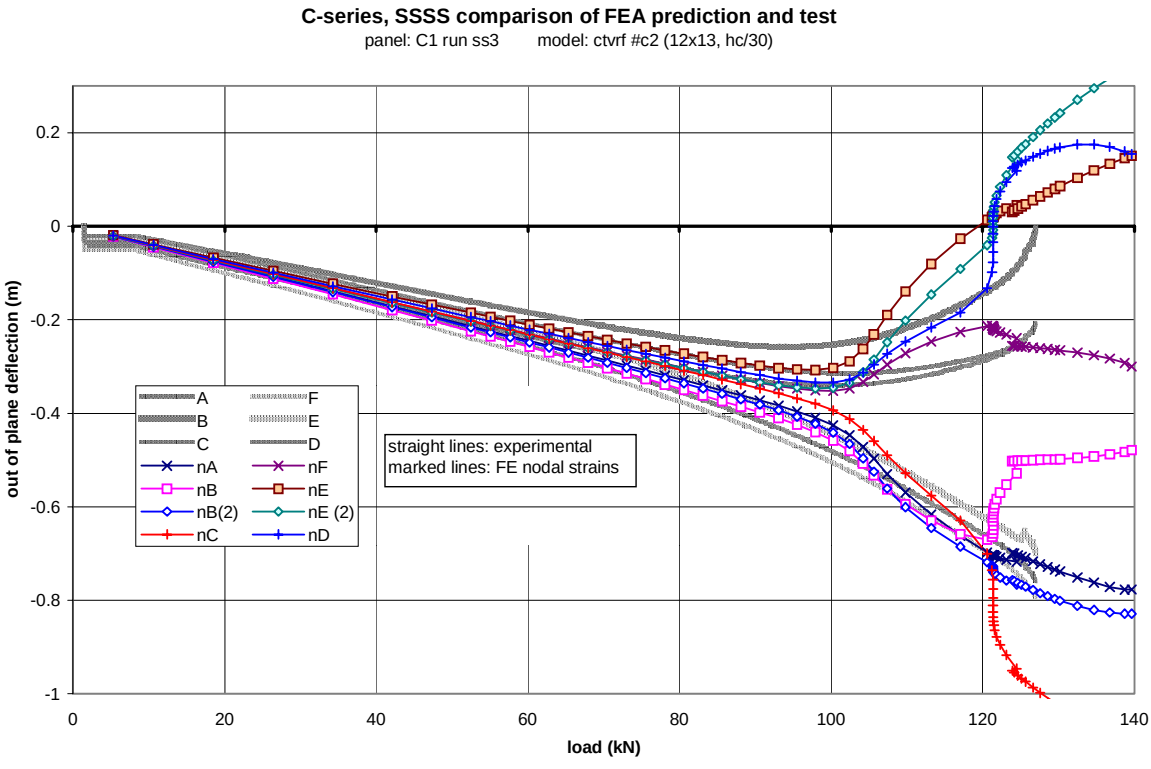

Figure 6-30. C-series, SSSS, FE model and test run comparison

In conclusion, the FEA panel techniques are valid into the early postbuckling response of the C-series sandwich panels. The correct mode shape is predicted by all of the techniques as well as an accurate critical buckling load. The early postbuckling response tends to be fairly accurate and on the conservative side. No conclusions on the validity of the late postbuckling response can be surmised due to early failure, however, the mode shift problem which invalidated the strain data is again found for this lay-up.

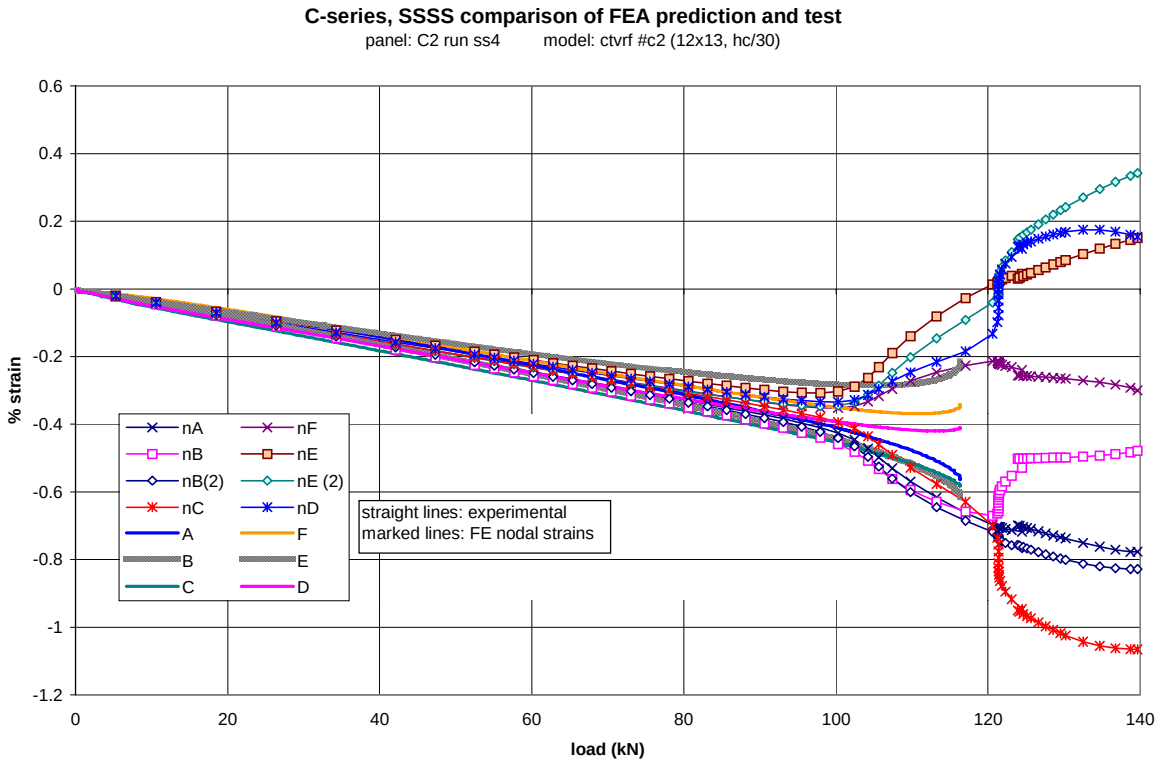

Figure 6-31. C-series, SSSS, comparison between a second test run and same FE model (from Figure 6-30)

Effect of Layup on the FEA predictions

The effect of layup upon sandwich panel buckling response is examined in Figure 6-32 in which the FEA and experimental data is plotted for the B and C-series panels in both the SFSF and SSSS support condition. The complicated differences between the B and C-series facesheets resulted in only small response changes. Both series experienced the same postbuckling response types for each support condition. The asymptotic buckling load of the SFSF panels dropped from ~45kN for the B-series, to ~35 kN for the C-series. However, for the SSSS critical buckling load, the C-series panels increased their buckling load slightly from the B-series even though their axial stiffness dropped significantly. The linear

and nonlinear FEA models had no problems accounting for the complex differences between the two facesheets. The nonlinear models predicted each series very well as far as the early postbuckling response. The problems the FEA techniques had predicting the late postbuckling response is due to mode shifting problems caused by the random perturbation technique. These resulting problems are governed by the boundary conditions and not the facesheet.

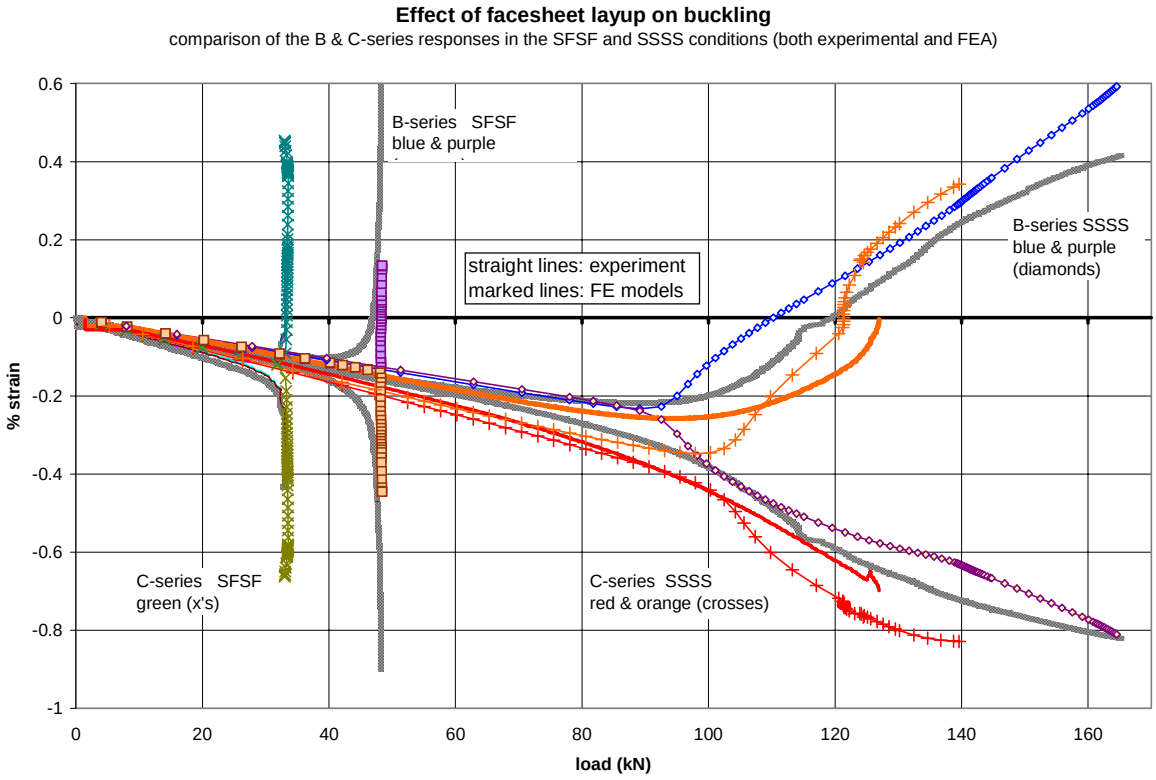

Figure 6-32. example effect of facesheet lay-up on buckling responses for both the SSSS and SFSF conditions for experiment and FE models

Core Thickness, Q-series

panel data: flat, (0/+45/b3/8)s, ~ 46x46 cm

The Q-series tests involved varying the core thickness for flat panels. The Q-series panels have 6.35 mm (1/4") balsa cores as opposed to the 9.35 mm (3/8") cores of the other series. The facesheets are (0/±45) laminates instead of the B-series (0/+45/0) because of sandwich modeling requirements in Ansys (the core thickness to total thickness must be above 5/7). The resulting thinner panel was expected to undergo more postbuckling before failure than the other two flat panel series. Therefore, the postbuckling response of the Q-series panels was of particular importance in validating the FEA predictions.

Q-series Test Results

SFSF Tests

Three Q-series panels were tested in the SFSF configuration, Q1,2 and 3, with the single piece load support fixture. A sample load-strain history for each panel is plotted in Figure 6-33. Due to dimension constraints of the knife edges, panel Q2 was unable to be tested in SSSS and therefore was tested deeply into the postbuckling response in the SFSF condition. Q2 never failed even though it deformed at least 30 cm in out of plane displacement. Although damage was heard, it was sporadic and no data was recorded. The Q2 sf3 test response demonstrates that the Q-series panel has a 'stable', neutral postbuckling response. Panels Q1 and Q3 were not carried as far into the postbuckling regime since they were to be tested in the SSSS configuration as well.

The Q-series SFSF responses followed the same trends found in the other two flat panel series (B&C); mode one shapes with the free edges deformed more than the center, neutral postbuckling, and consistent asymptotic buckling loads. Table 6.13 tabulates the statistical and buckling information gathered from the SFSF tests on the three Q-series panels. The five SFSF tests on Q3 show the dependence on initial imperfections of strain reversal buckling but the independence of the asymptotic buckling load. While no absolute correlation between the strain deviation between different gages and the reversal load can be found, the reversal loads of Q3 runs sf1-5 are seen to vary significantly as different shims are used and different resulting strain deviations found. Meanwhile, the asymptotic buckling load does not change more than 1% for these variations. The load-strain data from these five tests is plotted in Figure Q35. The

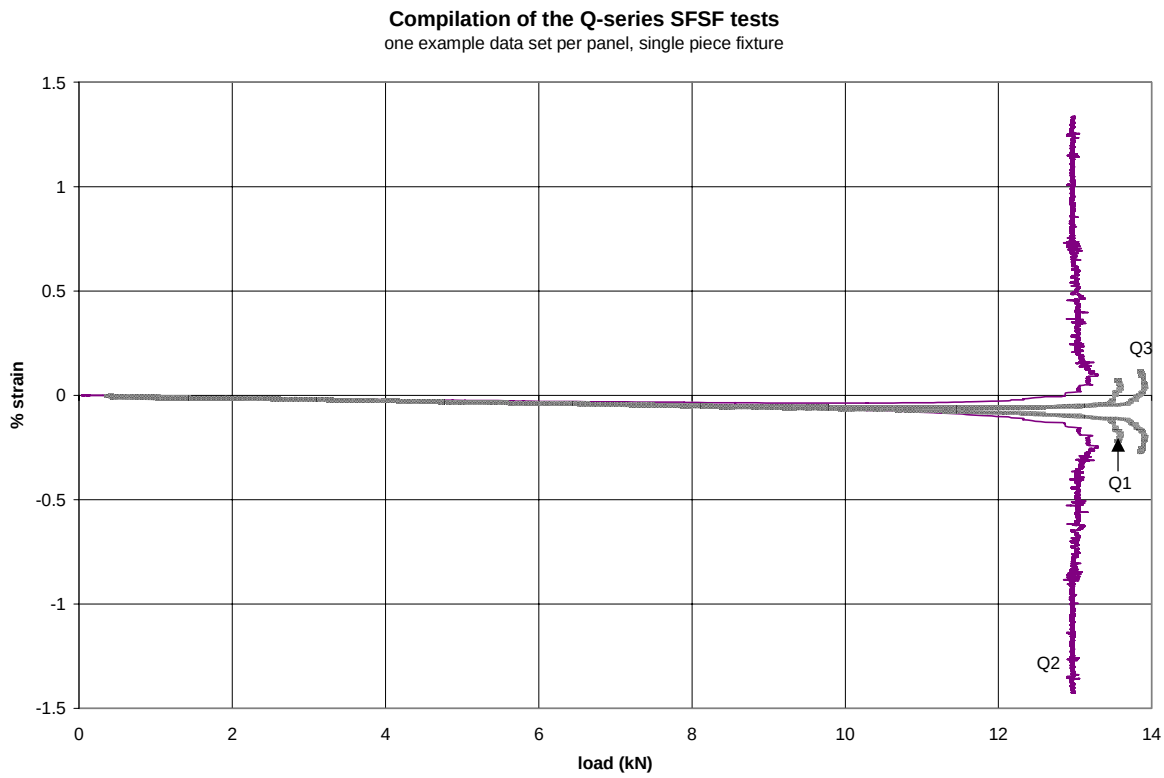

Figure 6-33. compilation of the Q-series panels SFSF buckling response

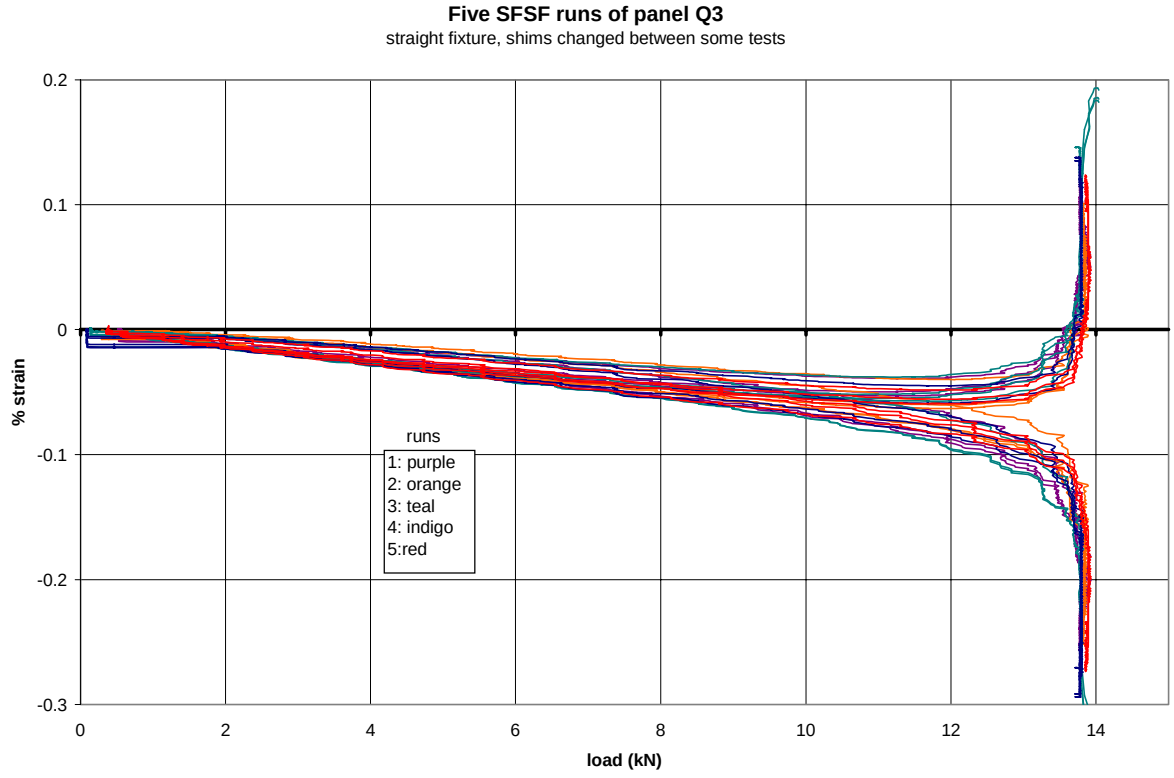

Figure 6-34. five SFSF buckling tests of panel Q3 (with shims changed between tests)

data are very consistent from test to test. The asymptotic buckling loads are within 0.1 kN of each other, while the critical buckling knees remain within a narrow band for all three gages across the width. The resultant asymptotic buckling loads, Nx, of the three panels are also consisitent at 29.1, 27.6 and 29.1 for Q1,2 and 3 respectively.

Table 6.13. statistical and buckling data for the Q-series SFSF buckling tests

			deviation statistics (%)			buckling data (kN)				
panel	run	shim	minimum	@ load	10 kN	reversal	*noise*	asymptote	*adjust*	comments
Q1	1	none	15.0	9.1	15.8	11.4	0.2	13.5	-0.2	softened slightly
Q2	3	NA	7.4	3.2	29.9	9.7	0.2	12.9	0	softened from 13.3
Q3	1	1A	20.4	7.9	22.5	11.2	0.2	13.8	-0.1	softened from 13.9
	2	1P	20.3	10.4	20.5	11.8	0.2	13.8	-0.1	barely softened
	3	1A	22.5	8.0	24.2	10.7	0.3	13.8	NA	shot up to 14.1 w/ quick loading
	4	both A	16.7	9.5	17.0	11.6	0.2	13.8	0	flat
	5	(CD)1A1P AF 2P	12.8	7.9	14.0	11.6	0.2	13.8	-0.1	flat

SSSS Tests

Only two Q-series panels were tested in the SSSS condition, Q1 and 3. Given the corroborating results obtained from the other two flat panel series and the three Q-series SFSF tests, the results from these two panels were viewed as adequate. Test data from each panel is plotted in Figure 6-35. Q3 was tested up to a load of 92 kN, but, only the portion below 58 kN is valid and shown in Figure 6-35. At 58 kN, the knife edges contacted the loading plates and began to transmit load directly. At this load, the strain data can be seen to take a significantly stiffer slope. The stiffness change is especially apparent for gage B (center convex). The knife edge contact was visually observed as well, in a load range around 58 kN. A similar slope change is seen in the response of Q1 at a load of 55 kN. A knife edge contact load was not recorded in the test logs, but, this quick, abrupt knee suggests that this occurred. Therefore, any data after 55 kN is suspect.

The linear, critical buckling and early postbuckling responses of Q1 and Q3 qualitatively agree very well with each other. Both follow similar response trends as the two previous series: a mode one shape, stable postbuckling response, gradual buckling knees, similar concave strains across the width, and the center bending strain discrepancy versus the sides. These tests, and experience with the B and C-series

responses, demonstrate Q-series FEA validation with only the two SSSS tests. The buckling and statistical data for these two panels are shown below in Table 6.14.

Table 6.14. the statistical and buckling data for the Q-series SSSS buckling tests

		deviation statistics (%)			buckling data (kN)			failure data			
panel	#	min.	@ load	10 kN	reversal	*noise*	damage	mode	load	@ strain (%)	comments
Q1	1	8.7	31.9	13.8	36.9	0.2	45	knife slipping below F, local	77.2	0.384/-0.651	lots of post buckling
Q3	1	7.8	22.4	12.6	34.8	0.2	none	none	NA	NA	max: 43.8
	2	8.9	19.9	11.9	31	0.5	45	none	NA	NA	knife edges hit roller @~58 kN

The range of critical buckling loads, 31 to 37 kN, is proportionally consistent with the range with the B-series. Damage occured at the same load of 45 kN, and was heard until the test ended. Notice that test Q3 ss1 was loaded to 43.8 kN and no damage was heard. Secondly, the center convex strains were very similar for Q1 and Q3 at 45 kN, suggesting very similar deformed shapes. With similar deformed shapes at the same loads, the width-wise strains would be nearly the same. It is these width-wise strains that cause the matrix cracking, and therefore the very consistent damage results are expected. None of the Q-series panels failed in either support condition.

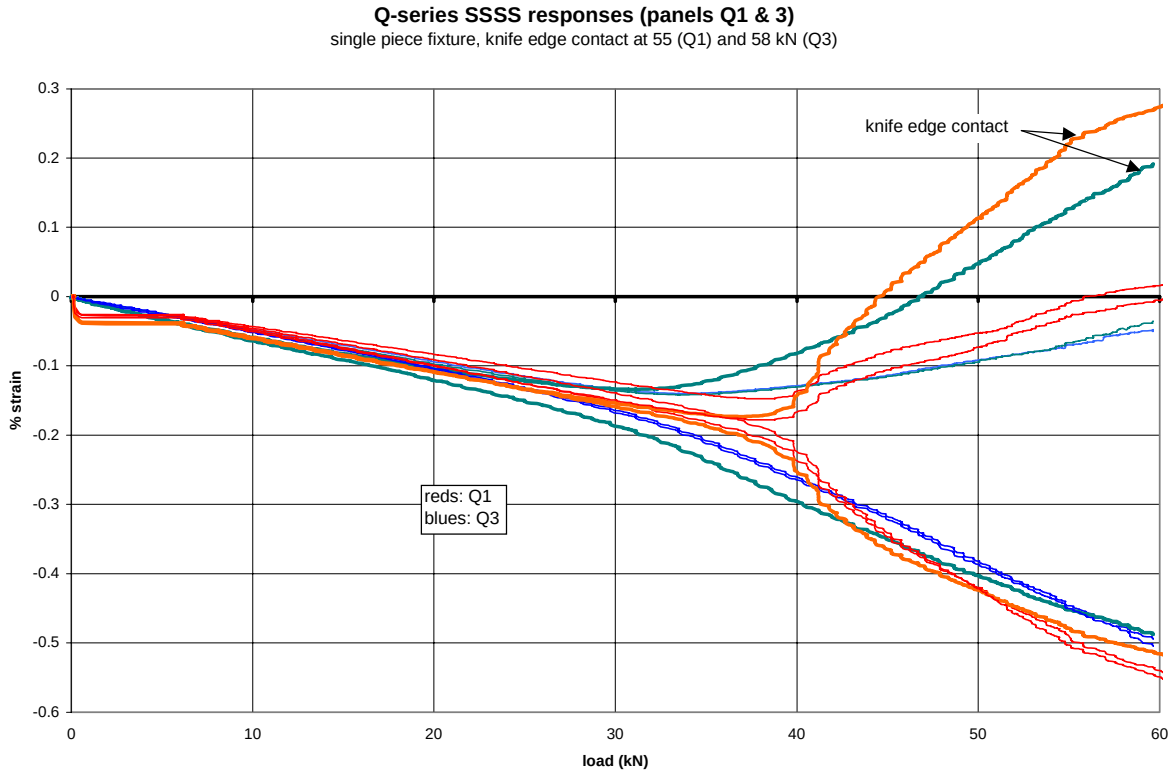

Figure 6-35. compilation of Q-series SSSS tests

FEA Validation

SFSF Validation

The three FEA models (linear and nonlinear) predicted the correct critical buckling shape, mode one, along with the extra edge deformations. The Q-series SFSF tests also use the asymptotic buckling load as the main factor in determining validity of the FEA predictions. Only one random perturbation model was run for the Q-series SFSF parameter, qf1 (fixture model, 17x18 panel mesh, rp = hc/50). The model is plotted along with three tests in Figure 6-36. The model did not experience the accustomed FEA random perturbation caused load drop even though it reached 0.175% strain, nor did it become non-convergent. With only one model, it is unclear whether this is due to the more compliant layup, thinner core, or just a statistical aberration.

Table 6.15. the experimental and FEA predicted buckling loads for the Q-series SFSF

experimental panels	asymptotic load (kN)	mode
Q1	13.5	1
Q2	12.9	1
Q3	13.8	1
FEA models	*(first)*	
nonlinear, qf1 (17x18, hc/50)	14.2	1
	critical buckling (kN)	
linear, ideal	14.7	1
linear, fixture	15.0	1

As can be seen visually in Figure 6-36, and numerically in Table 6.15, the FEA nonlinear model predicts an asymptotic load slightly higher than the experimental values. Curiously, the critical buckling load predicted by the FEA fixture model is higher than the asymptotic buckling load of the non-linear model. The B and C-series both had more conservative linear critical buckling loads than either the experiments or the FEA model. A closer inspection of Figure 6-36 may provide an explanation of this. The FEA model is consistently slightly stiffer than the tests. A slightly stiffer facesheet would produce a more bending stiff panel and a higher buckling load. The (0/$\pm$45) facesheet lay-up used the (0/$\pm$45/0) curve fitting equations for the thickness to fiber volume material property calculations, resulting in inherently erroneous results. No purely (0/$\pm$45) material property data was found in the MSU database, therefore the (0/$\pm$45/0) trend with fiber content was taken as the best approximation. Further investigation found that the

facesheet axial elastic modulus was stiffer for the FEA model than the experimental panels. The FEA model had an axial modulus of 21.3 GPa, while the test panels had moduli of 19.1, 18.0 and 17.5 GPa, for Q1,2 and 3. This averages a 17% higher modulus than the test panel average. In comparison, the FEA facesheet moduli for the B and C-series SSSS tests were only 7% and 0.1% higher than the test panel average respectively. As is expected, with the more accurate material properties, the predictions become more accurate. Additionally, accurate material properties tend to yield slightly conservative results, as shown by the B and C-series results compared to the Q-series. Therefore, with the caveat that the material properties must be at least within 10% to yield accurate results for the SFSF condition, the FEA techniques are valid for the thinner core SFSF sandwich panels.

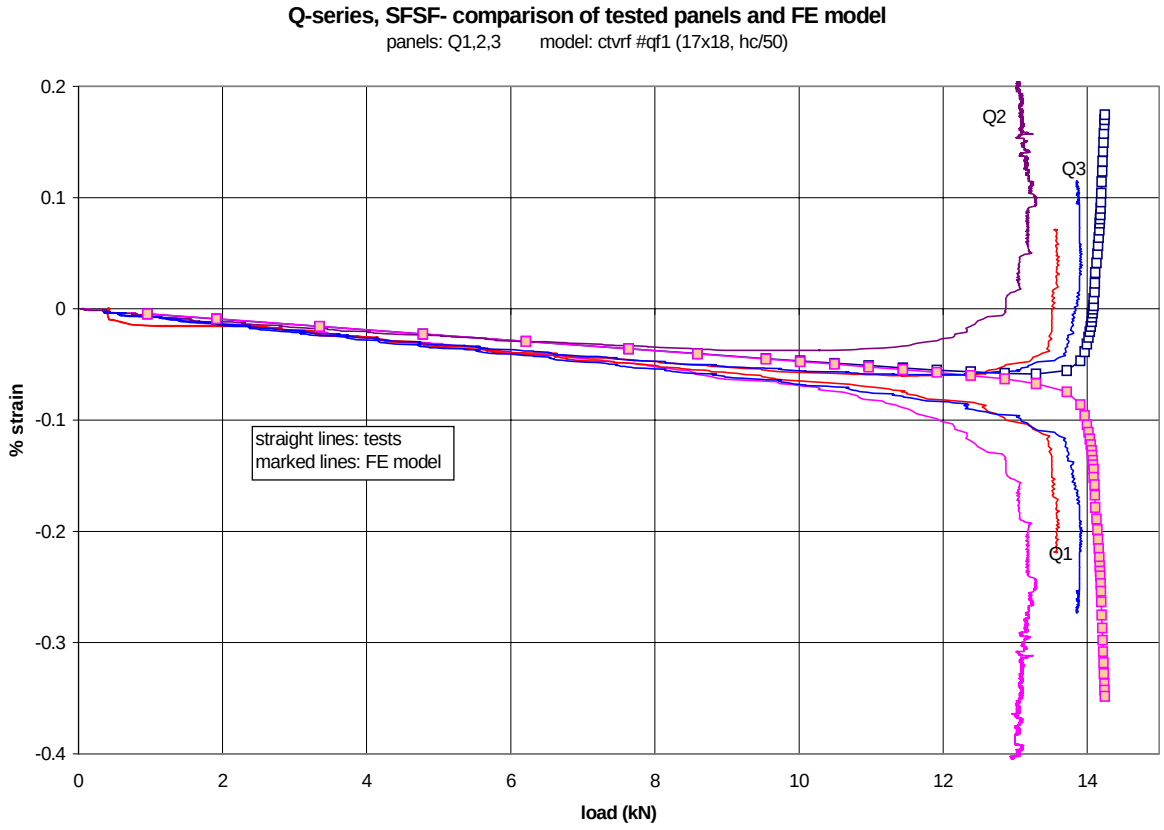

Figure 6-36. Q-series, SFSF comparison of tests and FE model

SSSS Validation

Like the SFSF condition, the Q-series results in Table 6.16 conform to the trends found in the previous flat series. The FEA models all predict the correct mode shape and critical buckling loads found within (or just conservative of) the experimental range. The three-layer theory models had difficulty predicting either the correct mode shape or the critical buckling loads, which were once again very low. For this series the three-layer predicted critical buckling loads were 20% and 60% of the actual experimental range. The consistency of the errors over the three flat panel models reinforces the belief that the closed-form models simply fail to model fiberglass/balsa sandwich panels for this range of dimensions. Lastly, the classical lamination theory results are predictably high, 50%, for the correct mode shape.

Table 6.16. CVS the critical buckling loads and mode shapes for the Q-series tested panels and all predictive analyses

	fixture models		ideal sandwich models		ideal sandwich models	
analyses	critical buckling (kN)	mode	critical buckling (kN)	mode	2^{nd} stability (kN)	2^{nd} mode
experimental	**(36.9) , (34.8,31.0)**	**1**				
random method FEA	32.5 , 32.1	1		1		
eigenbuckling FEA	36.5	1	30.6	1	56.6	2
Vinson eqns			6.1	2	7.8	1
Com. Pro eqns.			19.1	2		
classical lamination theory (Jones)			46.1	1	89.3	2

The postbuckling response prediction is examined in Figures 6-37 and 6-38 by comparison with panels Q1 and Q3. The FE model ctvrf #qs12 (fixture model, 12x13 panel mesh, rp = hc/30) is shown in Figure 6-37 while #qs17 (fixture, 17x18, hc/50) is in Figure 6-38. The quarter series was chosen in part because the thinner sandwich panel was expected to buckle further into the postbuckling response before failure than the thicker C and B-series panels. Unfortunately, the more compliant panels deformed so far inplane that the knife edges were engaged, leaving only the early to middle postbuckling response for comparison with FEA.

The qualitative results found in Figure 6-37 and 6-38 are very similar to those found for the B-series. The same trends include: a slightly conservative critical buckling load, sharper knee, very similar concave strains across the width, converging early to middle postbuckling responses, and a late postbuckling mode shift which invalidates subsuquent strain predictions. This nearly exact agreement validates the FEA random perturbation nonlinear buckling analyses technique for different core thicknesses of fiberglass/balsa core sandwich panels.

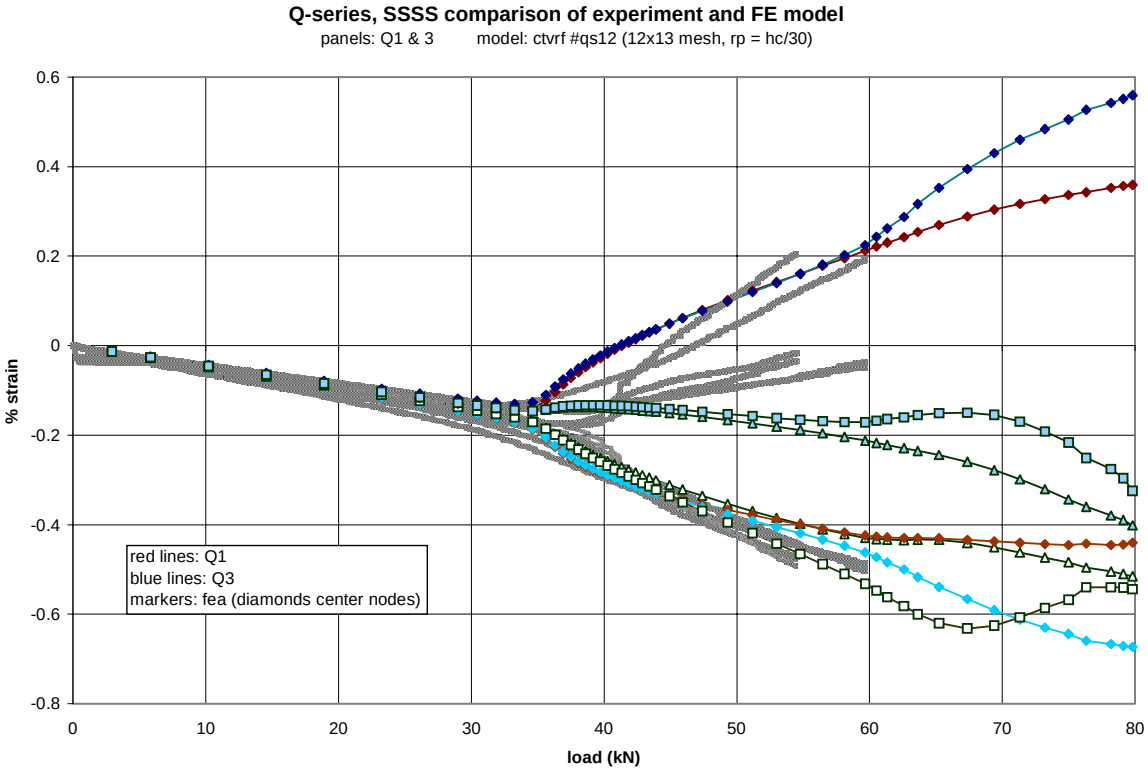

Figure 6-37. comparison of panels Q1&3 and FE model ctvrf #qs12

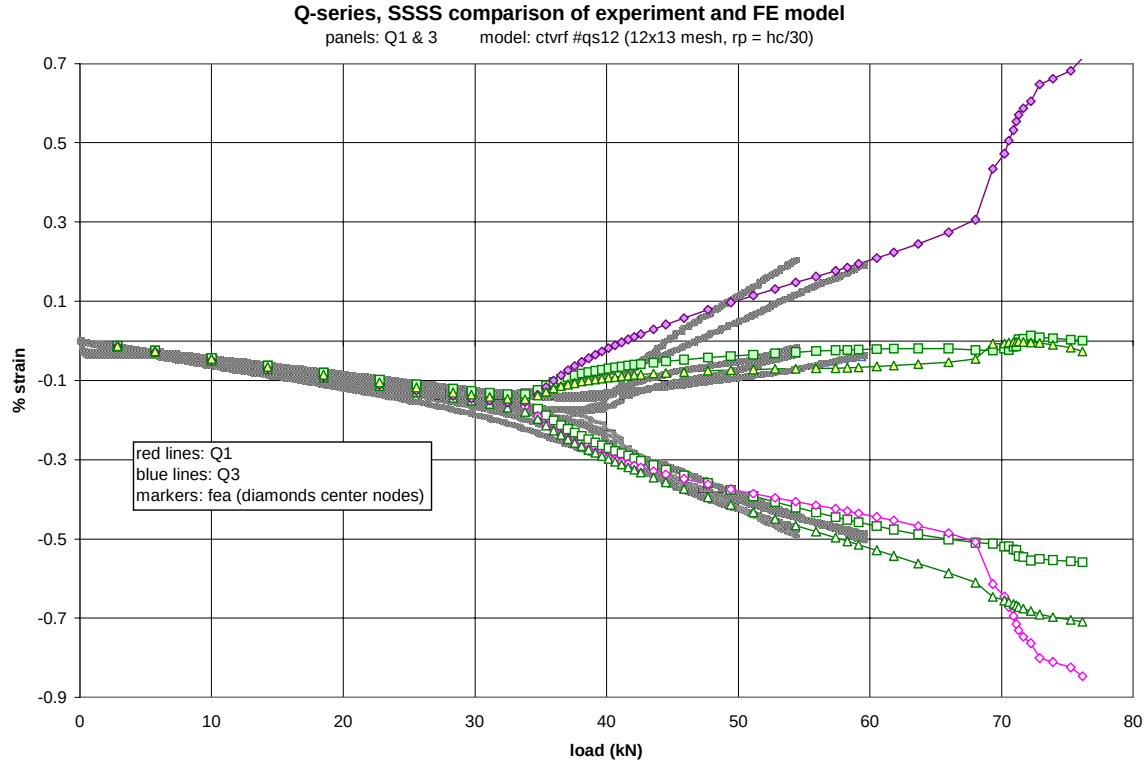

Figure 6-38. comparison of panels Q1&3 and FE model ctvrf #qs17

Effect of core thickness

As noted earlier, the FEA linear and nonlinear techniques were both able to predict the correct structural response of the flat sandwich panels for different core thicknesses. The same trends were found for the B and Q-series response prediction, suggesting that the core thickness has little or no effect on the accuracy of the FEA technique sandwich panel responses for sandwich panels with these dimension ranges (which are suitable for fiberglass wind turbine blades). For completeness, the B and Q-series experimental and FEA load-strain responses are plotted together in Figure 6-39, which visually reiterates the core thickness conclusion. Increasing the core thickness produces the predicted increase in buckling resistance.

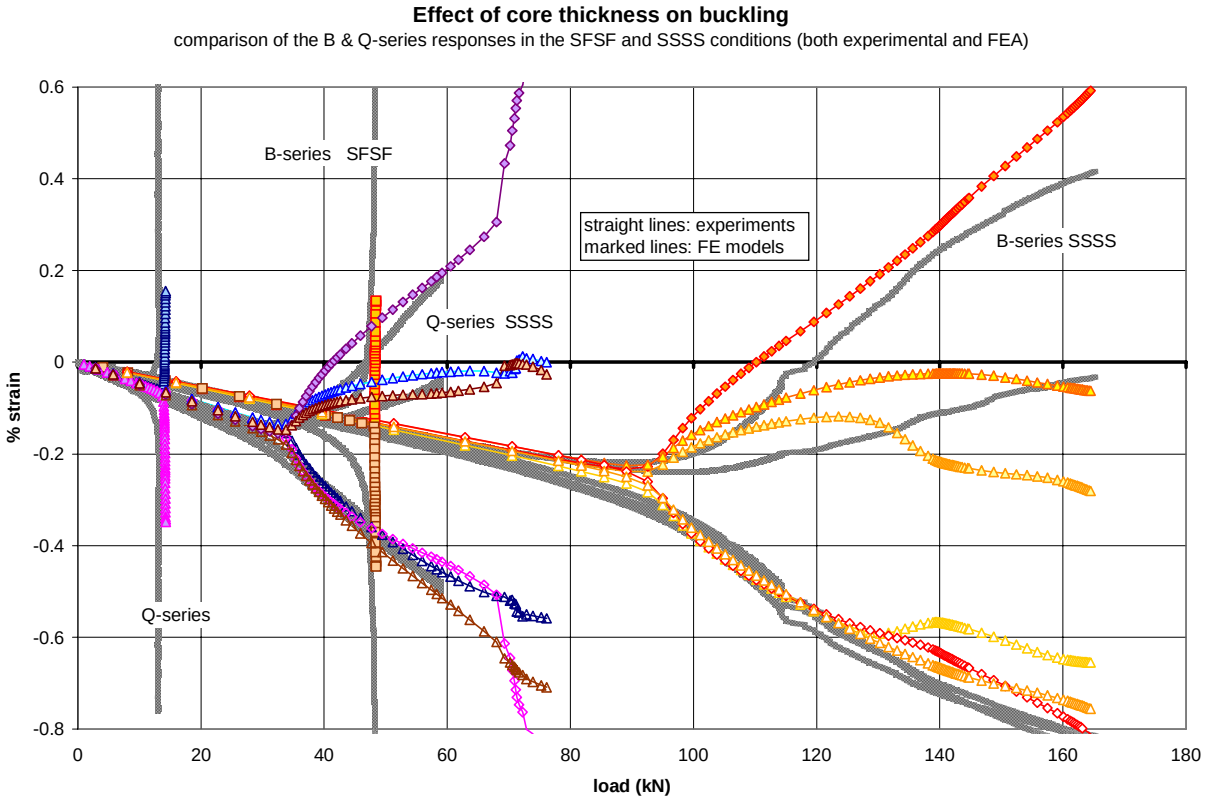

Figure 6-39. effect of core thickness on buckling (B & Q-series SFSF and SSSS results)

Shallow Radius of Curvature Panels

panel data: 70p-series, cylindrical (r = 1.78 m), $(0/\pm45/0/b_{3/8})$, ~46 x 46 cm

For flat panels, the effect of core thickness and layup were predictable by the FEA technique. The critical buckling load would change, sometimes significantly, but, the general response types remained the same. The SFSF conditions would always postbuckle with the neutral response, while the SSSS condition would assume the stable response. The reason for the similar responses was that the basic geometry of the flat panels remained similar, a flat 0.46 x 0.46 cm sandwich panel. The sandwich linear and random perturbation nonlinear buckling analyses were easily able to predict these response types for these materials. The effect of the final parameter, radius of curvature, was expected to change the responses more severely. With either of the support conditions, the panel might undergo an unstable response. Two curvatures were investigated, shallow and deep. The 70p series is the shallow curved panel studied which is a cylindrical panel with a radius of 1.78 m. It was expected to show response changes from the baseline flat panels with which it shares a common facesheet lay-up and core thickness.

70p-series Test Results

SFSF Test Results

Three 70p-series panels were tested in the SFSF support condition, 70p1,2 and 3. The panels were loaded through the piecewise support fixture as dictated by its curvature. For the B-series, the piecewise support fixture had the effect of lowering the asymptotic buckling load only slightly relative to the single piece fixture, so no problems were expected for the curved panels in the SFSF condition. Each panel also used the wide gage set to better monitor the effects of the free edges better.

The first test result was that each panel buckled towards the convex side consistently with a mode one shape. The other response characteristics can be garnered from the load-strain histories of the tests. Load-strain history results from each panel are plotted together in Figure 6-40. Several response characteristics can be observed from this figure. The general response type is a slowly unstable response. 70p1 and 3 definitely show significant load drops while 70p2 was not buckled enough to discern between the neutral and unstable postbuckling responses. The 70p3 panel in particular drops from a maximum load of 56 kN down to 50.5 and the slope suggests further load drop. This drop is much more than any of the

flat panels experienced, and an asymptotic response was never obtained even though strains as high as 0.5% occurred. Because of the unstable postbuckling response, it is easy to see that the middle gages experience lower absolute strains than the edge gages. The effect was so pronounced in late postbuckling that the width effect could be seen visually in the buckled shape. The free edges were seen to deform out of plane so much that, at the midplane, a straight line could be traced from one free edge to the other. The top and bottom of the panel remained at the manufactured radius of 178 cm.

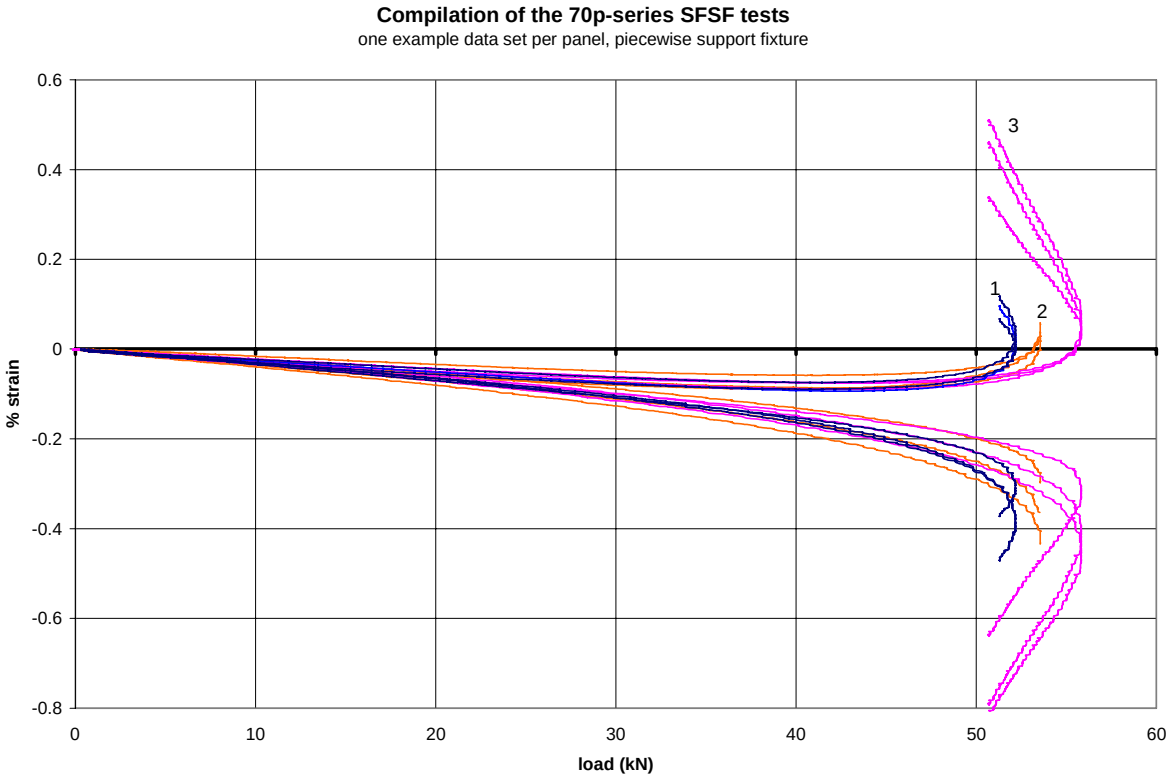

Figure 6-40. compilation of the 70p-series SFSF tests

Four buckling SFSF tests were performed on 70p3 and the results from each are plotted in Figure 7F3. Only two were postbuckled, sf11 and 12, while sf2 and 6 were buckled just past critical buckling range. 70p3 sf2 and 6 follow almost exactly the same paths as sf11, with sf6 reaching the same maximum load and appearing to begin inflection towards the unstable response at the same strain as well. Meanwhile, the last test, sf12, buckled earlier than the first three and reached a lower maximum load. Eventually sf12 converged to nearly the same late postbuckling response as sf11 at the end of the test run. Test run sf12

most likely followed the more compliant buckling knee due to damage incurred during the deep postbuckling of sf11. Therefore, once the new initial imperfections were overcome by the general buckling shape, the response converged with the earlier test. Test sf12 also has a peculiar spike in the strain of gage E at around 10 kN. The reason for this spike is unknown; however, after an initial offset due to the spike the path of E converges back to its convex neighbors at around 30kN. These four tests show that consistent results were found for the curved panels with the piecewise fixture from test to test for a single panel. They also again demonstrate that the critical buckling load and knee may vary with the initial imperfections (shown in CV from damage or shimming) but the postbuckling response will converge once significant out of plane deformation occurs (different for each series).

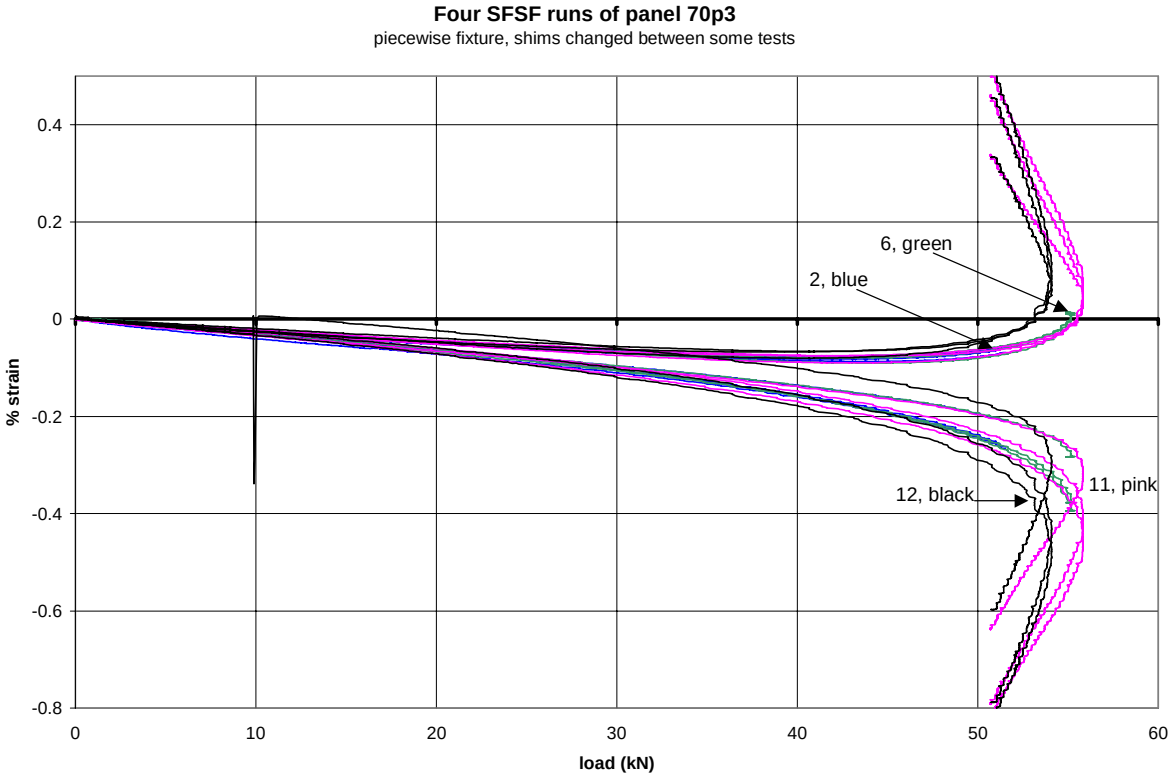

Figure 6-41. four SFSF runs for panel 70p3

The effect of the spike upon the coefficient of variation can be seen in Table 6.17. The minimum load was taken just prior to 10 kN and had a c.v. of 19%; just after the spike while still at 10 kN the coefficient of variation jumped to 66%. The new strain path caused the change in the response. Due to the lack of a neutral postbuckling response, the asymptotic buckling load had could not be used as the main

value determining the buckling response of the SFSF condition panels. Instead, the earlier approach used with the SSSS of strain reversal and qualitative postbuckling observations was adopted.

Table 6.17. the statistical and buckling data from the 70p-series SFSF tests

			st. deviation statistics (%)			buckling data (reversal)					
panel	#	shim	min	@load	@10 kN	AA	B	CC	*noise*	response	comments
70p1	1	none	20	18	28						
	2	1P AF	10	5	12						
	3	1P AF	9	6	12	43.7	42.2	42	0.5	none, unstable	max load:52.4
	4	1P AF	12	6	14	42.5	40.8	40.5	0.3	unstable	max load: 52.2
70p2	3	3P CD	27	19	29	42	40	39.5	0.5,1, 0.5	NA	max load: 53.55 runs 1&2 have no load data, 1 is 10kN cv run, 2 buckled
70p3	1	3P CD			36						
	2	1A CD	18	17	22	43.7	42.2	42	0.5		max load:
	3	3P CD			33						
	4	3P CD			27						
	5	4P CD			15						
	6	4P CD	14	12	15	44	40.6	42	0.5		max load: 51.5
	11	4P CD	15	15	10	42	40.5	42.5	0.5	unstable	max load: 55.8, still dropping at 50.5
	12	4P CD	19	10	66	39.6	38	40.2	0.5	unstable	max load: 54.1, still dropping at 50.5, very similar deep post to sf11

Oddly, even though the edges buckled more in postbuckling than the center, gage B produced on average lower strain reversal buckling loads than the edge gages. For consistency, to eliminate the effects of the edges, and to be conservative, gage B was chosen to define the critical buckling load. Thereby, the critical buckling loads for the 70p-series ranged from 38 to 42 kN.

SSSS Test Results

Two of the three 70p-series panels were tested in the SSSS support condition, 70p1 and 3. Due to size constraints, both knife edges could not be engaged and tested for 70p2. However, one knife edge could be engaged and tested, so panel 70p2 was tested in the SSSF support condition. That test will be considered in the FEA validation subsection. As with the SFSF tests, these tests also used the wide gage set and the piecewise fixture. It was noted that the piecewise supports caused B7 and 8 to develop an unstable postbuckling response. This occurrence would raise questions as to the meaning of the unstable postbuckling response of a 70p-series panel.

unstable postbuckling response. This occurrence would raise questions as to the meaning of the unstable postbuckling response of a 70p-series panel.

However, neither of the two panels developed a definite postbuckling response due to early failure or testing problems. The results from the 70p1 and 3 SSSS tests are shown in Figure 6-42. Panel 70p3 had knife edge engagement just after reversal and therefore only the valid portion is shown; this panel never failed. Panel 70p1 buckled further into the postbuckling range, and was nearing the onset of tension in gage B when it failed. Damage was observed in panel 70p1 just before failure. Except for the center strains (gage B and E) the responses of the two panels were almost identical. The wide convex gages for both panels undergo only very slight bending. Both AA and FF never get enough tension from bending to reverse the strain slope to a positive value. As with the flat panels, the center concave strain does not receive as much bending strain as the convex side. For 70p1, gages CC and DD actually converge to the same value as E at failure. The two panels buckled at strain reversal loads which were 10% apart, 96 and 105 kN, with the expected mode one response.

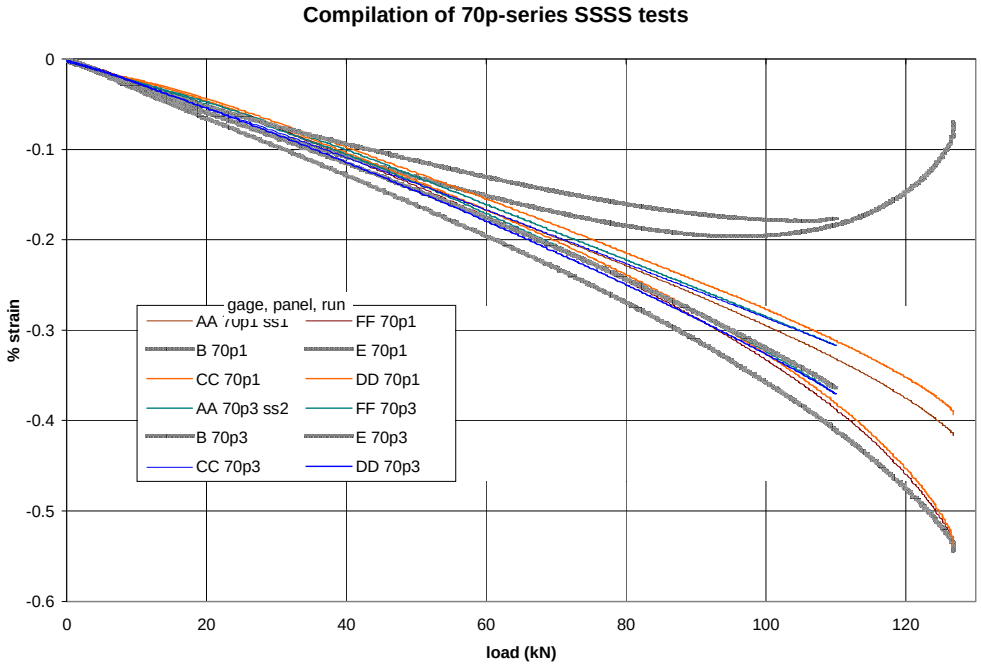

Figure 6-42. compilation of 70p-series SSSS tests

Table 6.18. the statistical and buckling data for the 70p-series SSSS tests

panel	#	shim	deviation statistics (%) min	@load	@10 kN	buckling data (kN) reversal	*noise*	damage	failure data load	@strain (%)	comments
70p1	1	1P AF	9	52	16	96	(+-1)	just before failure	126.5	-.0061/-0.544% fs wrinkling, concave side only, at top where gap found	panel looked pre-bent to start knife edges tight at bottom w/ gap at top when tightened seemed to introduce strain to gages, max 4 microstrain, rezeroed at 17 lbs slight separation on CD side near failure
70p2	not possible due to preparation error										
70p3	1	4P CD	4	11	5	no data available, knife edge engagement near reversal, no cracking heard					max load: 140.5
	2	4P CD	7	29	7	105	(+-1)		no failure		max load: 114 knife edge engagement just after reversal

FEA Validation

A closed form, three-layer analytical critical buckling solution was not found for a cylindrical sandwich panel and therefore the experimental results were only compared to FEA. As mentioned in the preceding chapter, the effect of modeling the fixture had a more prominent effect on the curved panels. The effect on the 70-series panels is apparent in Figure 6-43 in which three convergent, nonlinear, (one fixture, two ideal cases) SSSS models are plotted as LOD histories. The fixture model had an earlier critical buckling load (90 versus 92 and 97) and a much more gradual buckling knee. The postbuckling responses were also different, the ideal cases followed a much more compliant path than the fixture model. Only the fixture model will be compared to the experimental data.

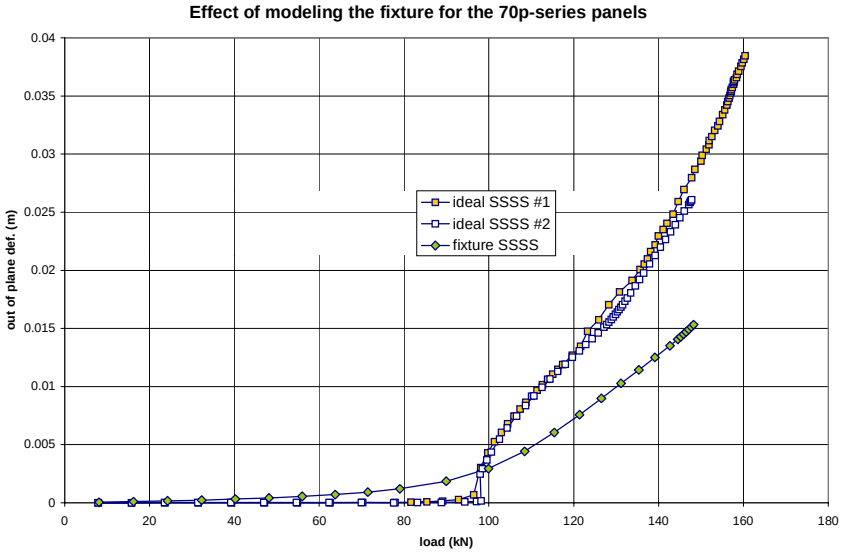

Figure 6-43. effect of modeling the fixture for shallowly curved panels

SFSF Validation

The 70-p series SFSF FEA validation procedure must take on the form of the SSSS procedure because of its unstable postbuckling response (no asymptotic buckling load). All FEA models predicted the correct critical buckling mode shape (mode one). Table 6.19 tabulates the critical buckling results for the 70p-series FEA predictions and experiments. The nonlinear model used the random perturbation method with a panel mesh of 17x18 elements and rp = hc/50.

Table 6.19. the 70-series SFSF critical buckling FEA predictions and experimental results

analyses	critical buckling (kN) AA	B	CC
experimental	40-44	38-42	39.5-42.5
random method FEA	47.3	48.1	46.8
eigenbuckling FEA	60.4		

The FEA predictions were consistently conservative for the flat panels; however, the FEA 70-series SFSF predictions are consistently higher than the experimental values. The 70 and B-series have the same facesheets, and therefore the same FEA material properties. The B-series FEA predicted stiffness was within 7% of the experimental values. The 70 and B-series panels were manufactured using the same spacers, and consequently the same thickness and fiber content. The plates used for the 70 series mold had the same radius of curvature resulting in slightly thinner sides than center. This was not included in buckling predictions. However, this consistent initial imperfection could have produced the lower experimental buckling loads. Since this hypothesis could not be validated, the original criteria for validity was used, and the FEA buckling techniques could not predict accurate or conservative results for this case. However, the nonlinear model predicts a buckling load which is only about 15% too high.

The nonlinear model predicts the more intuitive buckling results in terms of the width-wide buckling shape. It predicts the edges to buckle first since they deform more out of plane in the postbuckling response. This can be confirmed in Figure 6-44 which gives the nonlinear FEA model results along with the three test panel experimental results. The middle node (squares) can be seen to be slightly stiffer during the buckling knee and to drop at a lower rate (especially the convex side) than the side locations. The severity of the additional deformation of the free edges is predicted by the linear FE model and shown in its critical mode shape found in Figure7EO.

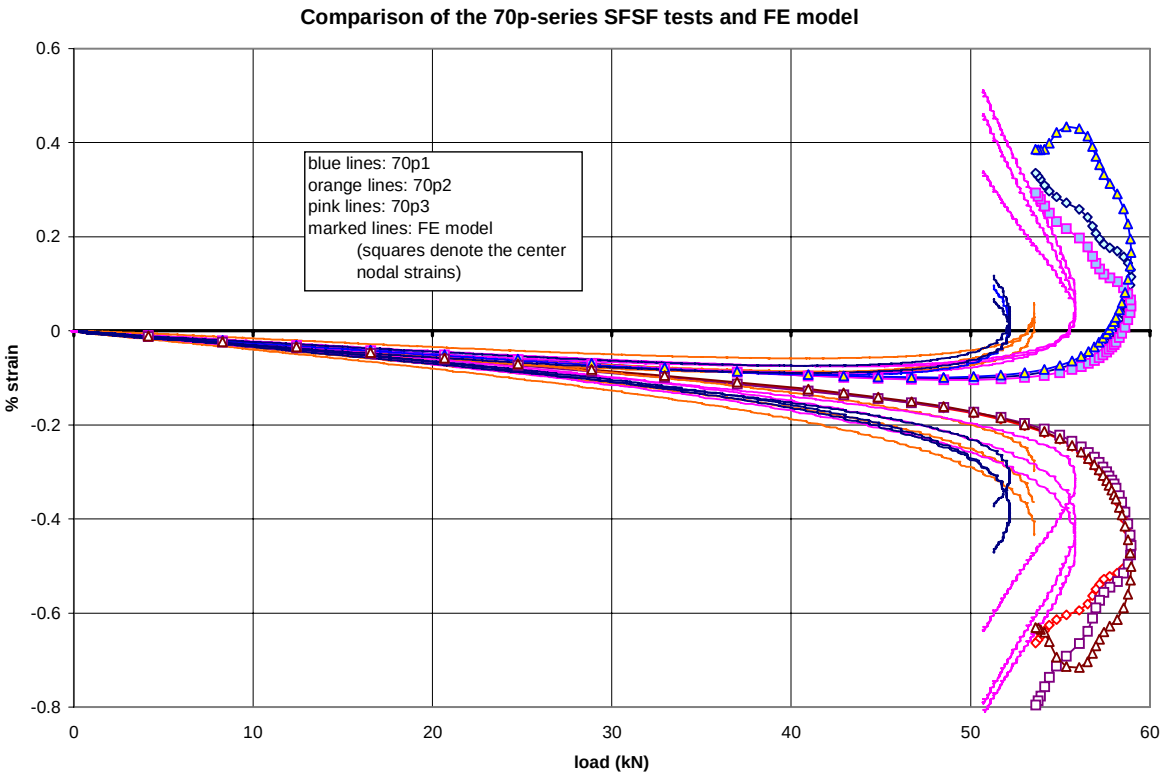

Figure 6-44. comparison of the shallow curved panel tests and FE model predictions

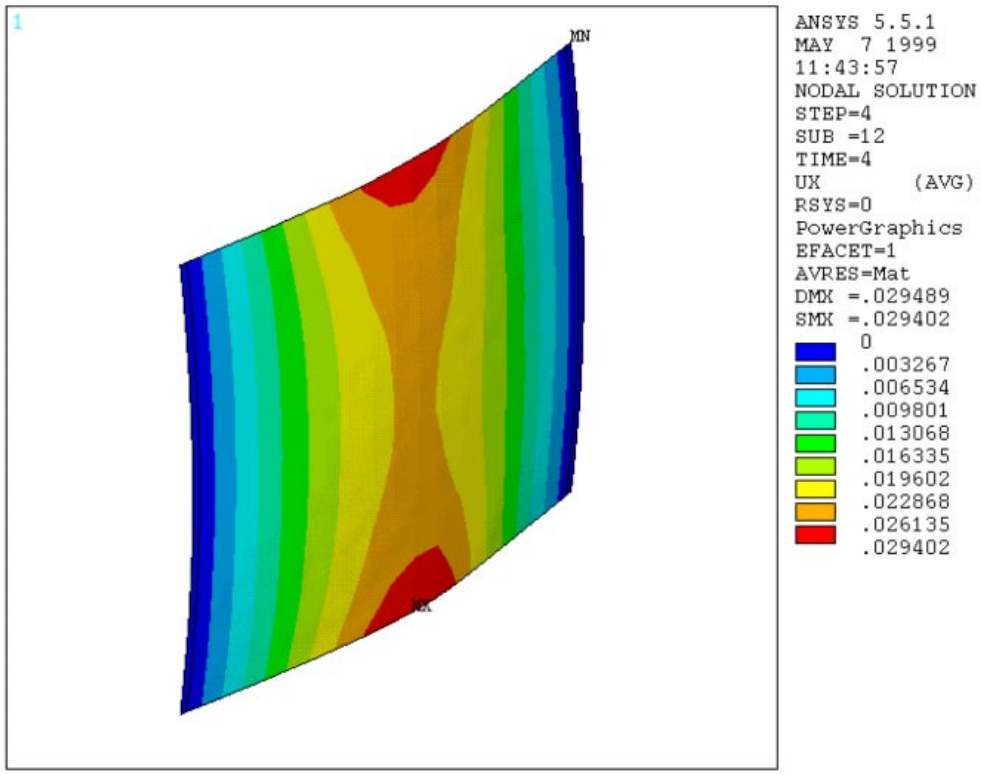

Figure 6-45. out of plane deformation contour plot of the shallow curved FE model

While the critical buckling load might be slightly high for the nonlinear model, it correctly predicts the unstable buckling response. As is becoming the norm, the model predicts good strain results until a mode shift occurs late into the postbuckling response. The early indication from the 70p SFSF validation is that the FEA techniques are having a more difficult time with the cylindrically curved sandwich panels. However, the SSSS 70p and 23p-series cases have yet to be studied.

SSSS Validation

As with the SFSF condition, a single nonlinear FEA fixture model (17x18, hc/50) was compared to the experimental data for validation. The linear and nonlinear models both predicted a mode one response. The mode shape does not resemble a sinusoidal wave as the did flat panels, as shown in Figure 7WA**.** Instead, the sine wave has elongated axially to develop a flat crest with quickly sloping areas near the load ends. The same shape was found for the ideal (pure) SSSS models, and was consistent for both linear and nonlinear models.

The critical buckling loads for the FEA predictions and experimental values are compiled in Table 6.18. The results from this table are quite interesting when viewed in conjunction with the SFSF condition. The nonlinear model again predicts a critical buckling load significantly lower than the linear model. The SFSF linear model was 26% higher than the nonlinear, while the SSSS linear model was 31% higher. However, while both FEA analyses were nonconservative for the SFSF case, for the SSSS case, the nonlinear FEA 70p model was slightly conservative, by about the same amount as for the flat panels.

Table 6.20. 70p-series SSSS critical buckling FEA predictions and experimental results

analyses	critical buckling (kN)
experimental	96 , 105
random method FEA	89.9
eigenbuckling FEA	117.5

Figure 6-46 is the load-strain history plot of the nonlinear model overlaying the experimental data for 70p1 ss2. The center convex strain is very close to the experimental strains until test failure. The nonlinear model continues on a stable postbuckling response until the now expected mode shift. After the mode shift, the model still continues on its stable postbuckling path for a short time before nonconvergence at around 145 kN. The other five nodal strains follow very similar, but consistently slightly stiffer response

paths. Overall, this nonlinear model predicts the 70p SSSS tests very well. The problems that the SFSF models had seem only to be present for the linear models with the SSSS support condition.

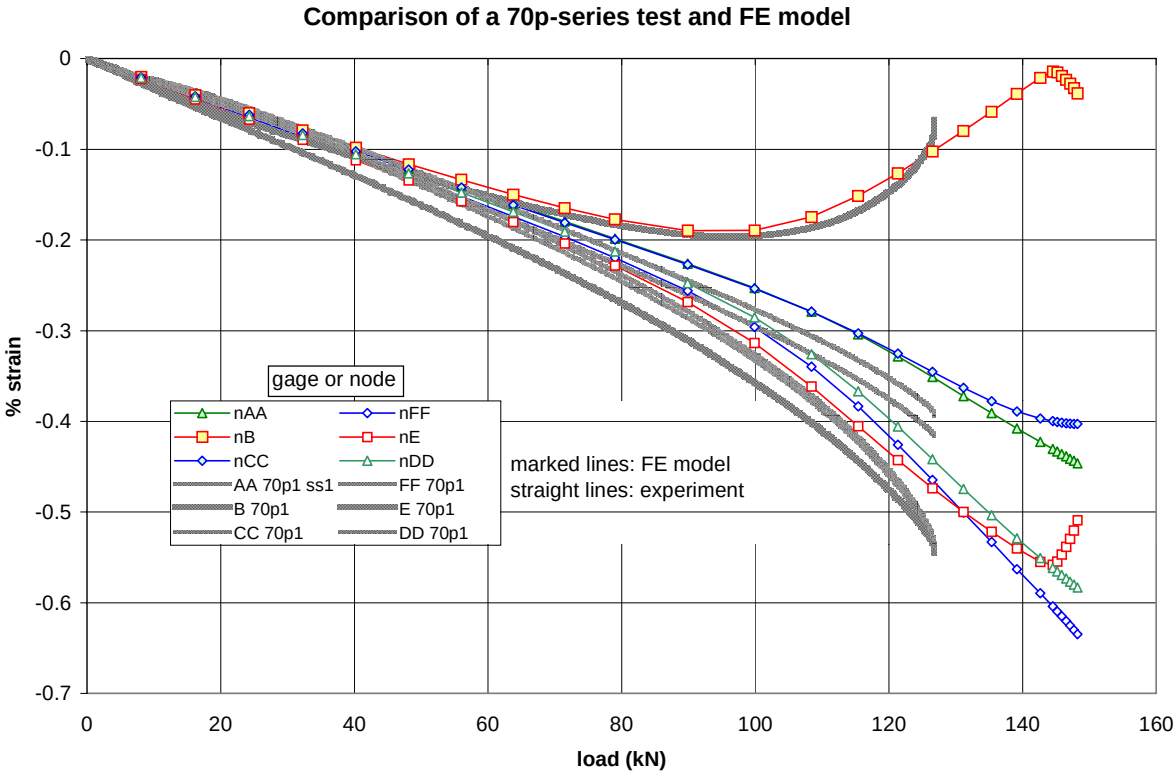

Figure 6-46. comparison results from a shallow curved panel test and FE model

SSSF Validation

The problems associated with testing the 70p2 panel in SSSS led to this curious test. The panel was expected to develop a nonlinear response somewhere between the SFSF and SSSS critical buckling loads. From this nonlinear behavior, the panel was expected to yield strain responses that would vary widely from the free edge gage (AA), through the width to the simply supported side gage (CC). Secondly, three different strain reversal loads were also expected depending on gage. This presented another challenge to the FEA buckling analysis technique. The experimental and FEA responses are plotted together in Figure 6.17 while examples of all three support conditions (SSFSF, SSSF & SSSS) are shown together in Figure 6-47.

The overall response was a stable postbuckling response, with nonlinear behavior starting around 55 kN. As expected, for 70p2, the free edge gage (CC) experienced significantly more strain than the

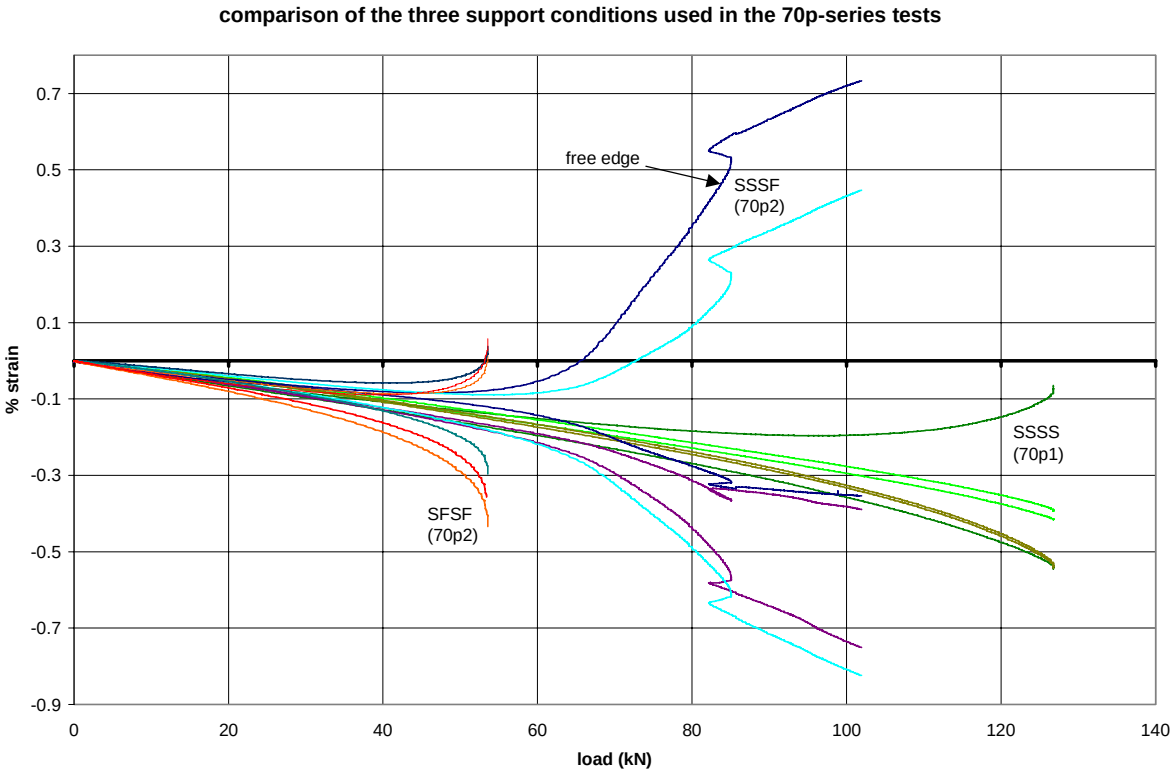

Figure 6-47. comparison of the three support conditions tested for the shallow curved panels

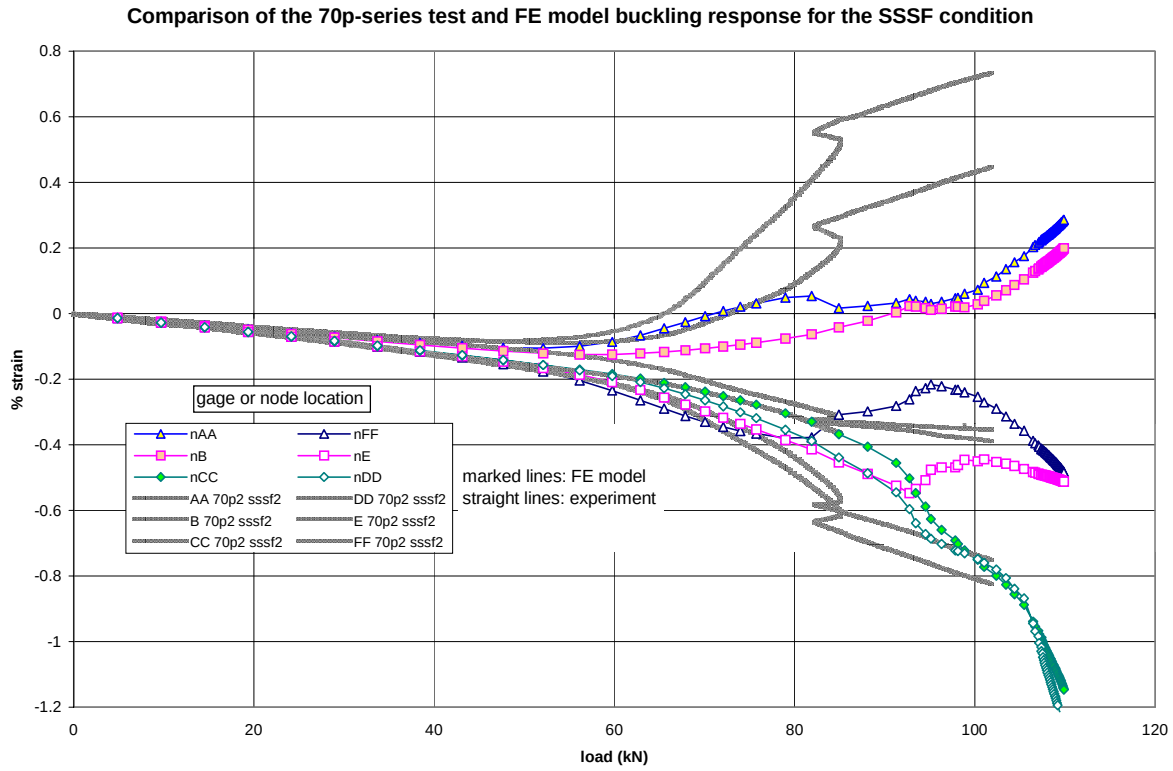

Figure 6-48. comparison of the test and FE model for the shallow curved panel in the SSSF condition

center gage. The simply supported side gage responded much as the pure SSSS wide gages did, with strains higher than the concave side, but never experiencing a slope reversal. The experimental critical buckling loads were 46 and 53 kN for the free edge and center gages respectively. The panel response was a mixture of the SFSF and SSSS responses, with critical buckling loads closer to the SFSF loads, but a postbuckling response typical of SSSS panels. The FEA model predicted the buckling response as a mixture as well. The critical buckling loads predicted by the model were 48.6 and 55.7 kN respectively. These were slightly higher than the experiment, but not nearly as over predicted as the SFSF nonlinear models. During the linear and early postbuckling response, the strains were slightly too stiff and the slope a little low, also consistent with the SFSF models. However, the model prediction was still within 5% of the experimental result for critical buckling loads at each gage. Considering that only one model was compared to a single test, along with the wide ranges found for the other tests and the uniqueness of each random perturbation model, these results are very good. Unfortunately, the mode shift appears early in the postbuckling response. The early and mode shifted FEA deformed shapes are shown in Figure 6-49. Overall, the SSSF model performed similar to the SSSS, with an accurate, valid strain field prediction until the postbuckling mode shift.

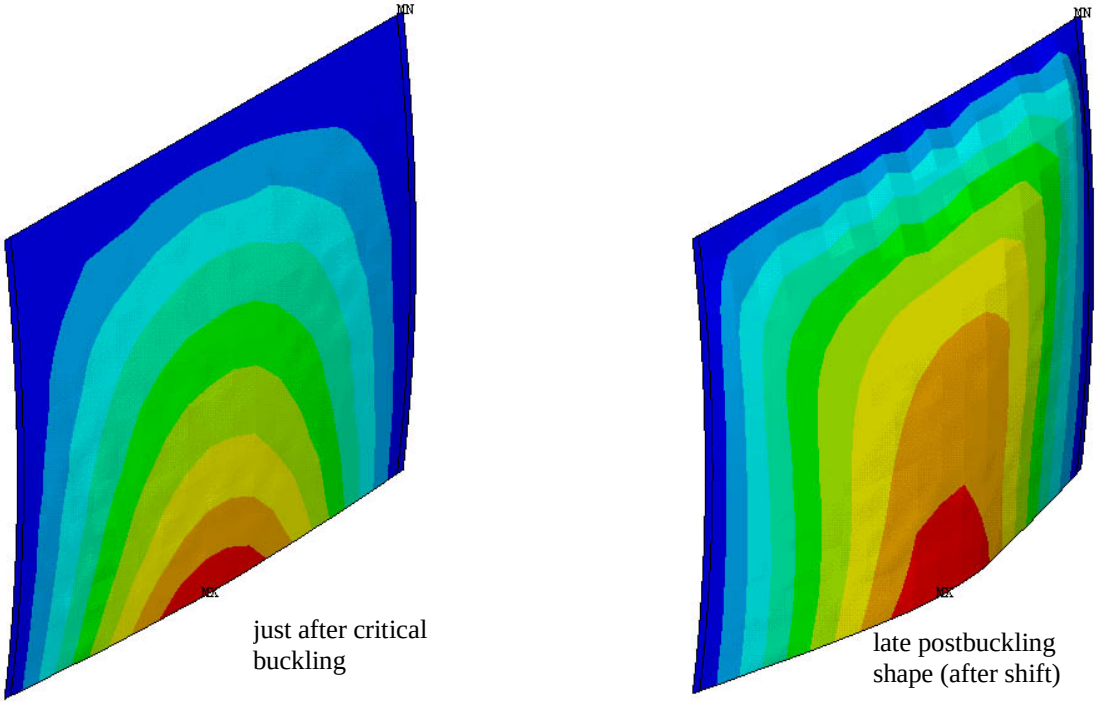

Figure 6-49. the out of plane deflection contour plots for the 70p-series model in the SSSF condition

Deep Radius of Curvature

panel data: 23p-series, cylindrical- r = 54 cm, (0/±45/b3/8)s, ~ 46x46 cm

The 23-p series sandwich panels have 58.4 cm radii of curvature. This very significant curvature was expected to drive the critical buckling load of the $(0/\pm45/0/b_{3/8})s$ sandwich panels higher for both support conditions due to the increased moment of inertia. No postbuckling response type was intuitively expected, although the unstable response is typical of thin shell cylinders. However, the panel was not expected to buckle very far into the postbuckling response due to the higher critical buckling load. The resulting high stress state in the early postbuckling range might cause failure before large out of plane deflections occur.

23-p series Test Results

SFSF Test Results

Of the three 23p-series panels tested, only two were buckled in the SFSF condition. Neither of these were buckled far into the postbuckling region; however, both experienced strain reversal. As with the other series, the outside gages tended to strain more. Therefore, the outer gages (A,F,C,D) are shown in the series SFSF compilation load-strain plot in Figure 6-50 for panels 23p1,2 & 3, rather than the center gages (B,E). Panel 23p1 has not buckled by 85 kN, although bending tension can be seen to be starting. It is reasonable to expect that 23p1 will buckle in the same load region as the other two panels. From Figure 6-50, 23p2 may be surmised to be following a neutral response, or even a barely stable response.

The full strain response for panel 23p2, shown in Figure 6-51, reveals some interesting information which may contradict that early conclusion. The data logs show that side AF buckled (deformed) more than CD. Gages A and F certainly experienced the highest bending strains of the eight gages recorded. If gages AA and FF were recorded, it is reasonable to expect that they would have strained even more, with AA perhaps even reaching tension. Gage C, along with B, possessed the most compliant responses across the panel. Gage B finally undergoes reversal at nearly 115 kN. Gage C begins on a path towards reversal, but, at about 105 kN the tension affect disappears. In fact, Gage C inflects towards a bending compression response. Gages CC and DD show this inflection even more emphatically. Gage DD reverses back with tension and CC with compression. This strain behavior suggests a mode shift from pure

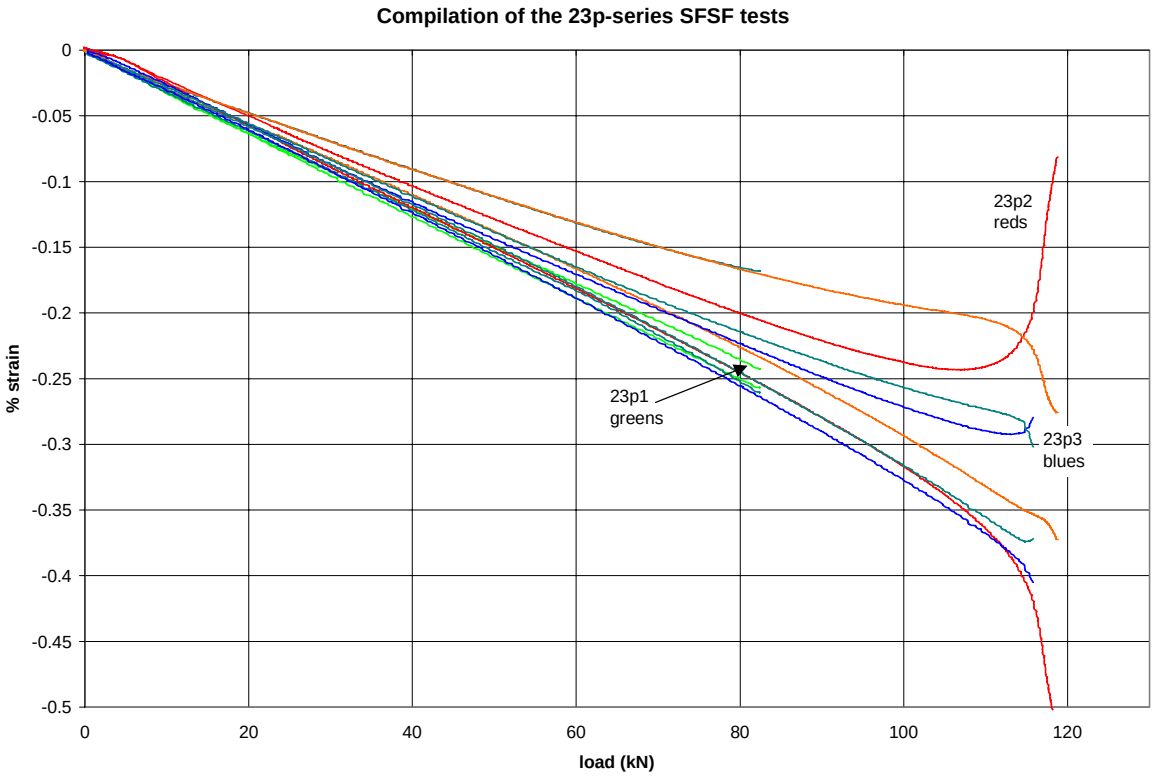

Figure 6-50. compilation of the SFSF tests on the deeply curved panels

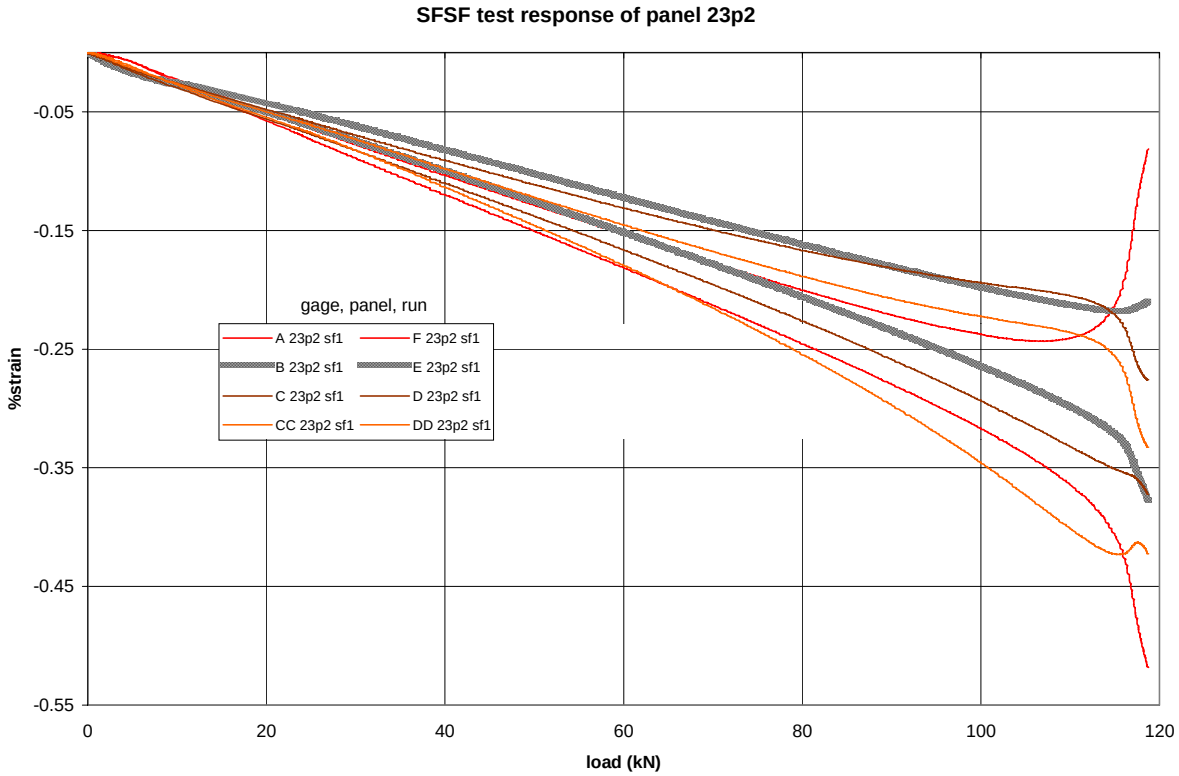

Figure 6-51. example SFSF test data set for a deeply curved panels

mode one to a shifted mode one (1xs hereafter), which has outward buckling at one free edge and inward at the other (in the radial direction). Deflections during this mode shift are not as severe as one might expect of snap-through behavior. Instead, a smooth but relatively quick shift is occurring. Since this mode shift seems to be still occurring at the end of the test, and the strains are changing quickly for that reason, it is difficult to conclusively determine the postbuckling response type.

A closer look at the response of panel 23p3 in Figure 6-52 shows that the same mode shift occurs. In 23p3 the shift occurs in a more complicated fashion. The mode shift seems to be slowly transitioning as with 23p2, then the load drops off slightly and a pop was heard. The pop coincides with the vertical lines seen at 114 kN, which seem to reinforce the mode shift behavior. Unfortunately the snap-through behavior suggested by the lines occurred because of a localized failure at the piecewise roller on the outside edge below gage C. Due to preparation problems, the sides of the aluminum C-channel were cut off entirely. this allowed the aluminum to slip off one of the facesheets during buckling and crush the balsa. The mode shift behavior is therefore not entirely conclusive. The system was replaced for the SSSS tests. The buckled shape of the AF side of 23p2 sf1 is pictured in Figure 6-53 just before the loading was stopped.

Again, without the neutral response, strain reversal gives the best buckling load. Table 6.21 tabulates the SFSF support condition tests for numerical comparisons. The buckling loads cited in Table 6.21 are the minimum loads for each run, located at a side gage (A or C). The middle gage strain reversal loads are slightly higher; for example 23p2 gage B reverses at 115 kN as compared to 107 for gage A. The strain deviation statistics show an approximately uniform uniformity of load

Table DFT. the statistical and buckling data from the 23p-series SFSF tests

			st. deviation statistics (%)			buckling data (kN)			
panel	#	shim	min	@load	@10 kN	reversal	noise	response	comments
23p1	1	1P CD	10	6	12	NA		NA	max load: 35 kN
	2	1P CD	6	4	11	NA		NA	max load: 82.4
23p2	1	none	8	11	9	106.5	+-1	NA	max load: 118.8 shift from mode 1 to mode 1xs
23p3	1	3P CD	3	22	22	112.8	+-0.5	NA	max load: 115.8 early mode 1

.

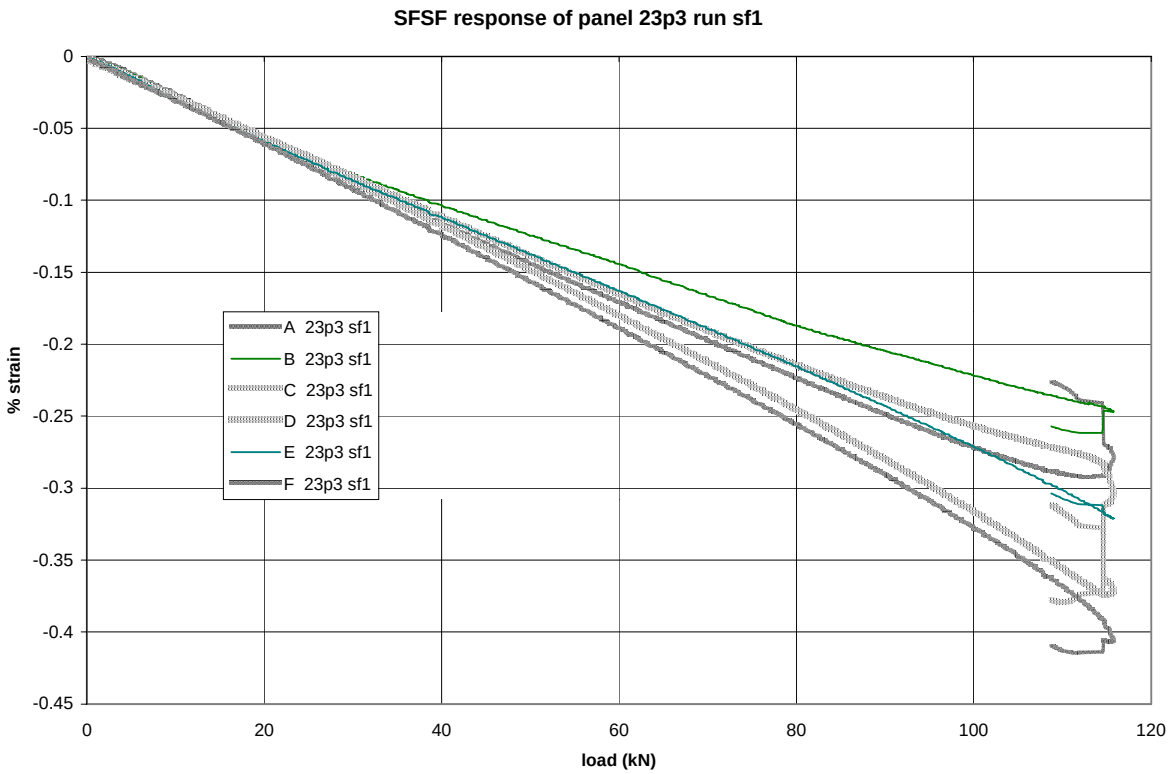

Figure 6-52. second example of a deeply curved panel tested in the SFSF condition

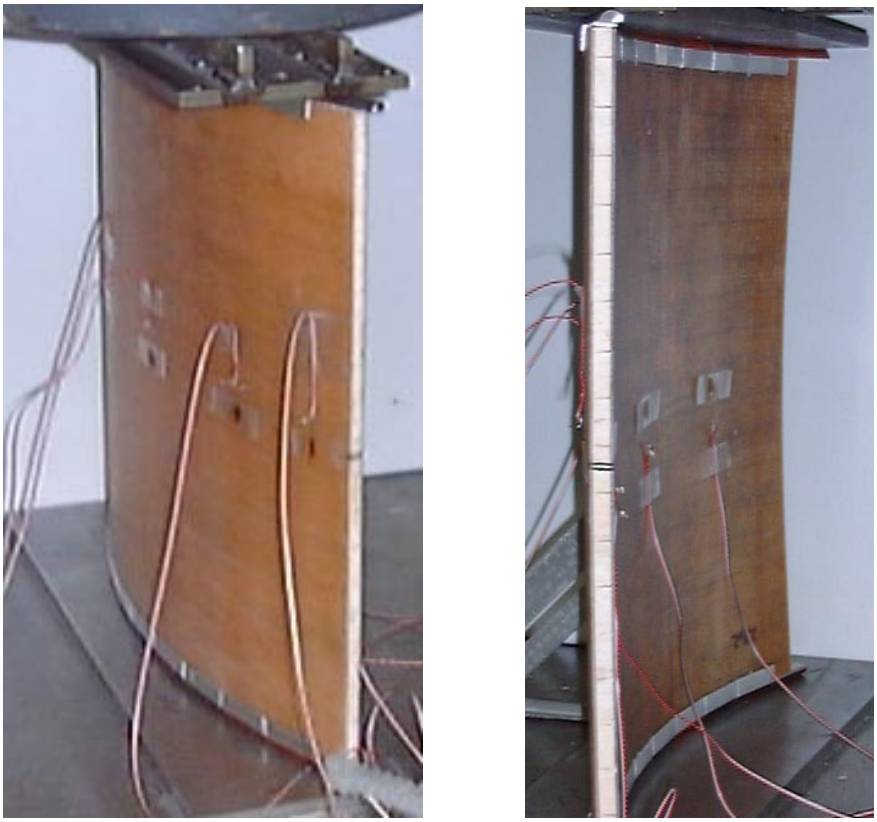

Figure 6-53. panel 23p2 shown before testing (left) and buckling during test run sf1 (right)

SSSS Test Results

All three 23p-series panels were tested in the SSSS condition. Of the three panels, only 23p1 and 2 buckled through strain reversal before failure, although all three developed or were developing a mode one buckling shape. All three test runs to failure are plotted in Figure 6-54 with only the center gages shown for clarity. The mode shift in the response of 23p3 indicated by the vertical lines is believed to be caused by the localized failure from the final SFSF test. Panel 23p3 is very close to strain reversal before a mode shift occurs suddenly which lowers the bending strains significantly at the center. If the mode shift is neglected, a strain reversal critical buckling load can be extrapolated by the strain-load differential plot within 5 kN. Due to the early failures, none of the tests reached past the early postbuckling stage, and therefore a definite postbuckling type could not be determined.

All of the recorded strain data until failure for panel 23p2 run ss1 is shown in Figure 6-55. Behavior typical of the other series is also found here; bending strain discrepancy of the center gages as compared to the sides; and a gradual buckling knee. It would also appear that the deformed shape is skewed towards the CD side. Gage C receives enough bending induced tension to reverse its strain, while gage A still remains fairly linear. In fact, gages C and B follow very similar buckling knees. This off-

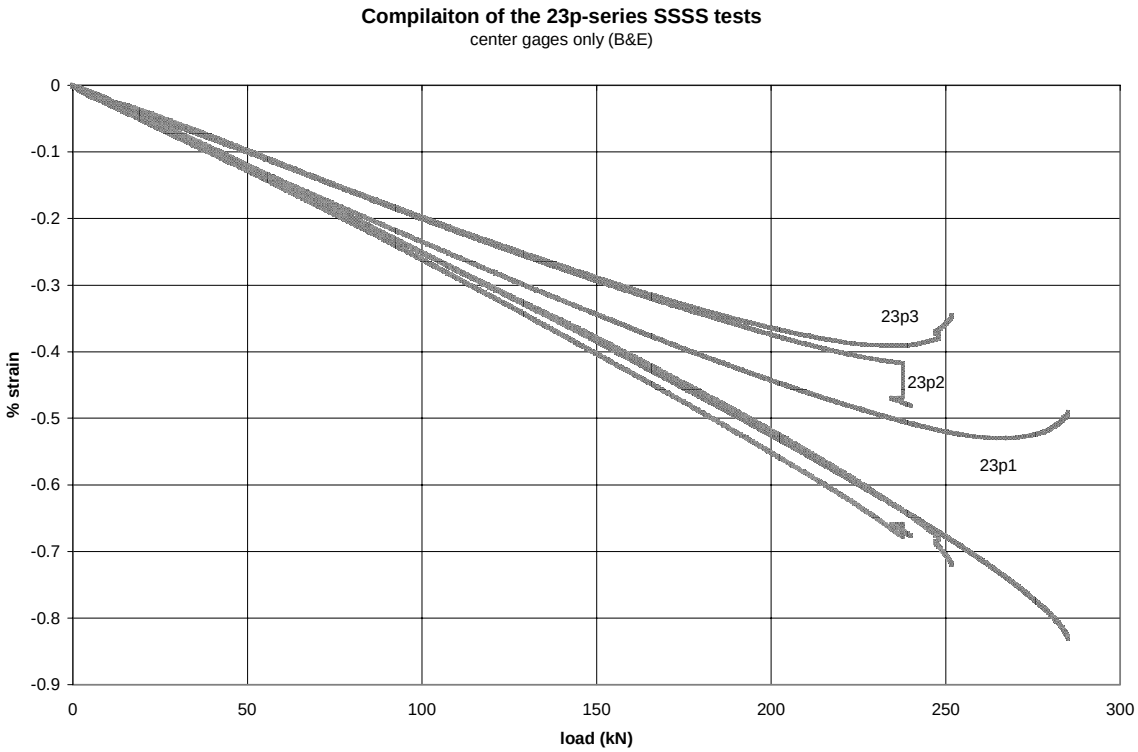

Figure 6-54. compilation of the deeply curved SSSS tests

center mode shape is also present in panel 23p1, as it deforms significantly more on the AF side, while side CD remains straight. Unfortunately, this trend cannot be confirmed by panel 23p3 whose data set is not complete because gage C was inoperative for the SSSS tests.

The critical buckling range for the 23p-series was from 233 to 263 kN; this was proportionally similar to the B-series range (97-115 kN). The failure mode was also similar to the B-series, although the facesheets received more damage and fiber failure with a more irregular delamination zone. As with the other series tests, the effect of the fixture on failure is complex and believed to be greatly influencing the failure mode. Examples of the 23p-series failures are shown in Figure 6-56.

Table 6.22. the statistical and buckling data from the 23p-series SSSS tests

			deviation statistics (%)			buckling data (kN)			failure data			
panel	#	shim	min	@load	@10 kN	reversal	*noise*	damage	load (kN)	%strain	mode	comments
23p1	1	1P CD	8	84	18	263	+-2.5	267	285	-0.390/ -0.832	delam & fiber	earplugs in, cracking might have begun earlier
23p2	1	none	12	12	13	233	+-2	231	251	-0.345/ -0.720	delam & fiber	cracking maybe 5-7 earlier
23p3	1	3P CD	6	9	7	238	extrapolated (up to +3)		237	-0.481/ -0.677	facesh. delam & fiber failure	strain jump occured at 237, less middle buckling, extrap reversal before jump load drop, then increase till failure

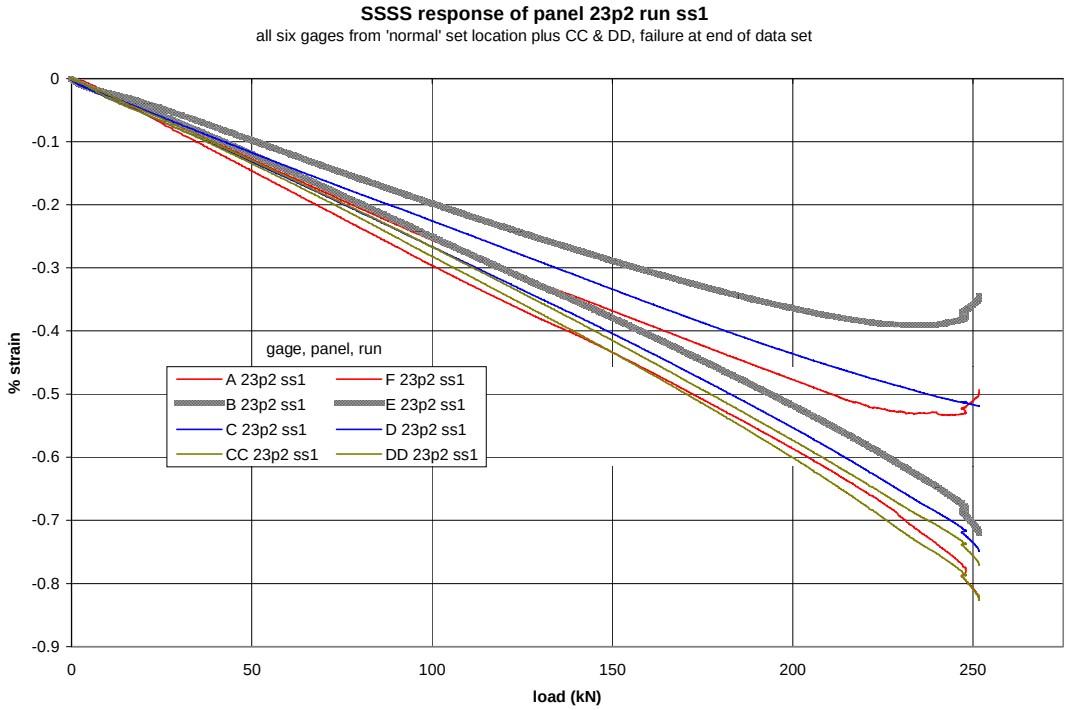

Figure 6-55. example of a full results set for a deeply curved panel tested in the SSSS support condition

(a). panels 23p1 & 2

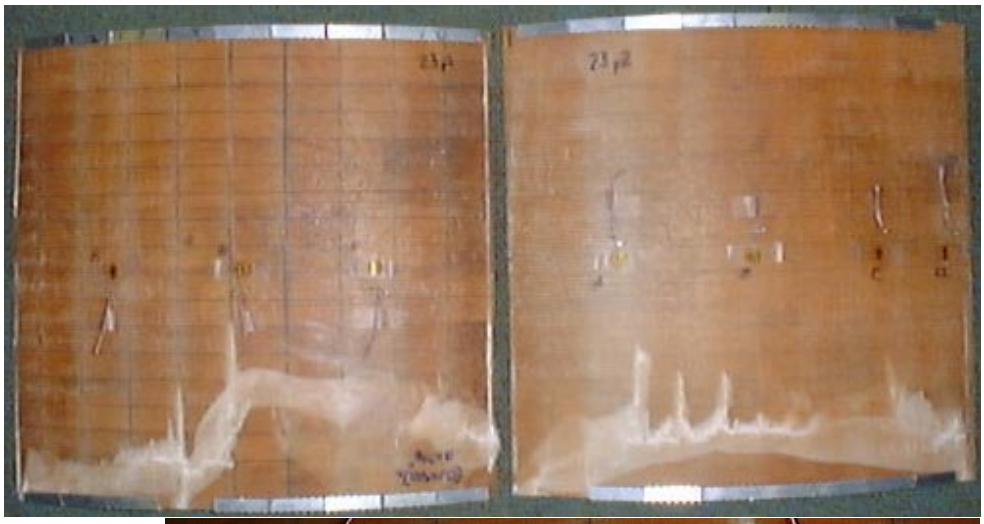

(b). close-up the damage zone of panel 23p1

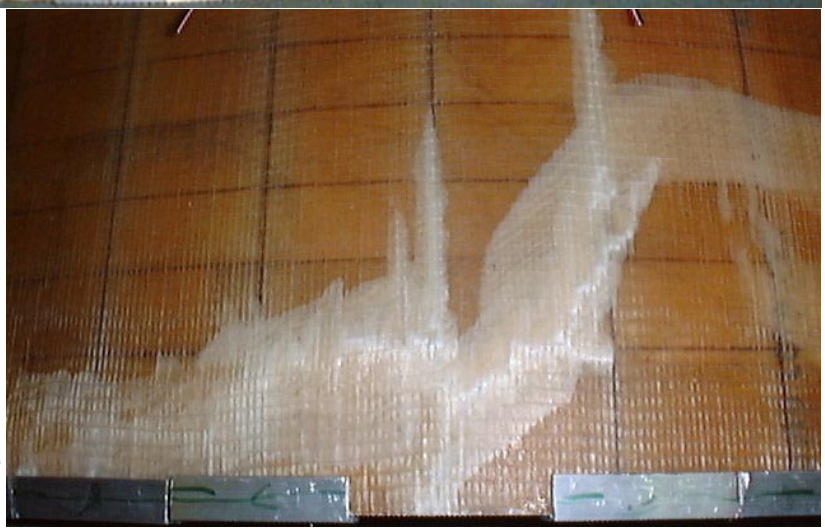

Figure 6-56. examples of the deeply curved panel failures (SSSS support condition)

FEA Validation

As with the other curved series, a cylindrical three-layer closed form buckling solution was not found. Therefore, only FEA predictions are compared to the experiments. Special attention is paid to whether those problems or trends found in the 70p-series become more pronounced with the deeper curvature of the 23p-series. The models used here in the comparisons are the single piece fixture models. The effect of modeling the load support fixture is very significant and was discussed in Chapter 4. The reader is encouraged to read that section for a complete understanding of the predictions.

SFSF Validation

The two experimental test panels are compared against two nonlinear FEA models and two eigenbuckling models (fixture and ideal). One of the most intriguing results from the experiments was the apparent transition from an early mode one shape to a side shifted mode (1xS) in which the free edges buckle in opposite directions. The predicted and experimental results are tabulated below in Table 6.23. The linear fixture model predicts this 1xs mode at a load which compares favorably with the experiments. The lowest experimental strain reversal is 107 kN, while the fixture model predicts 115 kN. An ideal SFSF model was also solved to determine whether the fixture influenced the likelihood of the mode shape. The ideal model yielded the same mode shapes, in the same order, at predictably lower loads, thereby reinforcing confidence in the 1xs mode as the critical buckling mode. In contrast, the shallow curved model (70p) predicted the more intuitive mode one response, although it had difficulties predicting the correct load (over-predicting by about 50%). For these more deeply curved panels, mode one is the second stability mode and again the buckling load over predicted by about 40-50%.

Table 6.23. the 23p-series SFSF critical buckling for the experiments and FEA

	critical buckling (kN)				
analyses	AA	A	B	C	CC
exp. panel 23p2	-	107	115	>	116 (DD)
exp. panel 23p3	-	113	>	115 (D)	-
random method, #1	107	124	151	119	116
random method, #2	119	122	147	123	110
eigenbuckling FEA	1 x s	1	2 x s	2	3 x s
fixture model	115	150	172	180	210
ideal model	90	96	-	-	-

note: the symbol, > signifies reversal was not reached for that gage, - signifies that data was not available

For the 70p-series, the nonlinear models had more success in predicting the corrrect critical buckling loads than the linear models. They were still non-conservative, but predicted the correct mode shape and postbuckling response. The 23p-series nonlinear models shared several of these trends and problems. Both nonlinear FEA models predicted a mode one response throughout an postbuckling region. At critical buckling, the experimental panels were just beginning their transition, although the free edge which did not transition had already reversed its strain. Therefore, a mode one prediction would still be a comparable one. The models tended to over-predict by about ~10% at gages A and C (120 kN versus 110

kN) which is consistent with the shallow series. However, the middle locations do not compare favorably, with the nonlinear model over-predicting by about 30% (150 to 115).

The problems the nonlinear model has predicting the buckling response are further identified in the load-strain plots shown in Figure 6-57. The critical buckling knee of the FEA model is very gradual in contrast with the experiments (and especially compared with the flat panels). The FEA model reaches a maximum load of 155 kN before becoming unstable. Even if the postbuckling type is yet undefined, the experimental results follow a completely different path. While the critical buckling loads are reasonably accurate, the nonlinear model has difficulty describing the buckling response, even the early postbuckling response for the 23p-series SFSF panels. Even the mode shape predicted remains questionable. The nonlinear FEA models seem to have great difficulty with the combination of curvature and free edges. However, the linear model, which had difficulty with the shallow curved panels, seems to give good, even if non-conservative, results. This could be the result of a slow transition from mode one to 1xs as curvature is increased from a flat panel.

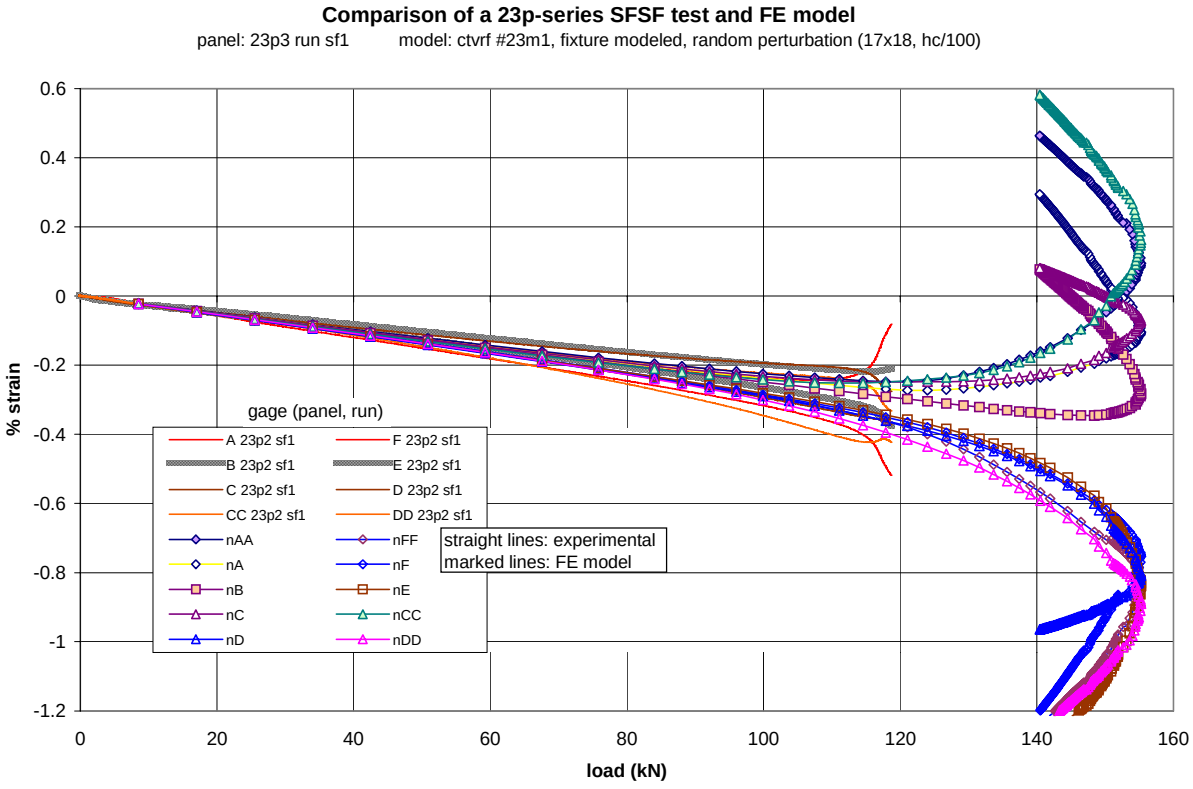

Figure 6-57. comparison between a example deeply curved SFSF test and FE model

SSSS Validation

As found for the shallow curvature, the problems contributed by curvature to the SFSF models did not appear in the SSSS models. The 70p random perturbation model had great success predicting the mode shape, critical buckling load and postbuckling response. Similarly, the 23p-series nonlinear SSSS models had much more success in modeling the buckling response than the did SFSF models. However, the linear fixture models had very severe problems. The results for all analyses on the 23p-series are compiled in Table 6.24.

Table 6.24. DVF the 23p-series SSSS critical buckling for the experiments and FEA

analyses	critical buckling (kN)	mode
experimental range	**233- 263**	1
random method FEA runs	222 , 224	1
fixture linear FEA	- -	- -
4x5 mesh	252	1
8x9 mesh and up	252	4+
ideal linear FEA		
15x16 mesh and below	157	1
16x17 mesh and above	205	2

The mesh convergence studies described in chapter 4 revealed that the linear models had a difficult time predicting the correct mode shape, and therefore the correct critical buckling load, when mesh densities were high for curved sandwich panels. The results are again presented here to compare against the fixture model, which has even more severe problems. The addition of the fixture caused the required mesh density for the mode drop to lower to the coarse mesh of 4x5. At this mesh, a critical buckling load of 252 kN is predicted, which falls within the experimental range. Oddly, the finer meshes also predict critical buckling loads of 252 kN. This occurs because a number of mode shapes and stability loads are grouped around 252 and 253 kN. Such a grouping is not infrequent for very complicated structures; however this structure is only a highly curved sandwich panel. Therefore, the results must be viewed with some skepticism.

As found for the ideal nonlinear curved sandwich models, the fixture models did not have such a mesh density problem. Two cases were solved with panel mesh grids of 12x13 and 17x18 respectively and convergent random perturbations. Slightly conservative critical buckling loads were found (about 5%) for

both, as well as the correct mode shape (mode one). The response of the 17x18 model is plotted over the 23p2 ss1 test in Figure DVS for qualitative comparisons. All of the models solved in the fixture model study (Chapter 4) had unstable postbuckling responses which had mode shifts occurring early into postbuckling. Unfortunately, the general, unstable postbuckling response cannot be validated due to the early failures during postbuckling. The FEA results in Figure 6-58 only shows the pre-shifted response for clarity. The panels failed at a similar load to where the mode shift occured. The buckling knee of the FEA model is sharper than the experimental knees, but significantly more gradual than for the flat panel models gave. The path of the strain of nodal location nA is odd for a convex side path, but the path of nF (same node) demonstrates that the outside layer is in fact the convex side of the deformed shape as expected. The almost exact agreement of the 70p series experiment and FEA run is partly luck, which makes the 23p-series prediction look worse than it is. Qualitatively, these results are in fact quite good.

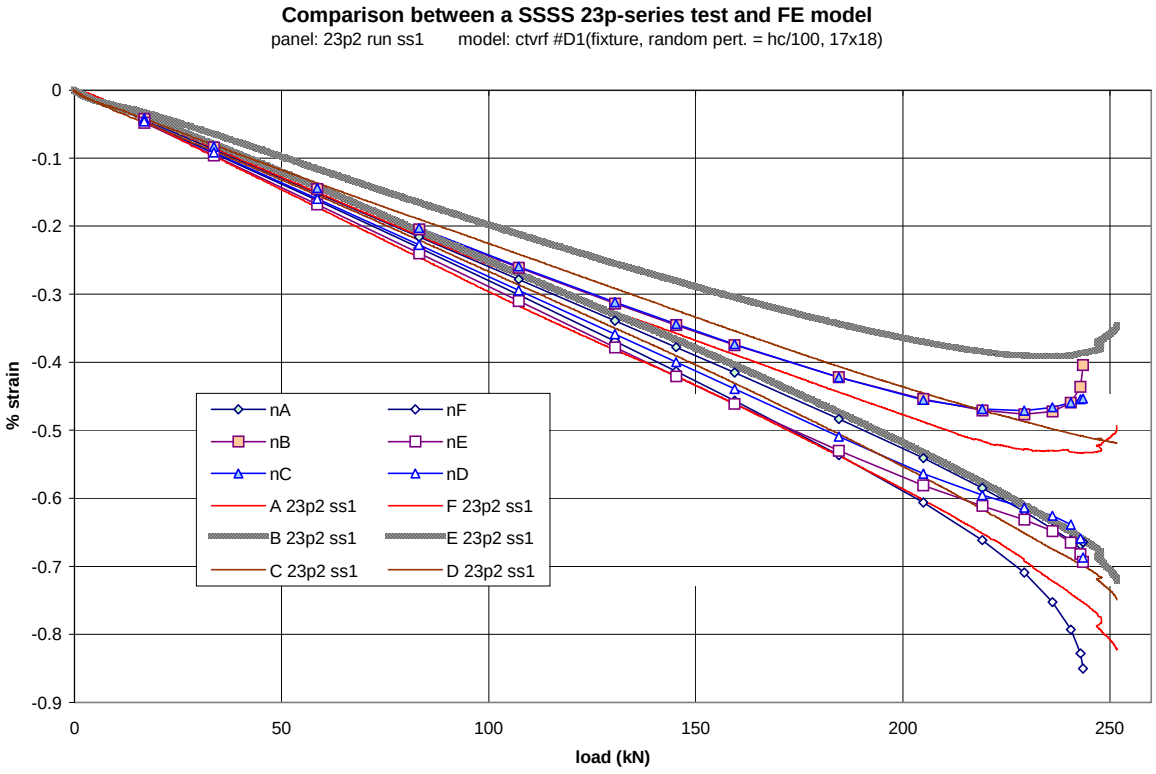

Figure 6-58. comparison between a deeply curved panel and FE model in the SSSS support condition

Effect of radius of curvature

While the first two parameters, lay-up and core thickness had various effects upon the buckling loads the general responses were very similar and predictable. Curvature has a more significant effect upon the response, changing the critical buckling loads and the response characteristics and type. The effect of curvature on the buckling response of sandwich panels and the ability of FEA to predict that response, can be clearly seen in Figures 6-59 and 6-62. All five series of SFSF responses are plotted together in Figure 6-59, while the SSSS responses are shown in Figure CUV (minus the C-series for clarity).

Curvature causes the SFSF buckling response to be unstable. Deeper curvatures predictably cause higher critical buckling loads because of their higher moment of inertia. It would seem that at least for the FEA models, the deeper the curvature the more unstable the response (faster the load drops). One hypothesis which might explain this is best understood when applied to the 70p-series. The 70p-series panels were observed to have a buckling shape that became flat across the middle section (the edges deformed farther), deep into the postbuckling response. It would seem that at with shape, the effect of

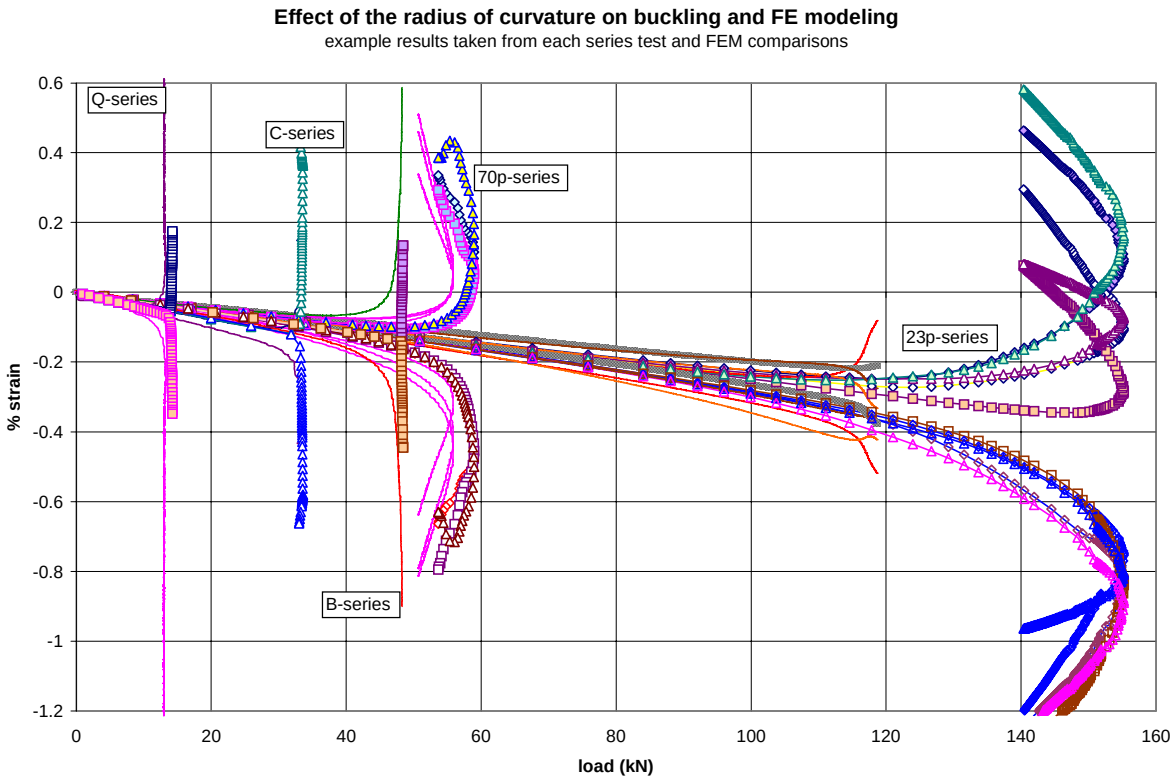

Figure 6-59. effect of all parameters on buckling and FE modeling

curvature was negated, and a response more typical of a flat panel would occur. In this case, the 70p panels would begin behaving as a similar lay-up flat panel, a B-series panel. The late 70p experimental postbuckling response seems to be following this hypothesis and flattening out at a load just above the B-series asymptotic load. With this theory in mind, a more curved panel would probably take a path which would approach the flat panel faster; however, it would necessarily begin at a much higher load. This appears to be the case for the 23p FEA model.

The SSSS panels have stable responses because of the two side supports which keep the local panel configuration straight and continue to take increasing loads even if the buckled middle does not. The 23p experimental SFSF panels seem to be developing a 1xS mode shape, which incorporates a straight center line (the nodal line created by the asymmetric mode shape). This might be a reason for the beginnings of a compliant postbuckling response shown by the 23p2 panel, rather than the intuitive and FEA predicted unstable response.

The FEA modeling techniques seem to have a difficult time dealing with curvature in the SFSF condition. Both the linear and non-linear techniques have problems which share similar origins, predicting the proper mode shape. For the linear models the symmetric (edges buckle to same side) deformed shape causes overprediction the critical buckling load (see 70p SFSF validation). Curvature causes the likelihood of an asymmetric mode (nxS, edges to opposite sides) to increase, as the curvature increases, and eventually this becomes the critical buckling mode according to linear analyses. This trend occurs for the higher modes as well as seen in Figure 6-60 which plots the stability loads versus radius of curvature for the linear fixture models. If the asymmetric predictions are accurate, or become more accurate as the radius drops, then this hypothesis is correct. The end result is that linear analyses are accurate for the flat and deeply curved panels but tend to overpredict the shallow curved panels.

The nonlinear models are affected by the curvature in a different, more predictable manner. The flat panels are predicted very well with respect to both critical buckling and postbuckling response. The introduction of curvature causes the model to predict high critical buckling loads, but the postbuckling response is predicted accurately. However, the nonlinear models seem to have difficulty developing the antisymmetric mode shapes which become more prevalent at the deeper curvatures. Therefore, they predict the second stability shape, the symmetric mode one, and predict a correspondingly high critical buckling

load. The analyst who is trying to predict buckling of a sandwich structure which has free edges should be careful by using both linear and nonlinear techniques for any panel with curvature. As the facesheet and core properties and thicknesses change, so to will the radius ranges over which the linear or nonlinear techniques perform the best. So, both methods should be used with the more conservative results being the most accurate.

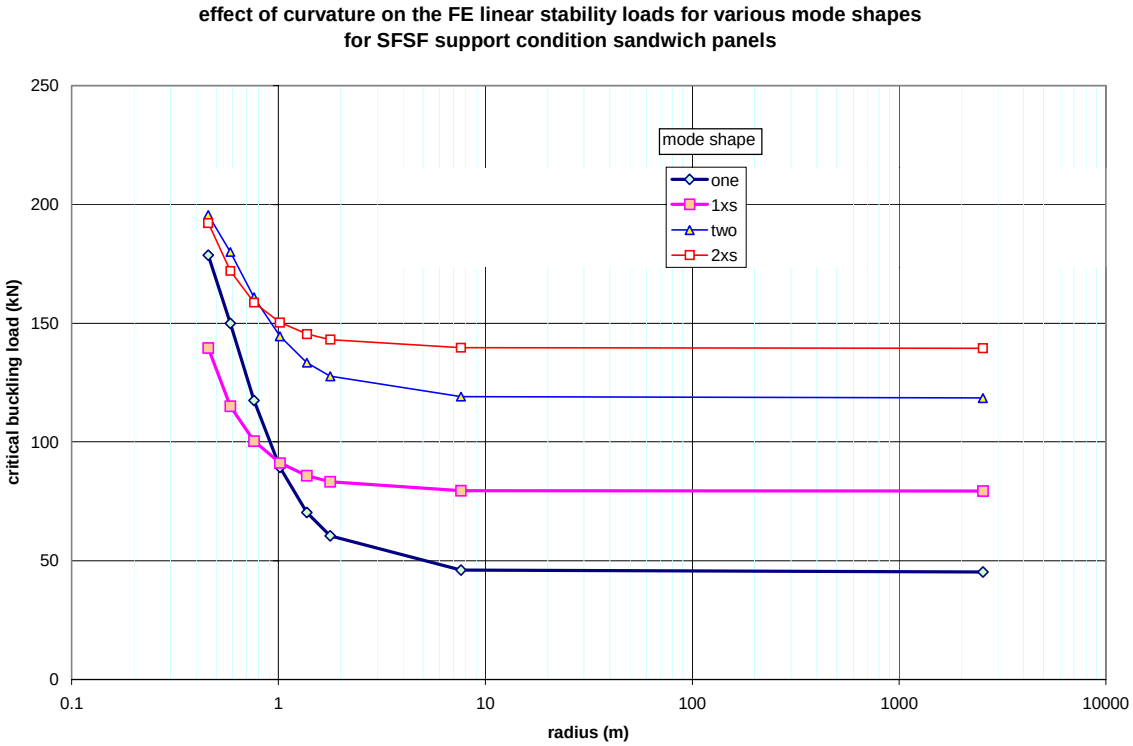

Figure 6-60. effect of curvature on the FE stability loads of SFSF support condition sandwich panels

The effect of curvature on SSSS panels, which better simulate blade panels, is more predictable and straightforward. As expected, the critical buckling load increases as the curvature is increased and the postbuckling response is shortened. The panels fail due to a higher stress state at lower out of plane deflections, while the FEA models experience earlier mode shifts which might reduce the accuracy of the predictions (more experimental data is required).

If the hypothesis espoused earlier to explain the curved SFSF responses is generalized, it can be applied to the SSSS panels: the more buckled/deformed a panel becomes, the more it behaves like a flat panel. If this is the case, a curved panel postbuckling response would become more compliant as the curvature was increased until an unstable response was obtained. This result is shown to exist in Figure 6-62, which has the LOD plots for each (0/±45/0/b3/8) panel series (B, 70p, 23p) nonlinear models, for the

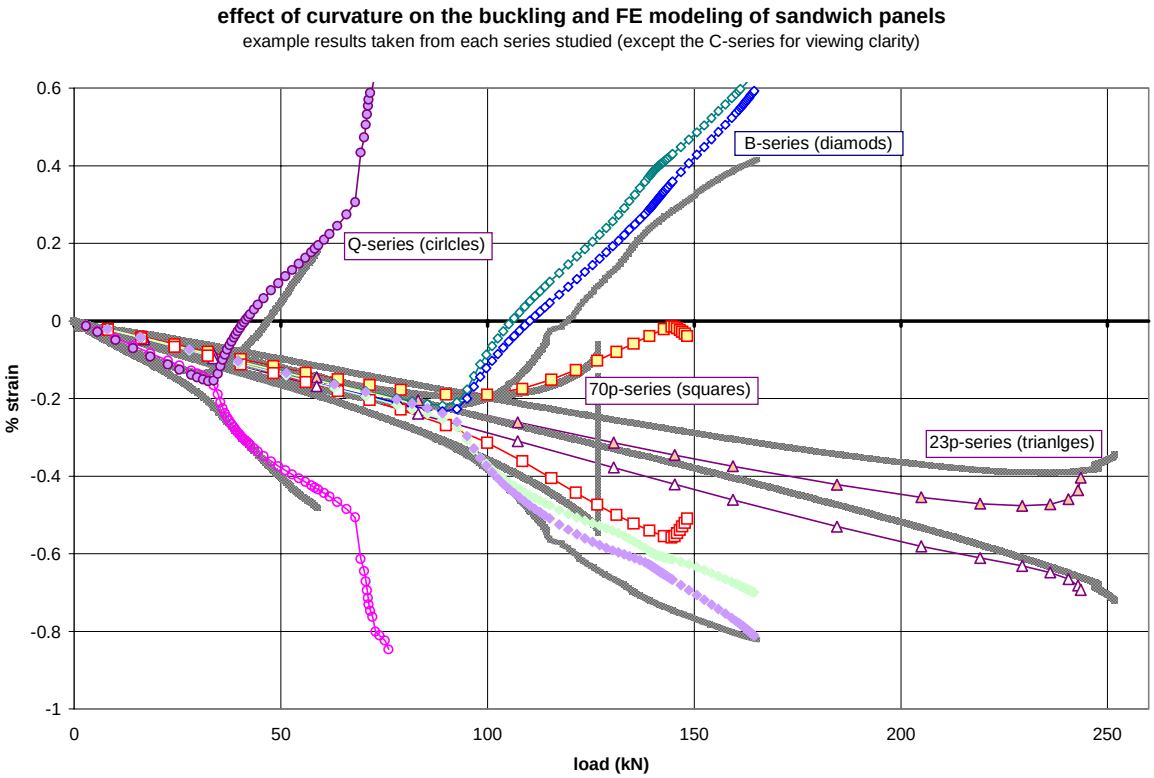

Figure 6-61. effect of curvature on the buckling and FE modeling of sandwich panels with SSSS supports

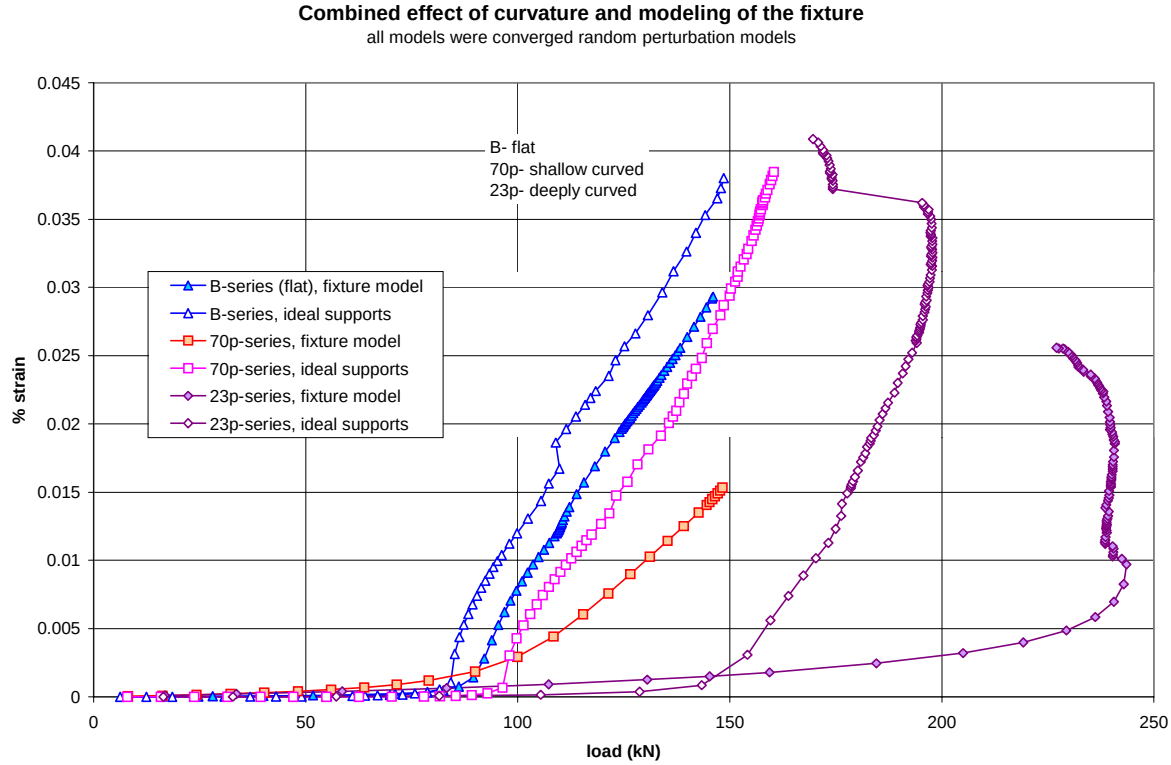

Figure 6-62. combined effect of curvature and fixture modeling on the buckling response of SSSS sandwich panels

ideal and fixture cases. The effect is most clearly seen for the ideal support models. The shallow curved model definitely follows a more compliant path than the flat panel while the deeply curved model follows an unstable response. However, the load drop does not occur for the 23p model until very late in postbuckling when the panel has deformed out of plane almost three panel thicknesses. At such a large deformation, the three models have loads which are within 25 kN (about 15%) of each other, even though their critical buckling loads differ significantly (~70 kN, 80%). These results lend more confidence in this hypothesis.

The FEA techniques have fewer problems predicting SSSS sandwich panel buckling responses for curved panels. The nonlinear models do not seem to have a problem predicting the critical buckling loads of curved panels. However, the mode shift which appears in almost all of the random perturbation models occurs earlier in the postbuckling response of curved panels. The linear models however, seem to be mesh size dependent at some deep curvatures. The mesh convergence study on the 23p series ideal support models (see Chapter 4, mesh convergence) shows that above certain high mesh densities the first mode shape is lost and the second stability load is predicted to be the critical buckling mode at the correspondingly high load. This problem is exacerbated by complex models, such as the modeling of the fixture. In the case of the 23p fixture model, linear analyses predict the wrong mode shape above 5x5 mesh grids. Most likely, complex structures and/or boundary conditions could also intensify this mesh dependence problem. The analyst is therefore encouraged to perform a nonlinear buckling analysis in addition to linear solutions to get confident results for complex models. When a conflict in results arises between the linear and nonlinear analyses, the results from the present study suggest the nonlinear model gives more accurate and dependable results (for models without free edges).

Chapter 7

CONCLUSIONS AND FUTURE WORK

The results from the testing, finite element validation and modeling studies are summarized in this chapter. The three sets of conclusions are separated for more convenient reference and some conclusions may be repeated between the three sections. Lastly, the suggested future work items, both extensions from and side projects of the present study, are presented in the final section.

Experimental Testing

Perfomance of the Fixture

- The whole fixture performed well in the linear, critical buckling and early postbuckling ranges. It performed adequately in the late postbuckling response. However, it was believed that the extra half inch of steel in the load direction would have a geometric, and elastic effect on the system response. The fixture also had a definite, but non-quantifiable, affect on all panel failures.

  - *load support fixture* Both the single piece and piecewise load supports rotated well to approximate a simply supported condition. Neither became plastically deformed in the axial direction due to pressure. The major drawback of this load support system was the large preparation time and test turnover reduced to a maximum of one panel per day due to the need for the epoxy filler to cure.

    - *single piece* The single piece fixture became permanently twisted torsionally due to repeated tests into the late postbuckling region. Afterwards, the fixture began to influence testing results by forcing the panel to buckle to a particular side, regardless of the panels imperfections, and therefore was rendered invalid for further testing.

    - *piecewise continuous set* This fixture accommodated any curved panel. It allowed for different rotations through the width of the support with minimal torsional resistance supplied by the fixture itself. It also affected the postbuckling response of the two B-series, four sided simply supported (SSSS) postbuckling response types from stable with the single piece to unstable with the piecewise set.

- *knife edge side supports* The knife edges were easy to assemble and generally performed adequately if sufficient force was applied to the bolts to keep the knife edges from separating. It was easy to see poor performance visually as a large gap between the panel and knife edge, and to confirm the observation in the load-strain response of the panel.

- *Alignment* The most uniform loads were produced when a layer of epoxy was placed between the panel and load support system. The epoxy fills any gaps created by uneven flatness of the panel (even after extensive sanding) and helps to create a more parallel loading.

- *Test Reproducibility* In general, the postbuckling response of a panel was governed mostly by the panel and the support condition, with little effect contributed by the imperfections and/or non-uniformity of loading. The critical buckling loads were more sensitive to initial imperfections, and therefore to non-uniform loading due to the fixture. Overall, from geometric differences of the panels and imperfections in the panel and due to the fixture, the critical buckling loads of each series varied by about ± 10% maximum from the mean average. Due to the relatively low number of tests, a critical buckling load range was used qualitatively rather than an average load with standard deviation quantitative approach.

  - *within one panel* When no changes were made to the system, and no significant damage observed audially, subsequent testing yielded very similar load-strain responses (critical buckling about ± 2%). With damage, the load-strain response would vary slightly more.

Performance of the Data Acquisition

- The strain gage data (and load) provided the main test data for all test results in this study. It did not have significant noise and could be differentiated with respect to the load to yield useful information.

  - *strain reversal technique* Due to the data available, the strain reversal technique provided the best method for the determination of the critical buckling load. This technique could be directly imported to the FEM results and could also be used on full structure buckling tests if the mode shape is known prior to testing so that the gage location could be chosen correctly.

- The strain pot deflection data proved to be too noisy to be useful. Therefore no load-deflection plots or mode shape contours were available.

Test Results

- Each of the five panel series tested responded and failed in a self similar fashion (3 flat, 2 curved). The five series and two support conditions, four sided simply supported (SSSS) and simple-free-simple-free (SFSF), provided a wide range of response types, critical buckling loads and mode shapes for the FE models to validate.

- *Flat panels, SFSF condition*: critically buckled at loads of around 13, 35 and 45 kN (Q, C, and B-series respectively) with neutral postbuckling types and mode one shapes (with the free edges deflecting more)
- *Flat panels SSSS condition:* buckled at 35, 100 & 95 kN (Q,C,B), stable postbuckling type, mode one
- *Shallow curved SFSF:* buckled at about 50 kN, unstable response, mode one
- *Shallow curved SSSS:* buckled at about 100 kN, stable response (failed early), mode one
- *Deeply curved SFSF:* buckled at about 110 kN, most likely stable response, mode one shifted (one free edge buckled out, the other in)
- *Deeply curved SSSS:* buckled between 230-260 kN, unknown response type (failed early), mode one

Validation of Modeling

- The finite element linear and nonlinear (shell) models with sandwich modeling provide accurate predictions of the experimentally determined critical buckling and postbuckling responses for most flat or singly curved sandwich panels. However, several cases exist which pose problems for these techniques and partially, or fully invalidate the results.

  exceptions (invalid cases)

  - most nonlinear models experience a mode shift or mesh rippling phenomenon (see next section) somewhere in the postbuckling response. After this occurrence the strain data becomes irregular and often invalid, while the deflection data still yields rough approximations.

  - The combination of curvature and free edges causes problems in predicting the correct mode shapes (and hence loads) for both the linear in nonlinear methods, but manifest themselves at different curvatures. The linear technique gives better results for deep curvatures while the nonlinear works better with shallower curves. The more conservative of the two results tends to agree better with experiments although it is still often nonconservative.

  - The linear analyses are sensitive to certain combinations of curvature and mesh density with further enhancement of the problem by complex boundary conditions. Deep curvatures combined with high mesh densities can cause the lower mode shapes to disappear, of which one is likely to be the critical mode, thereby yielding incorrect and nonconservative results. This problem is exacerbated by complex boundary conditions (such as the modeling of the test fixture) which cause the mesh at which these problems begin to be as low as four elements per buckling wave.

- The three-layer closed form solutions found in the literature [Vinson (1987), MIL-HDBK-23A (1968)] gave poor results, as used in this study, for fiberglass/balsa sandwich panels of the dimensions used in the present study (which are typical wind turbine blade dimensions). They tended to give results which are very conservative (as low as 25% of more accurate predictions) and predicted higher mode shapes than were correct or expected.

- The mixed element models (shell facesheets, solid brick cores) were difficult to construct properly and yielded critical buckling loads that were about two times too high, and postbuckling responses which were much stiffer than those of the experiments or shell models.

FEM Buckling Analysis Guidelines

Nonlinear versus Linear Modeling

- The nonlinear models tend to be more conservative and less sensitive to curvature and complex boundary conditions.
    - Linear model predictions are not valid for certain parameters, especially deep curvatures with high mesh densities or shallow curvatures with free edges (see previous section).
- The random perturbation method is susceptible to skipping the first mode shape (see below), and therefore, should always be accompanied by a linear model. If the linear model predicts a different critical buckling mode which has a lower load than the nonlinear model, more nonlinear runs are required. If the linear model predicts a different critical buckling mode, but at a higher load, the results from the nonlinear model should be used.

Sandwich Modeling

- The introduction of sandwich theory to the shell model significantly affects the critical buckling load and postbuckling response. In the models studied here, the critical buckling loads dropped 30-40%, down into the experimental buckling range, while the postbuckling responses became considerably more compliant.
- Two possible problems are also introduced with sandwich modeling
    - *Mode Shifting*. Somewhere in the postbuckling response most sandwich models will experience a mode shift. When this occurs, the symmetric deformed shape will move towards one of the corners (or occasionally a side). Accompanying this shift is a slightly more compliant postbuckling path (and for the random perturbation method, irregular nodal strain responses)
    - *Mesh Rippling*. High transverse shear strains in the core, along with composite facesheets (orthotropic oriented layers) often cause mesh rippling. Mesh rippling appears as local out of plane waveforms with half wavelengths the same size as the elements. The waves are often superimposed on to the global buckling mode shape. The high transverse shear strains can be caused by curvature or soft cores (which may produce local buckling before global). As with mode shifting, the postbuckling path becomes more compliant (sometimes unstable) and the strains irregular.
- Only approximate core properties are required for good results. In this study, varying the core properties by a factor of 4 changed the critical buckling load only by 15%.
- Facesheet properties affect buckling differently for each support condition.
    - *SFSF*. Axial stiffness dominates the critical buckling loads, with high stiffnesses producing high critical buckling loads.

- *SSSS*. The directional properties and buckling interactions are more complex for this case. Lower axial stiffnesses may actually increase buckling loads by allowing the panel to deform more in-plane in the linear region thereby delaying buckling.

Random Nodal Perturbation Method

- The random nodal perturbation method yields unique solutions for each case run due to unique original shapes. The results are relatively consistent for both critical buckling and postbuckling response. A statistical study of eighteen case runs found a standard deviation of 3.7%, which fell to 2.2% for cases with smoothly developed critical buckling knees. The statistical study also demonstrated two other characteristics of the random perturbation method:

  - *numerical pop-in.* Occasionally a model would remain linear past the critical buckling load (6 of 18 runs). Typically, these models would eventually pop/snap into the correct mode shape and immediately converge to the proper postbuckling path with a subsequent drop in load. These models over-predict the critical buckling load by from 5% higher compared to the 'smooth' responses, to as much as just below the second stability load (about 75% too high). The postbuckling path (after the pop-in) remains as valid as would a smoothly developed knee case.

  - *Higher mode predictions.* Rarely, a model will remain linear past the critical buckling load and reach the second stability load (2 of 20 runs). In this load region it may buckle into the second mode shape, or once again pass this stability point to pass on to the next higher mode (one of each occurred here). When the model buckles in a higher stability mode, the same modeling characteristics apply as to those found for the critical mode.

- *versus other methods.* The random perturbation method performs favorably compared to more conventional perturbation methods such as the moment method with characteristics as follows:

  - *perturbation size* The critical buckling load of the moment method is very sensitive to perturbation size while the random perturbation method is not (ignoring snap through or higher mode prediction behavior). However, the moment method has a convergent postbuckling path while the random perturbation responses generally become slightly more compliant with larger pertrubations.

  - *mesh size* The random perturbation method is mildly sensitive to mesh size while the moment method is not very sensitive. For the random method, the critical buckling load lowers slightly with higher mesh densities and the postbuckling response becomes more compliant with the lower mesh densities until approaching the stiffer, convergent postbuckling paths of the moment method.

  - *random perturbation side effects* The random method causes mode shifting and mesh rippling to occur earlier in the postbuckling response. With allowances for the uniqueness of each model, the larger the perturbation size the earlier the shift.

- The random perturbation method contains various logistical problems. The most prominent are:
  - local curvatures are created which may violate sandwich modeling restrictions depending on the size of the perturbations, the mesh density and their unique sequence.
  - Numerical pop-in behavior is likely with random perturbations which are too small.
    - The local curvature and snap-through problems conspire to create difficulties finding convergent perturbation and mesh sizes for certain models. For these models, the largest permissible perturbation size may be prone to snap-through behavior and several cases must be run to obtain a smooth critical buckling knee and corresponding critical buckling load prediction.
- The random perturbation method has difficulties predicting failure using common classical lamination theory failure models in the facesheets, due to strain field discontinuites resulting from the nodal perturbations.

Boundary Conditions

- Correct implementation of the boundary conditions is very important to the buckling problem. It is especially important if the boundary conditions are idealizations of structural parts. Those parts should be modeled; avoid over-use of simplifying assumptions. The effects of the complex boundary conditions are increased considerably with the introduction of curvature.
  - In the present study, the modeling of the fixture was necessary to accurately predict the critical buckling load of the deeply curved panels. For these, the critical buckling load increased by about 75% from the ideal support condition case.

Future Work

Testing

- It would be beneficial to test panels for which the first two linear stability loads are very close to each other, as well as a panel which buckled in a higher mode shape. The easiest way to do this would be to increase the aspect ratio to various values between 1.5 and 2 depending on the panel lay-up. This would provide good results on how well the buckling analyses (particularly the random perturbation method) worked for higher modes. These tests would also provide information on the effect of transverse shear on the transitions from one mode to another as the aspect ratio rises.
- To further define the validity of the buckling analyses, a number of additional tests could be performed so that a critical buckling load average and standard deviation calculated for one of the test series rather than a buckling load range (B-series recommended).
  - These extra tests may also provide a good opportunity to investigate the unstable responses found for the B-series tests using the piecewise load fixture.

- It would be useful to know if there is an upper limit on the core thickness for the linear or nonlinear analyses. To accomplish these tests, significant additions to the current fixture, or an entirely new test fixture may be required.

- The final step in testing would be to test actual blades and use them to fully validate the FE buckling models. An intermediate step could be taken by testing larger, more complex substructures such as full cross-sections lengths.

Modeling

- Other failure modes (beyond facesheet overstressing/straining and core transverse shear overstressing) could be incorporated into the shell models by using the three possible user defined failure criteria slots. In particular, core shear buckling and facesheet wrinkling could be attempted. Additional tests would most likely be required (also suggested above).

- The difficulties that the closed form solutions had predicting critical buckling modes and corresponding loads could be explored further. Two different paths could be followed to understand why the predictions were inaccurate. First, new lay-ups (especially much thicker cores) and different material systems could be tested and modeled to find out whether the problems were universal or tied to certain parameters in the present panels. Second, an intensive mathematical investigation could be initiated to accomplish the same feat. Both approaches could provide bounds on accurate results for these solutions.

- The initial questions that prompted the mixed element model were not sufficiently answered due to the problems encountered. Guidelines for the proper modeling of solid core models could be generated similar to those found for the shell models. Or the possibility remains that the mixed models can not accurately model these types of sandwich panels (see Chapter 5, mixed element model section for specific modeling suggestions).

Failure Prediction and Structural Interaction

- One useful direction to study from the base of knowledge supplied by this study is to fully incorporate failure predictions into the nonlinear response of FE models for whole structures. Several possible steps to reach this end are:

    1. Investigate the linear closed form solutions for facesheet wrinkling and core shear buckling and validate them with testing. New geometries, materials and/or test fixtures would be required to obtain these failures within the linear elastic response.

    2. Incorporate the closed form solutions into the FE models using the user defined failure criteria and validate them using the same linear tests from the first step.

3. Implement the valid linear predictions into non-linear models and validate with another round of testing. These tests would most likely also require another test fixture and must fail within the non-linear response (either through buckling, or in a bending test).

4. Scale the simple substructures tests and models up to full blade cross sections to obtain true structural interactions. From comparing these results to the simple substructures, the effects of structural interactions on failure can be determined.

REFERENCES CITED

1. Akkas N., Bauld Jr. N.R. (1971), Buckling an initial postbuckling behavior of clamped shallow spherical sandwich shells, *Journal of Applied Mechanics, ASME 39(3),* 163-171.

2. Allen H.G. (1969), *Analysis and Design of Structural Sandwich Panels*, Pergamon Press, Oxford, UK.

3. ANSYS. (Revision 5.5), *Engineering analysis system*. Houston, PA.

4. Bauld Jr. N.R. (1974), Imperfection sensitivity of axially compressed stringer reinforced cylindrical sandwich panels, *International Journal of Solids and Structures 10(8),* 883-902.

5. Bushnell D. (1981), Buckling of shells—pitfalls for designers. *AIAA Journal*, 19(9), 1183-1226.

6. Cairns D.S., Mandell J.F., McKittrick L.R., Rabern D., Combs, D.C., & VanLuchene R.D. (1999), Design/manufacturing synthesis of a composite blade for the AOC15/50 wind turbine. *AIAA, Aerospace Sciences Meeting and Exhibit, 37th, 1999 ASME Wind energy symposium,* Reno, NV, Jan 11-14 1999 (p. 58-65). AIAA Paper 99-0027.

7. Chamis C.C., Aiello R.A., Murthy P.L.N. (1988), Fiber composite sandwich thermostructural behavior: computational simulation, *Journal of Composite Technology and Research 10(3),* 93-99.

8. Chia C.Y. (1980), *Nonlinear analysis of plates*. McGraw-Hill, New York, NY.

9. Elspass W., Flemming M. (1990), Analysis of precision sandwich structures under thermal loading, *ICAS Proceedings 1990, 17th Congress of the International Council of Aeronaautical Science (ICAS-90-4.8.1),* Stockholm, Sweden, Sept. 9-14, 1990, Vol 2, 1513-1518.

10. Eppinga J. (2000), *Interim Mater's Thesis Work (to be published)*, Montana State University-Bozeman.

11. Gere J.M., Timoshenko S.P. (1984), *Mechanics of Materials (3rd Ed.),* PWS-KENT Publishing Co. Boston.

12. Hanagud S. , Chen H.P., Sriram P. (1985), A study of the static postbuckling behavior of composite sandwich plates, *Proceedings of the International Conference on Rotorcraft Basic Research,* Research Triangle Park, NC, Feb. 19-21, 1985, American Helicopter Society, Alexandria VA, 13.

13. Hedley, C.W., (1994) *Mold Filling Parameters in Resin Transfer Molding of Composites*. Masters Thesis, Montana State University-Bozeman, MT

14. Jones R.M. (1975), *Mechanics of Composite Materials*, Hemisphere Publishing Corporation, New York, NY.

15. Jeussette J-P., Laschet G. (1990), Pre- and postbuckling finite element analysis of curved composite and sandwich panels, *AIAA Journal 28(7),* 1233-1239.

16. Kanematsu H.H., Hirano Y., Iyama H. (1988), Bending and vibration of CFRP-faced rectangular sandwich plates, *Composite Structures 10(2),* 145-163.

17. Mandell J.F., & Samborsky D.D. (1997), *DOE/MSU composite material fatigue database: Test methods, materials, and analysis* (Contractor Report No. SAND97-3002). Albuquerque, NM: Sandia National Laboratiories.

18. McKittrick L.R., Cairns D.S., Mandell J.F., Combs D.C., Rabern D.A., & VanLuchene R.D. (1999), *Design of a composite blade for the AOC/50 wind turbine using a finite element model* (Interim Report). Albuquerque, NM: Sandia National Laboratiories

19. Monforton G.R., Ibrahim I.M. (1975), Analysis of sandwich plates with unbalanced cross-ply faces, *International Journal of Mechanical Science 19(6),* 335-343.

20. Mukhopadhyay A.K., Sierakowski R.L. (1990), On sandwich beams with laminate facings and honeycomb cores subjected to hygrothermal loads: Part I – Analysis, Part II – Application. *Journal of Composite Materials 24*, 382-418.

21. Noor A.K., Burton W.S., Bert C.W. (1996), Computational models for sandwich panels and shells *Applied Mechanics Review 49(3),* 155-199.

22. Noor A.K., Burton W.S., Peters J.M. (1994), Hierarchical adaptive modeling of structural sandwiches and multilayered composite panels, *Applied Numerical Mathematics 14*, 69-90.

23. Parida B.K., Prakash R.V., Ghosal A.K., Mangalgiri P.D., Vijayaruju K. (1997), Compression buckling behavior of laminated composite panels. *Composite Materials: Testing and Design, 13th Volume, ASTM STP 1242,* S.J. Hooper, Ed., American Society for Testing and Materials, 1997, 131-150.

24. Plantema F.J. (1966), *Sandwich construction: The bending and buckling of sandwich beams, plates and shells.* Wiley, New York, NY.

25. Schimdt R. (1976), Large deflections of multi-sandwich shells of arbitrary shape, *Journal of the Franklin Institute* 287(5), 423-437.

26. Sesto E., Ancona D.F. (1995), Present and prospective role of wind energy in electric supply. *International conference on new electricity (21st), Paris, France, May 22-24.*

27. Skramstad J.D. (1999), *Evaluation of hand lay-up and resin transfer molding in composite wind turbine blade manufacturing* Unpublished master's thesis, Montana State University-Bozeman, Bozeman MT.

28. Structural Sandwich Composites, *MIL-HDBK-23A* (Dec. 1968), Department of Defense, Washington D.C.

29. Sun B.H. (1992), *Buckling Problems of Sandwich Shells*, Delft Univ. Tech., Netherlands, LR-690.

30. Troshin V.P. (1986), Stress-strain state of three-layer cylindrical shells under the effect of axisymmetric loads, *Mechanics of Composite Materials* 22(3), 350-353.

31. Vinson J. (1987), Minimum weight solid core composite sandwich panels subjected to in-plane compressive loads. *Proceedings of the American Society for Composites (2nd tech. conf.), Newark DE, Sept. 23-25, 1987* Lancaster, PA, 329-337.

32. Wang S.S., Kuo A.Y. (1979), Nonlinear deformation and local buckling of deployable Kevlar fabric/polyurethane foam composites, Modern Developments in Composite Materials and Structures, Vinson J.R. (ed), ASME, 235-251.

33. Whitney J.M. (1987), *Structural analysis of laminated anisotropic plates.* Technomic, Lancaster, PA.

APPENDICES

```
FIXTURE SHELL DECK

/filnam,ctvrf_23m6


!*********************************************
!******************** parameters ********************
!*********************************************
cl=.0254*18
a=cl/2
r=0.0254*23
alpha=acos(a/r)
beta=((3.1415926/2)-alpha)*180/3.1415926
ar=1
gz=cl*ar-(.5*.0254)

ra=.0254*(0.25+(1/16)*(74/200))  !roller plus aluminum
addition with stiffness factor
ta1=.0254*.5                     !roller dia
ta2=.0254*.284                   !thickness at end for equal area-
stiffness calc of circle
taav=(ta1+ta2)/2
!ta1=taav
!ta2=taav


hc=3/8*.0254
iter=100
!*********************************************
!*********************************************

!******* fiber volume/thickness thang ************

!******* inputs, tt, nl **********
t=.5
tt=25.4*(t-.375)/2               !total (mm) lam thickness
(face sheet for symmetric sandwich)
rep1=0                                   !# of times
layup 1 occurs
rep2=1                                   !similiar
zeros=0                                  !# of zeros (not
counting layup 1&2 zeros)
fsl=rep1*3+rep2*3+zeros                  !# of layers (one
/ ply)
tave=tt/fsl                      !aver. ply th. , nl is # of
layers/plies
!*********************************

!********** pick a layup ***************
!* (45/0/45)=1, dd (0/45/0)=2, zeros=3 *

layup=2



*if,layup,eq,1,then
!******* (45/0/45) **********
n0=1*rep1 !# of zero plies/layers
n45=2*rep1           !# of 45's
a=0.000340           !a,b,c are coeff. of empirical poly fit
b=-0.03773
c=1.3642-tave
!*****************************

*elseif,layup,eq,2
!******** (0/45/0) **********
h=.5*.0254
ta130=(.0254*.125)/6

meshdiv=6
msize=gz/meshdiv
ms=msize/20

rp=hc/30
FC=-.0016
FC2=FC*2
FC3=FC*4
FC4=FC*8


T1=.1
TMIN=.05                         !time step vars
TMAX=.15
T2=.05
T2MIN=.01
T2MAX=.05
T3=.05
T3MIN=.01
T3MAX=.1
T4=.05
T4MIN=.01
T4MAX=.1

n0=2*rep2
n45=1*rep2
a=.000165
b=-0.0253
c=1.22-tave
!*****************************

*elseif,layup,eq,3
!******** zeros *************
n0=fsl
n45=0
a=.000361
b=-0.0441
c=1.701-tave
!*****************************

*else
a=0                  !in case of invalid layup #
b=0                  ! -should crash it
c=0
n0=0
n45=0

*endif
!*****************************************

!****** % fiber volume calc*****
!* the quadratic eqn. *
fv=(-b-sqrt(b*b-(4*a*c)))/(2*a)
!*********************************

!****** fiber fraction *********
!* f=tt45/tt0, empirical *
f=(2.847e-5*fv*fv*fv)-(2.306e-3*fv*fv)+(4.678e-
2*fv)+.5967
vf=fv/100
!*********************************

!***** ply thickness calcs ******
```

```
tmm0=tt/(n0+(f*n45))                    !from mm to m
tmm45=(tt-(n0*tmm0))/n45
tcheck=(tmm0*rep1+tmm45*rep1*2)+(tmm0*rep2*2+tmm4
5*rep2)+zeros*tmm0
t0=tmm0*.001
t45=tmm45*.001
!*********************************


!*** for a130, tt=.5, 03/b
!vf=.4

/prep7
!******* material props as function of vf ************
!*************************************************
*****
! a130's
mp,ex,1,(36.3e9)*(3.1+65.8*vf)/32.71
mp,ey,1,(8.76e9)*(1+0.836*vf)/((1-.836*vf)*2.206)
mp,ez,1,(8.76e9)*(1+0.836*vf)/((1-.836*vf)*2.206)
mp,prxy,1,.32*(.385-.15*vf)/0.318,
mp,pryz,1,.32*(.385-.15*vf)/0.318,
mp,prxz,1,.32*(.385-.15*vf)/0.318,
mp,gxy,1,3.48e9*(1+1.672*vf)/((1-.836*vf)*2.809)
mp,gyz,1,3.48e9*(1+1.672*vf)/((1-.836*vf)*2.809)
mp,gxz,1,3.48e9*(1+1.672*vf)/((1-.836*vf)*2.809)

tb,fail,1,1             !mat 1, 1 temp
tbtemp,,crit                    ! keys failure crit
tbdata,1,1,1                    ! max strain & stress
tbtemp,0                        ! 0 deg
        !max strain
tbdata,1,.0253,-.0092,.0039,-.0105,1,-1
tbdata,7,1,1,1
        !max stress
tbdata,10,868e6,-334e6,33.8e6,-93e6,3e6,-100e9
tbdata,16,87.1e6,100e9,100e9

!*  db120
mp,ex,2,(26.5e9)*(3.1+65.8*vf)/32.71
mp,ey,2,(7.52e9)*(1+0.836*vf)/((1-.836*vf)*2.206)
mp,ez,2,(7.52e9)*(1+0.836*vf)/((1-.836*vf)*2.206)
mp,prxy,2,.39*(.385-.15*vf)/0.318,
mp,pryz,2,.32*(.385-.15*vf)/0.318,
mp,prxz,2,.32*(.385-.15*vf)/0.318,
mp,gxy,2,4.12e9*(1+1.672*vf)/((1-.836*vf)*2.809)
mp,gyz,2,3.1e9*(1+1.672*vf)/((1-.836*vf)*2.809)
mp,gxz,2,3.1e9*(1+1.672*vf)/((1-.836*vf)*2.809)

tb,fail,2,1
tbtemp,,crit
tbdata,1,1,1
tbtemp,0
tbdata,1,.0249,-.0208,.0033,-.0121,1,-1
tbdata,7,1,1,1
tbdata,10,610e6,-551e6,24.9e6,-90.8e6,100e9,-100e9
tbdata,16,84.9e6,100e9,100e9,100e9


!*  balsa
MP,ex,3,1.48e8
MP,prxy,3,.3

tb,fail,3,1
tbtemp,,crit
tbdata,2,1
tbtemp,0
tbdata,10,100e9,,100e9,,100e9
tbdata,16,222e6,2.89e6,2.98e6

!* d155's
mp,ex,4,(37e9)*(3.1+65.8*vf)/32.71
mp,ey,4,(8.99e9)*(1+0.836*vf)/((1-.836*vf)*2.206)
mp,ez,4,(8.99e9)*(1+0.836*vf)/((1-.836*vf)*2.206)
mp,prxy,4,.31*(.385-.15*vf)/0.318
mp,pryz,4,.31*(.385-.15*vf)/0.318
mp,prxz,4,.31*(.385-.15*vf)/0.318
mp,gxy,4,4.1e9*(1+1.672*vf)/((1-.836*vf)*2.809)
mp,gyz,4,4.1e9*(1+1.672*vf)/((1-.836*vf)*2.809)
mp,gxz,4,4.1e9*(1+1.672*vf)/((1-.836*vf)*2.809)

tb,fail,4,1
tbtemp,,crit
tbdata,1,1,1
tbtemp,0
tbdata,1,.0283,-.0198,.004,-.0167,1,-1
tbdata,7,1,1,1
tbdata,10,986e6,-746e6,27.2e6,-129e6,100e9,
tbdata,16,94.2e6,100e9,100e9

!* steel (rollers)
uimp,5,ex,ey,ez,200e9,200e9,200e9
uimp,5,prxy,pryz,prxz,.3,.3,.3
!*************************************************
*****
finish


csys,1

/PREP7


!********** sandwich area thru kp ******
k,1,r,beta,0
k,2,r,-beta,0
k,3,r,-beta,gz
k,4,r,beta,gz

A,1,2,3,4

!*** steel rollers
k,5,r,-beta,-ra
k,6,r,beta,-ra
A,1,2,5,6
k,7,r,-beta,gz+ra
k,8,r,beta,gz+ra
A,4,3,7,8
!*********************************


ET,1,SHELL91
KEYOPT,1,9,1            !sandwich = 1
KEYOPT,1,6,1        !pr inter shear=1
KEYOPT,1,5,3        !pr positions
KEYOPT,1,8,1            !store for all (1) layers
KEYOPT,1,11,0       !node location (0=middle)
!*
KEYOPT,1,2,1

!*******define layers***********
R,1
RMODIF,1,1,9,0,
!*
```

```
!** defines according to theta, (or 90 deg off) ***
RMODIF,1,13,4,90,t0
RMODIF,1,19,2,45,t45/2
RMODIF,1,25,2,-45,t45/2
RMODIF,1,31,4,90,t0
RMODIF,1,37,3,90,hc
RMODIF,1,43,4,90,t0
RMODIF,1,49,2,-45,t45/2
rmodif,1,55,2,45,t45/2
rmodif,1,61,4,90,t0
rmodif,1,67,1,34,1
!*********************************

!** mesh att.*****
TYPE,1,
MAT,1,
REAL,1,
ESYS,0,

!********** mesh *****
ESIZE,gz/meshdiv,0

AMESH,1
!***********************

et,2,shell91
keyopt,2,2,1

r,2
r,2,1,1,0
rmodif,2,13,5,0,ta1,ta1,ta2,ta2

et,3,shell91
keyopt,3,2,1

type,2
mat,5
real,2
amesh,2
amesh,3


u_def,rp,0,0
allsel



/solu

!* output controls************
outres,NSOL,all
outres,RSOL,all

outres,nload,all
outres,misc,all

outres,strs,all
outres,epel,all
!*********************************

!************ DOF constraints *****
nsel,s,loc,z,-ra-ms,-ra+ms
D,ALL,UX,0
D,ALL,UZ,0

nsel,s,loc,y,-beta-beta/40,-beta+beta/40
D,ALL,UX,0

nsel,s,loc,z,gz+ra-ms,gz+ra+ms
D,ALL,UX,0

nsel,s,loc,y,beta-beta/40,beta+beta/40
D,ALL,UX,0


nsel,r,loc,z,-ra-ms,-ra+ms
d,all,uy,0
allsel



nsel,s,loc,z,gz+ra-ms,gz+ra+ms
D,ALL,UX,0
!**** load *****
D,ALL,UZ,FC
!*************************************
allsel

!*******loadstep 1*****
LNSRCH,ON
NLGEOM,ON
NROPT,AUTO, ,
LUMPM,0
EQSLV,FRONT,1e-08,0,
SSTIF
PSTRES
TOFFST,0,

NEQIT,iter
TIME,
AUTOTS,1
DELTIM,T1,TMIN,TMAX,0
KBC,0
!*****************************

LSWRITE,

!**** load step 2 *****
nsel,s,loc,z,gz+ra-ms,gz+ra+ms
D,ALL,UZ,FC2
allsel

TIME,
DELTIM,T2,T2MIN,T2MAX,0
!*****************************

LSWRITE,

!**** load step 3 *****
nsel,s,loc,z,gz+ra-ms,gz+ra+ms
D,ALL,UZ,FC3
allsel

TIME,
DELTIM,T3,T3MIN,T3MAX,0
!*****************************

LSWRITE,

!**** load step 4 *****
nsel,s,loc,z,gz+ra-ms,gz+ra+ms
D,ALL,UZ,FC4
allsel
```

```
TIME,
DELTIM,T4,T4MIN,T4MAX,0
!*****************************

LSWRITE,
!lssolve,1,4,1


save



!******* analysis helpers
************************************
!********** d155's ****************
exd=(37e9)*(3.1+65.8*vf)/32.71
prd=0.31*(.385-.15*vf)/0.318
eyd=(8.99e9)*(1+0.836*vf)/((1-.836*vf)*2.206)
prdsq=prd*prd*eyd/exd
q12d=prd*eyd/(1-prdsq)
!************************************

!************ db120's **************
ex45=(26.5e9)*(3.1+65.8*vf)/32.71
ey45=(7.52e9)*(1+0.836*vf)/((1-.836*vf)*2.206)
pr45=0.39*(.385-.15*vf)/0.318
g45=4.12e9*(1+1.672*vf)/((1-.836*vf)*2.809)

prsq=pr45*pr45*ey45/ex45
q11=ex45/(1-prsq)
q12=pr45*ey45/(1-prsq)
q22=ey45/(1-prsq)
q66=g45

cs45=.7071*.7071*.7071*.7071
q11b=(q11*cs45)+(2*(q12+2*q66)*cs45)+(q22*cs45)
q12b=(q11+q22-4*q66)*cs45+(q12*2*cs45)
q22b=q11b
q66b=(q11+q22-2*q12-2*q66)*cs45+(q66*2*cs45)
!************************************

!*** face sheet elastic constants ***
a11=2*((q11b*n45*t45)+(exd*n0*t0))
a12=2*((q12b*n45*t45)+(q12d*n0*t0))
!****************************************
!*************************************************
**************
```

```
IDEAL SUPPORT CONDITION DECK

/filnam,pertconv_hc1000


!*************************************************
!****************** parameters ******************
!*************************************************
cl=.0254*18
a=cl/2
r=0.0254*1e5
alpha=acos(a/r)
beta=((3.1415926/2)-alpha)*180/3.1415926
ar=1
gz=cl*ar

ra=.0254*(0.25+(1/16)*(74/200))  !roller plus aluminum
addition with stiffness factor
ta1=.0254*.5                                  !roller dia
ta2=.0254*.284              !thickness at end for equal area-
stiffness calc of circle
taav=(ta1+ta2)/2
!ta1=taav
!ta2=taav


hc=3/8*.0254
h=.5*.0254
ta130=(.0254*.125)/6

meshdiv=12
msize=gz/meshdiv
ms=msize/20

rp=hc/1000
FC=-.0008
FC2=FC*2.5
FC3=FC*5
FC4=FC*10

T1=.1
TMIN=.05                      !time step vars
TMAX=.1
T2=.05
T2MIN=.01
T2MAX=.05
T3=.05
T3MIN=.01
T3MAX=.1
T4=.05
T4MIN=.01
T4MAX=.1

iter=100
!*************************************************
!*************************************************

!******* fiber volume/thickness thang ************

!******* inputs, tt, nl **********
t=.5
tt=25.4*(t-.375)/2            !total (mm) lam thickness
(face sheet for symmetric sandwich)
rep1=0                                        !# of times
layup 1 occurs
rep2=1                                        !similiar
zeros=0                                       !# of zeros (not
counting layup 1&2 zeros)
fsl=rep1*3+rep2*3+zeros                       !# of layers (one
/ ply)
tave=tt/fsl                   !aver. ply th. , nl is # of
layers/plies
!*********************************

!********** pick a layup ***************
!* (45/0/45)=1, dd (0/45/0)=2, zeros=3 *

layup=2



*if,layup,eq,1,then
!******* (45/0/45) **********
n0=1*rep1 !# of zero plies/layers
n45=2*rep1          !# of 45's
a=0.000340          !a,b,c are coeff. of empirical poly fit
b=-0.03773
c=1.3642-tave
!*****************************

*elseif,layup,eq,2
!******** (0/45/0) **********
n0=2*rep2
n45=1*rep2
a=.000165
b=-0.0253
c=1.22-tave
!*****************************

*elseif,layup,eq,3
!******** zeros *************
n0=fsl
n45=0
a=.000361
b=-0.0441
c=1.701-tave
!*****************************

*else
a=0                 !in case of invalid layup #
b=0                 ! -should crash it
c=0
n0=0
n45=0

*endif
!*****************************************

!****** % fiber volume calc*****
!* the quadratic eqn. *
fv=(-b-sqrt(b*b-(4*a*c)))/(2*a)
!*********************************

!****** fiber fraction *********
!* f=tt45/tt0, empirical *
f=(2.847e-5*fv*fv*fv)-(2.306e-3*fv*fv)+(4.678e-
2*fv)+.5967
vf=fv/100
!*********************************

!***** ply thickness calcs ******
tmm0=tt/(n0+(f*n45))                  !from mm to m
tmm45=(tt-(n0*tmm0))/n45
```

```
tcheck=(tmm0*rep1+tmm45*rep1*2)+(tmm0*rep2*2+tmm4
5*rep2)+zeros*tmm0
t0=tmm0*.001
t45=tmm45*.001
!*********************************


!*** for a130, tt=.5, 03/b

!vf=.4

/prep7
!******* material props as function of vf ************
!************************************************
*****
! a130's
mp,ex,1,(36.3e9)*(3.1+65.8*vf)/32.71
mp,ey,1,(8.76e9)*(1+0.836*vf)/((1-.836*vf)*2.206)
mp,ez,1,(8.76e9)*(1+0.836*vf)/((1-.836*vf)*2.206)
mp,prxy,1,.32*(.385-.15*vf)/0.318,
mp,pryz,1,.32*(.385-.15*vf)/0.318,
mp,prxz,1,.32*(.385-.15*vf)/0.318,
mp,gxy,1,3.48e9*(1+1.672*vf)/((1-.836*vf)*2.809)
mp,gyz,1,3.48e9*(1+1.672*vf)/((1-.836*vf)*2.809)
mp,gxz,1,3.48e9*(1+1.672*vf)/((1-.836*vf)*2.809)

tb,fail,1,1                !mat 1, 1 temp
tbtemp,,crit                        ! keys failure crit
tbdata,1,1,1                        ! max strain & stress
tbtemp,0                            ! 0 deg
            !max strain
tbdata,1,.0253,-.0092,.0039,-.0105,1,-1
tbdata,7,1,1,1
            !max stress
tbdata,10,868e6,-334e6,33.8e6,-93e6,3e6,-100e9
tbdata,16,87.1e6,100e9,100e9

!*  db120
mp,ex,2,(26.5e9)*(3.1+65.8*vf)/32.71
mp,ey,2,(7.52e9)*(1+0.836*vf)/((1-.836*vf)*2.206)
mp,ez,2,(7.52e9)*(1+0.836*vf)/((1-.836*vf)*2.206)
mp,prxy,2,.39*(.385-.15*vf)/0.318,
mp,pryz,2,.32*(.385-.15*vf)/0.318,
mp,prxz,2,.32*(.385-.15*vf)/0.318,
mp,gxy,2,4.12e9*(1+1.672*vf)/((1-.836*vf)*2.809)
mp,gyz,2,3.1e9*(1+1.672*vf)/((1-.836*vf)*2.809)
mp,gxz,2,3.1e9*(1+1.672*vf)/((1-.836*vf)*2.809)

tb,fail,2,1
tbtemp,,crit
tbdata,1,1,1
tbtemp,0
tbdata,1,.0249,-.0208,.0033,-.0121,1,-1
tbdata,7,1,1,1
tbdata,10,610e6,-551e6,24.9e6,-90.8e6,100e9,-100e9
tbdata,16,84.9e6,100e9,100e9


!*  balsa
MP,ex,3,1.48e8
MP,prxy,3,.3

tb,fail,3,1
tbtemp,,crit
tbdata,2,1
tbtemp,0
tbdata,10,100e9,,100e9,,100e9
tbdata,16,222e6,2.89e6,2.98e6

!* d155's
mp,ex,4,(37e9)*(3.1+65.8*vf)/32.71
mp,ey,4,(8.99e9)*(1+0.836*vf)/((1-.836*vf)*2.206)
mp,ez,4,(8.99e9)*(1+0.836*vf)/((1-.836*vf)*2.206)
mp,prxy,4,.31*(.385-.15*vf)/0.318
mp,pryz,4,.31*(.385-.15*vf)/0.318
mp,prxz,4,.31*(.385-.15*vf)/0.318
mp,gxy,4,4.1e9*(1+1.672*vf)/((1-.836*vf)*2.809)
mp,gyz,4,4.1e9*(1+1.672*vf)/((1-.836*vf)*2.809)
mp,gxz,4,4.1e9*(1+1.672*vf)/((1-.836*vf)*2.809)

tb,fail,4,1
tbtemp,,crit
tbdata,1,1,1
tbtemp,0
tbdata,1,.0283,-.0198,.004,-.0167,1,-1
tbdata,7,1,1,1
tbdata,10,986e6,-746e6,27.2e6,-129e6,100e9,
tbdata,16,94.2e6,100e9,100e9

!* steel (rollers)
uimp,5,ex,ey,ez,200e9,200e9,200e9
uimp,5,prxy,pryz,prxz,.3,.3,.3
!************************************************
*****
finish


csys,1

/PREP7


!********** sandwich area thru kp ******
k,1,r,beta,0
k,2,r,-beta,0
k,3,r,-beta,gz
k,4,r,beta,gz

A,1,2,3,4


ET,1,SHELL91
KEYOPT,1,9,1                !sandwich = 1
KEYOPT,1,6,1          !pr inter shear=1
KEYOPT,1,5,3          !pr positions
KEYOPT,1,8,1                !store for all (1) layers
KEYOPT,1,11,0          !node location (0=middle)
!*
KEYOPT,1,2,1

!*******define layers***********
R,1
RMODIF,1,1,9,0,
!*
!** defines according to theta, (or 90 deg off) ***
RMODIF,1,13,4,90,t0
RMODIF,1,19,2,45,t45/2
RMODIF,1,25,2,-45,t45/2
RMODIF,1,31,4,90,t0
RMODIF,1,37,3,90,hc
RMODIF,1,43,4,90,t0
RMODIF,1,49,2,-45,t45/2
rmodif,1,55,2,45,t45/2
rmodif,1,61,4,90,t0
```

```
rmodif,1,67,1,34,1
!*********************************

!** mesh att.*****
TYPE,1,
MAT,1,
REAL,1,
ESYS,0,

!*********** mesh *****
ESIZE,gz/meshdiv,0

AMESH,1
!**********************

nsel,s,loc,z,0.00001,gz-0.00001
u_def,rp,0,0
allsel

/solu

!* output controls************
outres,NSOL,all
outres,RSOL,all

outres,nload,all
outres,misc,all

outres,strs,all
outres,epel,all
!*******************************

!************ DOF constraints *****
nsel,s,loc,z,-ms,+ms
D,ALL,UX,0
D,ALL,UZ,0

nsel,s,loc,y,-beta-beta/40,-beta+beta/40
D,ALL,UX,0

nsel,s,loc,z,gz-ms,gz+ms
D,ALL,UX,0

nsel,s,loc,y,beta-beta/40,beta+beta/40
D,ALL,UX,0

nsel,r,loc,z,-ms,+ms
d,all,uy,0
allsel


nsel,s,loc,z,gz-ms,gz+ms
D,ALL,UX,0
!**** load *****
D,ALL,UZ,FC
!*************************************
allsel

!*******loadstep 1*****
LNSRCH,ON
NLGEOM,ON
NROPT,AUTO, ,
LUMPM,0
EQSLV,FRONT,1e-08,0,
SSTIF
PSTRES
TOFFST,0,

NEQIT,iter
TIME,
AUTOTS,1
DELTIM,T1,TMIN,TMAX,0
KBC,0
!*****************************

LSWRITE,

!**** load step 2 *****
nsel,s,loc,z,gz-ms,gz+ms
D,ALL,UZ,FC2
allsel

TIME,
DELTIM,T2,T2MIN,T2MAX,0
!*****************************

LSWRITE,

!**** load step 3 *****
nsel,s,loc,z,gz-ms,gz+ms
D,ALL,UZ,FC3
allsel

TIME,
DELTIM,T3,T3MIN,T3MAX,0
!*****************************

LSWRITE,

!**** load step 4 *****
nsel,s,loc,z,gz-ms,gz+ms
D,ALL,UZ,FC4
allsel

TIME,
DELTIM,T4,T4MIN,T4MAX,0
!*****************************

LSWRITE,
!lssolve,1,2,1


save



!******* analysis helpers
************************************
!*********** d155's ****************
exd=(37e9)*(3.1+65.8*vf)/32.71
prd=0.31*(.385-.15*vf)/0.318
eyd=(8.99e9)*(1+0.836*vf)/((1-.836*vf)*2.206)
prdsq=prd*prd*eyd/exd
q12d=prd*eyd/(1-prdsq)
!************************************

!************ db120's **************
ex45=(26.5e9)*(3.1+65.8*vf)/32.71
ey45=(7.52e9)*(1+0.836*vf)/((1-.836*vf)*2.206)
pr45=0.39*(.385-.15*vf)/0.318
g45=4.12e9*(1+1.672*vf)/((1-.836*vf)*2.809)

prsq=pr45*pr45*ey45/ex45
```

```
q11=ex45/(1-prsq)
q12=pr45*ey45/(1-prsq)
q22=ey45/(1-prsq)
q66=g45

cs45=.7071*.7071*.7071*.7071
q11b=(q11*cs45)+(2*(q12+2*q66)*cs45)+(q22*cs45)
q12b=(q11+q22-4*q66)*cs45+(q12*2*cs45)
q22b=q11b
q66b=(q11+q22-2*q12-2*q66)*cs45+(q66*2*cs45)
!************************************

!*** face sheet elastic constants ***
a11=2*((q11b*n45*t45)+(exd*n0*t0))
a12=2*((q12b*n45*t45)+(q12d*n0*t0))
!************************************
!*************************************************
**************
```

```
LINEAR STABILITY SHELL DECK (EIGEN BUCKLING)

/filnam,cross_eigen


!*********************************************
!****************** parameters ******************
!*********************************************
cl=.0254*18
a=cl/2
r=0.0254*1e5
alpha=acos(a/r)
beta=((3.1415926/2)-alpha)*180/3.1415926
ar=1
gz=cl*ar-(.5*.0254)

ra=.0254*(0.25+(1/16)*(74/200))  !roller plus aluminum
addition with stiffness factor
ta1=.0254*.5                                  !roller dia
ta2=.0254*.284                !thickness at end for equal area-
stiffness calc of circle
taav=(ta1+ta2)/2
!ta1=taav
!ta2=taav


hc=3/8*.0254
h=.5*.0254
ta130=(.0254*.125)/6

meshdiv=12
msize=gz/meshdiv
ms=msize/20

rp=hc/50
FC=-.0001
FC2=FC*2
FC3=FC*4
FC4=FC*8


T1=.1
TMIN=.05                      !time step vars
TMAX=.15
T2=.05
T2MIN=.01
T2MAX=.05
T3=.05
T3MIN=.01
T3MAX=.1
T4=.05
T4MIN=.01
T4MAX=.1

iter=100
!*********************************************
!*********************************************

!******* fiber volume/thickness thang ***********

!******* inputs, tt, nl **********
t=.5
tt=25.4*(t-.375)/2            !total (mm) lam thickness
(face sheet for symmetric sandwich)
rep1=0                                        !# of times
layup 1 occurs
rep2=1                                        !similiar
zeros=0                                       !# of zeros (not
counting layup 1&2 zeros)
fsl=rep1*3+rep2*3+zeros                       !# of layers (one
/ ply)
tave=tt/fsl                   !aver. ply th. , nl is # of
layers/plies
!*********************************

!********** pick a layup ***************
!* (45/0/45)=1, dd (0/45/0)=2, zeros=3 *

layup=3



*if,layup,eq,1,then
!******* (45/0/45) **********
n0=1*rep1 !# of zero plies/layers
n45=2*rep1          !# of 45's
a=0.000340          !a,b,c are coeff. of empirical poly fit
b=-0.03773
c=1.3642-tave
!*****************************

*elseif,layup,eq,2
!******** (0/45/0) **********
n0=2*rep2
n45=1*rep2
a=.000165
b=-0.0253
c=1.22-tave
!*****************************

*elseif,layup,eq,3
!******** zeros *************
n0=fsl
n45=0
a=.000361
b=-0.0441
c=1.701-tave
!*****************************

*else
a=0                   !in case of invalid layup #
b=0                   ! -should crash it
c=0
n0=0
n45=0

*endif
!*****************************************

!****** % fiber volume calc*****
!* the quadratic eqn. *
fv=(-b-sqrt(b*b-(4*a*c)))/(2*a)
!*********************************

!****** fiber fraction *********
!* f=tt45/tt0, empirical *
f=(2.847e-5*fv*fv*fv)-(2.306e-3*fv*fv)+(4.678e-
2*fv)+.5967
vf=fv/100
!*********************************

!***** ply thickness calcs ******
tmm0=tt/(n0+(f*n45))                          !from mm to m
tmm45=(tt-(n0*tmm0))/n45
```

```
tcheck=(tmm0*rep1+tmm45*rep1*2)+(tmm0*rep2*2+tmm4
5*rep2)+zeros*tmm0
t0=tmm0*.001
t45=tmm45*.001
!*********************************


!*** for a130, tt=.5, 03/b
!vf=.4

/prep7
!******* material props as function of vf ***********
!************************************************
*****
! a130's
mp,ex,1,(36.3e9)*(3.1+65.8*vf)/32.71
mp,ey,1,(8.76e9)*(1+0.836*vf)/((1-.836*vf)*2.206)
mp,ez,1,(8.76e9)*(1+0.836*vf)/((1-.836*vf)*2.206)
mp,prxy,1,.32*(.385-.15*vf)/0.318,
mp,pryz,1,.32*(.385-.15*vf)/0.318,
mp,prxz,1,.32*(.385-.15*vf)/0.318,
mp,gxy,1,3.48e9*(1+1.672*vf)/((1-.836*vf)*2.809)
mp,gyz,1,3.48e9*(1+1.672*vf)/((1-.836*vf)*2.809)
mp,gxz,1,3.48e9*(1+1.672*vf)/((1-.836*vf)*2.809)

tb,fail,1,1             !mat 1, 1 temp
tbtemp,,crit                    ! keys failure crit
tbdata,1,1,1                    ! max strain & stress
tbtemp,0                        ! 0 deg
        !max strain
tbdata,1,.0253,-.0092,.0039,-.0105,1,-1
tbdata,7,1,1,1
        !max stress
tbdata,10,868e6,-334e6,33.8e6,-93e6,3e6,-100e9
tbdata,16,87.1e6,100e9,100e9

!*  db120
mp,ex,2,(26.5e9)*(3.1+65.8*vf)/32.71
mp,ey,2,(7.52e9)*(1+0.836*vf)/((1-.836*vf)*2.206)
mp,ez,2,(7.52e9)*(1+0.836*vf)/((1-.836*vf)*2.206)
mp,prxy,2,.39*(.385-.15*vf)/0.318,
mp,pryz,2,.32*(.385-.15*vf)/0.318,
mp,prxz,2,.32*(.385-.15*vf)/0.318,
mp,gxy,2,4.12e9*(1+1.672*vf)/((1-.836*vf)*2.809)
mp,gyz,2,3.1e9*(1+1.672*vf)/((1-.836*vf)*2.809)
mp,gxz,2,3.1e9*(1+1.672*vf)/((1-.836*vf)*2.809)

tb,fail,2,1
tbtemp,,crit
tbdata,1,1,1
tbtemp,0
tbdata,1,.0249,-.0208,.0033,-.0121,1,-1
tbdata,7,1,1,1
tbdata,10,610e6,-551e6,24.9e6,-90.8e6,100e9,-100e9
tbdata,16,84.9e6,100e9,100e9


!*  balsa
MP,ex,3,1.48e8
MP,prxy,3,.3

tb,fail,3,1
tbtemp,,crit
tbdata,2,1
tbtemp,0
tbdata,10,100e9,,100e9,,100e9
tbdata,16,222e6,2.89e6,2.98e6

!* d155's
mp,ex,4,(37e9)*(3.1+65.8*vf)/32.71
mp,ey,4,(8.99e9)*(1+0.836*vf)/((1-.836*vf)*2.206)
mp,ez,4,(8.99e9)*(1+0.836*vf)/((1-.836*vf)*2.206)
mp,prxy,4,.31*(.385-.15*vf)/0.318
mp,pryz,4,.31*(.385-.15*vf)/0.318
mp,prxz,4,.31*(.385-.15*vf)/0.318
mp,gxy,4,4.1e9*(1+1.672*vf)/((1-.836*vf)*2.809)
mp,gyz,4,4.1e9*(1+1.672*vf)/((1-.836*vf)*2.809)
mp,gxz,4,4.1e9*(1+1.672*vf)/((1-.836*vf)*2.809)

tb,fail,4,1
tbtemp,,crit
tbdata,1,1,1
tbtemp,0
tbdata,1,.0283,-.0198,.004,-.0167,1,-1
tbdata,7,1,1,1
tbdata,10,986e6,-746e6,27.2e6,-129e6,100e9,
tbdata,16,94.2e6,100e9,100e9

!* steel (rollers)
uimp,5,ex,ey,ez,200e9,200e9,200e9
uimp,5,prxy,pryz,prxz,.3,.3,.3
!************************************************
*****
finish


csys,1

/PREP7


!********** sandwich area thru kp ******
k,1,r,beta,0
k,2,r,-beta,0
k,3,r,-beta,gz
k,4,r,beta,gz

A,1,2,3,4

!*** steel rollers
k,5,r,-beta,-ra
k,6,r,beta,-ra
A,1,2,5,6
k,7,r,-beta,gz+ra
k,8,r,beta,gz+ra
A,4,3,7,8
!*********************************


ET,1,SHELL91
KEYOPT,1,9,1            !sandwich = 1
KEYOPT,1,6,1        !pr inter shear=1
KEYOPT,1,5,3        !pr positions
KEYOPT,1,8,1            !store for all (1) layers
KEYOPT,1,11,0       !node location (0=middle)
!*
KEYOPT,1,2,1

!*******define layers***********
R,1
RMODIF,1,1,7,0,
!*
!** defines according to theta, (or 90 deg off) ***
RMODIF,1,13,4,0,t0
```

```
RMODIF,1,19,4,90,t0
RMODIF,1,25,4,0,t0
RMODIF,1,31,3,90,hc
RMODIF,1,37,4,0,t0
rmodif,1,43,4,90,t0
rmodif,1,49,4,0,t0
rmodif,1,55,1,34,1
!*********************************

!** mesh att.*****
TYPE,1,
MAT,1,
REAL,1,
ESYS,0,

!********** mesh *****
ESIZE,gz/meshdiv,0

AMESH,1
!***********************

et,2,shell91
keyopt,2,2,1

r,2
r,2,1,1,0
rmodif,2,13,5,0,ta1,ta1,ta2,ta2

et,3,shell91
keyopt,3,2,1

type,2
mat,5
real,2
amesh,2
amesh,3


!u_def,rp,0,0
allsel



/solu

!* output controls************
outres,NSOL,all
outres,RSOL,all

outres,nload,all
outres,misc,all

outres,strs,all
outres,epel,all
!*******************************

!************ DOF constraints *****
nsel,s,loc,z,-ra-ms,-ra+ms
D,ALL,UX,0
D,ALL,UZ,0

nsel,s,loc,y,-beta-beta/40,-beta+beta/40
D,ALL,UX,0

nsel,s,loc,z,gz+ra-ms,gz+ra+ms
D,ALL,UX,0

nsel,s,loc,y,beta-beta/40,beta+beta/40
D,ALL,UX,0


nsel,r,loc,z,-ra-ms,-ra+ms
d,all,uy,0
allsel



nsel,s,loc,z,gz+ra-ms,gz+ra+ms
D,ALL,UX,0
!**** load *****
D,ALL,UZ,FC
!*************************************
allsel


!****** static solution ***
NLGEOM,0
NROPT,AUTO, ,
LUMPM,0
EQSLV,FRONT,1e-08,0,
PSTRES,ON
TOFFST,0,
!*
! /STAT,SOLU
SOLVE
!*
!*
!*
FINISH

!***** eigenbuckling soln********
/solu
ANTYPE,1
!*
!*
BUCOPT,SUBSP,8,0,0
!*
SUBOPT,0,0,0,0,0,ALL
! /STAT,SOLU
SOLVE


!* output controls************
outres,all,all



save



!******* analysis helpers
************************************
!*********** d155's ****************
exd=(37e9)*(3.1+65.8*vf)/32.71
prd=0.31*(.385-.15*vf)/0.318
eyd=(8.99e9)*(1+0.836*vf)/((1-.836*vf)*2.206)
prdsq=prd*prd*eyd/exd
q12d=prd*eyd/(1-prdsq)
!************************************

!************ db120's **************
ex45=(26.5e9)*(3.1+65.8*vf)/32.71
```

```
ey45=(7.52e9)*(1+0.836*vf)/((1-.836*vf)*2.206)
pr45=0.39*(.385-.15*vf)/0.318
g45=4.12e9*(1+1.672*vf)/((1-.836*vf)*2.809)

prsq=pr45*pr45*ey45/ex45
q11=ex45/(1-prsq)
q12=pr45*ey45/(1-prsq)
q22=ey45/(1-prsq)
q66=g45

cs45=.7071*.7071*.7071*.7071
q11b=(q11*cs45)+(2*(q12+2*q66)*cs45)+(q22*cs45)
q12b=(q11+q22-4*q66)*cs45+(q12*2*cs45)
q22b=q11b
q66b=(q11+q22-2*q12-2*q66)*cs45+(q66*2*cs45)
!************************************

!*** face sheet elastic constants ***
a11=2*((q11b*n45*t45)+(exd*n0/3*t0)+(eyd*2/3*n0*t0))
a22=2*((q11b*n45*t45)+(eyd*n0/3*t0)+(exd*2/3*n0*t0))
a12=2*((q12b*n45*t45)+(q12d*n0*t0))
!************************************
!************************************************
**********
```

```
MIXED ELEMENT MODEL DECK (SHELL
FACESHEETS, SOLID BRICK CORE)

/filnam,ctmixcpe



!*************************************************
!****************** parameters ******************
!*************************************************
cl=.0254*18
a=cl/2
r=0.0254*23
alpha=acos(a/r)
beta=((3.1415926/2)-alpha)*180/3.1415926
ar=1
gz=cl*ar

hc=0.0254*.375

FC=-.00001

meshdiv=12
msize=hc/2
ms=msize/4

!*************************************************
!*************************************************

!******* fiber volume/thickness thang ************

!******* inputs, tt, nl **********
t=.5
tt=25.4*(.5-.375)/2                !total (mm) lam thickness
(face sheet for symmetric sandwich)
rep1=0                                        !# of times
layup 1 occurs
rep2=1                                        !similiar
zeros=0                                       !# of zeros (not
counting layup 1&2 zeros)
fsl=rep1*3+rep2*3+zeros                       !# of layers (one
/ ply)
tave=tt/fsl                        !aver. ply th. , nl is # of
layers/plies
!*********************************

!********** pick a layup ***************
!* (45/0/45)=1, dd (0/45/0)=2, zeros=3 *

layup=2



*if,layup,eq,1,then
!******* (45/0/45) **********
n0=1*rep1 !# of zero plies/layers
n45=2*rep1              !# of 45's
a=0.000340              !a,b,c are coeff. of empirical poly fit
b=-0.03773
c=1.3642-tave
!*****************************

*elseif,layup,eq,2
!******** (0/45/0) **********
n0=2*rep2
n45=1*rep2
a=.000165
b=-0.0253
c=1.22-tave
!*****************************

*elseif,layup,eq,3
!******** zeros *************
n0=fsl
n45=0
a=.000361
b=-0.0441
c=1.701-tave
!*****************************

*else
a=0                     !in case of invalid layup #
b=0                     ! -should crash it
c=0
n0=0
n45=0

*endif
!***************************************

!****** % fiber volume calc*****
!* the quadratic eqn. *
fv=(-b-sqrt(b*b-(4*a*c)))/(2*a)
!*********************************

!****** fiber fraction **********
!* f=tt45/tt0, empirical *
f=(2.847e-5*fv*fv*fv)-(2.306e-3*fv*fv)+(4.678e-
2*fv)+.5967
vf=fv/100
!*********************************

!***** ply thickness calcs ******
tmm0=tt/(n0+(f*n45))                          !from mm to m
tmm45=(tt-(n0*tmm0))/n45
tcheck=(tmm0*rep1+tmm45*rep1*2)+(tmm0*rep2*2+tmm4
5*rep2)+zeros*tmm0
t0=tmm0*.001
t45=tmm45*.001
!*********************************

/prep7
!******* material props as function of vf ************
!*************************************************
*****
! a130's
mp,ex,1,(36.3e9)*(3.1+65.8*vf)/32.71
mp,ey,1,(8.76e9)*(1+0.836*vf)/((1-.836*vf)*2.206)
mp,ez,1,(8.76e9)*(1+0.836*vf)/((1-.836*vf)*2.206)
mp,prxy,1,.32*(.385-.15*vf)/0.318,
mp,pryz,1,.32*(.385-.15*vf)/0.318,
mp,prxz,1,.32*(.385-.15*vf)/0.318,
mp,gxy,1,3.48e9*(1+1.672*vf)/((1-.836*vf)*2.809)
mp,gyz,1,3.48e9*(1+1.672*vf)/((1-.836*vf)*2.809)
mp,gxz,1,3.48e9*(1+1.672*vf)/((1-.836*vf)*2.809)

tb,fail,1,1             !mat 1, 1 temp
tbtemp,,crit                    ! keys failure crit
tbdata,1,1,1                    ! max strain & stress
tbtemp,0                        ! 0 deg
        !max strain
tbdata,1,.0253,-.0092,.0039,-.0105,1,-1
tbdata,7,1,1,1
        !max stress
```

```
tbdata,10,868e6,-334e6,33.8e6,-93e6,3e6,-100e9
tbdata,16,87.1e6,100e9,100e9

!*  db120
mp,ex,2,(26.5e9)*(3.1+65.8*vf)/32.71
mp,ey,2,(7.52e9)*(1+0.836*vf)/((1-.836*vf)*2.206)
mp,ez,2,(7.52e9)*(1+0.836*vf)/((1-.836*vf)*2.206)
mp,prxy,2,.39*(.385-.15*vf)/0.318,
mp,pryz,2,.32*(.385-.15*vf)/0.318,
mp,prxz,2,.32*(.385-.15*vf)/0.318,
mp,gxy,2,4.12e9*(1+1.672*vf)/((1-.836*vf)*2.809)
mp,gyz,2,3.1e9*(1+1.672*vf)/((1-.836*vf)*2.809)
mp,gxz,2,3.1e9*(1+1.672*vf)/((1-.836*vf)*2.809)

tb,fail,2,1
tbtemp,,crit
tbdata,1,1,1
tbtemp,0
tbdata,1,.0249,-.0208,.0033,-.0121,1,-1
tbdata,7,1,1,1
tbdata,10,610e6,-551e6,24.9e6,-90.8e6,100e9,-100e9
tbdata,16,84.9e6,100e9,100e9

!*  balsa
UIMP,3,EX,EY,EZ,.187e9,.061e9,4.07e9,
UIMP,3,DENS, , ,.153,
UIMP,3,ALPX,ALPY,ALPZ,,,,
UIMP,3,REFT, , , ,
UIMP,3,PRXY,PRYZ,PRXZ,.67,.01,.02,
UIMP,3,NUXY,NUYZ,NUXZ,,,,
UIMP,3,GXY,GYZ,GXZ,.0203e9,.150e9,.220e9,

tb,fail,3,1
tbtemp,,crit
tbdata,2,1
tbtemp,0
tbdata,10,100e9,,100e9,,100e9
tbdata,16,222e6,2.89e6,2.98e6

!* d155's
mp,ex,4,(37e9)*(3.1+65.8*vf)/32.71
mp,ey,4,(8.99e9)*(1+0.836*vf)/((1-.836*vf)*2.206)
mp,ez,4,(8.99e9)*(1+0.836*vf)/((1-.836*vf)*2.206)
mp,prxy,4,.31*(.385-.15*vf)/0.318
mp,pryz,4,.31*(.385-.15*vf)/0.318
mp,prxz,4,.31*(.385-.15*vf)/0.318
mp,gxy,4,4.1e9*(1+1.672*vf)/((1-.836*vf)*2.809)
mp,gyz,4,4.1e9*(1+1.672*vf)/((1-.836*vf)*2.809)
mp,gxz,4,4.1e9*(1+1.672*vf)/((1-.836*vf)*2.809)

tb,fail,4,1
tbtemp,,crit
tbdata,1,1,1
tbtemp,0
tbdata,1,.0283,-.0198,.004,-.0167,1,-1
tbdata,7,1,1,1
tbdata,10,986e6,-746e6,27.2e6,-129e6,100e9,
tbdata,16,94.2e6,100e9,100e9

!* rigidium
uimp,5,ex,ey,ez,200e9,200e9,200e9
uimp,5,prxy,pryz,prxz,.3,.3,.3
uimp,5,gxy,gyz,gxz,200e9,200e9,200e9
!*************************************************
*****
finish
```

```
csys,1

/PREP7


!********** area thru kp ******
k,1,r-(hc/2),beta,0
k,2,r-(hc/2),-beta,0
k,3,r-(hc/2),-beta,gz
k,4,r-(hc/2),beta,gz

k,5,r+(hc/2),beta,0
k,6,r+(hc/2),-beta,0
k,7,r+(hc/2),-beta,gz
k,8,r+(hc/2),beta,gz

v,1,2,3,4,5,6,7,8

!*******************************


ET,1,SHELL91
KEYOPT,1,9,0          !sandwich = 1
KEYOPT,1,6,1        !pr inter shear=1
KEYOPT,1,5,3        !pr positions
KEYOPT,1,8,1          !store for all (1) layers
KEYOPT,1,11,1       !node location 1=bot
!*
KEYOPT,1,2,1

et,2,shell91
KEYOPT,2,9,0          !sandwich = 1
KEYOPT,2,6,1        !pr inter shear=1
KEYOPT,2,5,3        !pr positions
KEYOPT,2,8,1          !store for all (1) layers
KEYOPT,2,11,2       !node location 2=top
!*

KEYOPT,2,2,1

et,3,solid95

!*******define layers***********
R,1
RMODIF,1,1,4,0,
!*
!** defines according to theta, (or 90 deg off) ***
RMODIF,1,13,4,90,t0
RMODIF,1,19,2,45,t45/2
RMODIF,1,25,2,-45,t45/2
RMODIF,1,31,4,90,t0
!*************************************************
***


!***************** MESHING
**********************************
ESIZE,msize,0
!* volume *
type,3,
mat,3
vmesh,1

!* areas *
TYPE,1,
MAT,1,
```

```
REAL,1,
ESYS,0,

!********** mesh *****
AMESH,1

type,2
mat,1
real,1
esys,0

amesh,6

!*loaded ends*?
et,4,shell91
keyopt,4,2,1
r,4
rmodif,4,1,1,0
rmodif,4,13,5,0,t0

type,4
mat,5
real,4

amesh,2
amesh,4
!*sides too*?

!?*************?

!************************************************
*************

!************ DOF constraints *******
!***load***
nsel,s,loc,x,r-msize/100,r+msize/100
nsel,r,loc,z,gz
d,all,ux,0
d,all,uz,fc
!**********

nsel,s,loc,x,r-msize/100,r+msize/100
nsel,r,loc,z,0
d,all,ux,0
d,all,uz,0

nsel,s,loc,x,r-msize/100,r+msize/100
nsel,r,loc,y,beta
d,all,ux,0

nsel,s,loc,x,r-msize/100,r+msize/100
nsel,r,loc,y,-beta
d,all,ux,0

dk,2,uy,0



nsel,s,loc,x,r-msize/100,r+msize/100
nsel,r,loc,y,beta
cp,17,uy,all

nsel,s,loc,x,r-msize/100,r+msize/100
nsel,r,loc,y,-beta
cp,18,uy,all

!************************
!************************************
allsel

/solu

!****** static solution ***
NLGEOM,0
NROPT,AUTO, ,
LUMPM,0
EQSLV,FRONT,1e-08,0,
PSTRES,ON
TOFFST,0,
!*
! /STAT,SOLU
!SOLVE
!*
!*
!*
FINISH

!***** eigenbuckling soln********
!/solu
!ANTYPE,1
!*
!*
!BUCOPT,SUBSP,8,0,0
!*
!SUBOPT,0,0,0,0,0,ALL
! /STAT,SOLU
!SOLVE


!* output controls************
outres,all,all
save

finish


!******* analysis helpers
************************************
!*********** d155's ****************
exd=(37e9)*(3.1+65.8*vf)/32.71
prd=0.31*(.385-.15*vf)/0.318
eyd=(8.99e9)*(1+0.836*vf)/((1-.836*vf)*2.206)
g0=3.48e9*(1+1.672*vf)/((1-.836*vf)*2.809)
prdsq=prd*prd*eyd/exd
q12d=prd*eyd/(1-prdsq)
!************************************

!************ db120's **************
ex45=(26.5e9)*(3.1+65.8*vf)/32.71
ey45=(7.52e9)*(1+0.836*vf)/((1-.836*vf)*2.206)
pr45=0.39*(.385-.15*vf)/0.318
g45=4.12e9*(1+1.672*vf)/((1-.836*vf)*2.809)

prsq=pr45*pr45*ey45/ex45
q11=ex45/(1-prsq)
q12=pr45*ey45/(1-prsq)
q22=ey45/(1-prsq)
q66=g45

cs45=.7071*.7071*.7071*.7071
q11b=(q11*cs45)+(2*(q12+2*q66)*cs45)+(q22*cs45)
q12b=(q11+q22-4*q66)*cs45+(q12*2*cs45)
```

```
q22b=q11b
q66b=(q11+q22-2*q12-2*q66)*cs45+(q66*2*cs45)
!************************************

!*** face sheet elastic constants ***
a11=2*((q11b*n45*t45)+(exd*n0*t0))
a12=2*((q12b*n45*t45)+(q12d*n0*t0))
a22=2*((q11b*n45*t45)+(eyd*n0*t0))
a66=2*((q66b*n45*t45)+(g0*n0*t0))

ttt=2*tt*.001
afx=a11/ttt
afy=a22/ttt
a12av=a12/ttt
Gfxy=a66/ttt
pp=.05
Efx=afx*(1-pp)
Efy=afy*(1-pp)
v12=a12av*(1-pp)/Efy
v21=a12av*(1-pp)/Efx
ppp=v12*v21
!************************************
!************************************************
*************
```

u_def.mac
the random nodal perturbation macro

```
/COM ***************************************
/COM *** Modify nodal positions to simulate defective geometry for buckling ***
/COM ***************************************

/COM
/COM *** Check Plot Parameters ***
stdev_x = arg1
stdev_y = arg2
stdev_z = arg3

*MSG,NOTE,stdev_x,stdev_y,stdev_z
Standard deviation of nodal positions (x,y,z) is: %G, %G, %G.

/PREP7

modmsh,detach
! emid,remove,all

*get,n_count,node,,count
*get,node_num,node,,num,min

/COM Random Gaussian distribution is only PSUEDO-RANDOM
/COM & depends on number of time that gdis() has been called.
/COM Use time to add randomization
*get,clock,active,,time,wall
rungd = nint(clock*100)
*DO,i,1,rungd
  tmp = gdis(1,stdev_x)
*ENDDO
rungd= $ clock=

*DO,i,1,n_count
  node_x = gdis(nx(node_num),stdev_x)
  node_y = gdis(ny(node_num),stdev_y)
  node_z = gdis(nz(node_num),stdev_z)
  nmodif,node_num,node_x,node_y,node_z
  *get,node_num,node,node_num,nxth
*ENDDO
n_count= $node_num= $ node_x= $ node_y= $ node_z= ! Clean up unneeded param's

! emid,add,all

!!! End of File !!!
```

Mathcad Worksheet for 3-layer theory buckling and failure solutions
equations supplied by Vinson (1987)

$0/\pm45/0/b_{3/8}$

elastic properties

$E_{fx} := 25.08 \cdot 10^9$ $\quad \nu_{xy} := .3674$

$E_{fy} := 8.31 \cdot 10^9$ $\quad \nu_{yx} := .1217$

$G_{xy} := 8.033 \cdot 10^9$

$G_c := 1.345 \cdot 10^8$

$E_c := 3.793 \cdot 10^9$

thicknesses

$h_c := .0254 \cdot \frac{3}{8}$

$t_f := \frac{1}{16} \cdot .0254$

panel dimensions

$a := 18 \cdot .0254$

$b := 18 \cdot .0254$

OVERALL BUCKLING
terms for four sided simply supported panels

$n := 1, 2 .. 6$

$C_1(n) := \frac{a^2}{n^2 \cdot b^2}$ $\quad C_4(n) := \frac{a^2}{n^2 \cdot b^2}$ $\quad C_2 := 1$ $\quad C_3(n) := \frac{n^2 \cdot b^2}{a^2}$

$D_x := \frac{E_{fx} \cdot h_c^2 \cdot t_f}{2 \cdot \left(1 - \nu_{xy} \cdot \nu_{yx}\right)}$ $\quad D_y := \frac{E_{fy} \cdot h_c^2 \cdot t_f}{2 \cdot \left(1 - \nu_{xy} \cdot \nu_{yx}\right)}$ $\quad D_{xy} := \frac{G_{xy} \cdot h_c^2 \cdot t_f}{2 \cdot \left(1 - \nu_{xy} \cdot \nu_{yx}\right)}$

$B_1 := \sqrt{\frac{D_y}{D_x}}$ $\quad B_2 := \frac{D_y \cdot \nu_{xy}}{\sqrt{D_x \cdot D_y}}$ $\quad B_3 := \frac{D_{xy}}{\sqrt{D_x \cdot D_y}}$

$$A(n) := C_1(n) \cdot C_3(n) - B_2 \cdot C_2^2 + B_3 \cdot C_2 \cdot \left(B_1 \cdot C_1(n) + 2 \cdot B_2 \cdot C_2 + \frac{C_3(n)}{B_1}\right)$$

$V_x := \frac{\pi^2 \cdot \sqrt{D_x \cdot D_y}}{b^2 \cdot G_c \cdot h_c}$ $\quad V_y := \frac{\pi^2 \cdot \sqrt{D_x \cdot D_y}}{b^2 \cdot G_c \cdot h_c}$

$$K(n) := \frac{B_1 \cdot C_1(n) + 2 \cdot B_2 \cdot C_2 + A(n) \cdot \left(\frac{V_y}{C_4(n)} + V_x \right)}{1 + \left(B_1 \cdot C_1(n) + B_3 \cdot C_2 \right) \cdot \frac{V_y}{C_4(n)} + \left(\frac{C_3(n)}{B_1} + B_3 \cdot C_2 \right) \cdot V_x + V_y \cdot V_x \cdot \frac{A(n)}{C_4(n)}}$$

$$\sigma_2(n) := \frac{\pi^2}{4 \cdot \left(1 - \nu_{xy} \cdot \nu_{yx} \right)} \cdot \left(\sqrt{E_{fx} \cdot E_{fy}} \right) \cdot \frac{h_c^2}{b^2} \cdot K(n)$$

$\sigma_2(n)$

$1.671 \cdot 10^{7}$
$1.751 \cdot 10^{7}$
$3.531 \cdot 10^{7}$
$6.441 \cdot 10^{7}$
$9.921 \cdot 10^{7}$
$1.341 \cdot 10^{8}$

Pa

$N_x(n) := \sigma_2(n) \cdot \left(2 \cdot t_f \right)$

$N_x(n)$

$5.331 \cdot 10^{4}$
$5.551 \cdot 10^{4}$
$1.121 \cdot 10^{5}$
$2.041 \cdot 10^{5}$
$3.151 \cdot 10^{5}$
$4.281 \cdot 10^{5}$

$\frac{N}{m}$

$F_x(n) := N_x(n) \cdot a$ $F_x(n)$

$2.431 \cdot 10^{4}$
$2.541 \cdot 10^{4}$
$5.131 \cdot 10^{4}$
$9.351 \cdot 10^{4}$
$1.441 \cdot 10^{5}$
$1.951 \cdot 10^{5}$

N

CORE SHEAR BUCKLING

$$\sigma_3 := \frac{G_c \cdot h_c}{2 \cdot t_f}$$

$\sigma_3 = 4.037 \cdot 10^{8}$

$F_3 := \sigma_3 \cdot \left(2 \cdot t_f + h_c \right) \cdot a$

$F_3 = 2.344 \cdot 10^{6}$

FACESHEET WRINKLING

$$\sigma_4 := \left[\frac{2 \cdot t_f \cdot E_c \cdot \sqrt{E_{fx} \cdot E_{fy}}}{3 \cdot h_c \cdot \left(1 - \nu_{xy} \cdot \nu_{yx} \right)} \right]^{\frac{1}{2}}$$

$\sigma_4 = 2.524 \cdot 10^{9}$

$F_4 := \sigma_4 \cdot \left(2 \cdot t_f + h_c \right) \cdot a$

$F_4 = 1.465 \cdot 10^{7}$